Spring 2022

Light Microscopy of Proteins in Their Ultrastructural Context

Ons M'Saad
Yale University Graduate School of Arts and Sciences, onsmsaad1994@gmail.com

Abstract

Light Microscopy of Proteins in their Ultrastructural Context

Ons M'Saad

2022

Fluorescence light microscopy is an essential tool in biomedical research. In immunofluorescence, fluorophore-conjugated antibodies are used to detect specific proteins of interest in a fixed biological sample. With recently developed nanoscopy techniques, whole cells can be imaged at an isotropic spatial resolution of ~10 nm, revealing accurate protein distributions on the nanoscale. However, most localized proteins are imaged against a dark background, which forbids seeing the overall subcellular compartments (ultrastructural context) that encompass them. Electron microscopy (EM), on the other hand, offers a complete cellular overview on the scale of a few nanometers. However, EM fails to reliably detect specific molecules of interest. To this end, correlated light and electron microscopy (CLEM) techniques have emerged to combine the high molecular contrast of fluorescence microscopy with the ultrastructural imaging capabilities of EM. Despite the merits of CLEM, sample preparation and image alignment are extremely laborious, limiting this correlative approach to only proof-of-concept biological experiments.

This thesis poses this specific question: **why is light microscopy alone incapable of resolving the ultrastructural context of cells, despite extraordinary improvements in spatial resolution?** We argue that the limitation stems from the physical properties of fluorescent dyes: dyes are ~1 nm in diameter, a size comparable to the distance between proteins in the densely crowded cell. If labeled in bulk, fluorescent dyes would sterically hinder and self-quench via electron transfer and dipole-dipole interactions, which would limit the achievable staining density and thereby the sampling necessary to resolve the crowded cellular interior.

This thesis made the conceptual realization that if the sample protein content is isotropically expanded up to 20-fold in all three dimensions, the relative size of fluorescent dyes would shrink by the same factor. Here, the relative radius of a fluorescent dye would approach ~50 pm, which is comparable to the size of an osmium atom (~200 pm) used in heavy metal EM staining. Bulk fluorescence staining of the decrowded cell will therefore no longer be limited by sampling and quenching restrictions, and ultrastructural details, previously accessible with only EM, can now be revealed on a standard light microscope.

We call the underlying sample preparation technique **pan-Expansion Microscopy (pan-ExM)**. pan-ExM combines the philosophy of bulk- (pan-) staining of the total protein content with a newly developed Expansion Microscopy (ExM) protocol capable of 20-fold linear sample expansion and protein retention. We first develop pan-ExM in cultured cells as a proof-of-concept demonstration. We then develop the technique in dissociated neuronal cultures and in thick (~70 μm) mouse brain tissue sections (**pan-ExM-t**) to establish its applicability in neurobiological research. Finally, in a method we call **panception**, we demonstrate that the conceptual advance of pan-staining is also applicable to transmitted light microscopy. Using polymers of varying refractive indices and light-scattering analogs of fluorescent dyes, we show that sample ultrastructure can be imaged with brightfield microscopy, and that sample microstructure can be revealed with the un-aided eye.

Light Microscopy of Proteins in their Ultrastructural Context

A Dissertation

Presented to the Faculty of the Graduate School

of

Yale University

in Candidacy for the Degree of

Doctor of Philosophy

by

Ons M'Saad

Dissertation Director: Joerg Bewersdorf

May 2022

Table of Contents

List of Figures

Acknowledgements

I am grateful to the entire biological and biomedical community at Yale for creating an exceptional learning and research environment. I am thankful to my PhD advisor Joerg Bewersdorf. With his passion for exciting new ideas and openness to risk-taking, we were able to create new imaging technologies that I believe will have an enduring impact. I am grateful for his mentorship, integrity, guidance, and faith in my abilities.

I am thankful to all members of the Bewersdorf Lab, and in particular, my colleagues on the *2nd floor*. You gave me the respect of a scientist – and that made all the difference. I want to extend my gratitude to Phylicia Kidd who was a valuable colleague and friend, to Lena Schroeder for her mentorship and advice, to Hannahmariem Mekbib for being an inspirational mentee, and to Zach Marin who was always supportive of my work. I am also very grateful to Lukas Fuentes, Sonja Piehler, Yongdeng Zhang, Florian Schueder, Mark Lessard, Kenny Chung, and Dong-Ryoung Lee. Your support and friendships are greatly appreciated, and I enjoyed working alongside you.

Moreover, I want to thank my committee members Mingjiang Zhong, Derek Toomre, and Themis Kyriakides for their advice throughout this thesis. Your patience and integrity are greatly appreciated.

I am grateful to the Yale CCMI facility, and in particular Al Mennone, for maintaining the Leica SP8 confocal microscope that was necessary to conduct this thesis work.

My collaborators inspired many of the developments described in this thesis. I wish to extend my deepest grateful to James Rothman, who was the first outside my lab to see the potential of pan-ExM. Your encouragement and leadership markedly transformed my career trajectory, and I am very thankful. I thank members of the Rothman lab, especially Ravi Kiran Kasula, who was my collaborator on the pan-ExM-t project and a good friend. I thank Andreas Ernst, Pascal Ziltener, and Maohan Su

for their advice on labeling the Golgi. I also want to thank Thomas Biederer and Ilona Kondratiuk who helped push the brain pan-ExM-t project forward and provided guidance and samples. I thank Kattie Watters, Anthony Koleske, Juliana Shaw, Robert Niescer, Pietro De Camilli, Hanieh Falahati, Berrak Ugur, Antonio Giraldez, Alice Sherrard, Diane Krasue, Shangqin Guo, Nayoung Kwon, Brett Lindenbach, Shuo Zhang, Moi Bhattacharyya, Anthony Quinnert, and Xinran Liu for providing diverse cell and tissue samples and for their continued interest in pan-ExM. I thank Mengxue Cao and Yazhen Xue for their purification of sodium acrylate and synthesis of small molecules. I also thank Jens Rittscher, Mariia Dmitrieva, Reto Fiolka, Kevin Dean, and Bo-Jui Chang for exploring the optical imaging and image segmentation potential of pan-ExM. Your trust in the pan-ExM technology is a privilege and an honor I deeply appreciate.

I also really want to thank the Yale Office of Cooperative Research (OCR) and the entire *panluminate* venture team. I am deeply indebted to Thomas Friedlander, James Boyle, James Locker, Thomas Jasinski, Konstantine Drakonakis, Javier Sanchez Cortes, and Richard Andersson. I am grateful to all of you for turning the research that emerged from this thesis into a new commercial venture – I want you to know that I cannot be more excited for this next chapter of my career.

Moreover, I also want to thank Stefano Santaguida who first taught me the science of immunofluorescence and hydrogel synthesis as an undergraduate at MIT. Both skills were incredibly important to this dissertation work. I also want to thank the late Angelika Amon for first introducing me to biological research in her lab when I had minimal experience.

Finally, I want to thank my entire family, whose support throughout this journey I am forever indebted to. I thank my incredibly generous parents Hichem M'Saad and Nada Abdelhedi. Words cannot express my gratitude to you. This PhD would not have been possible without your endearing love, extraordinary sacrifices, and unwavering support – be it emotional, financial, everything. You are the

real pioneers to this American dream, and any success I achieve is only an extension of yours. I love you and I hope I have made you proud.

I thank my very loving husband Mohamed Aziz Bhouri, who was my rock and stronghold throughout this journey and beyond. The world is made for two, and I could not have chosen a better half. You stood by my side and supported me during every step of this journey. I am forever grateful, and I cannot wait for the rest of our lives together.

I thank my sister Sarah and my brother Amir. You were inspirational growing up. I am so privileged to be your big sister, and I hope I see you fulfill all your dreams in the future. I am grateful to my grandmother Latifa. You were - and always will be - my greatest influence and inspiration. I am so thankful for all the time you spent raising and caring for me. I am grateful for my loving grandparents Hamadi, Mohamed, and my late grandmother Essia. I am also thankful to Amira, my beloved childhood best friend and aunt. I am grateful for my uncles and aunts: Ibtissem, Walid, Bader, Anouar, Monia, Nawel, and ya Jamila. You have all shaped who I am today. Thank you for your support, including organizing the wedding of my dreams while I was in full PhD mode. I am so grateful, and I owe every success I achieve to you.

A mes parents,

Nada et Hichem

Cette thèse est la vôtre.

1. Introduction

Long before the advent of microbiology, amid the fearful infancy of our species, humans used to explain death from disease with enduring superstitious beliefs. Today, with the dissemination of microscopy, we are no longer perplexed by what we cannot see. There is a germ theory of disease [84]. Germs are seen, photographed, identified, and for the most part, destroyed. The 2019 coronavirus pandemic [85], during which most of this thesis was conducted, has set the course of microscopy to an extraordinary degree. From immunofluorescence identification of lung tissue biomarkers [86] to resolving the atomic structure of SARS CoV-2 spike proteins [87], microscopy was put to test, and it delivered with grace.

Microscopy is light and lens-based in its origins. The first use of magnifying material can be traced back to the 1st century AD when *Seneca* used flasks of water to magnify letters his book [88]. Interestingly, the silicate glass magnifying lenses we know today were first described by *Ibn al-Haytham* in 1021 [89]. While there remains a controversy regarding who invented the microscope, *Leeuwenhoek* in the 17th century is credited with revealing, bacteria, ciliates, spermatozoa, and muscle fibers using only a ~300-fold magnifying single-convex lens [90]. At the end of the 19th century, lenses reached the maximum numerical aperture, and the resolving resolution reached the diffraction limit of ~200-500 nm [46]. The attention of scientists shifted from looking at overall microstructure to exploring contrast agents capable of highlighting specific biomolecules of interest. Most notable of the contrast mechanisms adopted was the phenomenon of fluorescence, owing to its extraordinary sensitivity. *Coon* is credited with the invention of immunofluorescence [93] and *Shimomura* with the discovery of the Green Fluorescent Protein (GFP) [94]. These

labeling methods allowed imaging of single species of interest, namely single types of proteins, and they are still the gold standard labeling techniques today.

Although single protein species can be imaged, single proteins in intact cells were not resolved spatially until these past two decades. In the late 90s, the Abbe diffraction limit was revisited, and a new type of so-called super-resolution fluorescence microscopes (SRM) were developed. These circumvent the diffraction limit of light by selectively switching fluorophores between their on- and off- states, allowing up to ~10-20 nm spatial resolution in three dimensions [47][48][49].

In an orthogonal and chemical technique termed Expansion Microscopy (ExM) [6], it was demonstrated that physical magnification of fixed biospecimens can also bypass the diffraction limit of light. Developed in 2015, ExM proved that by isotropically separating protein labels from each other ~4-fold linearly using swellable polymer matrices, phantom images reminiscent of sub-diffraction microscopy can be produced. Today, with rapid advancements in molecular biology, chemical synthesis, optical hardware, and computing power, SRM and ExM techniques are active areas of development.

It took over 100 years from the development of a compound light microscopy to conceptualize a microscope that did not use light: Electron Microscopy (EM) was invented by *Knoll* and *Ruska* in 1931, and over the next century, became the standard modality to image cellular ultrastructure [95]. To form an image, (transmission) EM uses shaped magnetic fields as electron optical lenses and beams of accelerated electrons that are transmitted through a sample and detected on a charge-coupled device (CCD) camera [161]. Improvements in vacuum systems, electron guns and accelerating voltage would increase the resolution from ~10 nm to ~1 nm and allow for electron beams to adequately penetrate thin biological specimen. In the 1940-60s, with the development of fixatives and heavy metal stains by *Claude*, *Porter*, and *Palade* among many others, bulk sample

contrast enhanced substantially, revealing the many textbook subcellular imagery we are familiar with today [162][163].

Until now, EM was the only modality that provided a complete overview of cellular *ultrastructure*, while fluorescence microscopy remains the gold standard *molecular* imaging modality. With the order of magnitude enhancement in spatial resolution, fluorescence microscopy images can be correlated to grayscale EM images of the same field of view, providing ultrastructural context to fluorescent biomolecules of interest. This technique is known as correlative light and electron microscopy (CLEM) and it is of high interest to biologists who wish to characterize protein locations with previously unknown positions [164]. Despite its promise, however, CLEM is of prohibitive experimental difficulty, inherent low throughput, and elementally limited by a low (~20-80 nm) spatial correlation resolution [5]. Hence, the dream of looking down at a biological sample and probing its molecular content in context remains elusive and calls for an innovation.

This thesis establishes a new concept for an optical contrast analog to electron microscopy, enabling, for the first time, light-based contextual and molecular imaging on the scale of nanometers.

We discovered that by enlarging biological specimen up to 8,000 their volumes and labeling the bulk of their protein content with fluorescent dyes, familiar ultrastructural features that were previously inaccessible with light microscopy can now be revealed and analyzed.

We call this sample preparation technique **pan-Expansion Microscopy (pan-ExM)**, referencing to the philosophy of labeling the whole (Greek: pan) and the original concept of sample enlargement using Expansion Microscopy (ExM).

In the following chapter, I introduce the key concepts of fluorescence nanoscopy, the methods of Expansion Microscopy (ExM), and the challenges of contextual imaging. In Chapter 3, I present my published work titled "**Light microscopy of proteins in their ultrastructural context**" which demonstrates the feasibility of light-based contextual and molecular imaging in adherent cells. In Chapter 4, I present my submitted manuscript titled "**All-optical visualization of specific molecules in the ultrastructural context of brain tissue**" where I adapt pan-ExM to dissociated neuron cultures and thick mouse brain tissue sections. Several key developments in Chapter 4 are described in provisional patent. In Chapter 5, I develop a new concept for transmitted light nanoscopy and un-aided eye perception (panception) of fixed biological samples. Chapter 5 is described in my manuscript in preparation titled "**Panception: Pan-cellular Perception**". Chapters 1 and 5 are also described in published patent titled "**Methods and Systems for Physical Expansion and Imaging of Biological Samples"**. Finally, in Chapter 6, I summarize the key developments proposed in this thesis and reflect on the promise of light-based ultrastructural imaging. Several paragraphs in Chapters 1 and 6 are adapted from a solicited review article to be published in *Physiology*.

2. Background

2.1. Fluorescence Microscopy

2.1.1. Fluorescence Nanoscopy

A fluorescence microscope is a magnifying lens-based optical system that uses fluorescence contrast to visualize microscopic structures such as cellular organelles [43]. A biological sample is usually labeled with fluorescing dyes and illuminated with a specific light wavelength that is then absorbed by each dye and re-emitted at a longer wavelength. This emitted fluorescent light is observed as bright luminescence on a dark background, allowing labeled structures to be detected in extremely small amounts over relatively high noise levels [44]. The exceptional sensitivity of fluorescent dyes and their relative non-invasiveness make them ideal contrast agents to analyze the distribution and dynamics of the colorless biomolecules in question [45].

Despite the immense biological insight derived from fluorescence microscopy, the diffraction limit of light restricts the spatial resolution to ~250-500 nm [46]. This precludes conventional light microscopes from resolving organelle sub-structures, such as the cisternae of the Golgi apparatus and the cristae of mitochondria. Fortunately, super-resolution microscopy (SRM) techniques such as PALM, STORM, and STED developed in the last two decades have successfully overcome Abbe's diffraction limit. These control the number of fluorescing fluorophores in a diffraction limited volume, allowing for an order of magnitude improvement in spatial resolution [47][48][49][50][51]. Combined with breakthroughs in 3D imaging techniques, data acquisition speed, and probe design, SRM now routinely achieves ~20 nm isotropic spatial resolution in fixed

specimen and ~50 nm resolution in live cells and animal tissue [52][53][54][55][56][57][58][60]. Super-resolution microscopy (nanoscopy) today is a critical tool for biological discovery, revealing for example the convoluted cis-medial-trans subcompartments of the Golgi complex in adherent cells [1] and the fine structures of dendritic spines in the living mouse brain [59].

2.1.2. Tissue Clearing Techniques

Proteins are translucent in aqueous solution while lipid bilayers have high refractive indices (RI~1.45, [165]). Because biological tissue is composed mostly of proteins and lipids assembled heterogeneously in three dimensions, visible light that encounters these surfaces bend and scatter. This scattering limits the optical depth of light microscopy, pushing many scientists over the century to chemically transparentize (clear) their tissue specimens. Here the refractive indices of tissue components are homogenized by either dissolving the lipid content or *uniformizing* the density of scattering molecules [166].

Historically, the first clearing technique used organic solvents (e.g., methanol, hexane, and tetrahydrofuran) to dissolve scattering lipids and dehydrate the underlying tissue. This process leaves behind a homogenous, proteinaceous, and high RI sample [167] and is usually followed by incubation in organic solvents of high RIs (e.g., benzyl alcohol) to match that of the now dehydrated and delipidated sample. BABB [169], 3DISCO [168], and iDISCO [170] are all modern clearing techniques that fall within this category. Although powerful, particularly in anatomy studies, organic solvents quench fluorescent proteins and significantly shrink and distort the tissue in question.

Aqueous clearing methods emerged to circumvent tissue dehydration artifacts present in organic solvent based clearing techniques. In what is known as *simple immersion* methods, tissue samples

are simply immersed in high RI solutions (e.g., formamide [173], sucrose [171], fructose [172], and 2,2′-thiodiethanol [174]) to match the RI of the *average* tissue components. This strategy preserves lipids and is experimentally less demanding. However, it provides relatively low clearing efficiency, and it is used mostly to process small samples (e.g., monolayer cells and thin tissue sections).

Methods known collectively as *hyperhydration*, on the other hand, provide enhanced clearing efficiency compared to *simple immersion* methods. These remove lipids with detergents (e.g., Triton X-100) and hydrate the hydrophobic core of proteins with chaotropic reagents (e.g., urea), thereby reducing the overall RI of the sample to ~1.38. *Hyperhydration* techniques (e.g., *Scale* [175] and CUBIC [176][177]) have been effective at clearing whole mice bodies, fish organs, and skin layers.

Despite the high clearing efficiency of *hyperhydration* methods and their compatibility with fluorescent proteins, the high concentrations of detergents used (e.g., 50% (v/v) Triton X-100) extract not only the lipid content but also a high fraction of the protein content (up to ~20-40%) [68]. This weakens antibody stainings, which is very undesirable, particularly when imaging at high resolution. To this end, in 2013, and in a method known as CLARITY, *Chung* and colleagues developed polyacrylamide hydrogel scaffolds that can covalently crosslink the protein and RNA contents *prior* to lipid extraction and subsequent RI matching. This revolutionized the field of tissue clearing, as harsher lipid extraction (e.g., with sodium dodecyl sulfate (SDS)) can now be applied, while the proteome and transcriptome can still be preserved in their totality and probed with fluorescent dyes after clearing [68]. Although preserving tissue with polyacrylamide hydrogels can be traced back to 1981 [179][180], CLARITY conceptualized the use of hydrogels for transparentizing tissue, enabling 3D imaging of *intact* whole organs. Follow-up techniques

such as PACT and PARS further optimized this hydrogel-based clearing method and widely increased its dissemination [178].

2.1.3. Fundamentals of Expansion Microscopy

Multiple tissue clearing methods reported sample expansion (enlargement) after processing. In fact, prior to 2015, expansion was considered a dreadful artifact of clearing [178][68][70][176]. Hyperhydration with urea was particularly notorious at expanding samples by linear factors ranging from ~1.5 to ~2 [176][175] and hydrogel based clearing methods CLARITY and PACT frequently reported ~1.5-fold tissue expansion [178][68]. To this end, post-fixation with 4% formaldehyde (in the case of PACT) or dehydration with glycerol and sorbitol (in the case of CUBIC and *Scale*) were usually employed to counterbalance the expansion artifact.

A new microscopy technique however would take the conceptual leap of purposely expanding hydrogel-embedded tissue to achieve higher resolution imaging. In 2015 and in a method known as Expansion Microscopy (ExM), *Chen* and colleagues combined hyperhydration with hydrogel embedding and proved that *isotropic* ~4.5-fold linear enlargement of biological is possible [6]. Here, a fixed cell or tissue sample is infused with sodium acrylate monomers and bisacrylamide crosslinker and a hydrogel is formed *in situ*. After mechanical homogenization of the sample and water dialysis, electrostatic repulsion between the polyacrylate chains cause the underlying hydrogel to absorb 4.5^3 ~ 100-fold its volume in water, pulling crosslinked biomolecules apart as polymer chains linearly elongate in solution. This way, labels spaced closer than the optical diffraction limit are separated in space and optically resolved by conventional light microscopy. The apparent spatial resolution is now the diffraction limit of light (~300 nm) divided by the linear expansion factor (300 nm / ~4.5-fold = ~70 nm). Although ExM is the first method to

systematically and isotropically enlarge tissue components, the first recorded instance of purposeful tissue expansion can be dated back to 1994, when *North* and colleagues inverted thin cryosections of smooth muscle cells on the surface of Tris-buffered saline to separate cytoskeletal elements and allow for higher resolution imaging [210][211]. The method was even dubbed *artificial expansion*.

ExM methods can be broadly classified into two categories. The first category requires pre-expansion immunofluorescence (IF), while the second category is compatible with post-expansion IF. In the former approach, antibody labels are crosslinked to the ExM hydrogel with either the use of acryloyl-functionalized DNA oligonucleotides (ExM 1.0) [6] or acryloyl-conjugated NHS ester small molecules (pro-ExM [7] and ExM-GA [8]). The sample is then treated with detergents that permeabilize lipid membranes and digested with unspecific proteases. Although proteases remove most of the protein content, they allow for roughly half of the dye-conjugated antibody fragments to remain anchored to the hydrogel, permitting their subsequent imaging. Finally, the hydrogel scaffold is dialyzed with repeated exchanges in pure water. The linear expansion factor for poly(acrylamide/sodium acrylate) co-polymers of sufficient mechanical integrity is ~4.5-fold. Lowering the crosslinker concentration can allow for expansion factors up to ~10-fold (x10 expansion [11] and TREx [78]) but this is usually at the expense of rendering the hydrogels too brittle to handle. Moreover, ExM gelation in this category can also be done iteratively (iExM) [10]. With the use of cleavable acrylamide crosslinkers and a combination of complementary DNA oligonucleotides that transfer antibody labels from one gel to the next, a second iteration of ExM yields an expansion factor of ~20-fold. Here, the effective spatial resolution is ~25 nm which is lower than 300 nm / 20 ~ 15 nm because the resolving power is limited effectively by the size of antibody labels used (~ 20 nm).

The second category of ExM methods circumvents the use of harsh proteases for sample homogenization by preventing inter-protein crosslinking after formaldehyde (FA) fixation [9][12]. It is hypothesized that by incubating FA-fixed cells in an excess of acrylamide monomers at high temperatures, acrylamide will crosslink FA-modified amines (formaldimines) on proteins via a nucleophilic addition reaction, thereby preventing the formation of methylene bridges between closely spaced proteins while functionalizing proteins with acrylamide handles [98][99][100][101]. After hydrogel embedding, the sample is denatured and has its lipid content removed using anionic surfactants like sodium dodecyl sulfate (SDS) and heat. Electrostatic bonds between proteins are therefore severed and mechanically rigid lipids are discarded. This allows the protein-hydrogel hybrid to expand ~4-fold in pure water without significant loss of proteomic content. This category of ExM methods borrows heavily from CLARITY protocols and it has been used to expand whole mouse organs (MAP [9]) as well as cells and microbes (U-ExM [12]). Importantly, since the proteome is preserved, these methods are compatible with post-expansion IF techniques, allowing users to access a new dimension of fluorescence microscopy: one where the linker error of fluorescent labels is small enough to not limit the achievable imaging resolution.

ExM methods have evolved rapidly these past few years, with protocols allowing for expansion of: whole mouse brains, mouse lungs, mouse spleens, mouse pancreas slices [8][9], ovaries of Drosophila [103], whole organisms like planaria [104], zebrafish [102][106], C. elegans [38], human biopsies that are fresh-frozen or formalin-fixed and paraffin-embedded (FFPE) [105], multiple bacteria communities [107][114], fungal species [112], and plants [115]. Engineering of small acryolated molecules have enabled ExM to retain antibodies [34][109], RNA [108], actin [34], protein self-labeling tags like SNAP and Clip [109], as well as synthetic lipids [34][35]. Expansion microscopy has been combined with *in situ* transcriptomic sequencing methods like

multiplexed-error robust fluorescence in situ hybridization (MERFISH) [111] and fluorescence *in situ* sequencing (FISSEQ) [110]. ExM has also been combined with optical super-resolution techniques like structured illumination microscopy (SIM) [103][117], STED microscopy [113], and STORM microscopy [109][116], providing even higher spatial resolutions. Moreover, ExM has been especially popular with light sheet microscopy modalities since expanded samples are optically transparent (>99% water) and usually too large in volume to be thoroughly imaged with lower throughput techniques [33][118].

The fundamental limit on spatial resolution in ExM is the mesh size of the embedding hydrogel. Small-angle X-ray scattering (SAXS) studies show that polyacrylamide hydrogels with similar monomer and crosslinker concentrations to the hydrogels used in ExM exhibit mesh sizes that are on the order of ~1-2 nm [182]. However, polyacrylamide hydrogels prepared with free radical polymerization are known to harbor structural inhomogeneities on the ~1-10 nm scale (e.g., dangling ends and loops) [183]. To obtain a more ideal hydrogel network, one study synthesized a polyanionic hydrogel using end-linking of tetra-arm polyacrylate and polyethylene glycol (PEG) polymers with Click Chemistry (tetra-gel or TG) [119][120]. Here, it was demonstrated that ~10-fold expansion of the herpes simplex virus type 1 (HSV-1) capsid using TG gels yields 9.2 nm spatial error instead of 14.3 nm using free radical polymerization, resulting in a more preserved capsid sphericity [119]. However, TG gels did not prove superior in expanding structures within cells and thick tissue (e.g., microtubules and dendrites). This could be due to the limited permeability and diffusion extent of the highly charged and bulky tetrahedral polyacrylate and PEG TG monomers (~28 carboxyl groups per monomer). Nevertheless, most ExM methods still use *in situ* free radical polymerization of small acryloyl monomers and crosslinkers that are widely available.

Whether the expansion mechanism in ExM separates biomolecules apart equally on the single nanometer scale is a major question in the field. An ideal expansion would imply that (1) all biomolecules are tethered to polymer chains in a 1-to-1 ratio, (2) that all proteins are 'uncrosslinked' and their interactions annulled, and (3) that the hydrogel polymer network itself is homogenous and equally spaced. However, biomolecules can be technically considered 'defects' within the polymer network, and the extent of sample fixation (and reversal of fixation) is still an area of large speculation. Still, inhomogeneities in ExM are repeatedly proven to average out on the ~10 nm scale [185]. To validate the isotropy of expansion, the standard in the community is to register pre-expansion images to their post-expansion counterparts. Here local deformities are calculated and the error of image registration over several micrometers is reported in biological units [6]. Alternatively, measuring nanoscale structures with defined symmetry and stoichiometry such as nuclear pore complexes (NPCs) and centrioles can also be excellent validation metrics [12][184]. Nonetheless, if implemented properly and factors such as strength of fixation and sample homogenization are well accounted for during sample preparation, ExM methods can be deemed isotropic on the ~10 nm scale, with errors possibly equivalent to the size of individual proteins [185] *and* no different in magnitude than fluorescent probe linker errors frequently reported in optical super-resolution microscopy techniques [186].

2.2. The Challenge of Contextual Imaging

2.2.1. What is Ultrastructural Context?

Ultrastructure is defined as the fine nanometer-sized structures that constitute cells, typically those that cannot be imaged with diffraction limited microscopy or are only accessible with electron microscopy (EM) techniques. **Ultrastructural *context* is defined as the totality of fine structures that thoroughly represent a cell.** In one embodiment, this could refer to the total electron or amino acid density of the sample. In other paradigm, this could be the bulk of proteins or lipids that constitute the sample. In all embodiments, this molecular contrast must be able to resolve familiar organelles or cellular compartments that are ~1-20 nm apart. It follows that if a contrast reagent is used, it must be smaller in relative size than the molecule class it aims to accentuate. Preceding this work, the only available options to localize proteins to their ultrastructural context was to use immuno-EM or correlative light and electron microscopy (CLEM).

2.2.2. Immuno-Electron Microscopy

Electron microscopy (EM) techniques display electron densities within a sample with spatial resolutions on the order of a few nanometers. In the context of biological imaging, EM provides the wide and familiar ultrastructural cellular context we often find in textbooks [161]. If a sample is imaged following chemical fixation or freeze-substitution, it is often stained in bulk with heavy metals such as osmium tetroxide and uranium acetate [122]. These enhance membrane and protein contrast and allow for higher definition imaging of major subcellular compartments like the cisternae of the Golgi apparatus and cristae of mitochondria.

To identify functional molecules of interest, such as a specific protein type, immunodetection with electron dense nanoparticles conjugated to antibodies (immuno-EM) can be an option [187]. Immuno-EM can be performed before sample embedding in plastic resin (pre-embedding immuno-EM) [188] or after (post-embedding immuno-EM) [189]. Despite its promise, immuno-EM is of limited popularity in the cell biology research community for immanent disadvantages. For example:

(1) The electron-opaque markers that are conjugated to antibodies are imaged in the same channel as the underlying ultrastructural context and may therefore be mistaken for biological material. These markers (e.g., gold nanoparticles) are often designed to be larger than most macromolecules (~6-25 nm), to not be mistaken for electron dense proteins such as ribosomes. However, the larger marker size combined with the size of antibodies (~15 nm) often render the conjugate too large (~20-40 nm) to precisely localize the protein of interest to its subcellular compartment and often obscures the structure itself.

(2) In pre-embedding immuno-EM, the sample must be permeabilized with harsh detergents to allow for antibody penetration, particularly if the protein of interest is located within a double-membrane-bounded organelle. Permeabilization, however, perforates lipid membranes and extracts specific lipids which are necessary for ultrastructure delineation in EM, resulting in low-definition images.

(3) In post-embedding immuno-EM, antibodies must bind antigens exposed on the surface of thin and resin-embedded tissue sections. Because of antigen masking from excessive fixative and resin crosslinking as well as the hydrophobic nature of the resin, antibody labeling is usually inefficient.

(4) More importantly, this method is inherently 2D. Hundreds of thin sections must be labeled separately to achieve a 3D rendering.

2.2.3. Correlative Light and Electron Microscopy

Correlative light and electron microscopy (CLEM) is the technique of spatially correlating both electron and fluorescence microscopy data sets [164]. In its origin, CLEM was designed to bridge the gap between live-cell imaging and EM (Live-cell CLEM). A cell would be imaged live using fluorescent proteins, fixed at a temporal frame of interest, and subsequently visualized by EM using either immunolabeling or photoconversion of specific electron opaque substrates [190]. Here the fluorescence signal is converted to an EM signal that is used to localize specific cells or organelles. This way, cellular events such as cell division, synaptic release, membrane dynamics, or organelle biogenesis can be studied at the dynamic level first and at the ultrastructural level second, providing important biological insight [191][192][193].

In the present-day, however, developments in CLEM attempt to accomplish what immuno-EM struggled to attain, and that is to quantitatively localize single proteins to their sub-cellular compartments. Here the fluorescence signal in a fixed cell is *overlaid* directly with the EM image [5]. Briefly, a cell is (1) fixed, (2) immuno-stained with fluorescent dyes, (3) imaged usually with super-resolution fluorescence microscopy, (3) post-fixed with glutaraldehyde, (4) stained with heavy metals, (5) dehydrated, (6) embedded in plastic resin, and (7) imaged with EM. Lastly, images acquired with both microscopy modalities are correlated using sophisticated software. Unlike immuno-EM, proteins in CLEM are shown in a different ‘channel’ and not captured concurrently with total electron density. However, CLEM shares most of the disadvantages present

in immuno-EM methods and introduces new challenges that are unique to its correlative nature. For example:

(1) Like immuno-EM, antibodies in CLEM are bulky (~12 nm per antibody layer), lowering their localization precision.

(2) Unlike immuno-EM, signal from antibodies is registered before the additional sample preparation steps required for EM imaging, with the secondary fixation, heavy metal staining, dehydration, and plastic embedding all contributing to sample shrinkage and ultrastructure distortion. These factors also lower the precision of antibody localization.

(3) Software alignment methods currently achieve ~20 nm correlation resolution at best [194]. These alignment methods also require fiducials (e.g., embedded gold nanorods [194]), are nonlinear (since deformations are nonlinear), and in many cases, depend on user input. This means that there must be a priori knowledge of the target localization, limiting CLEM to proof-of-concept experiments.

(4) Like pre-embedding immuno-EM, detergents must be used to permeabilize cellular membranes, lowering the definition quality of EM imaging. Using fluorescent proteins (e.g., GFP and mEos) or self-labeling protein tags (e.g., Halo, SNAP, and Clip tags) can overcome some of the limitations associated with antibody labeling (such as points (1) and (3)), but these are only available for genetically engineered targets.

(5) Even with the advent of super-resolution microscopy (SRM), there is still an order of magnitude mismatch in spatial resolution between SRM and EM, particularly in the axial dimension.

(6) This method is mostly performed in 2D and in thin tissue sections. 3D EM uses focused ion beam scanning EM (FIB-SEM [195]) and diamond knife serial array [196] which

require weeks of continuous data acquisition (e.g., 1 month per 1 cell in 3D correlative light and FIB-SEM [5]), limiting this technique to proof-of-concept biological experiments.

3. pan-Expansion Microscopy of Adherent Cells

In this chapter, I reproduce my work titled:

*M'Saad O. & Bewersdorf J. Light Microscopy of Proteins in their Ultrastructural Context. Nature Communications, **11**, 3850 (2020)*

This work was recognized by a Yale News press release, an Editor's Highlight webpage, and is among the Top 50 Chemistry and Materials Sciences Articles in Nature Communications 2020 (>14,000 article accesses as of Oct. 9, 2021). My contributions to this section include the conceptualization of the underlying pan-ExM method and its implementation in adherent cells.

Abstract

Resolving the distribution of specific proteins at the nanoscale in the ultrastructural context of the cell is a major challenge in fluorescence microscopy. We report the discovery of a new principle for an optical contrast equivalent to electron microscopy (EM) which reveals the ultrastructural context of the cells with a conventional confocal microscope. By decrowding the intracellular space through 13 to 21-fold physical expansion while simultaneously retaining the proteins, bulk (pan) labeling of the proteome resolves local protein densities and reveals the cellular nanoarchitecture by standard light microscopy.

3.1. Introduction

Fluorescence microscopy has transformed the field of cell biology through its exceptional contrast and high specificity of labeling. With the advent of super-resolution microscopy, the three-

dimensional (3D) distribution of specific proteins of interest can be imaged at spatial resolutions down to ~10 nm, revealing their astounding sub-cellular organization at the nanoscale [1]. Fluorescence microscopy, unlike electron microscopy, is however fundamentally prohibited from resolving the ultrastructural context of the cell: the smallest fluorescent labels, organic dyes, are ~1 nm in diameter, a size comparable to the distance between proteins in the densely crowded cellular interior [2]. Many binding sites are therefore masked or unreachable and neighboring fluorescent labels sterically hinder or self-quench each other via electron transfer or dipole-dipole interactions [3]. This limits the achievable fluorophore density and thereby the contrast and sampling necessary to resolve the crowded and complex ultrastructural context of the cell [4]. Showing specific proteins in their ultrastructural context, has therefore largely relied on correlative light/electron microscopy (CLEM). These techniques combine the resolving power and global contrast of EM with the information provided by high molecular specificity of fluorescence microscopy. While CLEM can yield information-rich images of the 3D landscape of the cell [5], it requires highly specialized instruments and days to weeks of continuous data acquisition for a single 3D data set of a mammalian cell, thereby limiting its applicability.

Here, we demonstrate a straightforward method of imaging whole-cell ultrastructural context based on Expansion Microscopy (ExM). In ExM [6][7][8][9][10][11][12], a biological sample is embedded and hybridized to a swellable poly(acrylamide/sodium acrylate) co-polymer network. By absorbing water, the gel physically expands by a factor of ~4 in all three dimensions. In iterative expansion microscopy (iExM), iteratively anchoring DNA oligo-conjugated antibodies to hydrogel networks twice yields expansion factors of typically up to 20 [10]. The commonly used proteases, which digest proteins to allow for homogeneous expansion, however, result in the degradation of most cellular content. Variants of ExM such as Magnified Analysis of the Proteome

(MAP) and Ultrastructure-ExM (U-ExM) have addressed this problem by preventing inter- and intra-protein crosslinks during the tissue-hydrogel hybridization step and by using anionic surfactants and heat to isotropically separate neighboring proteins [9][12]. However, despite their promise, these techniques have been limited to an expansion factor of ~4 as they are not compatible with iterative expansion.

We hypothesized that by embedding a sample in a dense hydrogel prepared with a cleavable crosslinker in a second dense superabsorbent hydrogel, entanglements between polymer chains of the first and final hydrogels will physically interlock protein-polymer hybrids in this latter polymer network, thereby preserving the proteome while iteratively expanding it. This type of polymer entanglement, first described by Sam Edwards in 1967 [13], would retain most of the cellular proteome in the final hydrogel, while simultaneously expanding the sample by about a factor of $4 \times 4 = 16$. The hydrogel chemistry employed in this method is reminiscent of semi-interpenetrating polymer networks (semi-IPNs), where one polymer is crosslinked and the second is linear14. Because of their enhanced and tunable mechanical properties, semi-IPN hydrogels have been designed to entrap cells, proteins, and small molecule drugs for controlled drug release [15][16][17]. In this paper, we show that the application of semi-IPNs can be extended to the entrapment of polymer-protein hybrids to increase the sample expansion factor while retaining its protein content. This strategy combined with global fluorescent labeling, which targets all separated proteins, would reveal the overall landscape of the cell with a light microscope - resembling the contrast of heavy-metal EM stains.

Based on this concept, we developed an ExM method which we named, in reference to the philosophy of labeling the whole (Greek: pan) proteome, pan-ExM. In brief (**Supplementary Figs. 1** and **2**), previously fixed cells cultured on coverslips are incubated in a solution of acrylamide

(AAm) and formaldehyde (FA) to simultaneously prevent inter-protein crosslinks and tether proteins to the hydrogel. Next, the cells are embedded in a poly (acrylamide/sodium acrylate) co-polymer cross-linked with N,N′-(1,2-dihydroxyethylene)bisacrylamide (DHEBA), an acrylamide crosslinker with a cleavable amidomethylol bond. After polymerization, the sample is delipidated and denatured with sodium dodecyl sulfate (SDS) and heat. The hydrogel is then expanded ~4-fold in deionized water and embedded in a neutral polyacrylamide hydrogel cross-linked with DHEBA to maintain the gel in its expanded state during subsequent treatments. Afterwards, the gel is incubated in a solution of FA and AAm for additional anchoring of previously masked primary amines to the next hydrogel. This composite hydrogel is embedded in a third hydrogel, a poly(acrylamide/sodium acrylate) co-polymer cross-linked with N,N′-methylenebis(acrylamide) (BIS), a non-hydrolyzable acrylamide crosslinker. Next, sodium hydroxide is used to cleave the crosslinks of the first and second hydrogels and the sample is washed with PBS. Lastly, the hydrogel is labeled with fluorescent dyes and expanded to its final size in deionized water with an expected linear expansion factor of ~16 (**Supplementary Fig. 3**).

3.2. Results

3.2.1. pan-ExM reveals cellular ultrastructure

To test this concept, we labeled proteins in bulk with what we refer to as a pan-staining. For this first experiment we chose N-Hydroxysuccinimide (NHS) ester-dye conjugates, taking advantage of the abundance of primary amines on proteins (**Supplementary Fig. 4a**). A visual comparison of HeLa cells non-expanded, expanded once, or twice, imaged with a standard confocal microscope (**Fig. 1a–d**; **Supplementary Fig. 5**), confirms the validity of this concept: non-

expanded cells show essentially a uniform staining, revealing little information. Single-expanded cells start to show the outlines of organelles such as mitochondria, but fail to show ultrastructural details. Expanding cells twice, in contrast, allows to spatially resolve details too small to be distinguished by conventional light microscopy methods in standard samples. Analogous to EM, now resolvable hallmark features such as mitochondrial cristae (**Fig. 1e**, yellow arrowheads) or the stacking of Golgi cisternae (**Fig. 1e**, green arrowheads) allow for the identification of organelles by their morphological characteristics.

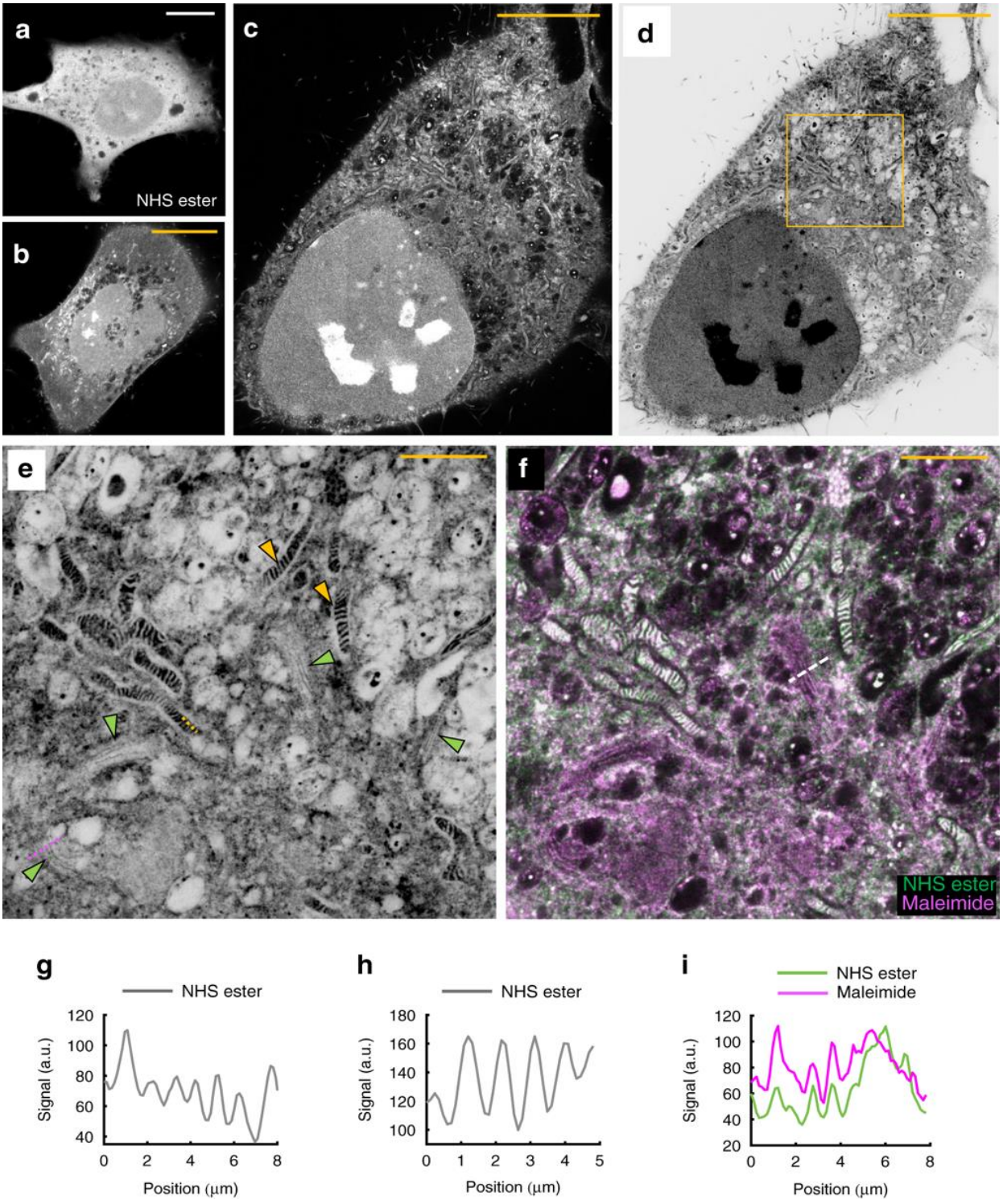

Figure 1: pan-ExM reveals cellular ultrastructure. a Non-expanded HeLa cell pan-stained with NHS ester dye. **b** HeLa cell expanded 4-fold and pan-stained with NHS ester dye. **c** pan-ExM expanded HeLa cell pan-stained with NHS ester dye. **d** Same image as c but shown with an inverted color table. **e** The area in the yellow box in **d** reveals hallmark cellular ultrastructure features such as mitochondrial cristae (yellow arrowheads) and Golgi cisternae (green

arrowheads). **f** Same image as in e but showing overlay of NHS ester pan-stain channel (green) and maleimide pan-stain channel (magenta; see Supplementary Fig. 23). Representative images from 3 (**a**, **b**) and 11 (**c–f**) independent experiments are shown. **g** Line profile along the magenta dashed line in **e** revealing Golgi cisternae. **h** Line profile along the yellow dashed line in **e** revealing mitochondrial cristae**. i** Line profile along the dashed line in **f** revealing the change in NHS ester to maleimide staining across a Golgi stack. Panels **a–c** are displayed with a black-to-white color table. Panels **d**, **e** are displayed with a white-to-black color table. Yellow scale bars are not corrected for the expansion factor. Scale bars, (**a**) 10 µm, (**b**) 40 µm, (**c, d**) 100 µm, (**e, f**) 20 µm.

3.2.2. pan-ExM is compatible with conventional fluorescent labels

Importantly, our protocol is compatible with immunofluorescence labeling as well as other established chemical stainings, enabling correlative studies which combine specific and contextual pan-labeling approaches. **Fig. 2a–c** and **Supplementary Fig. 6** show microtubules labeled by an antibody against α-tubulin. Similarly, we can visualize the outer mitochondrial membrane protein TOM20 by antibody-labeling in the context of the cellular ultrastructure revealed by our pan-staining (**Fig. 2d–f**). It is worth pointing out that these antibodies were applied after the expansion procedure. This approach allows us to take advantage of the molecular decrowding for improved epitope accessibility and leads to a negligible label size relative to the expanded structure sizes. Furthermore, **Fig. 2h** shows a pan-ExM sample labeled with a live-cell small molecule dye, MitoTracker Orange, which covalently binds to proteins in the matrix of mitochondria. The MitoTracker Orange staining overlays well with the striped pattern observed in the NHS ester channel (**Fig. 2g, j, k**), confirming that the latter represents the mitochondrial matrix. DNA-intercalating dyes such as SYTOX Green are equally compatible with pan-ExM and label, next to the nucleus, mitochondrial nucleoids (**Fig. 2i, j**). The resolution achieved with the used standard confocal microscope is good enough to reveal the partial exclusion of proteins from the nucleoids

(as represented by NHS-ester and MitoTracker staining; **Fig. 2k**) which have been reported to be about 110 nm in diameter [18].

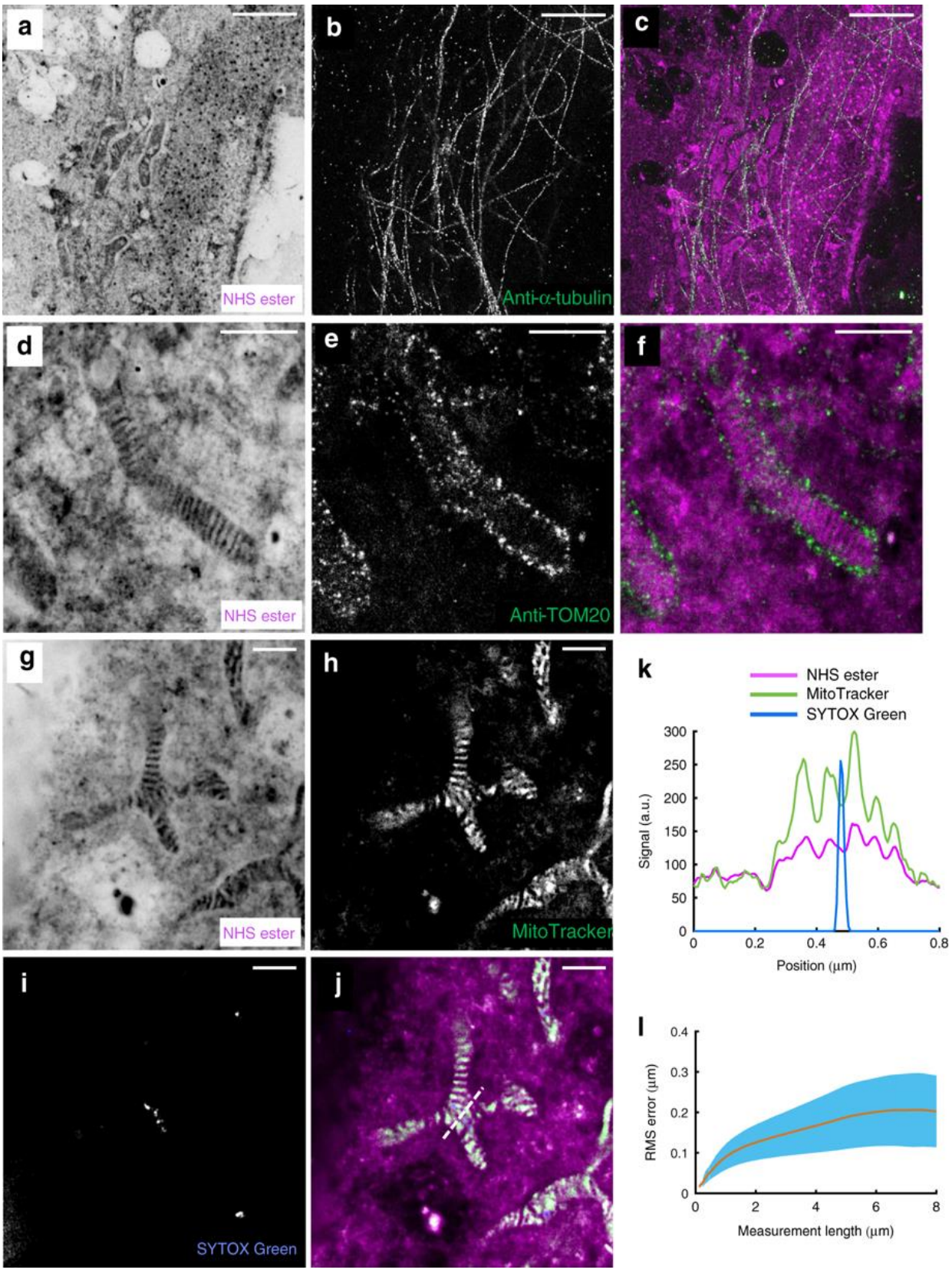
a
NHS ester
b
Anti-α-tubulin
c
d
NHS ester
e
Anti-TOM20
f
g
NHS ester
h
MitoTracker
i
SYTOX Green
j
k
NHS ester
MitoTracker
SYTOX Green
Signal (a.u.)
Position (μm)
l
RMS error (μm)
Measurement length (μm)

Figure 2: pan-ExM is compatible with standard fluorescent labeling techniques. **a** NHS ester pan-stained HeLa cell. **b** Anti-α-tubulin immunostaining in the same area. **c** Overlay of **a** and **b**. **d** NHS ester pan-stained mitochondrion. **e** Same area as in **d**, showing anti-TOM20 immunostaining and revealing the outer membrane of the mitochondrion. **f** Overlay of **d** and **e**. **g** NHS ester pan-stained mitochondrion. **h** MitoTracker Orange stain in the same area. **i** SYTOX Green stain showing DNA in mitochondrial nucleoids. **j** Overlay of **g–i**. **k** Line profile along the dashed line shown in **j**. Representative images from 3 (**a–f**) and 5 (**g–j**) independent experiments are shown. **l** Plot of root mean square (RMS) error over distance comparing pre- and post-pan-ExM images of microtubules (*n* = 5 cells). The orange line corresponds to the mean and blue error bars correspond to the standard deviation. Panels **a, d, g** are displayed with a white-to-black color table. Panels **b, e, h, i** are displayed with a black-to-white color table. Scale bars show expansion-corrected values. Scale bars, (**a–c**) 2 µm, (**d–f**) 1 µm, (**g–j**) 500 nm.

3.2.3. pan-ExM reveals nuclear ultrastructure

Focusing on the cell nucleus, we find that SYTOX Green produces a bright nuclear staining (**Fig. 3a–c**). Nuclear pore complexes appear as bright spots in the NHS ester pan-staining (also visible in **Fig. 2a**) and are clearly correlated with nuclear regions showing reduced SYTOX Green staining (**Fig. 3d–f, j**; **Supplementary Fig. 7**). This observation has been made by EM [19] and super-resolution microscopy [20] before. Similarly, the SYTOX Green staining is partially excluded from nucleoli identifiable by their strong NHS ester pan-staining (**Fig. 3g–i, k**; **Supplementary Fig. 7**). Nucleoli subcompartments such as the granular component, fibrillar center, and dense fibrillar components can easily be resolved [21]. Intriguingly, we can observe areas of strong nuclear acid staining in close vicinity of, but not overlapping with, the fibrillar components of the

nucleoli (**Fig. 3g–i, k**; **Supplementary Figs. 7** and **8** show nucleoli in U-2OS and HeLa cells, respectively).

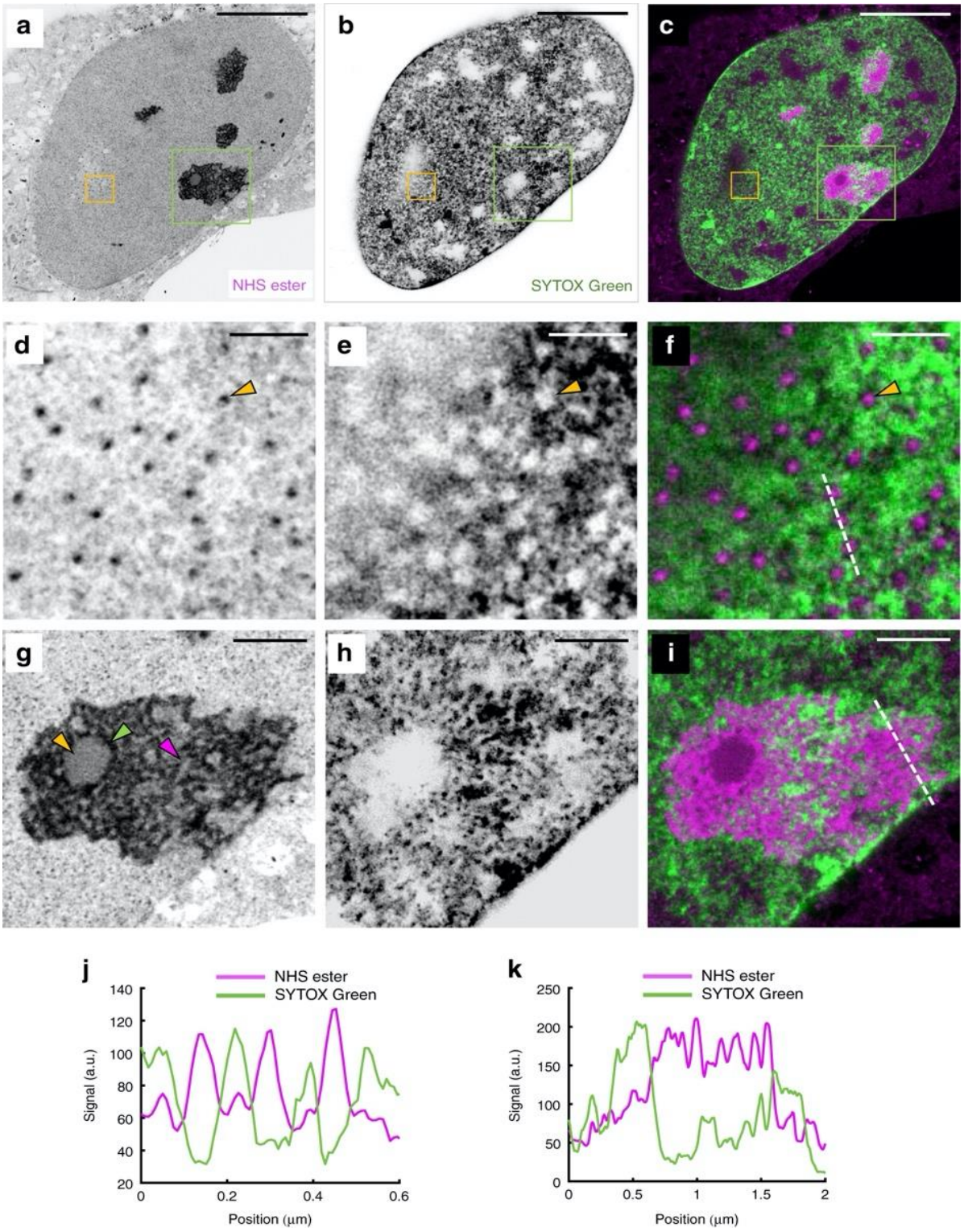

Figure 3: pan-ExM reveals nuclear ultrastructure in interphase. **a** Image of NHS ester pan-stained U-2OS cell in interphase. **b** SYTOX Green nucleic acid stain image of the same area. **c** Overlay of **a** and **b**. **d–f** Magnified view of the areas outlined by the yellow boxes in **a–c** showing amine-rich regions corresponding to nuclear pore complexes (NPCs) which coincide with circular channels excluding chromatin in the SYTOX Green image. The yellow arrowheads point at one NPC and the corresponding chromatin channel. **g–i** Magnified view of the areas outlined by the green boxes in **a–c** showing ultrastructural details of a nucleolus. The yellow, green and magenta arrowheads point at the fibrillar center (FC), the dense fibrillar component (DFC) and the granular component (GC), respectively. Representative images from 5 (**a–i**) independent experiments are shown. **j** Line profile along the dashed line shown in **f**. **k** Line profile along the dashed line shown in **i**. Panels **a, b, d, e, g, h** are displayed with a white-to-black color table. All scale bars are corrected for the determined expansion factor. Scale bars, (**a–c**) 5 µm, (**d–f**) 250 nm, (**g–i**), 1 µm.

3.2.4. pan-ExM reveals mitotic cell ultrastructure

Labeling a mitotic U-2OS cell with α-tubulin antibody and SYTOX Green in addition to our NHS ester pan-staining, reveals the mitotic spindle with individual filaments resolved within microtubule bundles (**Fig. 4**). Interestingly, NHS ester pan-staining appears to boost signal from α-tubulin antibody labeling, when applied after. This suggests that NHS ester also labels primary amines on antibodies, offering additional signal amplification. Additionally, kinetochores, easily identifiable by their association to chromosomes and microtubule ends, become clearly visible by their bright NHS ester signal (**Fig. 4e, f**). Individual chromosomes are resolvable in the SYTOX Green channel revealing fine chromatin fibers extending from the chromosomes (**Fig. 4a**) which are consistent with the polymer brush-like architecture model of mitotic chromosomes [22]. Similar chromatin organization can be observed in the mitotic HeLa cell image shown in **Supplementary Fig. 9**. Another hallmark structure of cell division, the cleavage furrow, also

shows strong contrast in NHS ester pan-stained samples, revealing the clearly discernible midbody and the very dense matrix of the Flemming body (**Supplementary Fig. 10**).

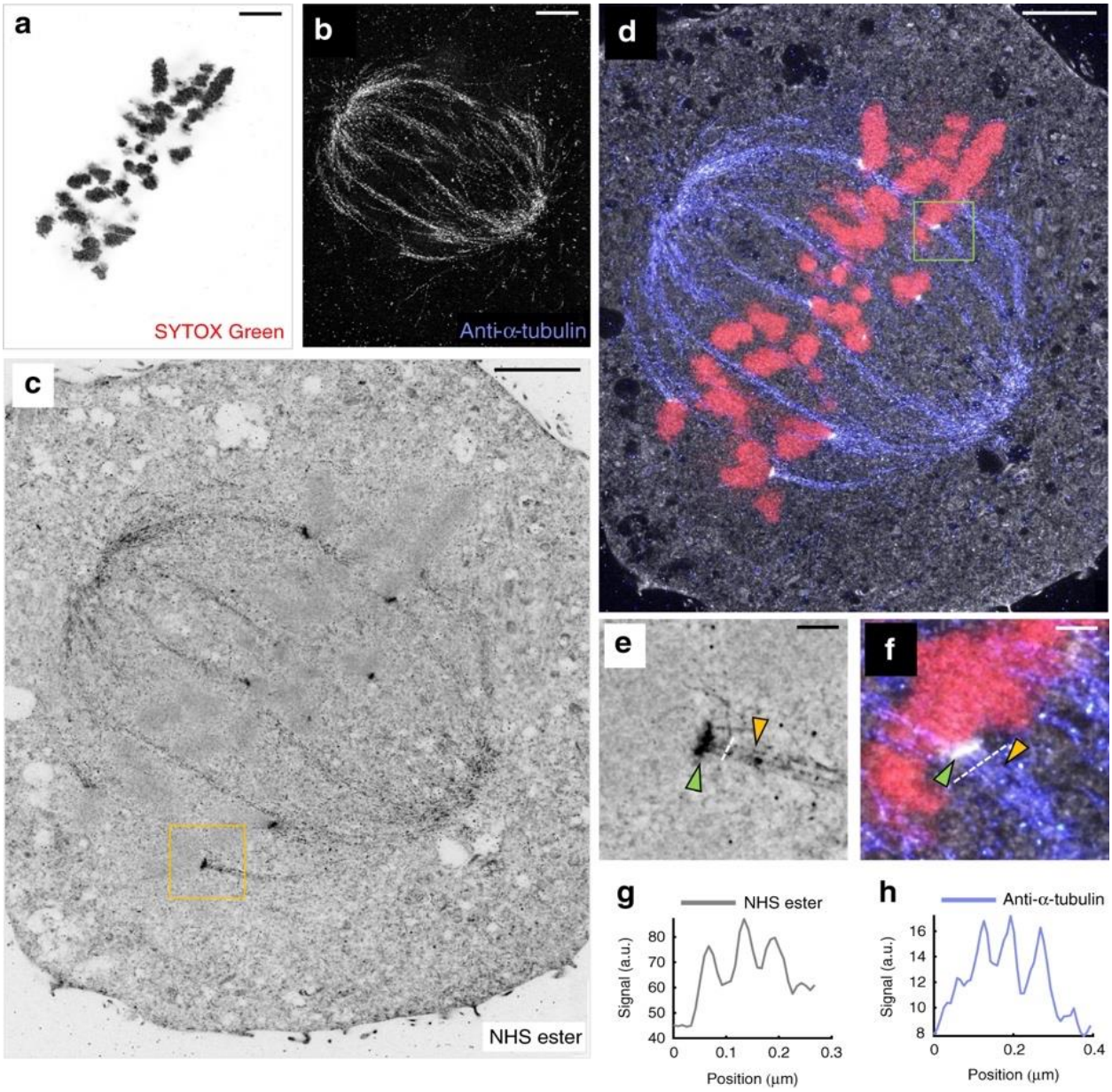

Figure 4: pan-ExM reveals mitotic cell ultrastructure. a SYTOX Green channel of a mitotic U-2OS cell revealing chromosomes. **b** Anti-α-tubulin immunostaining in the same area. **c** NHS ester pan-staining in the same area. **d** Overlay of **a–c. e** Magnified image of the area outlined by the yellow box in **c**. **f** Magnified image of the area outlined by the green box in d. The yellow arrowheads highlight individual microtubules within microtubule bundles, the green arrowheads point at kinetochores. Representative images from 3 (**a–f**) independent experiments. **g** Line profile along the dashed line shown in **e**. **h** Line profile along the dashed line shown in **f**. Panels **a, c, e** are displayed

with a white-to-black color table. Panel **b** is displayed with a black-to-white color table. All scale bars are corrected for the determined expansion factor. Scale bars, (**a–d**) 2 μm, (**e, f**) 300 nm.

3.2.5. Expansion factor and homogeneity

To determine the achieved linear expansion factors, we imaged SYTOX Green-stained HeLa cell nuclei in non-expanded samples and samples expanded using our standard protocol (see **Methods**) and compared the average nuclear cross-sectional area in both cases. On average, we obtained an expansion factor of 14.3 ± 0.9 (mean ± s.d.; N = 6 experiments; n = 21–58 nuclei per experiment; see **Methods** and **Supplementary Fig. 11b, c**). We next investigated the homogeneity of the expansion by imaging three different cellular structures, mitochondria, microtubules, and the nucleus, before and after expansion. Briefly, we registered the corresponding data sets with a similarity transform and then registered the similarity-corrected post-expansion image to the pre-expansion image with a B-spline non-rigid transform to detect local heterogeneities in expansion [6] (see **Methods**, **Supplementary Fig. 12**). Global expansion factors determined by this approach were 15.6 ± 0.3 (nuclei), 15.8 ± 0.7 (microtubules) and 17.1 ± 0.7 (mitochondria) (n = 5 fields of view, N = 1 sample, each; **Supplementary Fig. 11a**) and were largely in agreement with the value listed above. For structures 8–20 μm apart, we measured root-mean-square (RMS) errors of ~200–670 nm, corresponding to ~2.5–3.2% of the measurement length (**Fig. 2l**, **Supplementary Fig. 12**). The determined RMS error distributions are comparable to results published for other protease-free ExM methods [9][12]. To investigate if anisotropic stretching during sample handling contributes to these results, we replaced the similarity transform with an affine transform (**Supplementary Fig. 12**). The relative RMS errors dropped as a result to ~1.5–1.7% suggesting

that mechanical deformations from handling the sample are responsible for about half of the observed RMS error in the similarity transform data.

3.2.6. Validation of pan-ExM on the nanoscale

pan-ExM clearly can resolve ultrastructural features which are not accessible in conventional fluorescence microscopy. **Figure 5**, for example, shows two centrioles in human U-2OS cells, one in a lateral orientation (**Fig. 5a–c**) and one in an axial orientation (**Fig. 5d**). We observed that centrioles, which are massive protein complexes, are labeled very brightly by NHS ester pan-staining (**Supplementary Fig. 13**). Not only does pan-ExM reveal the dense hollow barrel geometry of the centriole but also its subdistal appendages, distal appendages, the nine-fold symmetry of microtubule triplets (**Supplementary Fig. 14**), and the pericentriolar material (PCM) surrounding the centrosome previously identified in EM data [23]. 3D image stacks of the centrosome (**Supplementary Movies 1** and **2**) also reveal the centriolar cartwheel structure and the procentrioles that associate with mature centrioles. When we immuno-labeled polyglutamylated tubulin, we observed that it labeled the centriolar wall on the central core (**Fig. 5c**) in agreement with previous reports [12][24]. Quantifying centriole roundness yielded a value of 0.91 ± 0.05 (mean ± s.d.; $n = 8$; **Supplementary Fig. 15a**), supporting the nanoscale isotropy of expansion.

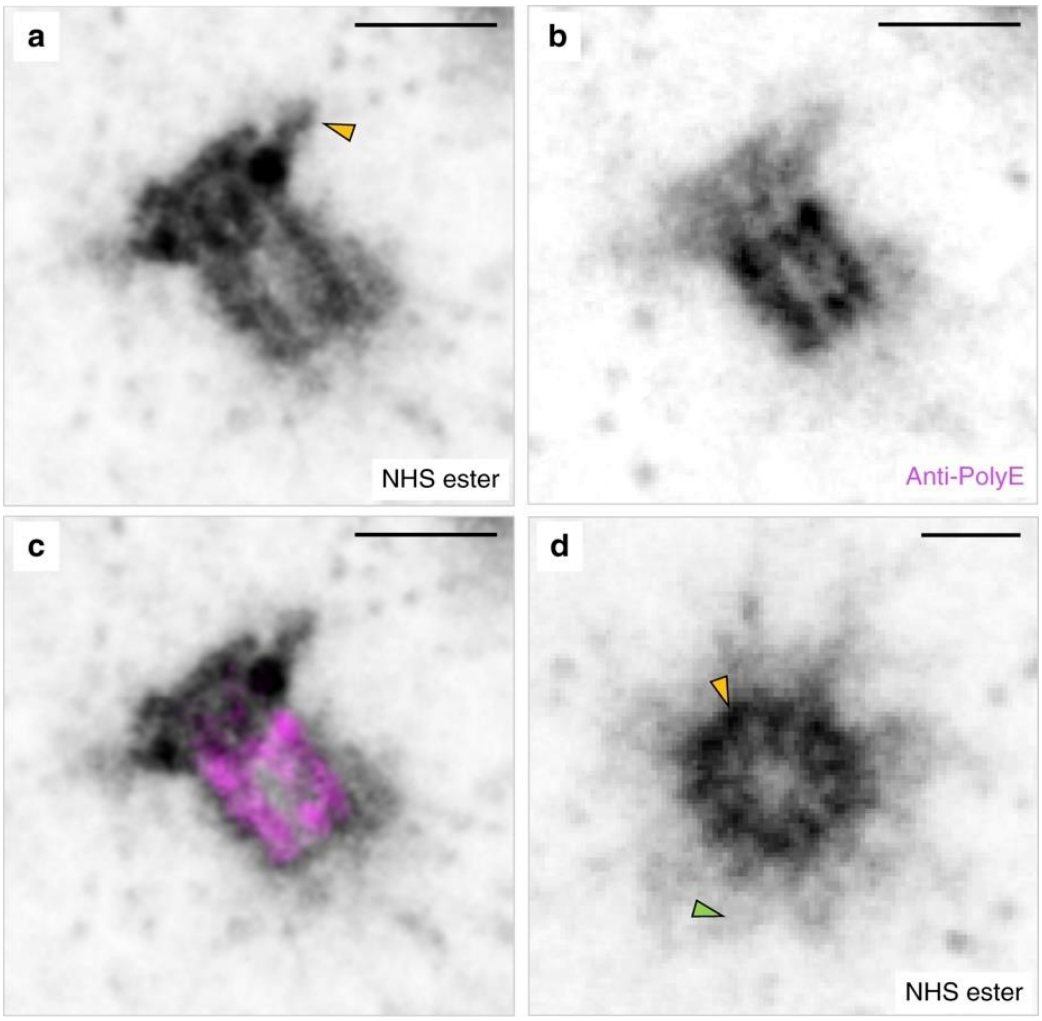

Figure 5: pan-ExM reveals ultrastructural details of centrosomes. a Lateral view of a NHS-ester pan-labeled mature centriole in a pan-ExM processed U-2OS cell revealing subdistal appendages (yellow arrowhead). **b** Anti-polyglutamate chain (PolyE) immunostaining in the same area revealing three distinct polyglutamylated microtubule triplets. **c** Overlay of **a** and **b**. **d** Axial view of a different NHS-ester pan-stained mature centriole revealing microtubule triplets (yellow arrowhead) and pericentriolar material (PCM) (green arrowhead). Representative images from 4 (**a, d**) and 1 (**b, c**) independent experiments. Panels **a, b, d** are displayed with white-to-black color tables. All scale bars are corrected for the determined expansion factor. Scale bars, (**a–c**) 200 nm, (**d**) 100 nm.

To further investigate structural preservation of features at the sub-organelle scale, we quantified the distance between mitochondrial cristae (**Fig. 6a, i**). The determined expansion-corrected distance of 85 ± 22 nm (mean ± s.d.) is in good agreement with previously published observations

in living HeLa cells [25]. We next investigated the preservation of the endoplasmic reticulum (ER) in HeLa cells. While the ER did not show a characteristic NHS-ester pan-staining that would make it directly identifiable, we could visualize it by overexpressing ER-membrane localized Sec61β-GFP and immunolabeling with an anti-GFP antibody (**Fig. 6b–e**), a strategy which we have previously employed successfully in optical super-resolution studies [1][26]. pan-ExM clearly resolves the two sides of ER tubules using a standard confocal microscope (**Fig. 6e**) as well as the inner and outer membrane of the nuclear envelope (**Supplementary Fig. 16**). The superior optical resolution of a STED super-resolution microscope applied to these samples reveals distinct clustering of the antibody staining (**Supplementary Fig. 17**). The expansion-corrected diameter of these tubules (47 ± 10 nm, mean ± s.d.; **Fig. 6j**) was slightly smaller than diameters determined previously by super-resolution light microscopy of non-expanded COS-7 cells [26] but consistent with diameters of ER tubules determined by EM [27]. Furthermore, we overexpressed the Golgi protein mannosidase II (ManII) fused to GFP in HeLa cells, labeled it with an anti-GFP antibody after applying our pan-ExM protocol and imaged it with a STED super-resolution microscope (**Fig. 6f–h**). It is known that ManII is located primarily in the medial cisternae of the Golgi and, when overexpressed, also in cis cisternae [1]. Consistent with this observation, we find the ManII stain to highlight 3 cisternae located at one side of the Golgi stack (**Fig. 6f–h**). The immunolabeled Golgi cisternae could be easily discerned by eye and overlaid well with similar structures visible in the NHS ester pan-channel. Quantifying the distance between neighboring Golgi cisternae (using conventional confocal data sets) yielded a value of 64 ± 16 nm (mean ± s.d.; n = 193; **Fig. 6k**), consistent with EM data [28].

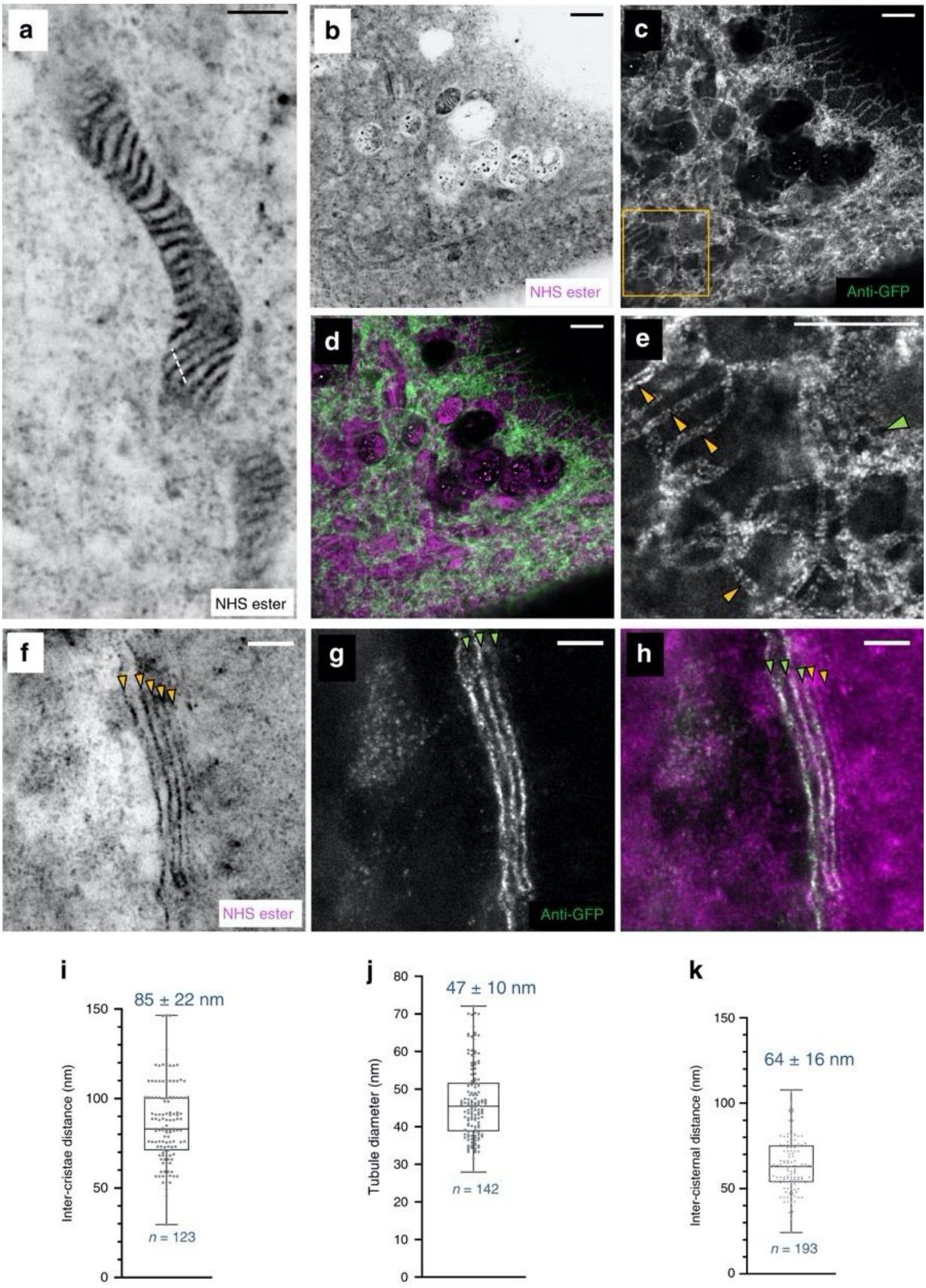
a
NHS ester
b
NHS ester
c
Anti-GFP
d
e
f
NHS ester
g
Anti-GFP
h
i
85 ± 22 nm
Inter-cristae distance (nm)
150
100
50
0
n = 123
j
47 ± 10 nm
Tubule diameter (nm)
80
70
60
50
40
30
20
10
0
n = 142
k
64 ± 16 nm
Inter-cisternal distance (nm)
150
100
50
0
n = 193

Figure 6: pan-ExM reveals ultrastructural details of cellular organelles. a NHS ester pan-stained mitochondrion in a NHS ester pan-stained HeLa cell. **b** NHS ester pan-stained HeLa cell expressing ER-membrane localized Sec61β-GFP. **c** Anti-GFP label in the same area revealing the ER. d Overlay of **a** and **b**. **e** Magnified image of the area outlined by the yellow box in **b**, revealing individual ER tubules clearly resolved as hollow tubules (yellow arrowheads) and a dense network of ER tubules (green arrowhead). **f** STED super-resolution image showing an NHS ester pan-stained Golgi stack in a ManII-GFP expressing HeLa cell. The yellow arrowheads show five distinct Golgi cisternae. **g** Anti-GFP STED image of the same area. The green arrowheads show three distinct Golgi cisternae. **h** Overlay of **f** and **g**. The green arrowheads point at ManII GFP-positive Golgi cisternae, the yellow ones at two ManII GFP-negative Golgi cisternae. Representative images from 11 (**a**), 2 (**b–e**), and 3 (**f–h**) independent experiments**. i** Distribution of distances between neighboring mitochondrial cristae (n = 123 line profiles, N = 4 independent experiments) calculated from cross-sections like those along the dashed line shown in **a**. **j** Distribution of ER tubule diameters (n = 142 cross-sections, N = 2 cells from 1 independent experiment). **k** Inter-cisternal distance distribution in Golgi stacks (n = 193 line profiles, N = 3 independent experiments). Medians and interquartile ranges are shown with whiskers drawn down to the minimum and maximum values. Means ± standard deviations are reported. Panels **a, b, f** are displayed with a white-to-black color table. Panels **c, e, g** are displayed with a black-to-white color table. All scale bars are corrected for the determined expansion factor. Scale bars, (**a**) 500 nm, (**b–e**) 1 µm, (**f–h**) 250 nm.

3.2.7. Polymer entanglement as a mechanism for pan-ExM expansion

We further tested if proteins indeed are retained throughout our sample preparation procedure. For this purpose, we compared fluorescence signal levels of antibodies applied without expansion and after one or two expansion steps. The quantification shows no decrease in signal (**Supplementary Fig. 18**), suggesting the good protein retention capabilities of our protocol. To further investigate the protein retention mechanism, we performed an additional experiment comparing structural preservation of centrioles using our standard protocol and one where we reduced possible Schiff base groups on proteins with sodium borohydride after denaturation [29]. Schiff bases are formed as a result of formaldehyde reacting with nucleophiles on proteins and they can react covalently with acrylamide monomers [30][31]. The denaturation step is located between the polymerization

of the first gel and the embedding in the second gel. Quenching reactive Schiff bases should therefore prevent crosslinking between the two gels. Additionally, we refrained from using the post-fixation step which is applied after the second gel embedding step of the standard protocol, further reducing possible crosslinking. **Supplementary Fig. 15** shows the quantification of centriole roundness and length/diameter ratios. Centriole roundness between the two conditions did not differ significantly ($p = 0.3$) and the observed small difference of 15% in the length/diameter ratio distributions was barely statistically relevant ($p = 0.047$). The lack of substantial quantitative differences between the two protocols is further supported by the visual similarity between overview pan-ExM images of HeLa cells expanded following the two different protocols (compare **Supplementary Fig. 19** with **Fig. 1c**). We conclude that while we cannot exclude a minor role of crosslinking between the gels, it does not play a major role and entanglement therefore seems to be the dominating mechanism responsible for the observed protein retention in pan-ExM.

3.2.8. pan-ExM is compatible with 3D imaging

Importantly, pan-ExM is fully compatible with 3D imaging, as demonstrated by the confocal 3D image stacks shown in **Fig. 7**, **Supplementary Fig. 20** and **Supplementary Movies 3–5**. The intricate structure of the convoluted Golgi ribbon and stacking of multiple cisternae is clearly revealed at all axial positions even with a conventional confocal microscope (**Fig. 7**; **Supplementary Fig. 21**). This organization has to our knowledge never before been resolved by conventional light microscopy.

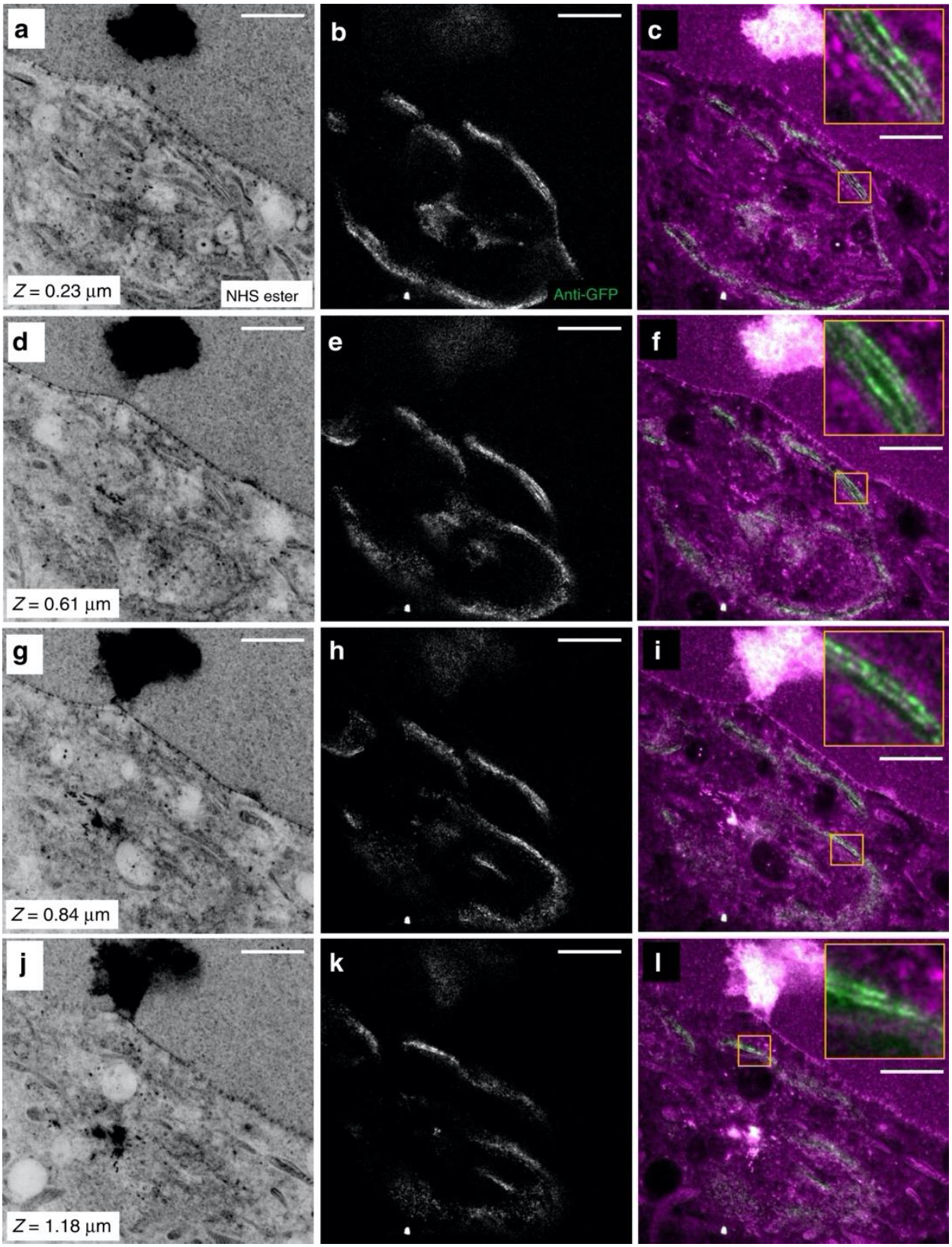
a
Z = 0.23 µm
NHS ester
b
Anti-GFP
c
d
Z = 0.61 µm
e
f
g
Z = 0.84 µm
h
i
j
Z = 1.18 µm
k
l

Figure 7: pan-ExM is compatible with 3D imaging. Images from a 3D image stack featuring the Golgi complex next to the nucleus in a HeLa cell expressing Golgi-localized ManII-GFP**. a, d, g, j** NHS ester images at axial positions 0.23, 0.61, 0.84 and 1.18 µm, respectively, displayed with a white-to-black color table. **b, e, h, k** Anti-GFP images of the same fields of view as **a, d, g, j** displayed with a black-to-white color table. **c, f, i, l** Overlay of the NHS ester and anti-GFP images. Representative images from 5 (**a–l**) independent experiments. The insets show the zoomed-in yellow boxes and reveal individual ManII-positive Golgi cisternae. Panels **b, e, h, k** were corrected for crosstalk (see Methods). Scale bar and axial positions are corrected for the determined expansion factor. Scale bars (**a–l**) 2 µm.

3.2.9. Differential pan-staining of proteins

One of the unique powers of pan-ExM is its capability to reveal the compartmentalization of biomolecule classes identifiable by a particular pan-staining such as NHS ester. Pan-stainings are, however, not restricted to NHS ester and other pan-stainings should show different distributions. For example, using metabolic incorporation of palmitic acid azide, one can use alkyne dyes to label palmitoylated proteins post-expansion (**Supplementary Fig. 4c**). Given that these proteins are insoluble in water, we expect an enriched staining in the vicinity of lipid membranes in the cell. Performing this experiment indeed produced a strong signal at the location of the plasma membrane and membrane-bound organelles (**Fig. 8**; **Supplementary Fig. 22**). Both labels are strongly enriched on structures resembling clathrin-coated pits (inset in **Fig. 8c**). The difference in the mitochondrial staining patterns between palmitate and NHS ester pan-stainings is particularly striking (**Fig. 8i**; **Supplementary Fig. 22f**). We note that this pattern is not visible in non-expanded cells pan-stained with the same labels (**Supplementary Fig. 22c**), emphasizing the role of molecular de-crowding in revealing the spatial compartmentalization of protein classes.

As another example of a pan-staining, we tested dye-conjugated maleimide (**Supplementary Fig. 4b**) which can reveal cellular domains with high cysteine-rich protein content. **Supplementary**

Figs. 23 and **24** show that the maleimide staining highlights in particular the Golgi complex, most likely due to the high levels of palmitoyltransferases in the Golgi which have cysteine-rich domains [32]. The combination with NHS ester labeling (**Fig. 1f** and **Supplementary Fig. 23**) shows intriguing patterns of differential staining which provide information well beyond the monochromatic, EM-like contrast achievable with a single pan-staining - analogous to Haemotoxylin and Eosin (H&E) staining but on the nanoscale.

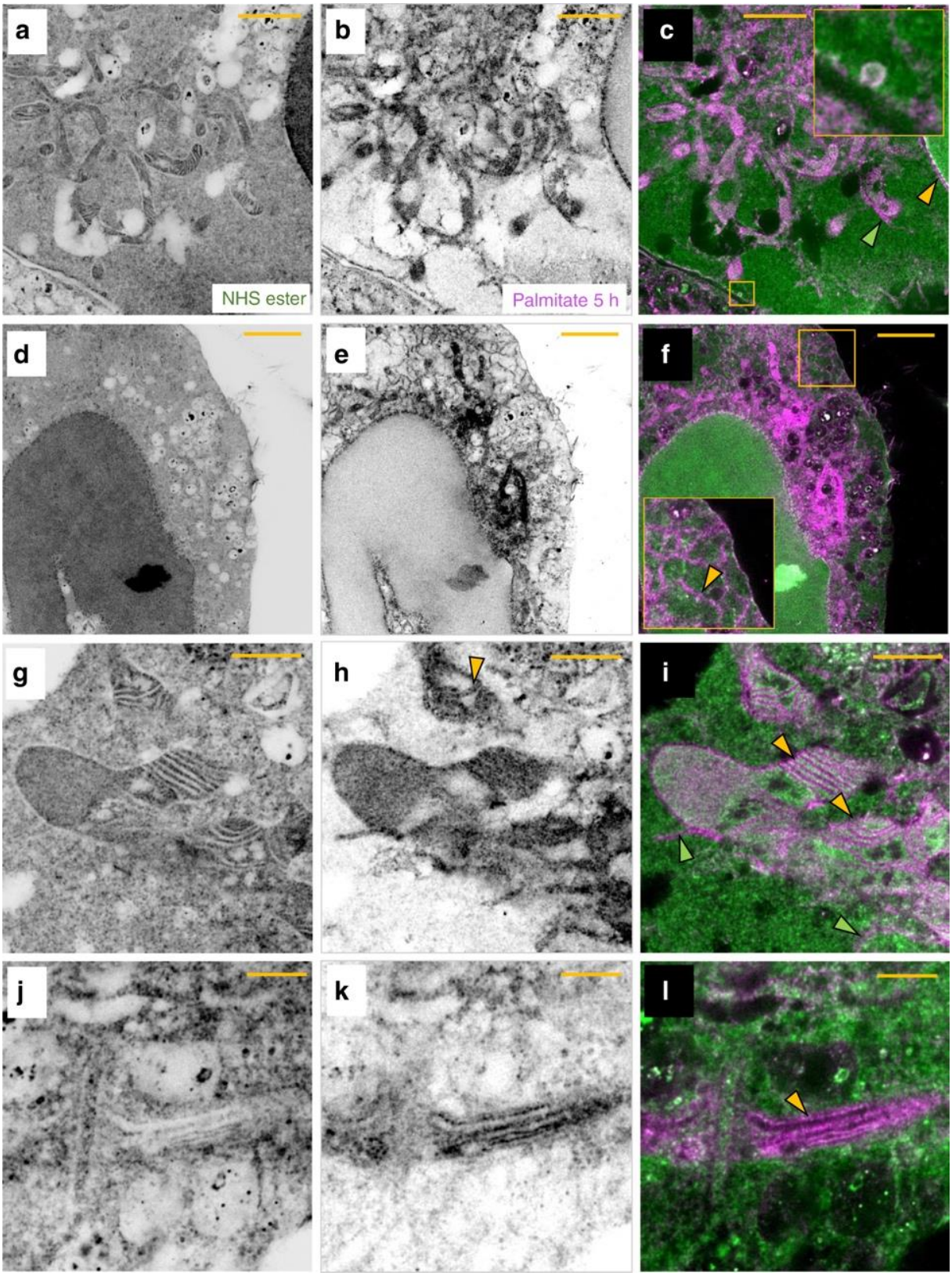
a
NHS ester
b
Palmitate 5 h
c
d
e
f
g
h
i
j
k
l

Figure 8: Differential pan-staining reveals compartmentalized palmitate distribution. a NHS ester pan-stained HeLa cell. **b** Palmitate pan-staining corresponding to the same area as shown in **a**. **c** Overlay of **a** and **b**. The area in the yellow box is shown in the inset and reveals a vesicular structure resembling a clathrin-coated pit. The yellow arrowhead points at the palmitate-rich nuclear envelope. The green arrowhead points at a tubular structure resembling an ER tubule near a mitochondrion. **d** NHS ester pan-stained HeLa cell. **e** Palmitate pan-staining corresponding to the same area as shown in **d**. **f** Overlay of **d** and **e**. The area in the yellow box is shown in the inset and reveals ER tubules (yellow arrowhead). **g** NHS ester pan-stained image of a HeLa cell showing mitochondria. **h** Palmitate pan-staining corresponding to the same area as shown in **g**. The yellow arrowhead points at a mitochondrial crista with two palmitate-rich membranes. **i** Overlay of **g** and **h**. The yellow arrowheads point at mitochondrial cristae and the green arrowheads point at tubule-like structures resembling ER tubules. **j** NHS ester pan-stained image of a HeLa cell showing a Golgi stack. **k** Palmitate pan-staining corresponding to the same area as shown in **j**. **l** Overlay of **j** and **k**. The yellow arrowhead points at a palmitate-rich Golgi cisterna. Representative images from 2 (**a–l**) independent experiments. Panels **a, b, d, e, g, h, j, k** are displayed with a white-to-black color table. Yellow scale bars are not corrected for the expansion factor. Scale bars, (**a–c**) 30 µm, (**d–f**) 50 µm, (**g–i**) 20 µm, (**j–l**) 10 µm.

3.3. Discussion

The data presented here demonstrates, from our perspective, pan-ExM's potential to revolutionize light microscopic imaging of cellular structures. pan-ExM combines, (i), 13 to 21-fold linear expansion (obtained through iterative expansion), and (ii), protein retention through direct anchoring of proteins to the first hydrogel and transfer of entrapped proteins to the final expansion hydrogel by polymer chain entanglement. While these individual techniques have demonstrated merit, we see their true power in their combination with labeling the whole proteome: staining the cell with NHS ester dyes shifts from a largely pointless exercise in a non-expanded cell (**Fig. 1a**) to a technique with EM-like contrast, capable of revealing nanoscopic structural hallmarks that allow users to identify organelles without the need for specific staining (**Fig. 1c**, **Supplementary Figs. 22, 23, 24**). While the obtained resolution does not reach the level of EM, its straightforward combination with single, or multiple, specific labels stands in stark contrast to the complex

protocols of immuno-gold EM or CLEM. Our sample preparation is completed in a few days; subsequent imaging takes less than a minute (2D image) to tens of minutes (3D data set; **Supplementary Movie 2**) per cell on a conventional light microscope. We anticipate that light-sheet microscopes or other instruments optimized for ExM [33] will accelerate future pan-ExM data acquisition substantially.

We have shown here, using anti-GFP, anti-α-tubulin, anti-PolyE and anti-TOM20 antibodies, that pan-ExM is compatible with immunolabeling. However, some antibodies we tested did not work as they were not compatible with glutaraldehyde fixation or protein denaturation. We anticipate that this caveat can be overcome in the future by (i) focusing on antibodies which have been shown to work well in western blots due to the commonality of the denaturing step and (ii) developing fixation protocols that preserve ultrastructure without compromising protein epitope integrity. We ruled out the possibility that base hydrolysis of DHEBA crosslinker, necessary for the dissolution of the first and second hydrogels, has a detrimental effect on antibody labeling efficiency. We incubated a once-expanded sample prepared with the non-hydrolyzable crosslinker N,N′-Methylenebisacrylamide (BIS) with sodium hydroxide for 1 h prior to antibody labeling and found no significant decrease in anti-α-tubulin and anti-TOM20 signal compared to a control sample. We also validated that the treatments used to cleave other commercially available crosslinkers (e.g., N,N′-Diallyltartramide (DATD) and N,N′-Bis(acryloyl)cystamine (BAC); **Supplementary Fig. 25**) do not decrease antibody labeling efficiency. These alternative crosslinkers could be used for additional rounds of expansion in the future.

Resolution can be best evaluated by the structures that can be resolved. The presented examples demonstrate that we consistently resolve structures that were only about 30–100 nm apart pre-expansion. The lateral resolution of the used confocal microscope is in the 250–300 nm resolution

range using a high-numerical aperture objective. Correcting this value by the measured expansion factors of ~13–21, suggests an effective expansion-corrected PSF size of 12–23 nm. Labeling samples post expansion, as usually done in our protocol, has the advantage that the label size plays essentially no role: a primary and secondary antibody pair spans at maximum a distance of 25 nm. Correcting the final image by the expansion factor shrinks this distance down to less than 2 nm. Overall, we therefore believe that it is safe to assume that the achievable lateral resolution of pan-ExM in combination with a high-end confocal microscope is in the 20–30 nm range. Combined with STED microscopy, this resolution can shrink by another factor of ~5 [26]. As shown in **Supplementary Fig. 26**, this increase in resolution allows, for example, to not only resolve individual cristae but to distinguish the two sides of a single crista with a light microscope. The practical limit on resolution is therefore currently not the optical resolution or the global expansion factor, but our limited understanding of the expansion factor on the molecular size scale. It remains to be investigated down to which size scale structures are preserved in pan-ExM. Based on our protocol, we expect that proteins lose their tertiary structure and unfold at least partially during the sample preparation process. At the tens-of-nanometer scale, our data shows that microtubules, centrioles, and membrane-bound organelles such as mitochondria, the Golgi complex and the ER are represented well after expansion. On the other extreme: lipid droplets, having a lipid core, are dissolved by the used detergents, leaving only a shadow image of their former shape. Future systematic studies, refinements to the protocols and engineered probes, such as cross-linkable lipid labels [34][35] and reversible protein crosslinking reagents, will answer these questions and promise further improvements.

On the positive side, pan-ExM leads to substantial molecular decrowding (~$163 \approx 4000$-fold by volume) of the sample. This effect is key to pan-ExM's success: the average distance of 3 nm

between proteins in the native cell becomes about 50 nm after expansion and the space in between proteins becomes easily accessible by probes even as large as antibodies (6–12 nm in size). Furthermore, the expansion protocol most likely disrupts protein clusters through denaturation, revealing previously inaccessible binding sites.

It is worth pointing out that, in contrast to optical super-resolution microscopy techniques which are ultimately limited in resolution by the size of the fluorescent labels, ExM is not constrained by label-size (if labeling is applied after expansion). Moreover, problems with labeling density which are a major limitation in optical super-resolution microscopy get alleviated: steric hindrance and fluorescence quenching in densely labeled samples become essentially irrelevant after 13- to 21-fold expansion. On the contrary, the created gaps between endogenous molecules provide space for potential biochemical amplification of the label [36], boosting the sensitivity of the technology.

The fact that many organelles can easily be identified by eye through their characteristic NHS ester stain suggests that pan-ExM is well-suited for automated segmentation and classification algorithms to identify organelles of interest. Training of machine learning algorithms can be facilitated by additional imaging channels showing specific stains of the target organelle, for example MitoTracker for mitochondria, during the learning phase.

The pan-staining approach can be easily generalized to many sub-proteomes. We have demonstrated NHS ester, maleimide, and palmitate pan-stainings in this work (**Supplementary Fig. 4**). Other options could include phosphorylated and glycosylated proteins. We believe that the combination of two or more of these pan-stainings has great potential for automated segmentation of organelles and other subcellular structures of interest, and can also reveal how different sub-proteomes are distributed in the cell. We emphasize that the success of our pan-staining approach fundamentally benefits from two key strengths: high levels of protein retention and molecular

decrowding provide access to large numbers of target sites; high levels of expansion offer the effective spatial resolution required to identify structures and their cellular context.

3.4. Methods

General comments

Please see **Supplementary Tables 1–3** for an overview of the reagents and materials used in this work.

Coverslip preparation

Before plating HeLa or U-2OS cells, 12-mm round glass coverslips (Electron Microscopy Sciences, catalog no. 72230-01) were cleaned in a sonic bath (Bronson) submerged in 1 M KOH (Macron Fine Chemicals; catalog no. 6984-04) for 15 min and then rinsed with MilliQ water three times. Glass was then sterilized with 100% ethanol, incubated with 5 μg/mL fibronectin (Sigma-Aldrich, catalog no. F1141) for 30 min, and rinsed with sterile phosphate-buffered saline (PBS; Gibco, catalog no. 10010023) before adding media and cells.

Cell culture

HeLa and U-2OS cells were grown in Dulbecco's modified Eagle medium (DMEM; Gibco, catalog no. 21063029), supplemented with 10% fetal bovine serum (FBS; Gibco, catalog no. 10438026), and 1% mL/L penicillin-streptomycin (Gibco, catalog no. 15140122) at 37 °C with 5% CO2. Cells were passaged twice to three times a week and used between passage number 2 and 20. Passaging was performed using 1× PBS and 0.05% Trypsin-EDTA (Gibco, catalog no.

25300054). Approximately 24 h before fixation, cells were seeded on fibronectin-coated glass coverslips at ~65,000 cells per well.

Plasmids

For labeling the medial Golgi in HeLa cells, GFP-ManII was expressed. GFP-ManII was made from pEGFP-N1 (Takara Bio Inc.) to include amino acids 1-137 of mouse MAN2A1 fused to GFP, such that GFP is expressed in the Golgi lumen. For labeling the ER membrane in HeLa cells, mEmerald-Sec61-C-18 was expressed. mEmerald-Sec61-C-18 was a gift from the late Michael Davidson (Florida State University, Tallahassee, FL; Addgene plasmid # 54249; referred to as GFP-Sec61β).

Transfection

GFP-ManII and GFP-Sec61β expression in HeLa cells used DNA transfection by electroporation1. DNA was introduced into the cells using a NEPA GENE electroporation device. Approximately 1 million cells were rinsed in Opti-MEM (Gibco, catalog no. 31985070) and then resuspended in Opti-MEM with 10 μg DNA in an electroporation cuvette with a 2-mm gap (Bulldog Bio, catalog no. 12358346). Cells were electroporated with a poring pulse of 125 V, 3-ms pulse length, 50-ms pulse interval, 2 pulses, with decay rate of 10% and + polarity; followed by a transfer pulse of 25 V, 50-ms pulse length, 50-ms pulse interval, 5 pulses, with a decay rate of 40% and ± polarity. After electroporation, the cells were seeded on fibronectin-coated coverslips (see **Coverslip preparation**). Samples were fixed 24–36 h after electroporation.

MitoTracker orange staining

Live HeLa cells were incubated with 0.5 μM of MitoTracker Orange CMTMRos (Invitrogen, catalog no. M7510) for 30 min at 37 °C and 5% CO2. Next, the cells were washed three times with cell media and fixed immediately after.

Cell fixation

Cells were fixed with 3% formaldehyde (FA) and 0.1% glutaraldehyde (GA) (Electron Microscopy Sciences, catalog nos. 15710 and 16019, respectively) in 1× PBS for 15 min at RT. Samples were rinsed three times with 1× PBS and processed according to the pan-ExM protocol immediately after.

pan-ExM reagents

Acrylamide (AAm; catalog no. A9099), N,N′-(1,2-dihydroxyethylene)bisacrylamide (DHEBA; catalog no. 294381), N,N′-Cystaminebisacrylamide (BAC; catalog no. 9809) were purchased from Sigma-Aldrich. Three different batches of sodium acrylate (SA) were used. The first batch (catalog no. 408220, lot no. MKCF0390) was purchased from Sigma-Aldrich. The second and third batches (catalog no. sc-236893C, lot nos. H3019 and L0619) were purchased from Santa Cruz Biotechnology. We noticed significant batch-to-batch variability in SA purity. To verify that SA was of acceptable purity, 38% (w/v) solutions were made in water and checked for quality [37]. Only solutions that were light yellow were used. Solutions that were yellow and/or had a precipitate were discarded. N,N′-methylenebis(acrylamide) (BIS; catalog no. J66710) was purchased from Alfa Aesar. Ammonium persulfate (APS; catalog no. AB00112), N,N,N′,N′-tetramethylethylenediamine (TEMED; catalog no. AB02020), tris [hyroxymethyl] aminomethane (Tris; catalog no. AB02000), and 20% sodium dodecyl sulfate solution in water (SDS; AB01922)

were purchased from American Bio. Sodium chloride (NaCl; catalog no. 3624-01) was purchased from J.T. Baker.

pan-ExM gelation chamber

The gelation chamber was constructed using a glass microscope slide (Sigma-Aldrich, catalog no. S8400) and two spacers, each consisting of a stack of two no. 1.5 22 × 22 mm coverslips (Fisher Scientific, catalog no. 12-541B), were glued with superglue to the microscope slide on both sides of the cell-adhered coverslip, with the cell-adhered coverslip glued in between. A no. 1.5 22 × 22 mm coverslip was used as a lid after adding the gel solution. This geometry yielded an initial gel thickness size of ~170 μm.

First round of expansion

HeLa and U-2OS cells, previously fixed as described in the **Cell fixation** section, were incubated in post-fix solution (0.7% FA + 1% AAm (w/v) in 1× PBS) for 6–7 h at 37 °C. Next, the cells were washed twice with 1× PBS for 10 min each on a rocking platform and embedded in the first expansion gel solution (19% (w/v) SA + 10% AAm (w/v) + 0.1% (w/v) DHEBA + 0.25% (v/v) TEMED + 0.25% (w/v) APS in 1× PBS). Gelation proceeded first for 15 min at room temperature (RT) and then 1.5 h at 37 °C in a humidified chamber. Coverslips with hydrogels were then incubated in ~1 mL denaturation buffer (200 mM SDS + 200 mM NaCl + 50 mM Tris in MilliQ water, pH 6.8) in 35 mm dishes for 15 min at RT. Gels were then transferred into denaturation buffer-filled 1.5 mL Eppendorf tubes and incubated at 73 °C for 1 h. Next, the gels were placed in petri dishes filled with MilliQ water for the first expansion. Water was exchanged at least twice every 1 h and then the gels were incubated overnight in MilliQ water. Gels expanded between 3.8× and 4.5× according to SA purity (see **Reagents**).

Re-embedding in neutral hydrogel

Expanded hydrogels were incubated in a fresh re-embedding neutral gel solution (10% (w/v) AAm + 0.05% (w/v) DHEBA + 0.05% (v/v) TEMED + 0.05% (w/v) APS in 1× PBS) three times for 20 min each on a rocking platform at RT. Immediately after, residual gel solution was removed by extensive but gentle pressing with Kimwipes. The gels were then sandwiched between two pieces of no. 1.5 coverslips and incubated at 37 °C for 1.5 h in a nitrogen-filled humidified chamber. Next, the gels were detached from the coverslip and washed three times with 1× PBS for 30 min each on a rocking platform at RT. Gels were incubated in post-fix solution (0.7% FA + 1% (w/v) AAm in 1× PBS) for 15 min at RT and then for 6–9 h at 37 °C. The gels were subsequently washed three times with 1× PBS for 30 min each on a rocking platform at RT.

Second round of expansion

Re-embedded hydrogels were incubated in a fresh second hydrogel gel solution (19% (w/v) SA + 10% AAm (w/v) + 0.1% (w/v) BIS + 0.05% (v/v) TEMED + 0.05% (w/v) APS in 1× PBS) four times for 15 min each on a rocking platform on ice. Immediately after, residual gel solution was removed by extensive but gentle pressing with Kimwipes. The gels were then sandwiched between two pieces of no. 1.5 coverslips and incubated at 37 °C for 2 h in a humidified nitrogen-filled chamber. To dissolve DHEBA, gels were incubated in 0.2 M NaOH for 1 h on a rocking platform at RT. Gels were next detached from the coverslip and washed three times with 1× PBS for 30 min each on a rocking platform at RT. Subsequently, the gels were labeled with antibodies and pan-stained with NHS ester dyes. Finally, the gels were placed in petri dishes filled with MilliQ water for the second expansion. Water was exchanged at least twice every 1 h at RT, and then the gels were incubated overnight in MilliQ water. Gels expanded between 3.8× and 4.0× according

to SA purity (see **Reagents**) for a final expansion factor of 13× to 20×. Note that for the ER images shown in **Fig. 6b–e**, the cleavable crosslinker BAC was used instead of BIS at a concentration of 0.1% (w/v).

Antibody labeling post-expansion

For microtubule samples, gels were incubated for 24 h with monoclonal mouse anti-α-tubulin antibody (DM1α; Sigma-Aldrich, catalog no. T6199) diluted to 1:250 in antibody dilution buffer (2% (w/v) BSA in 1× PBS). For mitochondria samples, gels were incubated for 24 h with rabbit anti-TOM20 antibody (Abcam, catalog no. ab78547) diluted to 1:250 in antibody dilution buffer. For centriole samples, gels were incubated for 24 h with rabbit polyclonal anti-polyglutamate chain (PolyE) antibody (Adipogen, catalog no. AG-25B-0030-C050) in antibody dilution buffer. For both Golgi and ER samples, gels were incubated for 36–40 h with polyclonal rabbit anti-GFP antibody (Invitrogen, catalog no. A11122) diluted to 1:250 in antibody dilution buffer. All primary antibody incubations were performed on a rocking platform at RT. Gels were then washed in PBS-T (0.1% (v/v) Tween 20 in 1× PBS) three times for 20 min each on a rocking platform at RT. Next, microtubule samples were incubated for 24 h with ATTO647N-conjugated anti-mouse antibodies (Sigma-Aldrich, catalog no. 50185) diluted to 1:250 in antibody dilution buffer, while mitochondria, ER, Golgi, and centriole samples were incubated for 24 h at RT with ATTO647N-conjugated anti-rabbit antibodies (Sigma-Aldrich, catalog no. 40839) diluted to 1:250 in antibody dilution buffer. All secondary antibody incubations were performed on a rocking platform at RT. The gels were subsequently washed in PBS-T three times for 20 min each, rinsed one time with 1× PBS, and stored in PBS at RT until subsequent treatments. Note that bovine serum albumin (BSA; catalog no. 001-000-162) was purchased from Jackson ImmunoResearch and Tween 20 (catalog no. P7949) was ordered from Sigma-Aldrich.

NHS ester pan-staining post-expansion

After antibody labeling, gels were incubated for 1.5 h with either 20 µg/mL NHS ester-ATTO594 (Sigma-Aldrich, catalog no. 08741), 20 µg/mL NHS ester-ATTO532 (Sigma-Aldrich, catalog no. 88793) or 200 µM NHS ester-DY634 (Dyomics, catalog no. 634-01 A), dissolved in 100 mM sodium bicarbonate solution (Sigma-Aldrich, catalog no. SLBX3650) on a rocking platform at RT. The gels were subsequently washed three to five times in either 1× PBS or PBS-T for 20 min each on a rocking platform at RT. Note that for the experiment where we compared HeLa cells expanded never, once, or twice (**Fig. 1**), the same concentration of NHS ester-ATTO594 and labeling conditions were used.

Palmitate pan-staining

Live 80%-confluent HeLa cells were incubated with 50 µM azide-functionalized palmitate (Thermofisher, catalog no. C10265) diluted in delipidated medium (DMEM + 10% charcoal-stripped FBS; Thermofisher, catalog no. A3382101) for 5 h at 37 °C and 5% CO2. Next, the cells were fixed with 3% FA + 0.1% GA in 1× PBS for 15 min at RT and processed according to pan-ExM protocols. Prior to NHS ester staining, CuAAC (Copper(I)-catalyzed Azide-Alkyne Cycloaddition) was performed using the Click-iT Protein Reaction Buffer Kit (Thermo Fisher, catalog no. C10276) according to manufacturer instructions. Alkyne-functionalized ATTO590 dye (Sigma-Aldrich, catalog no. 93990) was used at a concentration of 5 µM. After CuAAC, the gels were washed three times with 2% (w/v) delipidated BSA (Sigma Aldrich, catalog no. A4612) in 1× PBS for 20 min each on a rocking platform at RT.

Maleimide pan-staining post-expansion

pan-ExM processed gels were reduced with 50 mM Tris(2-carboxyethyl)phosphine hydrochloride solution (TCEP) (Sigma-Aldrich, catalog no. 646547) in 1× PBS for 30 min at RT and subsequently incubated for 1.5 h in an inert environment with 20 µg/mL maleimide-ATTO594 (Sigma-Aldrich, catalog no. 08717) dissolved in deoxygenated 150 mM Tris-Cl pH 7.4 solution. The gels were then washed three times in either 1× PBS or PBS-T for 20 min each on a rocking platform at RT.

SYTOX Green staining post-expansion

pan-ExM processed gels were incubated with SYTOX Green (Invitrogen, catalog no. S7020) diluted 1:3,000 in calcium- and magnesium-free HBSS buffer (Gibco, catalog no. 14170112) for 30 min on a rocking platform at RT. The gels were then washed three times with PBS-T for 20 min each on a rocking platform at RT.

pan-ExM sample mounting

After expansion, the gels were mounted on Poly-L-Lysine-coated glass-bottom dishes (35 mm; no. 1.5; MatTek). A clean 18-millimeter diameter Poly-L-Lysine-coated coverslip (Marienfeld, catalog no. 0117580) was put on top of the gels after draining excess water using Kimwipes. The samples were then sealed with a two-component silicone glue (Picodent Twinsil, Picodent, Wipperfürth, Germany). After the silicone mold hardened (typically 15–20 min), the samples were stored in the dark at RT until they were imaged. Note that gels imaged with an oil objective were incubated overnight in 30% glycerol (Teknova, catalog no. G1797) prior to mounting.

Image acquisition

Confocal and STED images were acquired using a Leica SP8 STED 3X equipped with a SuperK Extreme EXW-12 (NKT Photonics) pulsed white light laser as an excitation source and a Onefive Katana-08HP pulsed laser as depletion light source (775-nm wavelength). All images were acquired using either a HC PL APO 63×/1.2 water objective, HC PL APO 86×/1.2 water CS2 objective, HC PL APO 63×/1.40-0.60 oil objective, or a HC PL APO 100×/1.40 NA oil immersion CS2 objective. Application Suite X software (LAS X; Leica Microsystems) was used to control imaging parameters. ATTO532 was imaged with 532-nm excitation. ATTO594 was imaged with 585-nm excitation and 775-nm depletion wavelengths. ATTO647N was imaged with 647-nm excitation and 775-nm depletion wavelengths. DY634 was imaged with 634-nm excitation. SYTOX Green and MitoTracker Orange were excited by 488-nm and 555-nm excitation light, respectively.

Widefield images to measure protein retention were obtained with a Leica tissue culture microscope (DM IL LED FLUO) equipped with a 10×/0.22 NA air objective. An Andor Clara CCD camera operated by MicroManager was used to record images.

Protein retention assay

HeLa cells were transfected with either GFP-ManII or GFP-Sec61β and plated at 75,000 cells per 12-mm fibronectin-coated glass coverslip. Non-expanded cells from the same experiment were stored in 1× PBS at 4 °C after fixation and were permeabilized with 0.1% Triton X-100 (Sigma-Aldrich, catalog no. T8787) in 1× PBS prior to antibody labeling. All non-expanded, once- and twice-expanded samples were subjected to the same antibody labeling scheme described in Antibody labeling post-expansion. However, ATTO594-conjugated anti-rabbit antibodies (1:250; Sigma-Aldrich, catalog no. 77671) were used instead of ATTO647N-conjugated antibodies.

Additionally, samples were stained with SYTOX Green as described in SYTOX Green staining post-expansion. All samples were imaged in deionized water with a widefield Leica tissue culture microscope (DM IL LED FLUO) using a 10×/0.22 NA air objective (see **Image Acquisition**) and the same LED light intensity.

To measure protein retention in the first expansion step, we compared the total fluorescence signal (TFS) of ATTO594 between non-expanded and once expanded cells expressing GFP-Sec61β and immunolabeled against GFP. Since the ER spreads throughout the whole cytoplasm, TFS for these samples was quantified by measuring the total background-corrected mean fluorescence signal per field of view and dividing it by the number of cells in the field of view. Cells were counted based on the SYTOX Green nuclear staining using FIJI's 3D Objects counter. Cell numbers were manually corrected for nuclei which were so close that the automatic segmentation merged them into single objects (typically the case for 5–20% of the nuclei). Background levels were determined by averaging the signal determined in a manually selected area containing no cells. 5 fields of view containing between 419 and 653 cells each were analyzed for non-expanded samples; 10 fields of view containing 21–58 cells each were analyzed for samples expanded once.

Because signal-to-background levels dropped to values too low to provide reliable results using the described method for the ER staining in samples expanded twice, we chose a different approach using more localized labeling of the Golgi complex for these samples. To measure protein retention in the second expansion step, we compared the TFS of ATTO594 between once-expanded and twice-expanded cells expressing GFP-ManII and immunolabeled against GFP. TFS for these samples was quantified by multiplying the manually identified total area occupied by stained Golgi stacks in every cell with the background-corrected mean fluorescence signal in that area. Background levels were determined by averaging the signal determined in a manually selected

area within a cell containing no GFP-ManII signal. 60 cells in 10 fields of view were analyzed for samples expanded once and 67 cells in 45 fields of view were analyzed for samples expanded twice. For all measurements, TFS was corrected for the different camera exposure times used. Images were processed using FIJI/ImageJ software. Results are summarized in **Supplementary Fig. 18**.

Image processing

Images were visualized, smoothed, and contrast-adjusted using FIJI/ImageJ or Imspector software. STED and confocal images were smoothed for display with a 0.5 to 1-pixel sigma Gaussian blur. Minimum and maximum brightness were adjusted linearly for optimal contrast. The TOM20 data set (**Fig. 2d–f**) was corrected for bleedthrough of the NHS ester channel by subtracting a constant fraction of the latter from the former using Imspector. The confocal ManII (**Fig. 7**) and mitotic cell NHS ester (**Supplementary Fig. 9**) data sets were corrected for bleedthrough of the NHS ester and SYTOX Green channels respectively by subtracting a constant fraction of the latter from the former using the Image Expression Parser tool in FIJI.

Cristae and Golgi inter-cisternal distance measurements were performed using FIJI. 10-pixel thick line profiles were taken approximately perpendicular to the cristae and Golgi stack orientations and peak-to-peak distances were extracted from the profiles. For mitochondrial cristae, 123 line profiles were drawn from 4 independent experiments. For Golgi inter-cisternal distance measurements, 193 line profiles were drawn from 3 independent experiments. The diameter of ER tubules was determined in FIJI using the Point Tool by manually measuring two positions arranged perpendicular to the orientation of clearly discernible tubules and located at the crests of the signal denoting each side of the tubule. The Euclidean distance between them was used as a measure of

the ER tubule diameter. For this measurement, 142 ER tubule widths were extracted from 2 cells in 1 sample. Results are summarized in **Fig. 6i–k**.

All line profiles were extracted from the images using the Plot Profile tool in FIJI/ImageJ.

Expansion factor calculation

Images of HeLa cell nuclei in non-expanded and pan-ExM expanded samples stained with SYTOX Green (1:3,000) were acquired with a Leica SP8 STED 3X microscope using a HCX PL Fluotar 10×/0.30 dry objective. Average nuclear cross-sectional areas were determined using FIJI/ImageJ software. To calculate the expansion factor, the average nuclear cross-sectional area in pan-ExM samples was divided by the average nuclear cross-sectional area of non-expanded samples. The square root of this ratio represents an estimate of the linear expansion factor. Results are summarized in **Supplementary Fig. 11c**.

Expansion homogeneity calculation

To compare nuclei, mitochondria, and microtubules pre- and post-expansion, U-2OS cells were cultured as specified in Cell culture and live-labeled with MitoTracker Orange as described in **MitoTracker Orange staining**. After fixation with 3% FA + 0.1% GA in 1× PBS for 5 min at RT, cells were incubated in post-fix solution (0.7% FA + 1% (w/v) AAm in 1× PBS) for 7 h at 37 °C, permeabilized with 0.1% Triton X-100 in 1× PBS for 5 min on a rocking platform at RT, and labeled with a mouse monoclonal anti-α-tubulin antibody (MT antibody 1; Sigma-Aldrich, catalog no. T5168) diluted in cell antibody dilution buffer (1% (w/v) BSA + 0.2% TX-100 in 1× PBS) for 1 h on a rocking platform at RT. They were then washed three times with wash buffer (0.05% TX-100 in 1× PBS) for 5 min each, labeled with ATTO647N-conjugated anti-mouse antibodies (Sigma-Aldrich, catalog no. 50185) diluted to 1:1,000 in cell antibody dilution buffer for 1 h on a

rocking platform at RT, and stained with Hoechst (abcam, catalog no. ab228551) diluted to 1:10,000 in 1× PBS for 20 min on a rocking platform at RT. The samples were next washed three times with wash buffer for 5 min each and rinsed with 1× PBS.

Pre-expansion image stacks of nuclei (Hoechst), mitochondria (MitoTracker Orange), and microtubules (MT antibody 1) were acquired. The cells were then immediately processed with pan-ExM protocol. For post-expansion microtubule labeling, gels were labeled with a different mouse monoclonal anti-α-tubulin antibody (MT antibody 2; Sigma-Aldrich, catalog no. T6199) diluted 1:250 in antibody dilution buffer (2% (w/v) BSA in 1× PBS) for 6 h at 37 °C and 6 h on a rocking platform at RT, washed three times with PBS-T for 20 min each, and labeled with the same ATTO647N-conjugated anti-mouse antibodies as above. Gels were then stained with SYTOX Green dye diluted 1:3,000 in calcium- and magnesium-free HBSS buffer for 45 min on a rocking platform at RT, washed three times with PBS-T for 30 min each at 37 °C, and expanded in MilliQ water as described above. Post-expansion image stacks of nuclei (SYTOX Green), mitochondria (MitoTracker Orange), and microtubules (MT antibody 2) were acquired. Maximum projection images of corresponding pre- and post-expansion image stacks were generated with the FIJI/ImageJ z projection tool. Additionally, post-expansion images of mitochondria and microtubules were despeckled and masks were created manually to exclude regions of no features for microtubule samples.

To determine spatial sample distortion, post-expansion images were smoothed with a 2-pixel Gaussian blur and first registered to the pre-expansion image of the same field of view with either a similarity transform (uniform scaling, rotation, and translation) or an affine transform (scaling, shear, rotation, and translation). FIJI TurboReg plugin was used for this initial registration. The similarity- and affine-registered post-expansion images were registered again to the pre-expansion

images with a B-spline-based non-rigid registration package in Matlab **[8]**. The similarity measure (error) was set to squared pixel distance and the penalty of registration was set to 1e-1 (nuclei images) or 1e-2 (mitochondria and microtubule images). Using the deformation vector field from the output B-spline transformation parameters, the root mean square (RMS) error of expansion was calculated across different distance measurements. The deformation field was applied to the coordinates of either a binary outline of the pre-expansion image (nuclei images) or its binary skeleton (mitochondria and microtubule images). The distance between every two pairs of points in the pre-expansion image binary image (d_i) and the corresponding deformed coordinates (d_def) were calculated. The RMS error is the absolute difference of these distance measurements (RMS = abs(d_def - d_i)). RMS error was calculated for every combination of points across distances of 20 μm (nuclei images), 10 μm (mitochondria images), and 8 μm (microtubule images). For nuclei, 5 cells in 5 fields of view were analyzed. For mitochondria, 14 fields of view in 5 cells were analyzed. For microtubules, 5 fields of view in 4 cells were analyzed. Results are summarized in **Supplementary Fig. 12**.

To quantify the expansion factor of nuclei, mitochondria, and microtubules. Similarity-registered post-expansion images and the corresponding pre-expansion images were cropped using four manually-identified landmark features in both images. To determine the expansion factor, the area of the cropped post-expansion image was divided by the area of the cropped pre-expansion image. The square root of this ratio represents the linear expansion factor. Results are summarized in **Supplementary Fig. 11**.

pan-ExM modified protocol

To test whether the mechanism of the second expansion is primarily polymer entanglement or chemical crosslinking between the sample and the final expansion hydrogel, a modified pan-ExM protocol was developed. After denaturation (Step 3, **Supplementary Fig. 1**), possible reactive Schiff base groups on proteins that may react covalently with acrylamide monomers were quenched by incubating the gels in 0.1% sodium borohydride (Sigma-Aldrich, catalog no. 452882) in 1× PBS for 7 min at RT followed by an incubation with 100 mM glycine (Sigma-Aldrich, catalog no. G8898) in 1× PBS for 10 min at RT. Additionally, the second post-fixation step (Step 7, **Supplementary Fig. 1**) was omitted to prevent crosslinking of the sample to the second expansion hydrogel. The remaining steps are identical to the original protocol.

Centriole roundness quantification

Image stacks of PolyE-labeled U-2OS mature centrioles were acquired by confocal microscopy and axial-view centriole image stacks were selected for quantification. Volume Viewer plugin in FIJI was used to align image stacks that were not perfectly axial. Manually selected images of the distal region were smoothed with a 1-pixel Gaussian blur and converted to binary using automatic thresholding in FIJI. Using the shape descriptor tool in FIJI, centriole roundness was measured for both post-fixed centrioles (standard protocol; n = 7 centrioles) and quenched/no post-fix centrioles (pan-ExM modified protocol; n = 8 centrioles). Results are summarized in **Supplementary Fig. 15**.

Centriole length-to-width calculation

Image stacks of PolyE-labeled and NHS ester pan-stained mature centrioles were acquired by confocal microscopy and lateral view image stacks were selected for quantification. Similarly as above, Volume Viewer plugin in FIJI was used to align image stacks that were not perfectly lateral.

To compare the length-to-width ratio of centrioles, 5-pixel thick line profiles of NHS ester pan-staining along the length of the centrioles were drawn to measure centriolar length, and 5-pixel thick line profiles of PolyE staining along the width of the centriole were drawn to measure centriolar width. The peak-to-peak distances were extracted from these profiles and the ratio is the centriole length-to-width ratio12. This ratio was measured for both post-fixed centrioles (standard protocol; n = 17 centrioles) and quenched/no post-fix centrioles (pan-ExM modified protocol; n = 22 centrioles). Results are summarized in **Supplementary Fig. 15**.

Measurement of antibody labeling efficiency

To test whether the treatments required to dissolve several common cleavable crosslinkers (**Supplementary Fig. 27**) play a role in reducing post-expansion antibody labeling efficiency, four U-2OS cell samples live-labeled with MitoTracker Orange as described in MitoTracker Orange staining were expanded once (Steps 1–5, **Supplementary Fig. 1**) using a hydrogel prepared with 0.1% (w/v) BIS (instead of 0.1% (w/v) DHEBA). After the denaturation step (Step 4, **Supplementary Fig. 1**), one gel was expanded (CTRL) right after. The second gel was treated with 0.2 M NaOH for 1 h at RT (Treatment 1) and then expanded. The third gel was treated with 25 mM sodium periodate (Sigma-Aldrich, catalog no. 311448) diluted in 100 mM sodium acetate buffer (Sigma-Aldrich, catalog no. S7899), adjusted to pH 6.0, for 1 h at RT (Treatment 2) and then expanded. Finally, the fourth gel was treated with 0.25 M TCEP diluted in 1 M Tris-Cl buffer, adjusted to pH 7.5, for 18 h at RT (Treatment 3) and then expanded. Note that we verified that Treatment 1 can dissolve a gel composed of 19% (w/v) SA + 10% (w/v) AAm + 0.1% (w/v) DHEBA + 0.25% (w/v) APS + 0.25% (v/v) TEMED in 1 h at RT; Treatment 2 can dissolve a gel composed of 19% (w/v) SA + 10% (w/v) AAm + 0.2% (w/v) DATD + 0.25% (w/v) APS + 0.25% (v/v) TEMED in 1 h at RT; and Treatment 3 can dissolve a gel composed of 19% (w/v) SA + 10%

(w/v) AAm + 0.1% (w/v) BAC + 0.25% (w/v) APS + 0.25% (v/v) TEMED in 18 h at RT. After expansion, all four gels were immunolabeled with both a mouse monoclonal anti-α-tubulin antibody (1:500; Sigma-Aldrich, catalog no. T5168) and a rabbit polyclonal anti-TOM20 antibody (1:500; Abcam, catalog no. ab78547) diluted in antibody dilution buffer (2% (w/v) BSA in 1× PBS) for 12 h on a rocking platform at RT. The gels were washed three times with PBS-T for 20 min each and then immunolabeled with both ATTO647N-conjugated anti-mouse antibodies (1:500; Sigma-Aldrich, catalog no. 50185) and ATTO594-conjugated anti-rabbit antibodies (1:500, Sigma-Aldrich, catalog no. 77671) diluted in antibody dilution buffer for 6 h on a rocking platform at RT. The gels were washed with PBS-T for 20 min each on a rocking platform at RT and expanded again in MilliQ water to the final expansion factor of ~4.5. 3-color images of microtubules (anti-α-tubulin) and mitochondria (MitoTracker Orange and anti-TOM20) were acquired for each condition.

To measure TOM20 signal, background-corrected total fluorescence signal was calculated for each ROI containing mitochondria. This value was divided by the area occupied by mitochondria as calculated from the area of a mask generated from the corresponding MitoTracker Orange signal. Between 23 to 29 fields of view were quantified in 5 cells for every condition. To measure α-tubulin signal, line profiles of microtubules were drawn from the images using the Plot Profile tool in FIJI/ImageJ and the background-corrected peak value was extracted. Between 104 and 123 profiles were drawn in 5 cells for every condition. Results are summarized in **Supplementary Fig. 25**.

Statistics and reproducibility

For all quantitative experiments, the number of samples and independent reproductions are listed in the figure legends. An unpaired two-tailed t-test in Graphpad Prism 8 was used to analyze the data presented in **Supplementary Figs. 15**, **18** and **25**.

Data availability

The datasets generated and/or analyzed during the current study are available from the corresponding author on reasonable request.

Acknowledgements

We would like to thank Dr. James Rothman and Dr. Andreas Ernst for fruitful discussions. We are grateful to Dr. Lena Schroeder for her guidance on fluorescent staining methods, to Phylicia Kidd for providing cultured cells, and to Zach Marin and Dr. Kenny Chung for comments on the manuscript. This work was supported by grants from the Wellcome Trust (203285/B/16/Z) and NIH (P30 DK045735, S10 OD020142). During the revision phase of this manuscript, two papers were independently published that demonstrated the use of NHS ester stainings in non-expanded and once expanded tissue and cell samples further emphasizing the general utility of pan-stainings [38][39].

Contributions

O.M. developed the concept and sample preparation protocols and prepared the samples. O.M. and J.B. performed the imaging experiments and analyzed the data. J.B. provided guidance on the project. O.M. and J.B. wrote the manuscript.

Corresponding author

Correspondence to Joerg Bewersdorf.

Competing interests

J.B. has financial interests in Bruker Corp. and Hamamatsu Photonics. Both authors filed a patent application with the U.S. patent office covering the presented method (62989158).

4. pan-Expansion Microscopy of Neurons and Thick Brain Tissue

The work contained in this section is being prepared for publication in *Neuron*. It is titled:

M'Saad, O., Kasula, R., Kondratiuk, I., Kidd, P., Falahati, H., Gentile, J.E., Niescier, R., Watters, K., Sterner, R.C., Lee, S., Liu, X., De Camilli, P., Koleske, A.J., Rothman, J.E., Biederer, T. & Bewersdorf, J. All-optical visualization of specific molecules in the ultrastructural context of brain tissue (2021).

I am the first author of this manuscript. My contributions include the development and validation of the pan-ExM-t method. Culturing of dissociated neurons and perfusion of mouse brains were performed by collaborators.

Highlights

- pan-ExM-t visualizes proteins in the context of synaptic ultrastructure
- Lipid labeling in pan-ExM-t reveals organellar and cellular membranes
- All-optical, easily accessible alternative to correlative light/electron microscopy
- High potential for high throughput connectomics studies

Summary

Understanding the molecular anatomy and neural connectivity of the brain requires imaging technologies that can map the 3D nanoscale distribution of specific proteins in the context of brain

ultrastructure. Light and electron microscopy enable visualization of either specific labels or anatomical ultrastructure but combining molecular specificity with anatomical context is challenging. pan-Expansion Microscopy of tissue (pan-ExM-t) generates both contrast modalities with a standard confocal light microscope by combining ~24-fold linear expansion of biological samples with immunolabeling for specific protein imaging and pan-staining of protein densities for ultrastructural context. Here, we present pan-ExM-t, a protocol developed for mouse brain tissue. We demonstrate the versatility of this approach in neurobiological research by imaging established markers Homer1, Bassoon, PSD-95, Synaptophysin, GFAP, MBP and anti-GFP antibodies in dissociated neuron cultures and mouse brain sections. pan-ExM-t reveals these markers in the context of ultrastructural features such as pre and postsynaptic densities, 3D nanoarchitecture of neuropil, and the fine structures of cellular organelles. pan-ExM-t is adoptable in any neurobiological laboratory with access to a confocal laser scanning microscope and has therefore broad applicability in the research community.

4.1. Introduction

Three-dimensional microscopy techniques are instrumental to our understanding of brain organization with its complex morphology, spanning from the sub-synapse scale to neural circuitry maps. Despite significant advances in imaging, no microscopy method can provide a detailed molecular topography of the synapse [40]. While electron microscopy (EM) is the gold standard for ultrastructural analysis, localizing specific proteins still relies on immunogold labeling or electron-dense peroxidase substrates, neither of which are reliable nor quantitative [41]. Fluorescence microscopy, on the other hand, enables highly specific, multicolor labeling of proteins of interest. However, it fails to reveal the underlying ultrastructural context. Even with

the advent of super-resolution microscopy, where single molecules can be imaged in 3D with spatial resolutions down to ~10 nm [1], delineating context is unattainable: fluorescent dyes are comparatively bulky (~1 nm) and susceptible to quenching when densely packed, hindering imaging of crowded biomolecules [3][4]. To align specific molecular markers with sample ultrastructure, the only option currently is correlative light electron microscopy (CLEM) [5]. However, because of its hefty price tag and operational complexity, especially in 3D imaging, only a handful of research institutions worldwide have access to it. Not surprisingly, no study to date has correlated 3D images of synaptic proteins to sub-synaptic ultrastructural compartments.

We recently discovered a new principle for an optical contrast equivalent to EM heavy-metal stains, which allows for ultrastructural analysis using conventional light microscopy [42]. By physically expanding a biological sample ~20-fold in every dimension, bulk staining of proteins can now reveal the totality of subcellular compartments down to size scales of ~15 nm. We call this approach pan-ExM, referencing the philosophy of labeling the whole (Greek: pan) and the original concept of sample expansion in Expansion Microscopy (ExM) [6]. The 20^3=8,000-fold volume expansion decrowds the cellular environment and thereby overcomes the permeability, quenching, and sampling limitations associated with bulk staining of conventional samples. In our previous work, we showed how this approach allows for conventional light microscopes to acquire EM-like images of adherent monolayer cells, revealing subcellular features such as mitochondria cristae and Golgi cisternae by their anatomical characteristics [42].

The expansion mechanism in pan-ExM differs from other ExM approaches in that the sample expands ~20-fold while proteins are retained in the hydrogel for subsequent staining. To achieve this, pan-ExM avoids protease digestion and instead uses polymer entanglement [13] (as opposed to iterative labeling [10]) to expand sample components twice without losing them: by embedding

an already expanded sample prepared with a cleavable crosslinker in a second dense superabsorbent hydrogel, entanglements between polymer chains of the first and final hydrogels can physically interlock protein-polymer hybrids in this latter polymer network, thereby preserving the proteome while iteratively expanding it. The conceptual advance in pan-staining of highly expanded samples takes light microscopy to the realm of ultrastructural context imaging. In combination with well-established labeling methods in fluorescence microscopy, pan-staining provides nanoscale context to proteins of interest, analog to CLEM.

Here, we introduce pan-ExM-t, a pan-ExM protocol that enables contextual imaging of thick mouse brain tissue sections. Analogous to EM, we discovered that hallmark ultrastructural features such as pre- and postsynaptic densities can be identified by their morphological characteristics, allowing, for the first-time, ultrastructural imaging of putative synapses by light microscopy without specific labels. The developments we present in this paper will give every neurobiologist the power to perform routine 3D pan-ExM-t imaging of brain tissue sections using their standard confocal microscope.

Figure 9 shows an overview of our novel brain-tissue pan-ExM-t protocol. In brief, mice are transcardially perfused with fixative containing both formaldehyde (FA) and acrylamide (AAm) and their brains are extracted surgically and incubated in the same fixative overnight at 4°C. The brains are then sectioned at 50-100 µm thickness using a vibratome and stored in PBS until future use (**Fig. 9a**). Each tissue section to be expanded is embedded in a dense poly(acrylamide/sodium acrylate) co-polymer that is cross-linked with N,N′-(1,2-dihydroxyethylene)bisacrylamide (DHEBA), an acrylamide crosslinker with a cleavable amidomethylol bond (**Fig. 9b**). After polymerization, the now tissue-hydrogel hybrid is denatured with sodium dodecyl sulfate (SDS) in heated buffer (pH 6.8) for 4 hours (**Fig. 9c**) and expanded ~5-fold in deionized water (**Fig. 9d**,

blue). Next, a specific region of interest (ROI, ~8x8 mm2) is cut and re-embedded first in a neutral polyacrylamide hydrogel cross-linked with DHEBA (**Fig. 9d**, green) and then in a poly(acrylamide/sodium acrylate) co-polymer cross-linked with N,N′-methylenebis(acrylamide) (BIS), a non-hydrolysable acrylamide crosslinker (**Fig. 9d**, orange). The sample is then incubated in 200 mM sodium hydroxide to cleave DHEBA so that the crosslinked first and second hydrogel polymer networks are disentangled. After neutralization with multiple PBS washing steps, the sample is labeled with antibodies, pan-stained with fluorescent dyes, washed with detergents, and expanded to its final size (~24-fold) in ultrapure water (**Fig. 9e**). The sample is finally imaged on a standard confocal microscope (**Fig. 9f**) and can be stored at 4°C for months. As we previously demonstrated [42], no secondary fixation of proteins before the second re-embedding is required.

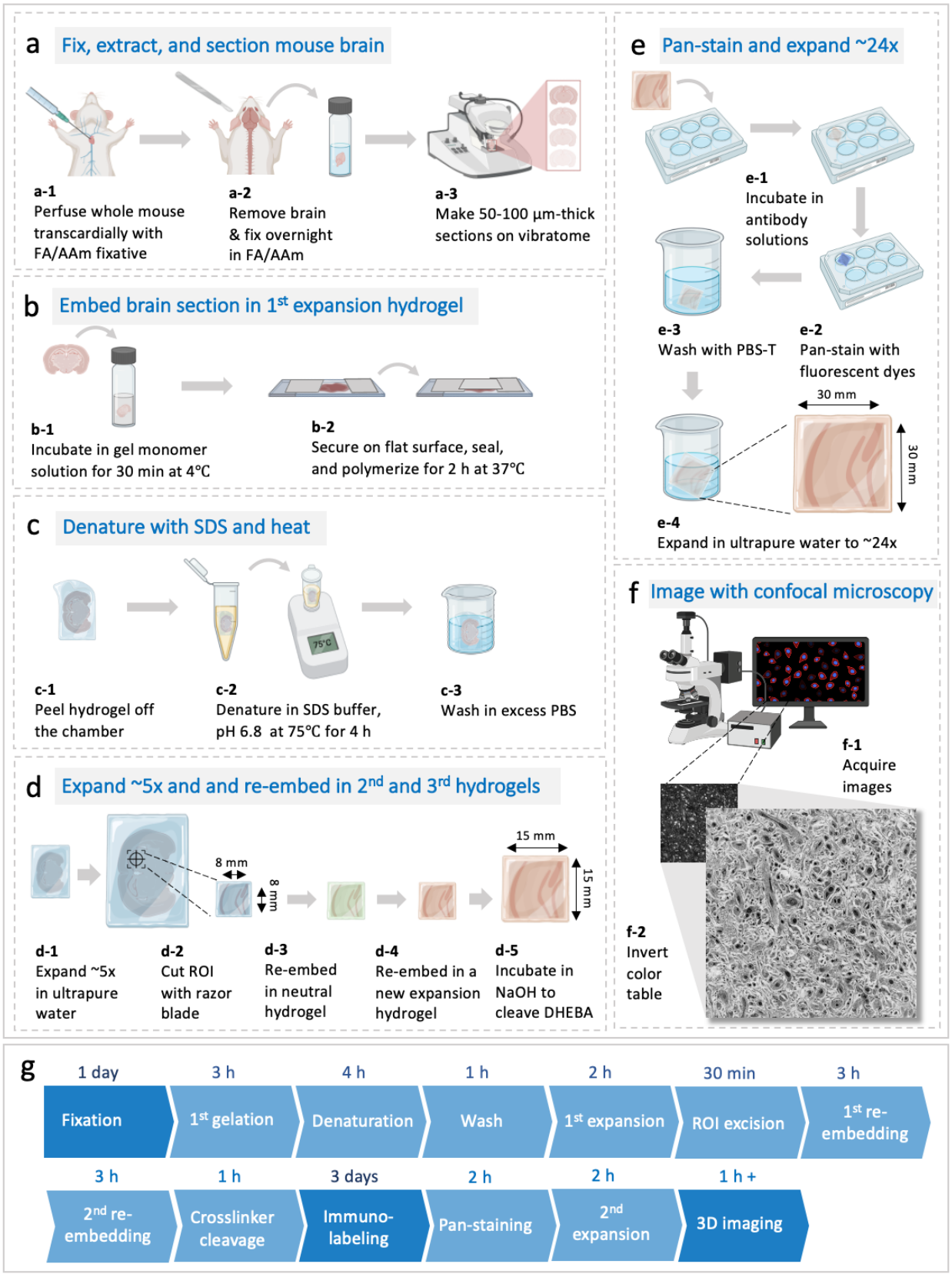
a Fix, extract, and section mouse brain
a-1
Perfuse whole mouse transcardially with FA/AAm fixative
a-2
Remove brain & fix overnight in FA/AAm
a-3
Make 50-100 µm-thick sections on vibratome
b Embed brain section in 1st expansion hydrogel
b-1
Incubate in gel monomer solution for 30 min at 4°C
b-2
Secure on flat surface, seal, and polymerize for 2 h at 37°C
c Denature with SDS and heat
75°C
c-1
Peel hydrogel off the chamber
c-2
Denature in SDS buffer, pH 6.8 at 75°C for 4 h
c-3
Wash in excess PBS
d Expand ~5x and and re-embed in 2nd and 3rd hydrogels
8 mm
8 mm
15 mm
15 mm
d-1
Expand ~5x in ultrapure water
d-2
Cut ROI with razor blade
d-3
Re-embed in neutral hydrogel
d-4
Re-embed in a new expansion hydrogel
d-5
Incubate in NaOH to cleave DHEBA
e Pan-stain and expand ~24x
e-1
Incubate in antibody solutions
e-2
Pan-stain with fluorescent dyes
e-3
Wash with PBS-T
30 mm
30 mm
e-4
Expand in ultrapure water to ~24x
f Image with confocal microscopy
f-1
Acquire images
f-2
Invert color table
g
1 day
Fixation
3 h
1st gelation
4 h
Denaturation
1 h
Wash
2 h
1st expansion
30 min
ROI excision
3 h
1st re-embedding
3 h
2nd re-embedding
1 h
Crosslinker cleavage
3 days
Immuno-labeling
2 h
Pan-staining
2 h
2nd expansion
1 h +
3D imaging

Figure 9: pan-ExM-t workflow for mouse brain tissue sections. (**a-f**) Experimental workflow. (g): Timeline summarizing the protocol. Abbreviations: FA: formaldehyde; AAm: acrylamide; NaOH: sodium hydroxide; DHEBA: N,N'-(1,2-dihydroxyethylene)bis-acrylamide; SDS: sodium dodecyl sulfate; PBS-T: 0.1% (v/v) TX-100 in PBS; ROI: region of interest.

4.2. Results

4.2.1. pan-ExM reveals synapse ultrastructure in dissociated neurons

Before experimenting with expanding mouse brain tissue sections, we tested pan-ExM in dissociated hippocampal rat and mice neurons using our published protocol with modifications in sample fixation (see **Methods**). We sought to test whether pan-ExM in neurons would reveal ultrastructural details previously too crowded or small to be efficiently resolved with conventional microscopy. A visual comparison of NHS ester bulk amine pan-staining of neurons that are non-expanded (**Fig. 10a**) or expanded with pan-ExM, (**Fig. 10d-k**, **Supplementary Videos 1 and 2**), confirms the validity of this approach: non-expanded synapses show essentially uniform staining, revealing little information, whereas expanding neurons ~16-fold allows to spatially resolve synapses by their protein density patterns. Analogous to phosphotungstic acid- (PTA-) staining of neurons in EM **(Fig. 10l**) [61], now resolvable hallmark features such as dense projections (DP) of the presynaptic bouton (**Fig. 10m**, lime arrow) and the postsynaptic density (**Fig. 10m**, salmon arrow) allow for the identification of synapses by their morphological characteristics. We see spines that are cupboard shaped **(Fig. 10h,j**), thin (**Fig. 10g,k**), and stubby (**Fig. 10f**). Strikingly, we also observe triagonal protein-dense patterns formed by presynaptic DPs (**Fig. 10e**), a discovery made using freeze-etched replica EM in 1972 [66]. A gallery of synapses imaged with pan-ExM is shown in **Supplementary Figure 1**.

To determine the achieved linear expansion factors, we imaged SYTOX Green-stained neuron nuclei in non-expanded samples and samples expanded using our standard protocol and compared the average nuclear cross-sectional area in both cases. On average, we obtained an expansion factor of 15.7 ± 0.3 (mean ± s.d.; $N = 4$ experiments; $n = 6–13$ nuclei per experiment). Dividing the measured distances between dense projections (DP) and the postsynaptic density (PSD) by the expansion factor determined from nuclei measurements, we obtained a value of 81.9 ± 25.8 nm (mean ± s.d.; $N = 4$ experiments; $n = 44$ synaptic profiles; **Fig. 10n**), which is consistent with the range of pre- and post-synaptic density distance measurements determined previously by super-resolution microscopy and electron tomography [60][62][63][64][65]. Similarly, dividing the distance between neighboring DPs by the nuclear expansion factor, we obtained a value of 67.2 ± 15.4 nm (mean ± s.d.; $N = 6$ experiments; $n = 78$ DP profiles; **Fig. 10o**), consistent with earlier reports in EM [64][67]. In all subsequent experiments, we used the DP-PSD distance as a metric for linear expansion factor calculation.

pan-ExM in dissociated neurons is compatible with immunofluorescence labeling as well as other established chemical stainings, enabling correlative studies which combine specific and contextual pan-staining approaches. Focusing on the synapse, **Figure 10t-ccc** shows the distributions of synaptic proteins Bassoon, Homer1, PSD-95, and Synaptophysin in the context of synaptic ultrastructure. We observe compartmentalization of active zone protein Bassoon into distinct puncta as dense projections (**Fig. 10t-bb**) with synaptic vesicle protein Synaptophysin intercalating in between neighboring dense projections (**Fig. 10xx-ccc**), supporting the model that DPs represent distinct sites for synaptic vesicle docking and fusion at the active zone. We also observe nanoclustering of postsynaptic density proteins Homer1 and PSD-95 along an otherwise macular and dense PSD, with Homer1 slightly offsetting the PSD further into the spine (**Fig. 10cc-**

hh,q) and PSD-95 concentrating directly over the PSD (**Fig. 10ll-qq,r**), consistent with previous work [212]. The expansion-corrected distributions of Bassoon, Homer1, and PSD-95 within the axial DP-PSD distances are all in agreement with previously published studies [60][62]. For instance, the distance between Bassoon and the PSD is 103.7 ± 24.4 nm (mean ± s.d.; $N = 3$ independent samples; $n = 50$ synaptic profiles; **Fig. 10p**); the distance between Homer1 and the DP is 82.86 ± 15.8 nm (mean ± s.d.; $N = 4$ independent samples; $n = 85$ synaptic profiles; **Fig. 10q**); and the distance between PSD-95 and the DP is 68.4 ± 11.0 nm (mean ± s.d.; $N = 2$ independent samples; $n = 25$ synaptic profiles; **Fig. 10r**). **Figure 10s** shows a plot of the positions of Bassoon, Homer1, and PSD-95 along the trans-synaptic axis defined as the center position between DP and PSD.

Double immunostainings are compatible with pan-ExM. **Figure 10rr-ww and Supplementary Video 3** show Bassoon-Homer1 immunofluorescence images at super-resolution and in their synaptic context. A gallery of images showing distributions of synaptic proteins Bassoon, Homer1, and PSD-95 is shown in **Supplementary Figs. 2-5**. This richness of information is inaccessible with conventional confocal microscopy of unexpanded or only ~5-fold expanded samples (**Supplementary Fig. 6**).

Optimizing antibody labeling parameters to achieve efficient and background-free staining is critical for pan-ExM imaging. Because the hydrogels used in pan-ExM are entangled and dense (~30% w/v monomer concentration), we suspect that many antibodies can become entrapped within this hydrogel matrix when used in high concentrations, often producing a granular background (**Supplementary Fig. 7b**). We found, for example, that lowering the concentrations of both Homer1 primary and dye-conjugated secondary antibodies from ~4 μg/mL to ~2 μg/mL strongly reduced the background without compromising signal levels (**Supplementary Fig. 7j**).

pan-ExM can clearly resolve subcellular structures in dissociated neurons that were previously inaccessible with standard confocal microscopy. **Figure 10ddd-fff** shows mtDNA inside a mitochondrion with visible cristae, **Fig. 10ggg-hhh** shows the hollow, circular structure of a nuclear pore complex, and **Fig. 10iii-jjj** reveals the cartwheel structure of basal bodies, their distal appendages, and the ciliary tip of a cilium. Furthermore, by combining NHS ester pan-staining with metabolic incorporation of palmitic acid azide, it becomes possible to examine the contact sites of membranous organelles, such as the tubules of the endoplasmic reticulum (ER) and mitochondria (**Supplementary Fig. 8**). A gallery of subcellular neuronal features is shown in **Supplementary Figs. 9-10**.

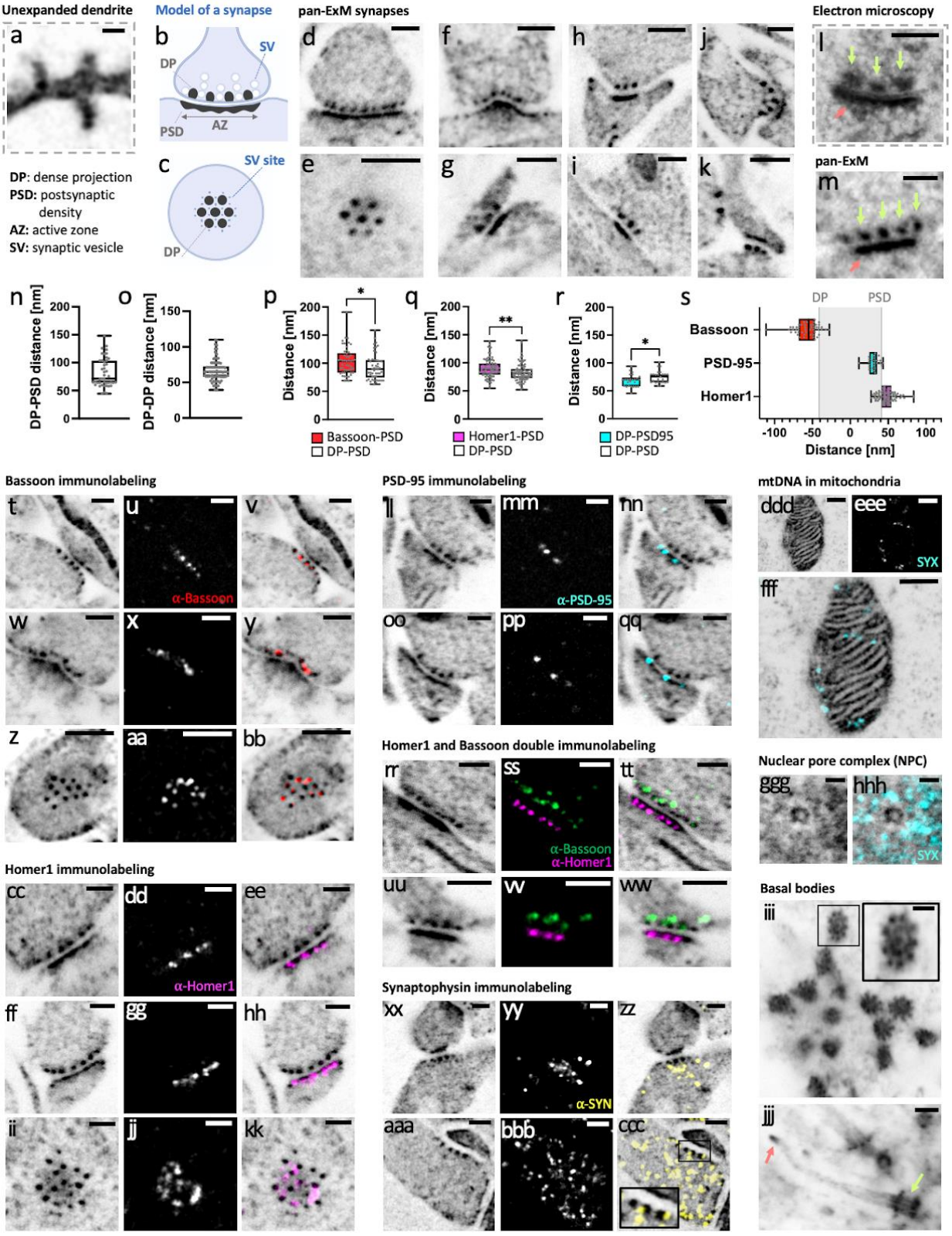

Figure 10: pan-ExM reveals synapse ultrastructure in dissociated neurons. a, NHS ester pan-stained dendrite in a non-expanded sample showing dendritic spines. **b**, axial view model of a synapse showing dense projections (DPs)

and synaptic vesicles (SVs) in the presynaptic bouton, and the postsynaptic density (PSD), and the active zone (AZ) in the postsynaptic dendritic spine. **c**, top view of a synapse showing hexagonal dense projections (DPs) in the presynaptic bouton and synaptic vesicle (SV) attachment sites. **d, f-k**, pan-ExM processed and NHS ester pan-stained spines including cupboard (**h**, **j**), stubby (**f**), and thin (**k**) shapes. **e**, NHS ester pan-stained synapse showing hexagonally arranged DPs. **l**, transmission EM (TEM) image of a phosphotungstic acid (PTA) stained synapse showing prominent DPs (lime arrows) and a PSD (salmon arrow). **m**, pan-ExM processed and NHS ester pan-stained synapse for comparison, showing similar hallmark ultrastructural features. **n**, DP-PSD distances (n = 44 measurements from 4 independent experiments). **o**, DP-DP distances (n = 78 measurements from 6 independent experiments). **p**, Comparison of Bassoon-PSD and DP-PSD distances (n = 50 measurements from 3 independent samples). **q**, Comparison of Homer1-PSD and DP-PSD distances (n = 85 measurements from 4 independent samples). **r**, Comparison of PSD95-DP and DP-PSD distances (n = 25 measurements from 2 independent samples). *: $p<0.05$; **: $p<0.01$. **s**, Relative spatial distributions of Bassoon, PSD-95, and Homer1 along the trans-synaptic axis. **t**, **w**, **z**, axial (**t**, **w**) and top (**z**) views of synapses pan-stained with NHS ester. **u**, **x**, **aa**, Bassoon immunolabeling of the same areas. **v**, **y**, **bb**, respective overlays. **cc-kk**, **ll-qq**, **rr-ww**, and **xx-ccc**, same as **t-bb** in samples labeled for Homer1, labeled for PSD-95, double-labeled for Homer1 and Bassoon, and labeled for Synaptophysin (SYN), respectively. The inset in **ccc** shows SYN puncta, representing synaptic vesicles, intercalated between neighboring DPs. **ddd**, NHS ester image of a mitochondrion in a hippocampal rat neuron. **eee**, SYTOX Green (SYX) staining of the same area. **fff**, overlay. **ggg**, NHS ester image of a nuclear pore complex (NPC). **hhh**, overlay of **ggg** with a SYTOX Green image of the same area. **iii**, NHS ester image of basal bodies in a mouse neuron. The inset shows the familiar centriolar cartwheel structure. **jjj**, NHS ester image of a cilium in a mouse neuron. Lime and salmon arrows point to the basal body and ciliary tip, respectively. Gamma corrections: (**d**, **e**) γ=0.8; (**h**, **j**, **k**, **m**, **cc**, **ll**, **oo**, **rr**, **uu**, **xx**, **aaa**, **iii**, **jjj**) γ=0.7; (**i**) γ=0.6. **jjj** is a z-projection (intensity average) of 5 images. All scale bars are corrected for the expansion factor. Scale bars, (**a**) 800 nm, (**d-m**, **t-ccc**, **jjj**) 200 nm, (**ddd-fff**) 300 nm, (**ggg, hhh**) 50 nm, (**iii**) 100 nm

4.2.2. pan-ExM-t reveals tissue ultrastructural features

Having established pan-ExM in dissociated neuron cultures, we adapted our technique to 70 µm-thick mouse brain tissue sections. Because of stark differences in thickness, lipid content, and presence of a highly connected extracellular matrix in tissue that is absent in dissociated neurons, brain fixation, sample denaturation, and antibody labeling parameters had to be optimized.

Ultrastructural analysis of brain tissue sections in EM has typically relied on formaldehyde (FA) and glutaraldehyde (GA) fixation to best preserve fine structures [122][124]. Because pan-ExM is an ultrastructural imaging method, structural preservation at the 10-nm scale is of utmost importance [42]. However, compatibility with immunolabeling is equally important to the core concept of our technique, and antigens are known to be masked by glutaraldehyde fixation [123]. To examine the effects of fixation and post-fixation on tissue preservation, we expanded 70 µm-thick mouse brain tissue sections that were fixed with 4% FA and not post-fixed (*Fix-1*), fixed with 4% FA and post-fixed with 0.7% FA + 1% acrylamide (AAm) (*Fix-2*), fixed with 4% FA and post-fixed with 4% FA + 20% AAm (*Fix-3*), fixed with 4% FA + 0.1% GA and post-fixed with 4% FA + 20% AAm (*Fix-4*), and fixed with 4% FA and post-treated with 0.1 mg/mL acryloyl-X SE (AcX) (*Fix-5*). **Supplementary Figs. 11-12** show that tissue treated with *Fix-1* has no distinguishable structural features beyond the outline of cell nuclei, suggesting little protein retention; tissue treated with *Fix-2* expands 18.5 ± 1.3-fold (mean ± s.d.; N = 6 fields of view; n = 38 synaptic profiles, **Supplementary Fig. 12p**) and shows resolved synapses and cell bodies, but no distinguishable neurites; tissue treated with *Fix-3* expands 16.0 ± 1.0-fold (mean ± s.d.; N = 9 fields of view; n = 81 synaptic profiles) and shows distinguishable neurites, but many detached cell bodies; tissue treated with *Fix-4* expands 11.6 ± 1.1-fold (mean ± s.d.; N = 8 fields of view; n = 77 synaptic profiles) and exhibits adequate neuropil and cell body preservation, and finally; tissue treated with *Fix-5* expands 11.8 ± 1.9-fold (mean ± s.d.; N = 9 fields of view; n = 74 synaptic profiles) and shows poor cell body preservation and multiple artifactual gaps in neuropil. These results suggest that the expansion factor increases with lower post-fixation strength and decreases with the addition of GA in the fixative. They also suggest that using AcX, a common

acryloylated and amine-reactive reagent in ExM [8], results in lower expansion factors as well as multiple artifacts in tissue ultrastructure when coupled with nonenzymatic homogenization.

Moreover, to examine tissue preservation further, we determined the extracellular space and lipid membrane (ECS+) fraction of neuropil across the different fixation schemes presented. The ECS fraction in live organotypic brain slices, determined by STED microscopy, ranges from 5% to 36% [125]. We therefore expect the ECS+ fraction to be within that range or higher by ~10% to account for unlabeled lipid membrane boundaries. **Supplementary Fig. 13** shows that indeed lowering the strength of the post-fixative (*Fix-2*) or using AcX (*Fix-5*) result in large ECS gaps (ECS+>60%) that are likely artifactual, while using stronger post-fixatives (*Fix-3* and *Fix-4*) result in an ECS+ fraction within an acceptable range (~30%). It is worth noting that in EM of chemically fixed tissue, the ECS fraction is notoriously underestimated because of tissue shrinkage from excessive fixation (ECS shrinkage is ~6 fold), giving the false notion that neurites are tightly apposed to one another [213][214].

We conclude based on our assessment of fixation effects on ultrastructural preservation in expanded brain tissue that strong post-fixation with FA and AAm (*Fix-3* and *Fix-4*) is necessary for good neuropil and ECS preservation. However, these still cause artifactual gaps in neuropil, and in the case of FA+GA-fixed tissue, result in a low expansion factor of ~11 fold. Therefore, we hypothesized that excessive interprotein crosslinking occurs in the initial fixation stage and predicted that transcardial perfusion with both FA and AAm along with post-fixation in the same fixative would result in a more uniform expansion. Inspired by CLARITY [68] and MAP [9] where FA is combined with acrylamide to simultaneously quench inter-protein crosslinking and functionalize proteins with an AAm group, we used 4% FA + 20% AAm in both the transcardial perfusion and overnight post-fixation solutions (*Fix-6*). We obtained an expansion factor of

24.1± 1.4-fold (mean ± s.d.; N = 10 fields of view from 3 independent experiments; n = 254 synaptic profiles, **Fig. 11i**; **Supplementary Fig. 12p**) as well as good neuropil preservation, very little artifactual tissue perforations (**Fig. 11a-c; Supplementary Figs. 11-12**), and an acceptable ECS+ fraction of ~38% (**Fig. 11j-l**; **Supplementary Fig. 13**). We therefore decided to use this fixation strategy for all subsequent experiments.

In the process of optimizing protein denaturation conditions, we found that increasing the denaturation temperature above 90 °C or using alkaline buffers resulted in hydrogel disintegration, possibly because of the lability of the DHEBA crosslinker molecule [126]. We therefore adopted the pH 6.8 SDS buffer of pan-ExM and used 75 °C as the temperature for denaturation, similar to 73 °C used in the original protocol [42]. We also found that tissue-hydrogel hybrids denatured for 4 h were macroscopically flat, while gels denatured for fewer than 4 h exhibited crumbled macrostructures, signifying incomplete mechanical homogenization. We therefore assessed denaturation times of 4 h (*Denat-4*), 6 h (*Denat-6*), and 8 h (*Denat-8*) for both expansion factor and relative protein retention (measured by reporting peak DP intensity). We found that *Denat-4* results in an expansion factor of 26.9 ± 1.2 (mean ± s.d.; N = 3 fields of view; n = 50 synaptic profiles, **Supplementary Fig. 14j**) and DP peak intensity of 1506.8 ± 243.8 (mean ± s.d.; N = 3 fields of view; n = 50 intensity measurements, **Supplementary Fig. 14k**), *Denat-6* yields a similar expansion factor of 26.0 ± 1.3 (mean ± s.d.; N = 3 fields of view; n = 42 synaptic profiles) and slightly lower DP peak intensity of 1353.3 ± 248.3 (mean ± s.d.; N = 3 fields of view; n = 42 intensity measurements), and finally Denat-8 shows an increase in expansion factor to 33.7 ± 1.6 (mean ± s.d.; N = 3 fields of view; n = 100 synaptic profiles) and partial protein loss with DP peak intensity of 1014.3 ± 209.1 (mean ± s.d.; N = 2 fields of view; n = 48 intensity measurements). Since we prioritize protein retention and argue that expansion factors of ~24 fold are sufficient to

resolve ultrastructural features of interest, we denatured our samples for 4 h at 75 °C in all subsequent experiments.

Equipped with a pan-ExM-t protocol that preserves ultrastructure well and allows for ~24-fold linear expansion, we imaged a wide variety of tissue nanostructures across both hippocampal and cortical regions of the mouse brain. Figure 3a shows a tiled ~1x1 mm2 image (corresponding to ~42x42 µm2 after correction for the expansion factor) of NHS ester pan-stained cortical tissue at synaptic resolution. Hallmark synaptic features such as pre- and postsynaptic densities can now be imaged and with a standard confocal microscope deep inside a brain tissue section (**Fig. 11d-h**; **Supplementary Figs. 15-17**; **Supplementary Videos 4 and 5**). For example, we could observe that putative excitatory synapses, defined by a prominent PSD (**Fig. 11m-cc**), often featured mitochondria in the vicinity of axonal boutons (**Fig. 11n, arrow**) and sometimes in the postsynaptic partner (**Fig. 11o**, arrow). Intriguingly, we can discern densely stained stacked structures in some postsynaptic compartments, suggestive of spine apparatuses (**Fig. 11dd-ii**) [215]. Moreover, the obtained resolution allowed us to classify synapses based on variations in PSD patterns and NHS ester pan-staining intensity into three classes inspired by the previously established [215][216][217][218] Gray classification of synapses: Class 1, where the PSD is dense and macular (**Fig. 11jj**); Class 2, where the PSD is dense and perforated (**Fig. 11kk**); and Class 3, where the PSD is barely visible (**Fig. 11ll**). Furthermore, pan-ExM-t images clearly reveal the spine neck (**Fig. 11q**, arrow) and multisynaptic boutons (**Fig. 11mm-vv**).

Next to synapses, centrioles in the perikarya are distinguished by a bright NHS ester pan-staining showing clear distal appendages (**Fig. 11ww**) and, in top views, the cartwheel structure (**Fig. 11xx**) and nine-fold symmetry (**Fig. 11zz**). The nine-fold symmetry is also visible in multiciliated ependymal epithelia lining the lateral ventricles of the mouse brain (**Fig. 13l**, **Supplementary**

Video 6, **Supplementary Fig. 18**). Moreover, we also observe that mitochondria morphologies vary strongly across neuropil (**Fig. 11zz-ooo**), some featuring clearly resolvable lamellar cristae, and shapes ranging from vesicular to teardrops with tubular extensions (**Fig. 11mmm-ooo**, arrows) reported to correlate with disease and synaptic performance [219][220]. A closer look at brain capillaries (**Fig. 11ooo, Supplementary Fig. 19**) reveals clearly discernible endothelial cells, tight junctions, pericytes, and the basement membrane [218].

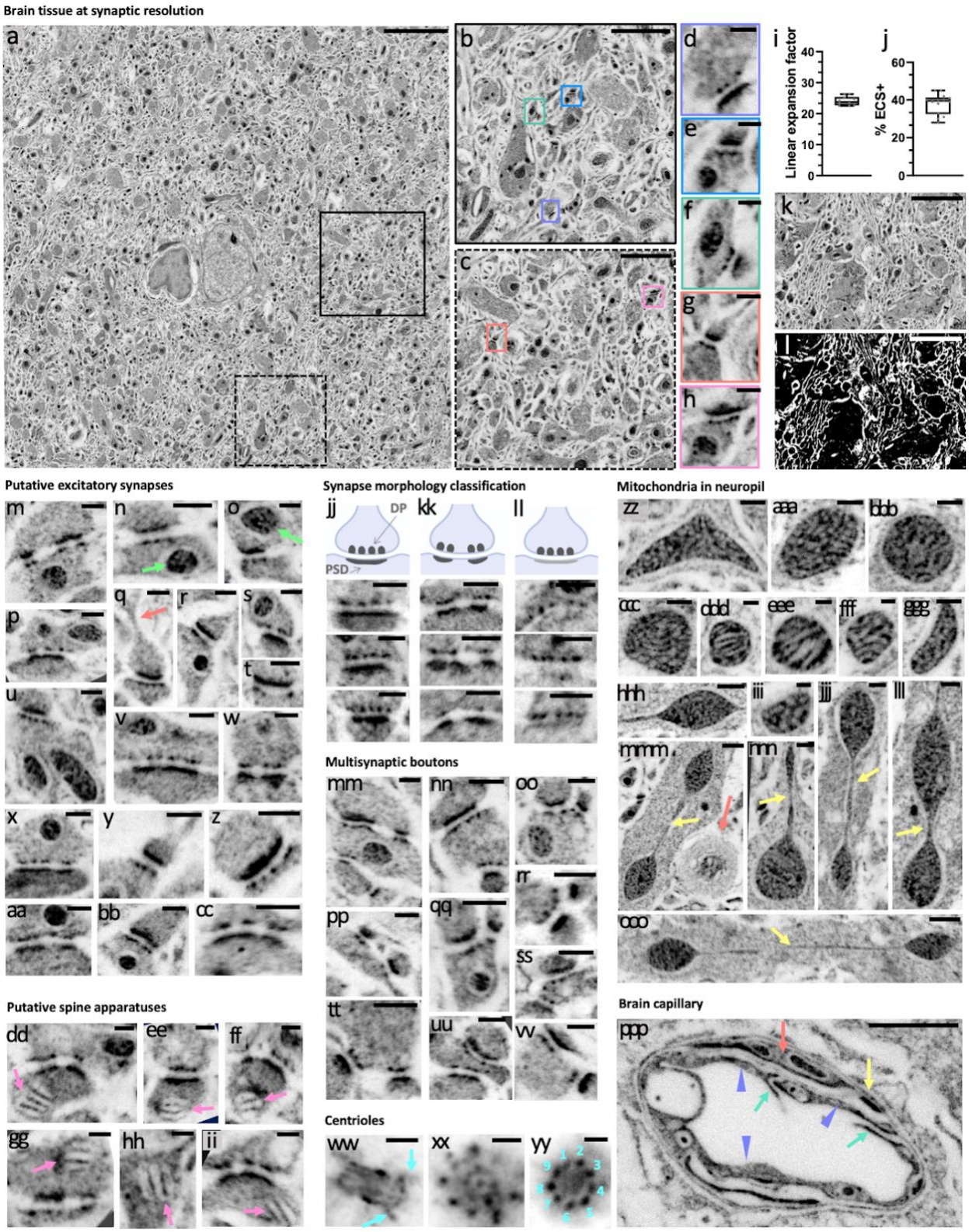

Figure 11: pan-ExM-t reveals mouse brain tissue ultrastructure. **a**, NHS ester pan-stained tissue section of the mouse cortex. **b**, **c**, magnified areas in the black and dotted black boxes in **a**, respectively. **d-h**, magnified areas identified by the correspondingly colored boxes in **b**, **c** showing putative excitatory synapses. **i**, linear expansion

factor (n = 254 measurements from 3 independent experiments). **j**, ECS + lipid membrane (ECS+) fraction (n = 14 measurements from 3 independent experiments). **k**, image of neuropil in the hippocampus. **l**, same area as **k** where white pixels represent the ECS+. **m-cc**, putative excitatory synapses defined by a prominent PSD. Lime arrows in **n** and **p** point to mitochondria in the presynaptic bouton and in the postsynaptic compartment, respectively. The salmon arrow in **q** points to a spine neck. **dd-ii**, putative spine apparatuses (pink arrows) in the postsynaptic compartment defined by a characteristic lamellar arrangement. **jj-ll**, classification of synapses based on the patterns and intensity of the PSD; **jj**, class 1: the PSD is prominent and macular; **kk**, class 2: the PSD is prominent and perforated; **ll**, class 3: the PSD, unlike DPs, is barely visible. **mm-vv**, NHS ester pan-stained multisynaptic boutons and their postsynaptic partners. **ww**, lateral view of a centriole showing distal and proximal ends as well as distal appendages (turquoise arrows). **xx**, **yy**, top views of centrioles showing the cartwheel structure (**xx**) and the 9-fold symmetry of microtubule triplets (**yy**). **zz-ooo**, mitochondria with vesicular cristae (**zz-ccc**, **ggg**, **iii**), lamellar cristae (**ddd-fff**), and teardrop-shaped with tubular extensions (yellow arrows) (**mmm-ooo**). Salmon arrow in **mmm** points to putative myelinated sheaths. **ppp**, brain capillary showing endothelial cells (lavender arrow heads), putative tight junctions (TJs; teal arrows) that link neighboring endothelial cells, putative pericyte branch (salmon arrow), and the basement membrane (BM; yellow arrow). Gamma corrections: (**a**, **ww-yy**, **ppp**) γ=0.7; (**m-vv**, **zz-ooo**) γ=0.8. All scale bars are corrected for the expansion factor. Scale bars, (**a**) 5 µm, (**b**, **c**, **ppp**) 1 µm, (**d-h**, **m-cc**, **jj-vv**, **xx**, **ww, zz-ccc**, **ggg**, **jjj**, **lll**) 200 nm, (**k**, **l**) 3 µm, (**dd-ii**, **xx**, **yy**, **ddd-fff**, **iii**, **nnn**) 100 nm, (**hhh**, **mmm**, **ooo**) 400 nm.

4.2.3. pan-ExM-t is compatible with antibody labeling of synapses in thick brain tissue sections

A particular strength of pan-ExM-t is its ability to localize specific proteins to sub-compartments revealed in the contextual pan-stained channel. Our protocol must therefore allow for efficient antibody staining, while also maintaining good ultrastructural preservation. Because hydrogels with high monomer concentrations are known to impede antibody diffusion, we investigated whether lowering the monomer concentration in the different interpenetrating hydrogels would result in better signal-to-noise antibody stainings. We assessed both antibody-labeling efficiency and ultrastructural preservation in hydrogels synthesized with different sodium acrylate (SA) monomer concentrations. We hypothesized that lowering this concentration would allow for larger effective hydrogel mesh sizes and therefore better antibody penetration. In summary, we used four

different hydrogel monomer combinations with either 19% (w/v) or 9% (w/v) SA in the first and second expansion hydrogels, referred to as *19SA/19SA*, *19SA/9SA*, *9SA/19SA*, and *9SA/9SA*. Comparing expansion factors, we found that *19SA/19SA* gels expand as we previously reported 24.1± 1.4-fold (mean ± s.d.; N = 10 fields of view from 3 independent experiments; n = 254 synaptic profiles, **Supplementary Fig. 20e**), *19SA/9SA* gels expand 20.3± 1.2-fold (mean ± s.d.; N = 12 fields of view from 2 independent experiments; n = 267 synaptic profiles), *9SA/19SA* gels expand 20.5± 1.8-fold (mean ± s.d.; N = 6 fields of view from 2 independent experiments; n = 88 synaptic profiles), and *9SA/9SA* gels expand 18.5± 1.7-fold (mean ± s.d.; N = 6 fields of view from 2 independent experiments; n = 86 synaptic profiles). While expansion factors are not radically affected by variations in SA monomer concentrations, we noticed visible ultrastructural differences. Judging tissue preservation by the frequency of gaps in neuropil and detachments of cell bodies from the underlying tissue, we observe equally good tissue integrity in *19SA/19SA*, *19SA/9SA*, and *9SA/19SA* gels (**Supplementary Fig. 20a-c**), but significantly distorted neuropil and dissociated cell bodies in *9SA/9SA* gels (**Supplementary Fig. 20d**). We suspect that this distortion effect is due to a decrease in hydrogel mechanical sturdiness when hydrogels of lower monomer concentrations, like the ones in ExR [127], are used. We therefore caution against synthesizing hydrogels that are mechanically too brittle to properly preserve the integrity of biological structures. As for antibody-staining efficiency, we observed equally efficient labeling in *19SA/19SA*, *19SA/9SA*, and *9SA/19SA* hydrogels for most antigens, with reduced background following synaptic protein immunolabeling in *19SA/9SA* hydrogels. Therefore, in all subsequent immunoassays, we used *19SA/9SA* gels for synaptic protein immunolabeling and *19SA/19SA* gels in immunolabeling structural markers.

With a now robust pan-ExM-t protocol capable of localizing specific proteins in their tissue ultrastructural context, we performed several immunostainings against commonly studied synaptic targets. **Figure 12** shows the distributions of synaptic proteins Homer1, Bassoon, PSD-95 (**Supplementary Video 6**), and Synaptophysin in the context of tissue and synaptic ultrastructure. The expansion-corrected distributions of Homer1, PSD-95, and Bassoon within the axial DP-PSD distances are all in agreement with published values as well as with values obtained from cultured neuron measurements in this work. For example, the distance between Bassoon and the PSD is 93.7 ± 16.9 nm (mean ± s.d.; $N = 3$ fields of view; $n = 74$ synaptic profiles; **Fig. 12ooo**); the distance between Homer1 and DP is 93.3 ± 16.1 nm (mean ± s.d.; $N = 5$ fields on views; $n = 120$ synaptic profiles; **Fig. 12ppp**); and the distance between PSD-95 and the DP is 76.4 ± 11.8 nm (mean ± s.d.; $N = 3$ fields of view; $n = 113$ synaptic profiles, **Fig. 12qqq**). **Figure 12rrr** shows a plot of the axial positions of Homer1, PSD-95, and Bassoon along the trans-synaptic axis defined as the center position between DP and PSD. In agreement with previous work, Homer1 is on average localized further inside the spine and away from the cleft than the PSD center [212]. Interestingly, in Class 3 synapses, defined by the absence of a protein-dense PSD, we found that while Bassoon scaffold protein is present (**Figs. 12q-s**) PSD proteins Homer1 (**Figs. 12jj-ll**) and PSD-95 (**Figs. 12ddd-fff**) are not, reminiscent of inhibitory synapses.

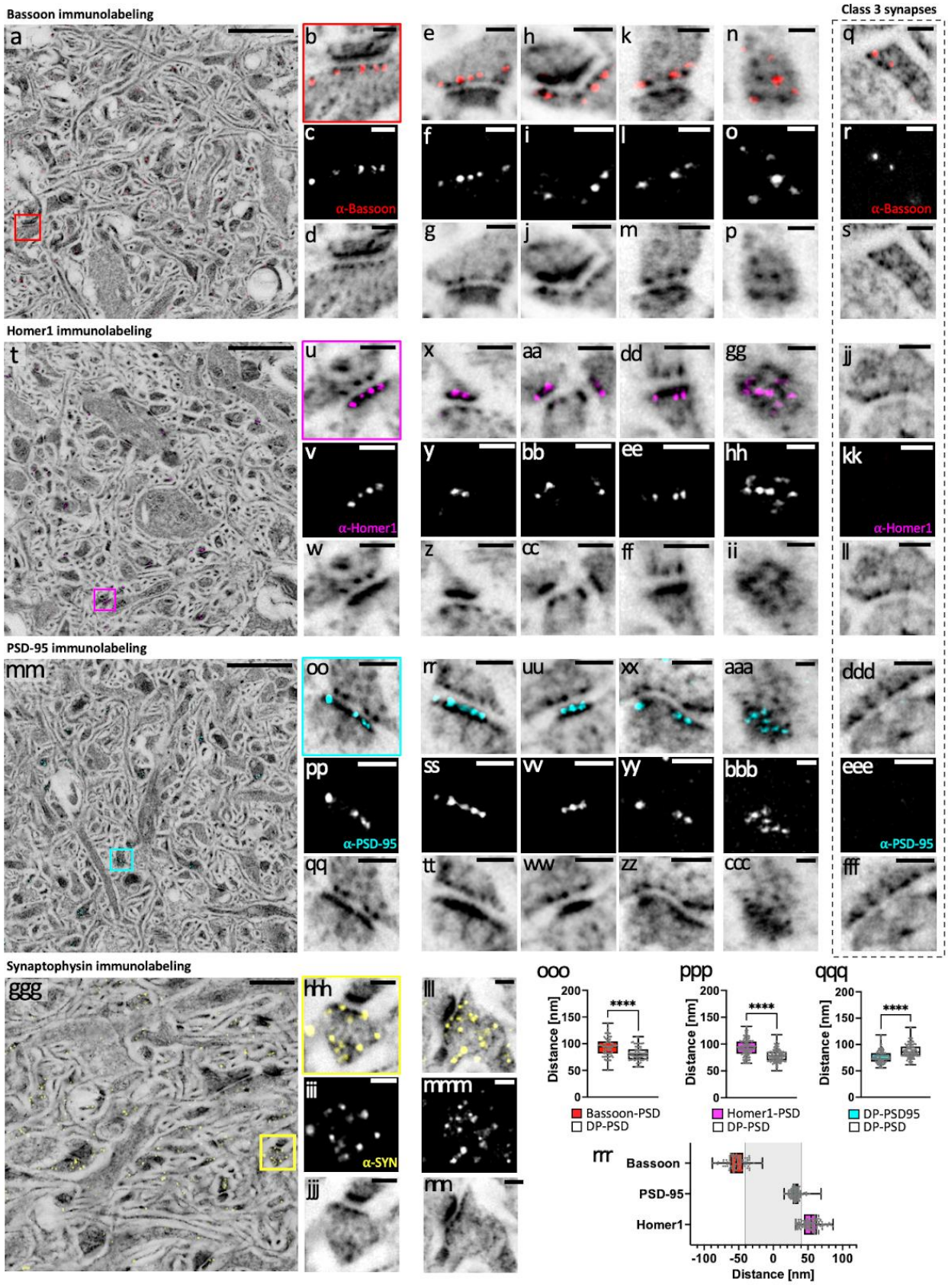
Bassoon immunolabeling
Class 3 synapses
α-Bassoon
Homer1 immunolabeling
α-Homer1
PSD-95 immunolabeling
α-PSD-95
Synaptophysin immunolabeling
α-SYN
ooo
ppp
qqq
Distance [nm]
****
Bassoon-PSD
DP-PSD
Homer1-PSD
DP-PSD
DP-PSD95
DP-PSD
rrr
Bassoon
PSD-95
Homer1
Distance [nm]

Figure 12: pan-ExM-t is compatible with antibody labeling of synaptic proteins in brain tissue. **a**, NHS ester (grayscale) pan-stained and Bassoon (red) immunolabeled brain tissue section. **b**, magnified area in the red box in a showing a synapse. **c**, Bassoon immunolabeling of the same area as in **b**. **d**, NHS ester pan-staining of the same area as in **b**. **e-p**, additional examples similar to **b-d** showing lateral (**e-m**) and top (**n-p**) views of Bassoon-immunolabeled synapses. **q-s**, lateral view of a Class 3 synapse pan-stained with NHS ester and immunolabeled with Bassoon antibody indicating that Class 3 synapses are positive for Bassoon protein. **t**, NHS ester (grayscale) pan-stained and Homer1 (magenta) immunolabeled brain tissue section. **u**, magnified area in the magenta box in t showing a synapse. **v**, Homer1 immunolabeling of the same area as in **u**. **w**, NHS ester pan-staining of the same area as in **u**. **x-ii**, additional examples similar to **u-w** showing lateral (**x-ff**) and top (**gg-ii**) views of Homer1-immunolabeled synapses. **jj-ll**, lateral view of a Class 3 synapse pan-stained with NHS ester and immunolabeled with Homer1 antibody indicating that Class 3 synapses are negative for Homer1 protein. **mm**, NHS ester (grayscale) pan-stained and PSD-95 (cyan) immunolabeled brain tissue section. **oo**, magnified area in the cyan box in mm showing a synapse. **pp**, PSD-95 immunolabeling of the same area as in **oo**. **qq**, NHS ester pan-staining of the same area as in **oo**. **rr-ccc**, additional examples similar to **oo-qq** showing lateral (**rr-zz**) and top (**aaa-ccc**) views of PSD-95-immunolabeled synapses. **ddd-fff**, lateral view of a Class 3 synapse pan-stained with NHS ester and immunolabeled with PSD-95 antibody indicating that Class 3 synapses are negative for PSD-95 protein. **ggg**, NHS ester (grayscale) pan-stained and Synaptophysin (SYN; yellow) immunolabeled brain tissue section. **hhh**, magnified area in the yellow box in **ggg** showing a synapse. **iii**, Synaptophysin immunolabeling of the same area as in **hhh**. **jjj**, NHS ester pan-staining of the same area as in **hhh**. **lll-nnn**, additional example similar to **hhh-jjj**. **ooo**, Comparison between Bassoon-PSD and DP-PSD distances (n = 74 measurements from 3 fields of view (FOVs) in one independent experiment). **ppp**, Comparison between Homer1-PSD and DP-PSD distances (n = 120 measurements from 5 FOVs in 2 independent experiments). **qqq**, Comparison between PSD95-DP and DP-PSD distances (n = 113 measurements from 3 FOVs in one independent experiment). ****: p<0.0001. **rrr**, relative spatial distributions of Bassoon, PSD-95, and Homer1 along the trans-synaptic axis. All images (with the exception of **ggg-nnn**) are z-projections (intensity average) of 2 images. All NHS ester images were Gamma-corrected with γ=0.7 with the exception of the Synaptophysin images (γ=0.6). All scale bars are corrected for the expansion factor. Scale bars (**a**, **t**, **mm**) 2 μm, (**b-m**, **q-s**, **u-ff**, **jj-ll**, **oo-zz**, **ddd-fff**, **hhh-nnn**) 200 nm, (**n-p**, **gg-ii**, **aaa-ccc**) 100 nm, (**ggg**) 1 μm.

4.2.4. pan-ExM-t is compatible with antibody labeling of tissue structures

pan-ExM-t is not limited to providing context to synaptic proteins. We found that SYTOX Green nucleic acid stain produces a bright nuclear staining that overlays perfectly with NHS ester pan-stained cell nuclei (**Fig. 13a-d**). Furthermore, we can resolve individual glial fibrillary acidic

protein (GFAP) filaments in astrocytes (**Fig. 13e-k**) including near multiciliated ependymal epithelia (**Supplementary Fig. 18**) and engulfing blood vessels (**Fig. 13k**; **Supplementary Video 7**). Interestingly, the distinctive pan-stain pattern of astrocyte nuclei and their thick and fibrous cytoplasmic branches allow for their identification without GFAP, analogous to heavy metal-stains in EM (**Supplementary Fig. 21**; **Supplementary Video 8**) [128][218]. We also observe that myelin basic protein (MBP-) labeled structures are devoid of surrounding pan-staining, suggesting these represent myelinated axons (**Fig. 13m-s**). Moreover, when we immunolabeled GFP in Thy1-GFP transgenic mice, we noticed the sparsity of this marker in both neuropil and neuron somas (**Fig. 13t-hh**; **Supplementary Video 9**). Originally designed to resolve individual dendrites and axons in densely packed neuropil [129], GFP-Thy1 imaged with pan-ExM-t reveals these transgenic neurons in their ultrastructural context. pan-ExM-t clearly shows the GFP surrounding, but being excluded from, mitochondria (**Fig. 13u-w**). The ability to distinguish GFP-positive dendritic spine heads (**Fig. 13x-z**) and axonal boutons (**Fig. 13aa-ff**) from their synaptic partners suggests that pan-ExM-t is especially suited for light-based neural tracing and connectomics.

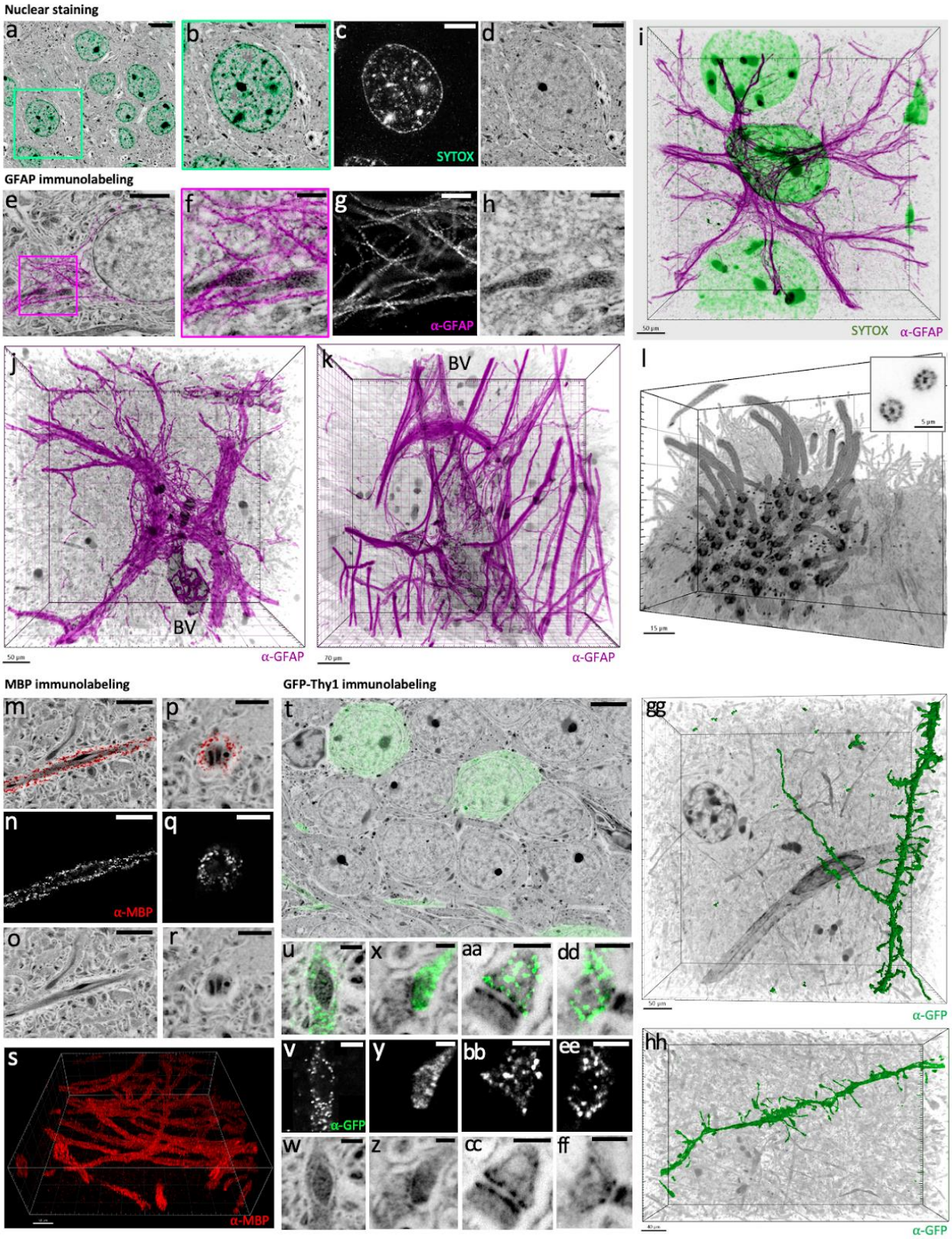
Nuclear staining
a
b
c
SYTOX
d
i
SYTOX α-GFAP
GFAP immunolabeling
e
f
g
α-GFAP
h
j
BV
α-GFAP
k
BV
α-GFAP
l
MBP immunolabeling
m
p
n
α-MBP
q
o
r
s
α-MBP
GFP-Thy1 immunolabeling
t
u
x
aa
dd
v
α-GFP
y
bb
ee
w
z
cc
ff
gg
α-GFP
hh
α-GFP

Figure 13: pan-ExM-t is compatible with antibody labeling of brain tissue structural markers. **a**, cortical neurons pan-stained with NHS ester (grayscale) and stained with SYTOX green (teal) showing a neuron nucleus. **b-d**, magnified view of the area in the green box in **a** and the SYTOX Green (**c**) and NHS ester (**d**) channels shown separately. **e**, astrocyte pan-stained with NHS ester (grayscale) and immunolabeled with glial fibrillary acidic protein antibody (α-GFAP; magenta). **f-h**, magnified view of the area in the magenta box in **e** showing GFAP filaments surrounding mitochondria, and the α-GFAP (**g**) and NHS ester (**h**) channels shown separately. **i**, 3D rendering of α-GFAP (magenta), SYTOX Green (green), and NHS ester (grayscale). **j**, **k**, 3D renderings of α-GFAP (magenta) and blood vessels (BV) pan-stained with NHS ester (grayscale). **l**, multiciliated ependymal epithelia pan-stained with NHS ester (grayscale). Inset shows 9-fold symmetry of cilia. **m-r**, lateral (**m-o**) and top (**p-r**) views of axons pan-stained with NHS ester (grayscale) and immunolabeled with myelin basic protein antibody (α-MBP; red). α-MBP (**n**, **q**) and NHS ester (**o**, **r**) channels of the areas shown in **m** and **p**. **s**, 3D rendering of anti-MBP showing multiple axons. **t**, cortical neurons pan-stained with NHS ester (grayscale) and anti-GFP (green) showing that only a sparse subset of neuron somas and neurites express GFP-Thy1. **u-w**, a neurite pan-stained with NHS ester (**w**) and immunolabeled with anti-GFP (**v**) showing that GFP-Thy1 is not expressed inside mitochondria. **x-ff**, a dendritic spine (**x-z**) and axonal boutons (**aa-ff**) pan-stained with NHS ester and immunolabeled with anti-GFP. **y**, **bb**, **ee**, anti-GFP channels of the areas shown in **x**, **aa**, and **dd**, respectively. **z**, **cc**, **ff**, NHS ester channels of the areas shown in **x**, **aa**, and **dd**, respectively. **gg**, 3D representation of a surface-rendered dendrite immunolabeled with anti-GFP (green) and NHS ester pan-staining (grayscale). **hh**, 3D rendering of a dendrite immunolabeled with anti-GFP (green) and NHS ester pan-staining (grayscale). Gamma corrections: (**a**, **e**, **m**, **p**, **t**, **u**, **x**, **aa**, **dd**) γ=0.7. 3D renderings were processed with Imaris with gamma corrections applied. A mask drawn manually in Fiji was created to remove background noise in images **m** and **t**. 3D image processing details for images **i-l**, **s**, **gg**, and **hh** are found in the **Methods** section. Scale bars in the 3D renderings **i-l**, **s**, **gg**, and **hh** are not corrected for the expansion factor. All other scale bars are corrected for the expansion factor. Scale bars (**a**, **t**) 5 μm, (**b-d**, **e**, **m-o**) 2 μm, (**f-h**, **u-w**) 500 nm, (**p-r**) 1 μm, (**x-ff**) 200 nm.

4.2.5. pacSph enables lipid labeling of tissue in pan-ExM-t

Neural connectomics analysis in EM generally relies on contrast from lipid membranes to delineate cellular boundaries. One way to achieve this in pan-ExM-t would be to preserve the lipid content. Since there are roughly 5 million lipids per 1 μm2 of membrane surface and 150-times more lipids than proteins on a typical cell membrane [73], we expect that even following detergent extraction with SDS, a fraction of these lipids would remain in the hydrogel. Interestingly, when we labeled

SDS-denatured and ~4-fold expanded brain tissue with BODIPY TR Methyl Ester (BDP), we achieved a distinct pan-staining (**Supplementary Fig. 22**). Here, BDP highlights the nuclear envelope, organelles like mitochondria, the Golgi complex, the ER, as well as myelinated axons. All these structures resemble those shown in mExM [35], but were acquired without using any specialized probes. Overlaid with sulfonated NHS ester dye pan-staining, we observe a striking differential hydrophilic-lipophilic pan-staining pattern (**Supplementary Fig. 23**), with significantly higher BDP staining levels achieved in 4% FA + 0.1% GA-fixed tissue than in 4% FA-fixed tissue (**Supplementary Fig. 24**). Similarly, in pan-ExM-t expanded tissue, we achieve distinctive and bright BDP labeling in 4% FA + 0.1% GA-fixed tissue (**Supplementary Fig. 25**), but almost no staining in 4% FA-fixed tissue, and we see major structural artifacts when supplementing the fixatives with 0.01% osmium tetroxide, known to better preserve lipids [74][75] (**Supplementary Fig. 24s-aa; Supplementary Fig. 26**). These results confirm that GA plays a major role in stabilizing and crosslinking the lipid content [122], and suggest that monoaldehydes like FA alone do not provide adequate lipid preservation when preceded by detergent extraction.

Next, we asked whether replacing the anionic detergent SDS in our denaturation buffer with the chaotropic reagent guanidine hydrochloride (G-HCl) would better preserve the lipid content and enable superior lipid staining in 4% FA + 0.1% GA-fixed, pan-ExM-t expanded tissue. Unlike SDS, hyperhydration with urea or guanidine HCl is known to disrupt hydrogen bonding in proteins without solubilizing lipids [69]. EM images of brain tissue samples fixed with only 4% FA and chemically cleared with the functionally similar chaotropic molecule urea show intact membrane ultrastructure and up to 70% lipid retention [70][71]. We chose to work with G-HCl and not urea, because the latter is known to decompose and carbamylate proteins at the elevated temperatures required for efficient denaturation [72]. **Supplementary Fig. 27** shows that BDP signal is in fact

higher in G-HCl-denatured neuron and tissue samples, giving credence to this approach. However, our data also show that BDP does not exclusively stain cell membranes and subjecting samples to no denaturation at all results in lower BPD signal. This observation is more evident in ~20-fold expanded samples where easily distinguishable neurite boundaries are not specifically stained with BDP (**Supplementary Fig. 28**). All these results suggest that lipophilic dyes like BDP do not exclusively label lipid membranes in denatured samples, but also label the hydrophobic core of proteins exposed following denaturation. In fact, in thermal denaturation assays, environmentally sensitive fluorescent dyes are commonly used to determine the temperature at which proteins denature (e.g., in differential scanning fluorimetry (DSF)) [130][131][132]. Protein denaturation, however, is a necessary step in enzyme-free ExM methods, since electrostatic interactions between proteins must be nulled for isotropic sample expansion.

Since strategies to preserve the lipid content for post-denaturation lipophilic labeling do not result in exclusive cell membrane delineation and require antigen-masking GA fixation [138], we decided to capitalize on pre-denaturation lipid labeling strategies. Here, proteins are not unfolded, and the lipid content may require less harsh fixatives for preservation after expansion. To label lipid membranes in ExM, all approaches have so far used trifunctional lipid probes in either live or fixed samples [34][35][76][78]. In these probes, one functional group is a membrane-intercalating lipid, the second is hydrogel-anchorable, and the third is a reporter molecule. In the live-labeling approaches, cells have been labeled with acryolated and fluorescent 1,2-distearoyl-sn-glycero-3-phosphoethanolamine (DSPE) [34], clickable palmitic acid [42], aminated α-NH2-ω-N3-C6-ceramide [76], or clickable choline [77]. The only strategy available to stain lipids in tissue with ExM after it is fixed is to use aminated (poly-lysine) membrane-intercalating probes such as pG5kb [35] and mCling [78][79]. These survive detergent disruption by covalent

attachment to the hydrogel matrix and contain a biotin group available for conjugation with dye-labeled streptavidin after expansion. When we tested mCling in 5-fold expanded brain tissue sections, we found that although it labeled tissue hydrophobic components, this labeling was limited to the tissue surface, likely because of diffusion limitations (**Supplementary Fig. 29**). When we tested mCling in pan-ExM-t samples, we observed little to no labeling. mCling [79] as well as an ExM-optimized version of it, pG5kb [35], have 5 to 7 lysine groups making them relatively highly charged and bulky (**Supplementary Fig. 30a-b**). mCling and pG5kb also require that the tissue is fixed with GA, which we previously found decreases synaptic protein antigenicity, introduces structural artifacts in the form of tissue perforations, as well as limits the expansion factor to ~12 fold, and so we did not explore this avenue any further.

We therefore developed a new pan-ExM-t lipid labeling strategy where we use a commercially available photocrosslinkable and clickable sphingosine (pacSph [221], **Fig. 14n**) as a lipid intercalating reagent in tissue fixed only with 4% FA + 20% AAm (to preserve antigenicity). In our protocol, we (1) label 70 µm-thick tissue sections with pacSph prior to hydrogel embedding, (2) irradiate the sample with UV light (365 nm) to photo-crosslink the probes onto neighboring proteins (from both directions to compensate for depth-dependent UV light absorption in the 70-µM thick tissue); and (3) probe the ligands with fluorescent dyes after expansion. It is worth noting that pacSph is smaller (335 Da) than mCling (1445 Da) or pG5kb (1158 Da), polar, and partially positively charged (amine pKa ~6.6), allowing for high probe packing and sampling. Sphingosines are also membrane bilayer-rigidifying: they stabilize gel domains in membranes, raise their melting temperature, and induce membrane permeabilization without micellar extraction of proteins or lipids [80][81]. We therefore expect sphingosine to diffuse efficiently in thick tissue. Furthermore, pacSph has a photoactivatable diazirine group that forms reactive carbene

intermediates capable of insertion in C-H or N-H, and O-H bonds of tissue components upon UV irradiation [82][83]. Since diazirine is on the lipid chain (**Fig. 14n**, pink diazirine), we expect that two pacSph lipids located on opposing sides of a membrane bilayer will photo-crosslink the embedded hydrogel polymer chains at the center of the hydrophobic phase of the bilayer, minimizing the linker error. This error is inevitable if we were to photo-crosslink the probes at the polar head group. Finally, retained lipids are conjugated with a hydrophobic azido dye at the lipid tail extremity (**Fig. 14n**, green alkyne). We believe all these factors make pacSph ideally suited for membrane delineation in pan-ExM-t.

Figure 14 confirms the plausibility of our approach. In the perikarya of brain tissue fixed with 4% FA + 20% AAm and pan-stained with pacSph, we can clearly discern both sides of ER tubules (**Fig. 14d-f**), ER and mitochondria contact sites (**Fig. 14g-i**), and both sides of the nuclear envelope (**Fig. 14j-l**). In neuropil, lipid membrane boundaries are now discernable (**Fig. 14o-oo**), revealing the boundaries of neurites and synaptic compartments. In brain capillaries, the different membranes are also differentially highlighted relative to NHS ester pan-staining (**Fig. 14pp-rr**). Moreover, when we experimented with irradiating pacSph pan-stained tissue with UV light before or after the first hydrogel embedding, we found that UV irradiation after hydrogel embedding results in significantly higher probe retention, suggesting that diazirine is being photo-crosslinked to the dense hydrogel mesh in addition to surrounding proteins (**Fig. 14m**; **Supplementary Fig. 31**). In fact, a recent study showed that diazirine has an affinity for reacting with proteins containing large negative electrostatic surfaces in cells (e.g., carboxyl groups) [139]. We suspect that diazirine in our probe is preferentially photo-crosslinked to carboxyl groups on the poly(acrylamide/acrylate) mesh, offering better retention of the lipid content. While benefiting from future investigation, our data shows that photo-crosslinking lipid-intercalating ceramides to

the expansion hydrogel represents an important strategy in labeling lipids in ~24-fold expanded and formaldehyde fixed brain tissue sections. A gallery of pacSph pan-stained tissue is found in **Supplementary Fig. 32**.

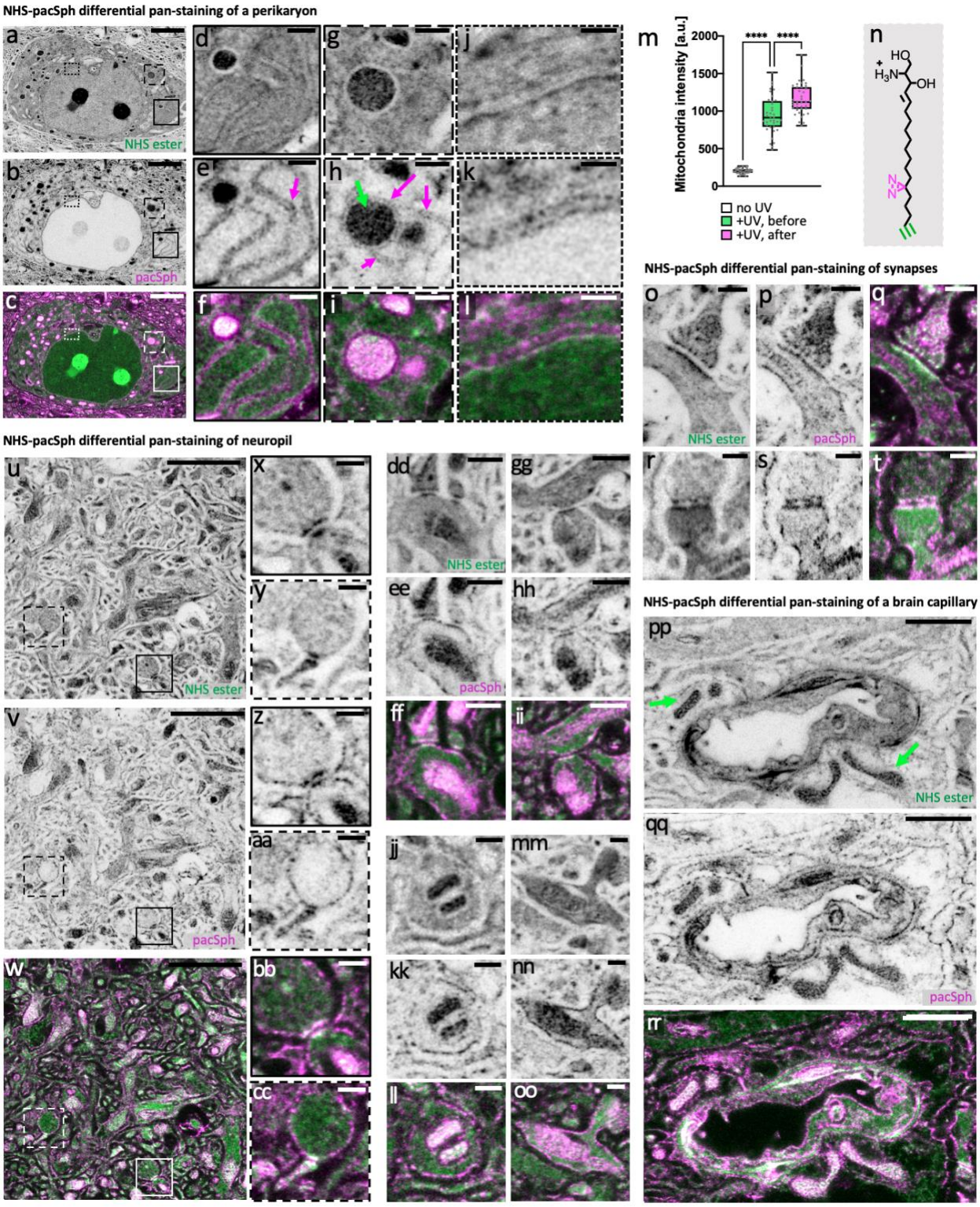

Figure 14: pacSph enables lipid membrane pan-staining of brain tissue in pan-ExM-t. **a-c**, perikaryon pan-stained both with NHS ester (**a**) and pacSph (b) (overlay shown in **c**). **d-l**, magnified areas of the solid boxes in **a-c** showing the two sides of ER tubules (magenta arrow; **d-f**), the dashed boxes in **a-c** showing a mitochondrion (green arrow) in

contact with the ER (magenta arrow; **g-i**), and the dotted boxes in **a-c** showing the nuclear envelope (**j-l**). **m**, mitochondria signal levels in tissue pan-stained with pacSph and not irradiated with UV (white; n = 35 measurements from 5 FOVs in one independent experiment); pan-stained with pacSph and irradiated with UV before hydrogel embedding (green; n = 37 measurements from 5 FOVs in one independent experiment); and pan-stained with pacSph and irradiated with UV after hydrogel embedding (pink; n = 39 measurements from 5 FOVs in one independent experiment). ****: p<0.0001. **n**, chemical structure of pacSph. The probe is photocrosslinked via its diazirine group (magenta) and labeled via its alkyne group (green). **o-t**, synapses pan-stained both with NHS ester (**o**, **r**) and pacSph (**p**, **s**) (overlays shown in **q**, **t**). **u-w**, neuropil pan-stained both with NHS ester (**u**) and pacSph (**v**) (overlay shown in w**). x-cc**, magnified areas of the solid (**x**, **z**, **bb**) and dashed (**y**, **aa**, **cc**) boxes in **u-w** showing synapses. **dd-oo**, neurites and synapses pan-stained both with NHS ester (**dd**, **gg**, **jj**, **mm**) and pacSph (**ee**, **hh**, **kk**, **nn**) (overlays shown in **ff**, **ii**, **ll**, **oo**). **pp-rr**, brain capillary pan-stained both with NHS ester (**pp**) and pacSph (**qq**) (overlay shown in **rr**). Green arrows point to mitochondria. Gamma corrections: (**a**) γ=0.7; (**p**, **r**, **u**, **dd**, **gg**, **jj**, **mm**, **pp**) γ=0.5. All scale bars are corrected for the expansion factor. Scale bars (**a-c**) 3 µm, (**d-i**, **dd-ii**) 500 nm, (**u-w**) 2 µm, (**j-l**, **o-t**, **x-cc**, **jj-oo**) 250 nm, (**pp-rr**) 1 µm

4.3. Discussion

Multiple ExM techniques have been developed to image the subcellular protein distribution of synaptic targets in brain tissue [6][8][9][10][11][78][106][127][119][222][223][224][225][226] as well as map RNA transcripts within axons and dendrites in the brain [110]. An excellent review can be found here [136]. However, capitalizing almost exclusively on antibody labeling, none of these methods demonstrate correlative molecular and contextual imaging with synaptic resolution. Notwithstanding the importance of specific protein imaging, we believe that sample expansion presents a new opportunity to explore a new dimension of light microscopy inaccessible to optical super-resolution techniques: one where the relative size of labels appears shrunken by the linear expansion factor. In this context, the relative radius of a fluorescent dye (~ 1 nm) would approach (~1 nm/20 = ~50 pm), which is comparable to the size of an osmium atom used in heavy metal EM staining (~200 pm). Here, bulk fluorescence staining of decrowded neuropil would no longer

be limited by the sampling and quenching restrictions of fluorescent dyes, and ultrastructural details, previously accessible with only EM, can now be examined on standard light microscopes.

The data we present in this paper demonstrates that pan-ExM-t can clearly resolve molecular targets in the context of brain tissue ultrastructure. By combining ~24-fold linear sample expansion with novel pan-stainings, we were able to (1) resolve and identify synapses and their substructures by their morphological characteristics, (2) localize protein markers to their subcellular compartments, and (3) delineate cellular membranes.

We have shown that brain tissue structures such as neurons, glia, axons, dendrites, blood capillaries, pericytes, the endothelium, basal bodies, as well as subcellular features like DPs, PSDs, the cristae of mitochondria, ER tubules, myelin sheaths, multisynaptic boutons, spine necks, spine apparatuses, and the cartwheel structure of centrioles can all be identified in the pan-stain channel alone, analogous to classical EM techniques. We have also demonstrated, for the first time, that chemical synapses can be distinguished in a light microscopic image by their characteristic protein density patterns. These patterns could be characterized using the Gray classification established for PTA and osmium stained synapses in EM [215][216]. Taking advantage of pan-ExM-t's strength of directly correlating synapse ultrastructure with immunolabeling against specific proteins, we observed that Class 1 and Class 2, but not Class 3, synapses are positive for Homer1 and PSD-95, supporting the functional Gray synapse concept that synapses with dense PSDs are likely excitatory. This example demonstrates our approach's capability to map the molecular makeup of different synapse types within the context of their distinct ultrastructural properties to systematically explore synapse diversity and determine synapse sub-types that are vulnerable to diseases.

To achieve the highest ultrastructural preservation of tissue while maximizing sample expansion, we have shown that it is important to optimize fixation and gelation parameters. NHS ester pan-staining in this context serves as a readily accessible readout to assess the preservation and retention of proteins. We have demonstrated that reducing interprotein crosslinking enables up to 26-fold expansion without resorting to protease treatments or harsh denaturation conditions. We have also shown that hydrogels of high monomer concentrations (~30% w/v) and sufficient crosslinker density (~0.1% w/v) must be used to ensure that proteins are adequately sampled by the polymer matrix. In this context, it is not surprising that pan-ExM-t gels are stiffer than the gels prepared using the original ExM protocol [6]. Moreover, we found that ECS preservation is sensitive to the strength of fixatives used, with higher fixation resulting in lower ECS fractions. In all cases, the ECS is significantly more prominent in pan-ExM-t than in EM, emphasizing that the familiar appearance of tightly apposed neurites, typically seen in EM, is artifactual, and consistent with a previous live-STED microscopy characterization of brain ECS [125].

In this work, we also explored the feasibility of imaging lipid membranes in 24-fold expanded brain tissue sections. We believe that efforts to preserve the endogenous lipid content and probe it after expansion are not necessarily productive. After all, since the free energy of lipid bilayers must be minimized, we hypothesized that even if we were to avoid detergent extraction, lipid membranes will eventually collapse into micelles following sample expansion. Our strategy was therefore to imprint lipid membranes onto the hydrogel before mechanical homogenization of the sample. We reasoned that the probe to-be-imprinted (1) had to be small to allow for maximum stacking, (2) was positively charged to intercalate negatively charged phospholipid bilayers, and (3) had the ability to be fixed onto neighboring proteins or the hydrogel itself in a mechanism that is orthogonal to protein intra-crosslinking. We have shown in this work that pacSph, a

photocrosslinkable and clickable sphingosine, fits these criteria, enabling neuronal membrane imaging in tissue fixed only with formaldehyde. We were able to delineate cellular organelles, synaptic anatomy, as well as membrane boundaries in neuropil. Our new contrast complements our established protein pan-stain and will in the future help facilitate segmentation and neuronal tracing algorithms for connectomics analysis.

Tracing lipid boundaries in neuropil using EM has enabled reconstruction of the neural wiring diagrams of a 1,500 μm3 volume in the mouse brain [133], the whole *Drosophila* larval mushroom body [134], and more recently, the whole brain of *Caenorhabditis elegans* [135]. To date, however, no light microscopy method has able to reconstruct a brain connectome, as these lack the ability of EM to reveal the ultrastructure of cells and their compartments without selective staining. Interestingly, one theoretical study supports the feasibility of reconstructing entire connectomes using lipid membrane labeling and *in-situ* molecular barcoding in 20-fold expanded tissue [141]. Based on our data, however, we assert that capitalizing on protein (instead of membrane) pan-staining in >20-fold expanded tissue is a more feasible step forward towards this goal. Our data shows that it is more straightforward to detect cell boundaries by the absence of protein pan-staining than it is to potentially reconstruct the membrane boundaries of very fine neural processes. After all, proteins have been repeatedly shown to survive the expansion process, while lipids need to be negatively imprinted onto the expansion hydrogel first, making this latter process inherently limited by pre-expansion sampling restrictions. Nevertheless, while we did not reconstruct neural connectivity in this work, we were able to resolve individual neighboring neurites and distinguish pre- and post-synaptic compartments, laying the groundwork to computational tracing of neurons. We envision that combining pan-ExM-t with microscopes optimized for high-resolution and large

field of view imaging with molecular optical barcoding techniques that are nucleic acid- [142] or protein-based [143] will revolutionize this active area of research.

Like in the early days of EM, we believe that future optimizations will be imperative to enhance this work. Sample fixation could be further improved, lipid pan-staining would benefit from systematic optimizations, and more experiments could be designed to characterize the multitude of ultrastructural patterns revealed by pan-stainings. However, our core concept holds true regardless: that with adequate sample preservation and expansion, pan-staining brings light microscopy to the realm of ultrastructural context imaging.

No longer in the dark, we now see the brain in its complex makeup, the totality of its diverse neural processes: from the microstructures of cells and neuropil down to synaptic densities. No longer in the void, fluorescing antigens are now localized to their nanoscopic compartments, providing functional information to the structures they embody.

4.4. Methods

Key resources table

Please see **Supplementary Tables 1–5** for an overview of the reagents and materials used in this work.

Resource availability

Lead contact

Further information and requests for resources and reagents should be directed to the lead contact, Joerg Bewersdorf (joerg.bewersdorf@yale.edu).

Materials availability

This study did not generate any new materials.

Neuron culture

Rat neuron cultures used to generate NHS ester and anti-Synaptophysin images were cultured as follows: hippocampal CA3-CA1 regions were isolated and dissected from E18 Sprague Dawley Rats (Charles River Laboratories) in the presence of chilled hibernate E media (BrainBits). Hippocampal neurons were then incubated at 37°C for 25 minutes in 0.25% trypsin (Corning; catalog no. 25–053 CI) and immediately washed with DMEM (Thermofisher; catalog no. 11965–118) containing 10% fetal bovine serum (Thermofisher; catalog no. 16000044). Following trypsinization, hippocampi were triturated and immediately plated in DMEM containing 10% fetal bovine serum on poly-D-lysine (Thermofisher; catalog no. ICN10269491) coated 18 mm glass coverslips (Warner instruments; catalog no. 64–0734 [CS-18R17]). After 1 hour of incubation at 37°C, DMEM was removed and replaced with Neurobasal-A (Thermofisher; catalog no. 10888–022) medium containing 2% B-27 (Thermofisher; catalog no. 17504001) and 2 mM Glutamax (Gibco; catalog no. 35050061). Experiments were performed 15-17 days after plating.

Mouse hippocampal cultures used to generate 5-fold expansion images were performed on BalbC P0 pups, in accordance with IACUC protocol number 2019-07912. Hypothermia was induced in pups using ice, followed by decapitation and hippocampal dissection. Hippocampi were dissociated using 200 units Papain (Worthington LS003124, 200 units) for 40 minutes at 37°C. Neurons were triturated and plated onto 12 mm Poly-D-lysine coated coverslips in a 24 well dish at a density of 150,000 cells per well in Neurobasal/B27 Plus media (Thermo-Fisher; catalog no. A3653401) supplemented with 10% FBS and 1% Penicillin/Streptomycin (Thermo-Fisher; catalog

no. 15140163). Following 3 hours of incubation at 37°C and 5% CO2, the media was replaced with Neurobasal/B27 Plus media (Thermo-Fisher; catalog no. A3653401) supplemented with 1% Penicillin/Streptomycin (Thermo-Fisher; catalog no. 15140163)). Fixation was performed at DIV 14-15.

Experimental models

Brain tissue experiments were conducted in 4 wild-type (C57BL/6) adult male mice and 1 Thy1-EGFP mouse (4-8 weeks), obtained from the Jackson Laboratory.

Neuron fixation

Neurons immunolabeled with Homer1, Bassoon, or PDS-95 were fixed with 4% formaldehyde in 1× PBS (Thermofisher; catalog no. 10010023) for 15 min at RT. Neurons immunolabeled with Synaptophysin were fixed with 3% FA and 0.1% glutaraldehyde in 1× PBS for 15 min at RT. Images showing nucleoids in mitochondria were from samples fixed with 3% FA + 0.1% GA in 1× PBS for 15 min at RT. Images showing centrioles and NPCs were from samples fixed with 4% FA in 1× PBS for 15 min at RT. After fixation, all samples were rinsed three times with 1× PBS and processed according to the pan-ExM protocol immediately after. Formaldehyde (FA; catalog no. 15710) and glutaraldehyde (GA; catalog no. 16019) were purchased from Electron Microscopy Sciences.

Brain perfusion

All experiments were carried out in accordance with National Institutes of Health (NIH) guidelines and approved by the Yale IACUC.

All wild-type (C57BL/6) adult male mice were between P30 and P35 and maintained in the vivarium with a 12-h light–dark cycle, stable temperature at 22 ± 1 °C and humidity between 20 and 50%. Mice were transcardially perfused first with ice-cold 1× PBS and then with either 4% FA, 4% FA + 0.1% FA, or 4% FA + 20% acrylamide (AAm; Sigma; catalog no. A9099) (all in 1× PBS, pH 7.4). Brains were isolated and post-fixed overnight in the same perfusion solution at 4 °C. Brains were subsequently washed and stored in PBS at 4 °C. Brains were mounted in ice-cold PBS and coronally sectioned at 70 μm using a vibrating microtome (Vibratome 1500, Harvard Apparatus). Medial hippocampal slices were selected and washed four times for 15 min in PBS at room temperature. Sections were stored in PBS at 4 °C for up to 3 months.

Thy1-EGFP mouse was anesthetized with ketamine (100 mg/kg, Butler Schein: 9952949) and xylazine (10 mg/kg, Akorn: NDC 59399-110-20) in saline (Hudson RCI: 200-59). The mouse was transcardially perfused first with ice cold 1× PBS (Fisher; BP2944-100) and then with 4% FA (J.T. Baker; S898-07) + 20% AAm in 1× PBS, pH 7.4. Brain was isolated and postfixed overnight in 4% FA + 20% AAm in 1× PBS at 4°C. Brain was then washed in PBS and coronally sectioned at 70 μm using vibrating microtome (Leica VT1000, Leica Biosystems, Nussloch, Germany). Sections were stored in 1× PBS with 0.01% sodium azide (Sigma-Aldrich, St. Louis, MO) at 4°C for up to 3 months.

pan-ExM-t reagents

Acrylamide (AAm; catalog no. A9099), N,N′-methylenebis(acrylamide) (BIS; catalog no. 146072) were purchased from Sigma-Aldrich. N,N'-(1,2-Dihydroxyethylene)bisacrylamide (DHEBA) was purchased from Sigma-Aldrich (catalog no. 294381) and Santa Cruz Biotechnologies (catalog no. sc-215503), with the latter being of better purity. Sodium acrylate

(SA) was purchased from both Sigma Aldrich (catalog no. 408220) and Santa Cruz Biotechnologies (catalog no. sc-236893C). To verify that SA was of acceptable purity, 38% (w/v) solutions were made in water and checked for quality as previously reported [37]. Only solutions that were light yellow were used. Solutions that were yellow and/or had a significant precipitate were discarded. Solutions with a minimum precipitate were centrifuged at 4000 rpm for 5 min and the supernatant was transferred to a new bottle and stored at 4 °C until use. Ammonium persulfate (APS) was purchased from both American Bio (catalog no. AB00112) and Sigma-Aldrich (catalog no. A3678). N,N,N′,N′-tetramethylethylenediamine (TEMED; catalog no. AB02020) was purchased from American Bio. 10X phosphate buffered saline (10X PBS; catalog no. 70011044) was purchased from Thermofisher. Sodium Dodecyl Sulfate (SDS; catalog no. AB01922) was purchased from American Bio and Guanidine hydrochloride (G-HCl; catalog no. G3272) was purchased from Sigma-Aldrich

pan-ExM gelation chamber for dissociated neurons

The gelation chamber was constructed using a glass microscope slide (Sigma-Aldrich, catalog no. S8400) and two spacers, each consisting of a stack of two no. 1.5 22 × 22 mm coverslips (Fisher Scientific, catalog no. 12-541B). The spacers were superglued to the microscope slide on both sides of the neuron-adhered coverslip, with this latter coverslip glued in between. A no. 1.5 22 × 22 mm coverslip was used as a lid after addition of the gel solution. This geometry yielded an initial gel thickness size of ~170 μm.

pan-ExM-t gelation chamber for brain tissue sections

The gelation chamber was constructed using a glass microscope slide (Sigma-Aldrich, catalog no. S8400) and two spacers, each consisting of one no. 1.5 22 × 22 mm coverslip (Fisher Scientific,

catalog no. 12-541B). The spacers were superglued to the microscope slide spaced ~ 1 cm from one another. After incubation in activated first expansion gel solution (as described below in First round of expansion for brain tissue sections), the 70 µm-thick brain tissue section was placed and flattened on an additional no. 1.5 22 × 22 mm coverslip which was used as a chamber lid after addition of more activated first expansion gel solution on the microscope slide in-between the spacers. This geometry yielded an initial gel thickness size of ~170 µm.

First round of expansion for dissociated neurons

Neurons, previously fixed as described in the **Neuron fixation** section, were incubated in post-fixation solution (0.7% FA + 1% AAm (w/v) in 1× PBS) for 6–7 h at 37 °C. Next, the neurons were washed twice with 1× PBS for 10 min each on a rocking platform and embedded in the first expansion gel solution (18.5% (w/v) SA + 10% AAm (w/v) + 0.1% (w/v) DHEBA + 0.25% (v/v) TEMED + 0.25% (w/v) APS in 1× PBS). Gelation proceeded for 10-15 min at room temperature (RT) and then for 1.5 h at 37 °C in a humidified chamber. Coverslips with hydrogels were then incubated in ~4 mL denaturation buffer (200 mM SDS + 200 mM NaCl + 50 mM Tris in MilliQ water, pH 6.8) in 6-well plates for 45 min at 37 °C. Gels were then transferred to denaturation buffer-filled 1.5 mL Eppendorf tubes and incubated at 73 °C for 1 h. Next, the gels were washed twice with PBS for 20 min each and stored in PBS overnight at 4 °C. Gels were then cut and placed in 6-well plates filled with MilliQ water for the first expansion. Water was exchanged twice every 30 min and once for 1 h. Gels expanded between 4.0× and 4.5× according to SA purity (see **pan-ExM-t reagents**).

First round of expansion for brain tissue sections

Brain tissue, previously fixed and sectioned to 70 µm as described in the **Brain perfusion** section, were first incubated in inactivated first expansion gel solution (19% (w/v) SA + 10% AAm (w/v) + 0.1% (w/v) DHEBA in 1× PBS) for 30-45 min on ice and then in activated first expansion gel solution (19% (w/v) SA + 10% AAm (w/v) + 0.1% (w/v) DHEBA + 0.075% (v/v) TEMED + 0.075% (w/v) APS in 1× PBS) for 15-20 min on ice before placing in gelation chamber. The tissue sections were gelled for 15 min at RT and 2 h at 37 °C in a humidified chamber. Next, the tissue-gel hybrids were peeled off of the gelation chamber and incubated in ~4 mL denaturation buffer (200 mM SDS + 200 mM NaCl + 50 mM Tris in MilliQ water, pH 6.8) in 6-well plates for 15 min at 37 °C. Gels were then transferred to denaturation buffer-filled 1.5 mL Eppendorf tubes and incubated at 75 °C for 4 h. The gels were washed twice with 1× PBS for 20 min each and once overnight at RT. Gels were optionally stored in 1× PBS at 4 °C. The samples were then placed in 6-well plates filled with MilliQ water for the first expansion. Water was exchanged three times every 1 h. Gels expanded between ~5× according to SA purity (see **pan-ExM-t reagents**).

Re-embedding in neutral hydrogel

Expanded hydrogels (of both dissociated neuron and tissue samples) were incubated in fresh re-embedding neutral gel solution (10% (w/v) AAm + 0.05% (w/v) DHEBA + 0.05% (v/v) TEMED + 0.05% (w/v) APS) two times for 20 min each on a rocking platform at RT. Immediately after, the residual gel solution was removed by gentle pressing with Kimwipes. Each gel was then sandwiched between one no. 1.5 coverslip and one glass microscope slide. Gels were incubated for 1.5 h at 37 °C in a nitrogen-filled and humidified chamber. Next, the gels were detached from the coverslips and washed two times with 1× PBS for 20 min each on a rocking platform at RT. The samples were stored in 1× PBS at 4 °C. No additional post-fixation of samples after the re-embedding step was performed.

Second round of expansion

Re-embedded hydrogels (of both dissociated neuron and tissue samples) were incubated in fresh second hydrogel gel solution (19% (w/v) SA + 10% AAm (w/v) + 0.1% (w/v) BIS + 0.05% (v/v) TEMED + 0.05% (w/v) APS in 1× PBS) two times for 15 min each on a rocking platform in 4 °C. Each gel was then sandwiched between one no. 1.5 coverslip and one glass microscope slide. Gels were incubated for 1.5 h at 37 °C in a nitrogen-filled and humidified chamber. Next, to dissolve DHEBA, gels were detached from the coverslips and incubated in 200 mM NaOH for 1 h on a rocking platform at RT. Gels were afterwards washed three to four times with 1× PBS for 30 min each on a rocking platform at RT or until the solution pH reached 7.4. The gels were optionally stored in 1× PBS at 4 °C. Subsequently, the gels were labeled with antibodies and pan-stained with NHS ester dyes. Finally, the gels were placed in 6-well plates filled with MilliQ water for the second expansion. Water was exchanged at least three times every 1 h at RT. Gels expanded ~ 4.5× according to SA purity (see **pan-ExM-t Reagents**) for a final expansion factor of ~16× (dissociated neurons) and ~24× (brain tissue).

Antibody labeling of neurons post-expansion

Samples immunolabeled with Homer1, Bassoon, and PSD-95 were fixed with 4% FA in 1× PBS for 15 min as described in the **Neuron fixation** section, processed with pan-ExM, and incubated overnight (~15 h) with monoclonal anti-Homer1 antibody (abcam, catalog no. ab184955), monoclonal anti-Bassoon antibody (abcam, catalog no. ab82958), or monoclonal anti-PSD-95 antibody (antibodiescinc, catalog no. 75-028) diluted 1:500 in antibody dilution buffer (0.05% TX-100 + 0.05% NP-40 + 0.2% BSA in 1× PBS). All primary antibody incubations were performed on a rocking platform at 4 °C. Gels were then washed with 0.1% (v/v) TX-100 in 1× PBS twice

for 20 min each on a rocking platform at RT and once overnight (~15 h) at 4 °C. Next, samples were incubated overnight with ATTO594-conjugated anti-mouse antibodies (Sigma-Aldrich, catalog no. 76085) or ATTO594-conjugated anti-rabbit antibodies (Sigma-Aldrich, catalog no. 77671) diluted 1:500 in antibody dilution buffer. All secondary antibody incubations were performed on a rocking platform at 4 °C. The gels were subsequently washed in 0.1% (v/v) TX-100 in 1× PBS twice for 20 min each at RT and once overnight at 4 °C. Gels were stored in PBS at 4 °C until subsequent treatments. Bovine serum albumin (BSA; catalog no. 001-000-162) was purchased from Jackson ImmunoResearch and NP-40 (catalog no. T8786) and Triton X-100 (TX-100; catalog no. T8787) was purchased from Sigma-Aldrich.

Samples immunolabeled with both Homer1 and Bassoon simultaneously were fixed with 4% FA in 1× PBS for 15 min as described in the **Neuron fixation** section, processed with pan-ExM, and incubated overnight (~15 h) with both monoclonal anti-Homer1 antibody (abcam, catalog no. ab184955) and monoclonal anti-Bassoon antibody (abcam, catalog no. ab82958) diluted 1:500 in antibody dilution buffer (0.05% TX-100 + 0.05% NP-40 + 0.2% BSA in 1× PBS). Primary antibody incubations were performed on a rocking platform at 4 °C. Gels were then washed with 0.1% (v/v) TX-100 in 1× PBS twice for 20 min each on a rocking platform at RT and once overnight (~15 h) at 4 °C. Next, samples were incubated overnight (~15 h) with both ATTO594-conjugated anti-rabbit antibodies (Sigma-Aldrich, catalog no. 77671) and ATTO647N-conjugated anti-mouse antibodies (Sigma-Aldrich, catalog no. 50185) diluted 1:500 in antibody dilution buffer. Secondary antibody incubations were performed on a rocking platform at 4 °C. The gels were subsequently washed in 0.1% (v/v) TX-100 in 1× PBS twice for 20 min each at RT and once overnight at 4 °C. Gels were stored in PBS at 4 °C until subsequent treatments.

Samples immunolabeled with Synaptophysin were fixed with 3% FA + 0.1% GA 1× PBS as described in the **Neuron fixation** section, processed with pan-ExM, and incubated for ~36-40 h at 37° C with rabbit anti-synaptophysin (Cell signaling technology, catalog no. 36406) diluted 1:250 in antibody dilution buffer (2% (w/v) BSA in 1× PBS). Gels were then washed in PBS-T (0.1% (v/v) Tween 20 in 1× PBS) three times for 20 min each on a rocking platform at RT. Next, samples were incubated for ~16-20 h at 37°C with donkey anti-rabbit CF568 (Biotium, catalog no. 20098) diluted 1:250 in antibody dilution buffer. The gels were washed in PBS-T three times for 20 min each at RT each before subsequent pan-staining.

Antibody labeling of brain tissue samples post-expansion

Brain tissue samples immunolabeled with Homer1, Bassoon, PSD-95, and Synaptophysin were previously fixed with 4% FA + 20% AAm in 1× PBS overnight at 4 °C and sectioned to 70 µm as described in the **Brain perfusion** section. Next, they were washed three times with 1× PBS for 30 min each on a rocking platform at RT and processed with the pan-ExM-t protocol with this modification: the monomer composition of the second expansion hydrogel was 10% (w/v) AAm + 9% SA (w/v). Samples were subsequently incubated for ~30 h with monoclonal anti-Homer1 antibody (abcam, catalog no. ab184955), monoclonal anti-Bassoon antibody (abcam, catalog no. ab82958), monoclonal anti-PSD-95 antibody (antibodiescinc, catalog no. 75-028), or anti-Synaptophysin antibody (SYSY, catalog no. 101 011) diluted 1:250 in antibody dilution buffer (0.05% TX-100 + 0.05% NP-40 + 0.2% BSA in 1× PBS). All primary antibody incubations were performed on a rocking platform at 4 °C. Next, samples were incubated for ~30 h with ATTO594-conjugated anti-mouse antibodies (Sigma-Aldrich, catalog no. 76085) or ATTO594-conjugated anti-rabbit antibodies (Sigma-Aldrich, catalog no. 77671) diluted 1:250 in antibody dilution buffer. Gels were then washed in 0.1% (v/v) TX-100 in 1× PBS four times for 30 min to 1 h each on a

rocking platform at RT and once overnight at 4 °C. All secondary antibody incubations were performed on a rocking platform at 4 °C. The gels were subsequently washed in 0.1% (v/v) TX-100 in 1× PBS four times for 30 min to 1 h each on a rocking platform at RT and once overnight at 4 °C. Gels were stored in PBS at 4 °C until subsequent treatments.

Brain tissue samples immunolabeled with GFAP, MBP, and GFP were previously fixed with 4% FA + 20% AAm in 1× PBS overnight at 4 °C and sectioned to 70 μm as described in the **Brain perfusion** section. Next, they were washed three times with 1× PBS for 30 min each on a rocking platform at RT and processed with the pan-ExM-t protocol. Samples were subsequently incubated for ~30 h with polyclonal anti-GFAP antibody (Thermofisher, catalog no. PA1-10019), monoclonal anti-MBP (BioLegend, catalog no. 808401), or polyclonal anti-GFP (Thermofisher, catalog no. A-1122) diluted 1:500 in antibody dilution buffer (0.05% TX-100 + 0.05% NP-40 + 0.2% BSA in 1× PBS). All primary antibody incubations were performed on a rocking platform at 4 °C. Gels were then washed in 0.1% (v/v) TX-100 in 1× PBS four times for 30 min to 1 h each on a rocking platform at RT and once overnight at 4 °C. Next, samples were incubated for ~30 h with ATTO594-conjugated anti-mouse antibodies (Sigma-Aldrich, catalog no. 76085) or ATTO594-conjugated anti-rabbit antibodies (Sigma-Aldrich, catalog no. 77671) diluted 1:500 in antibody dilution buffer. Gels were then washed in 0.1% (v/v) TX-100 in 1× PBS four times for 30 min to 1 h each on a rocking platform at RT and once overnight at 4 °C. All secondary antibody incubations were performed on a rocking platform at 4 °C. The gels were subsequently washed in 0.1% (v/v) TX-100 in 1× PBS four times for 30 min to 1 h each on a rocking platform at RT and once overnight at 4 °C. Gels were stored in PBS at 4 °C until subsequent treatments.

NHS ester pan-staining of neurons

After antibody labeling, gels were incubated for 1.5 h with 20 µg/mL NHS ester-ATTO532 (Sigma-Aldrich, catalog no. 88793) (Homer1, Bassoon, PSD-95, centriole, and NPC samples), or 20 µg/mL NHS ester-ATTO488 (Sigma-Aldrich, catalog no. 41698) (Synaptophysin samples), or 20 µg/mL NHS ester-ATTO594 (Sigma-Aldrich, catalog no. 08741) (mitochondria samples), dissolved in 100 mM sodium bicarbonate solution (Sigma-Aldrich, catalog no. SLBX3650) on a rocking platform at RT. The gels were subsequently washed four to six times in either 1× PBS or PBS-T for 20 min each on a rocking platform at RT.

NHS ester pan-staining of brain tissue sections

Gels were incubated for 2 h with either 30 µg/mL NHS ester-ATTO594 (Sigma-Aldrich, catalog no. 08741) (ultrastructural samples in **Fig. 11**) or 30 µg/mL NHS ester-ATTO532 (Sigma-Aldrich, catalog no. 88793) (all immunolabeled and lipid-stained samples), dissolved in 100 mM sodium bicarbonate solution on a rocking platform at RT. The gels were subsequently washed four to six times in either 1× PBS or PBS-T for 20 min each on a rocking platform at RT.

Palmitate pan-staining of neurons

Live and dissociated 80%-confluent hippocampal neurons were incubated with 50 µM azide-functionalized palmitate (Thermofisher, catalog no. C10265) diluted in delipidated medium (DMEM + 10% charcoal-stripped FBS; Thermofisher, catalog no. A3382101) for 5 h at 37 °C and 5% CO2. Next, the neurons were fixed with 3% FA + 0.1% GA in 1× PBS for 15 min at RT and processed according to the pan-ExM protocol. Prior to NHS ester pan-staining with ATTO532 , CuAAC (Copper(I)-catalyzed Azide-Alkyne Cycloaddition) was performed using the Click-iT Cell Reaction Buffer Kit (Thermo Fisher, catalog no. C10269) according to manufacturer instructions. Alkyne-functionalized ATTO590 dye (Sigma-Aldrich, catalog no. 93990) was used

at a concentration of 5 μM. After CuAAC, the gels were washed twice with 2% (w/v) delipidated BSA (Sigma Aldrich, catalog no. A4612) in 1× PBS for 20 min each on a rocking platform at RT and twice with 1× PBS for 20 min each at RT.

SYTOX Green staining post-expansion

pan-ExM and pan-ExM-t processed gels were incubated with SYTOX Green (Invitrogen, catalog no. S7020) diluted 1:5,000 (dissociated neuron samples) and 1:3,000 (brain tissue samples) in 1× PBS for 30 min on a rocking platform at RT. The gels were then washed three times with PBS-T for 20 min each on a rocking platform at RT.

pan-ExM and pan-ExM-t sample mounting

After expansion, the gels were mounted on glass-bottom dishes (35 mm; no. 1.5; MatTek). A clean 18-millimeter diameter coverslip (Marienfeld, catalog no. 0117580) was put on top of the gels after draining excess water using Kimwipes. The samples were then sealed with two-component silicone glue (Picodent Twinsil, Picodent, Wipperfürth, Germany). After the silicone mold hardened (typically 15–20 min), the samples were stored in the dark at 4 °C until they were imaged.

Image acquisition

All confocal images were acquired using a Leica SP8 STED 3X equipped with a SuperK Extreme EXW-12 (NKT Photonics) pulsed white light laser as an excitation source and a Onefive Katana-08HP pulsed laser as depletion light source (775-nm wavelength). Images were acquired using either an HC FLUOTAR L 25×/0.95 NA water objective, APO 63×/1.2 NA water objective, or an HC PL APO 86×/1.2 NA water CS2 objective. Application Suite X software (LAS X; Leica Microsystems) was used to control imaging parameters. ATTO532 was imaged with 532-nm excitation. ATTO594 was imaged with 585-nm excitation. CF568 was imaged with 568-nm

excitation. ATTO647N was imaged with 647-nm excitation. ATTO488 and SYTOX Green were imaged with 488-nm excitation.

Image processing

Images were visualized, smoothed, gamma-, and contrast-adjusted using FIJI/ImageJ software. STED and confocal images were smoothed for display with a 0.4 to 1.5-pixel sigma Gaussian blur. Minimum and maximum brightness were adjusted linearly for optimal contrast.

All line profiles were extracted from the images using the Plot Profile tool in FIJI/ImageJ. Stitching of tiled images was performed using the Pairwise Stitching tool in FIJI/ImageJ.

Neuron expansion factor calculation

Images of hippocampal mouse and rat neuron cell nuclei in non-expanded and pan-ExM expanded samples stained with SYTOX Green (1:5,000) were acquired with a Leica SP8 STED 3X microscope using a HCX PL Fluotar 10×/0.30 dry objective. Average nuclear cross-sectional areas were determined using FIJI/ImageJ software. To calculate the expansion factor, the average nuclear cross-sectional area in pan-ExM samples was divided by the average nuclear cross-sectional area of non-expanded samples. The square root of this ratio represents an estimate of the linear expansion factor. For nuclei cross-section measurements in pan-ExM samples, 38 nuclei were analyzed from 4 independent experiments. For nuclei cross-section measurements in non-expanded samples, 279 nuclei were analyzed from 4 independent experiments.

Using 2-pixel thick line profiles in FIJI, the peak-to-peak distances between the intensity distributions of the dense projection (DP) and postsynaptic density (PSD) NHS ester signals in the same samples were measured and divided by the nuclear expansion factor determined above. For this measurement, 44 line profiles were drawn from 4 independent experiments. The DP-PSD

value was determined to be 81.9 nm and was used to convert DP-PSD measurements to expansion factors in all subsequent experiments. Results are summarized in **Fig. 10n.**

General neuron and brain tissue expansion factor calculation

Using 2-pixel thick line profiles in FIJI, the peak-to-peak distances between the intensity distributions of the DP and PSD NHS ester signals were measured and divided by 81.9 nm, the DP-PSD length determined in **Neuron expansion factor calculation**.

Distance between individual DPs calculation

Using 2-pixel thick line profiles in FIJI, the peak-to-peak distances between the intensity distributions of individual dense projections (DPs) were measured and divided by the determined expansion factor. For this measurement, 78 line profiles were drawn from 41 synapses in 6 independent experiments. Results are summarized in **Fig. 10o**.

Measurements of synaptic protein distributions in neurons

Using 2-pixel thick line profiles in FIJI, the peak-to-peak distances between the intensity distributions between Homer1 and PSD, PSD-95 and DP, and Bassoon and PSD were measured and divided by the determined experiment expansion factor. For Bassoon-PSD measurements in neurons, 50 line profiles were drawn from 3 independent samples. For Homer1-DP measurements in neurons, 85 line profiles were drawn from 4 independent samples. For PSD95-DP measurements in neurons, 25 line profiles were drawn from 2 independent samples. Results are summarized in **Fig. 10p**-**s**.

Measurement of anti-Homer1 signal across dilution factors

Neuron samples were labeled with anti-Homer1 primary antibody and ATTO594-conjugated anti-rabbit antibodies as described in Antibody labeling of neurons post-expansion with this modification: Samples were labeled with primary and secondary antibodies both diluted 1:250 or 1:500 or 1:1000.

Relative protein retention was measured by comparing the peak intensity of Homer1 ATTO504 signal from 2-pixel thick line profiles in FIJI drawn across the punctate signal. For *1:250* measurements, 45 peak intensities were recorded from 7 FOVs. For *1:500* measurements, 13 peak intensities were recorded from 3 FOVs. For 1*:1000* measurements, 6 peak intensity measurements were recorded from 1 FOV. Results are summarized in **Supplementary Fig. 7j**.

Assessment of fixation effects in brain tissue ultrastructural preservation

Fix-1 brain tissue samples were previously fixed with 4% FA in 1× PBS overnight at 4 °C and sectioned to 70 µm as described in the **Brain perfusion** section. Next, they were washed three times with 1× PBS for 30 min each on a rocking platform at RT and processed with the pan-ExM-t protocol. *Fix-2* brain tissue samples were previously fixed with 4% FA in 1× PBS overnight at 4 °C and sectioned to 70 µm as described in the **Brain perfusion** section. Next, they were post-fixed in 0.7% FA + 1% AAm in 1× PBS for 7 h at 37 °C, washed three times with 1× PBS for 30 min each on a rocking platform at RT, and processed with the pan-ExM-t protocol. *Fix-3* brain tissue samples were previously fixed with 4% FA in 1× PBS overnight at 4 °C and sectioned to 70 µm as described in the **Brain perfusion** section. Next, they were post-fixed in 4% FA + 20% AAm in 1× PBS for 7 h at 37 °C, washed three times with 1× PBS for 30 min each on a rocking platform at RT, and processed with the pan-ExM-t protocol. *Fix-4* brain tissue samples were previously fixed with 4% FA + 0.1% GA in 1× PBS overnight at 4 °C and sectioned to 70 µm as described in the **Brain perfusion** section. Next, they were post-fixed in 4% FA + 20% AAm in 1× PBS for 12

h at 4°C, washed three times with 1× PBS for 30 min each on a rocking platform at RT, and processed with the pan-ExM-t protocol. *Fix-5* brain tissue samples were previously fixed with 4% FA in 1× PBS overnight at 4 °C and sectioned to 70 μm as described in the **Brain perfusion** section. Next, they were treated with 0.1 mg/mL acryloyl-X, SE (AcX; Thermofisher, catalog no. A20770) in 1× PBS for 3 h at RT, washed three times with 1× PBS for 30 min each on a rocking platform at RT, and processed with the pan-ExM-t protocol. *Fix-6* brain tissue was previously fixed with 4% FA + 20% AAm in 1× PBS overnight at 4 °C and sectioned to 70 μm as described in the **Brain perfusion** section. Next, they were washed three times with 1× PBS for 30 min each on a rocking platform at 4°C and processed with the pan-ExM-t protocol.

Expansion factors were calculated as described in the **General neuron and brain tissue expansion factor calculation** section. For Fix-2 DP-PSD measurements, 38 line profiles were drawn from 6 FOVs. For Fix-3 DP-PSD measurements, 81 line profiles were drawn from 9 FOVs. For Fix-4 DP-PSD measurements, 77 line profiles were drawn from 8 FOVs. For Fix-5 DP-PSD measurements, 74 line profiles were drawn from 9 FOVs. For Fix-6 DP-PSD measurements, 254 line profiles were drawn from 10 FOVs in 3 independent experiments. Results are summarized in **Supplementary Fig. 12**.

To calculate the ECS + lipid membrane (ECS+) fraction, ~250 x 250 μm2 large-FOV images that show predominantly neuropil pan-stained with NHS ester, were processed with a Gaussian blur of 1 sigma (*Fix-1*, *Fix-2* and *Fix-5*) or 0.5 sigma (*Fix-3*, *Fix-4* and *Fix-6*) in Fiji. A mask created with manual thresholding was used to exclude large gaps in the image that do not represent neurites. The images were then thresholded using the Otsu method with 100%, 70%, 50%, and 30% of the automatically determined threshold. The ECS+ fraction was calculated by dividing the total thresholded pixels by the total area represented by the masked pixels. For *Fix-2*, 8 FOVs from 1

independent experiment were processed. For *Fix-3*, 8 FOVs from 1 independent experiment were processed. For *Fix-4*, 8 FOVs from 1 independent experiment were processed. For *Fix-5*, 8 FOVs from 1 independent experiment were processed. For *Fix-6*, 14 FOVs from 3 independent experiments were processed. Results are summarized in **Supplementary Fig. 13**.

Assessment of denaturation effects in brain tissue expansion factor

Denat-4, *Denat-6*, and *Denat-8* brain tissue samples were previously fixed with 4% FA + 20% AAm in 1× PBS overnight at 4 °C and sectioned to 70 μm as described in the **Brain perfusion** section. Next, they were washed three times with 1× PBS for 30 min each on a rocking platform at RT and processed with the pan-ExM-t protocol with these modifications: *Denat-6* samples were denatured for 6 h and *Denat-8* samples were denatured for 8 h.

Expansion factors were calculated as described in the **General neuron and brain tissue expansion factor calculation** section. For *Denat-4* DP-PSD measurements, 50 line profiles were drawn from 3 FOVs. For *Denat-6* DP-PSD measurements, 42 line profiles were drawn from 3 FOVs. For *Denat-8* DP-PSD measurements, 100 line profiles were drawn from 3 FOVs. Results are summarized in **Supplementary Fig. 14**.

Relative protein retention was measured by comparing the peak intensity of DP NHS ester signal from 2-pixel thick line profiles in FIJI. For *Denat-4* measurements, 50 DP peak intensities were recorded from 3 FOVs. For *Denat-6* measurements, 42 DP peak intensities were recorded from 3 FOVs. For *Denat-8* measurements, 48 DP peak intensity measurements were recorded from 3 FOVs. The intensity values were multiplied by the cube of the expansion factor determined for every denaturation condition. Results are summarized in **Supplementary Fig. 14**.

Assessment of SA monomer concentration effects in brain tissue preservation

19SA/19SA, *19SA/9SA*, *9SA/19SA*, and *9SA/9SA* brain tissue samples were previously fixed with 4% FA + 20% AAm in 1× PBS overnight at 4 °C and sectioned to 70 μm as described in the **Brain perfusion** section. Next, they were washed three times with 1× PBS for 30 min each on a rocking platform at RT and processed with the pan-ExM-t protocol with these modifications: the monomer composition of the second expansion hydrogel in *19SA/9SA* samples was 10% (w/v) AAm + 9% SA (w/v); the monomer composition of the first expansion hydrogel in *9SA/19SA* samples was 10% (w/v) AAm + 9% SA (w/v); and the monomer composition of the first and second expansion hydrogels in *9SA/9SA* samples was 10% (w/v) AAm + 9% SA (w/v).

Expansion factors were calculated as described in **the General neuron and brain tissue expansion factor calculation** section. For *19SA/19SA* DP-PSD measurements, 254 line profiles were drawn from 10 FOVs in 3 independent experiments. For *19SA/9SA* DP-PSD measurements, 267 line profiles were drawn from 12 FOVs in 2 independent experiments. For *9SA/19SA* DP-PSD measurements, 88 line profiles were drawn from 6 FOVs in 2 independent experiments. For *9SA/9SA* DP-PSD measurements, 86 line profiles were drawn from 6 FOVs in 2 independent experiments. All results are summarized in **Supplementary Fig. 20e**.

Measurement of synaptic protein distributions in brain tissue

Using 2-pixel thick line profiles in FIJI, the peak-to-peak distances between the intensity distributions between Homer1 and PSD, PSD-95 and DP, and Bassoon and PSD were measured and divided by the determined experiment expansion factor. For Homer1-DP measurements in brain tissue, 120 line profiles were drawn from 5 FOVs in 2 independent experiments. For PSD-95-DP measurements in brain tissue, 113 line profiles were drawn from 3 FOVs in one independent

experiment. For Bassoon-PSD measurements in brain tissue, 74 line profiles were drawn from 3 FOVs in one independent experiment. Results are summarized in **Fig. 12ooo-rrr**.

Measurement of BDP signal in 4-fold expanded brain tissue across fixation conditions

To compare the effect of fixation on lipid retention, brain tissue was fixed with either 4% FA in 1× PBS (FA-fix) or 4% FA+ 0.1% GA in 1× PBS (*FA/GA-fix*) overnight at 4 °C and sectioned to 70 µm as described in the **Brain perfusion** section. Several *FA/GA-fix* tissue sections were post-fixed with 0.01% osmium tetroxide in 1× PBS for 1h at RT (*FA/GA/OsO4-fix*), washed three times with 1× PBS at RT, and stored in 4 °C until subsequent treatment. All tissue sections were post-fixed in 4% FA + 20% AAm in 1× PBS for 15 h at 4 °C, washed three times with 1× PBS for 30 min each on a rocking platform at 4°C, and processed only with the **First round of expansion for brain tissue** protocol with this modification: tissue sections were denatured in SDS buffer for 1 h. For NHS ester pan-staining, gels were incubated with 10 µg/mL NHS ester ATTO532 (Sigma-Aldrich, catalog no. 88793) in 1× PBS for 30 min on a rocking platform at RT and washed three times with 1× PBS for 30 min each. For BDP pan-staining, gels were incubated with 10 µM BODIPY TR Methyl Ester (Thermofisher, catalog no. C34556) in 1× PBS for 1 h on a rocking platform at RT and washed three times with 1× PBS for 30 min each. Gels were subsequently expanded in MilliQ water and imaged.

BDP pan-staining signal in axons was measured by recording the peak intensity of BDP signal from 10-pixel thick line profiles drawn across the width of axons in FIJI. For *FA-fix* measurements, 46 peak intensities were recorded from 5 FOVs. For *FA/GA-fix* measurements, 46 peak intensities

were recorded from 5 FOVs. For *FA/GA/OsO4-fix* measurements, 38 peak intensities were recorded from 5 FOVs. Results are summarized in **Supplementary Fig. 24bb**.

Measurement of BDP signal in 4-fold expanded brain tissue across denaturation conditions

To compare the effect of fixation on lipid retention, brain tissue was fixed with 4% FA+ 0.1% GA in 1× PBS overnight at 4 °C and sectioned to 70 µm as described in the **Brain perfusion** section. All tissue sections were post-fixed in 4% FA + 20% AAm in 1× PBS for 15 h at 4 °C, washed three times with 1× PBS for 30 min each on a rocking platform at 4°C, and processed only with the **First round of expansion for brain tissue** protocol with this modification: tissue sections were denatured with either SDS buffer at 75°C for 1 h (*SDS-1h*), or SDS buffer at 75°C for 4 h, (*SDS-4h*), non-denatured (**PBS**), or denatured with guanidine hydrochloride (*G-HCl*) buffer (6 M G-HCl + 5 mM DTT + 50 mM Tris in MilliQ water, pH 7.5) at 42°C overnight. For NHS ester pan-staining, gels were incubated with 10 µg/mL NHS ester ATTO532 (Sigma-Aldrich, catalog no. 88793) in 1× PBS for 30 min on a rocking platform at RT and washed three times with 1× PBS for 30 min each. For BDP pan-staining, gels were incubated with 10 µM BODIPY TR Methyl Ester (Thermofisher, catalog no. C34556) in 1× PBS for 1 h on a rocking platform at RT and washed three times with 1× PBS for 30 min each. Gels were subsequently expanded in MilliQ water and imaged.

BDP pan-staining signal in axons was measured by recording the peak intensity of BDP signal from 10-pixel thick line profiles drawn across the width of axons in FIJI. For *SDS-1h* measurements, 40 peak intensities were recorded from 4 FOVs. For *SDS-4h* measurements, 20 peak intensities were recorded from 1 FOV. For *PBS* measurements, 41 peak intensities were

recorded from 2 FOVs. For *G-HCl* measurements, 24 peak intensities were recorded from 1 FOV. Results are summarized in **Supplementary Fig. 27k**.

BDP pan-staining signal in mitochondria was measured by recording the peak intensity of BDP signal from 10-pixel thick line profiles drawn across the width of mitochondria in FIJI. For *SDS-1h* measurements, 40 peak intensities were recorded from 4 FOVs. For *SDS-4h* measurements, 18 peak intensities were recorded from 1 FOV. For *PBS* measurements, 41 peak intensities were recorded from 2 FOVs. For *G-HCl* measurements, 20 peak intensities were recorded from 1 FOV. Results are summarized in **Supplementary Fig. 27l**.

Measurement of pacSph pan-staining signal across UV irradiation conditions

To compare the effect of fixation on lipid retention, brain tissue was fixed with 4% FA+ 20% AAm in 1× PBS overnight at 4 °C and sectioned to 70 µm as described in the **Brain perfusion** section. Sections were incubated in 50 µM pacSph (PhotoClick Sphingosine; Avanti Polar Lipids, catalog no. 900600) in 1× PBS overnight at 4 °C, washed three times in 1× PBS for 1 h each at 4 °C, and either stored at 4 °C (*noUV*) or photo-crosslinked. Samples that were photo-crosslinked were kept on ice and irradiated with 365 nm UV light source 1 cm away from an 8W lamp surface for 30 min on both section surface sides, either before hydrogel embedding (*UV-before*) or immediately after **First round of expansion for brain tissue** while the tissue-hydrogel hybrid was still sandwiched between a glass microscope slide and glass coverslip (*UV-after*). Samples were processed with the remaining steps of the pan-ExM-t protocol with this modification: before NHS ester pan-staining, CuAAC was performed using the Click-iT Protein Reaction Buffer Kit (Thermo Fisher, catalog no. C10276) according to manufacturer instructions. Azide-functionalized ATTO590 dye (ATTO-TEC, catalog no. AD 590-101) was used at a concentration of 5 µM. After

CuAAC, the gels were washed once with 2% (w/v) delipidated BSA (Sigma Aldrich, catalog no. A4612) in 1× PBS for 20 min each and three times with 1× PBS for 20 min each on a rocking platform at RT.

pacSph pan-staining signal in mitochondria was measured by recording the peak intensity of ATTO590 signal from 10-pixel thick line profiles drawn across the width of mitochondria in FIJI. For *noUV* measurements, 35 peak intensities were recorded from 5 FOVs in one independent experiment. For *UV-before* measurements, 37 peak intensities were recorded from 5 FOVs in one independent experiment. For *UV-after* measurements, 39 peak intensities were recorded from 5 FOVs in one independent experiment. Results are summarized in **Fig. 14m**.

Statistics and reproducibility

For all quantitative experiments, the number of samples and independent reproductions are listed in the figure legends. An unpaired two-tailed t-test in GraphPad Prism 9 was used to analyze the data.

Data availability

The datasets generated and/or analyzed during the current study are available from the corresponding author on reasonable request.

Acknowledgements

We want to thank Mark Lessard for assisting with vibratome sectioning. This work was supported by grants from the Wellcome Trust (203285/B/16/Z) and NIH (P30 DK045735, S10 OD020142).

5. Panception of Adherent Cells

In this chapter, I reproduce my manuscript in preparation titled:

M'Saad O. & Bewersdorf J: *Panception: Pan-cellular Perception*. *(2021)*

My contributions include the development of transmitted light nanoscopy and un-aided eye perception of cell microstructure.

5.1. Abstract

The spatial resolution and color depth perception of the human eye is limited, restricting our ability to directly see subcellular structures. We report a new principle for un-aided eye cellular visualization in a method we call pan-cellular perception (panception). By expanding cells 20-fold linearly and pan-staining their bulk with light-scattering molecules of sufficient density, cells and their microstructures can be discerned with a contrast visible to the unaided eye.

5.2. Introduction

Fluorescence microscopy is one of the major light microscopy modalities in the life sciences. It uses refractive lenses to magnify objects of interest and relies on fluorescent labels that induce a highly sensitive contrast [43]. Fluorescence can be detected in single-molecule amounts, making it an ideal contrast mechanism to image the distribution of proteins on the nanoscale [45]. In super-resolution microscopy (SRM), selectively switching fluorophores in a diffraction limited volume

allows up to ~10 nm isotropic spatial resolution in cells and tissue samples, revealing precise sub-cellular protein distributions on the nanoscale [1][4].

The physical magnification of a fixed biological sample itself is also possible in a technique known as Expansion Microscopy (ExM) [6][7][8][9][10][12]. Here a sample is crosslinked to a polyacrylate hydrogel, mechanically homogenized, labeled with fluorescent molecules, and swelled 4- to 20-fold linearly in pure water. To capture nanoscale information, expanded samples are usually imaged on fluorescence microscopes and the total image magnification is the product between both physical and optical magnifications [6]. Using high-end confocal systems, the lateral spatial resolution achieved with ExM techniques ranges from 15 nm to 60 nm, depending on the expansion factor.

In our previous work, we demonstrated that by expanding cells 20-fold linearly while simultaneously retaining the proteins, bulk- (pan-) staining of the protein content can resolve local protein densities and reveal ultrastructural context by standard light microscopy [42]. We call this method pan-ExM. Analogous to electron microscopy (EM), organelle nanoarchitecture can now be imaged without the need for specific labels and with a lateral spatial resolution of ~15 nm.

While optical instrumentation is the common approach to visualizing cells, we wondered whether cells (~10 µm) and their microstructures (~5 µm) can be discerned with the human lens alone, without relying on additional optical manipulation. Such a development would represent a new way of studying biological microstructures, circumventing the need for an intermediary apparatus.

In fact, if a typical HeLa cell is expanded 20-fold linearly, its width would approach ~50 µm × 20 = ~1 mm. Since the human eye has a resolution of 35-60 seconds of arc, it could, at distance of ~1 cm, in principle, discern between objects that are ~100 µm apart, such as the fine microstructures

of an expanded HeLa cell [144]. However, after 20-fold linear expansion, the protein content of the cell (~1.1 mM [2]) will volumetrically expand 20^3=8,000-fold, resulting in a ~140 nM diluted protein content. Because of our limited color depth perception, we unfortunately cannot detect pigments at comparable concentrations.

We hypothesized that physical magnification of cells combined with an amplified and chromogenic pan-staining would result in a visible cellular contrast, with microstructures ultimately resolvable by the un-aided eye. We speculated that if we pan-stained expanded cells with peroxidases or photo-initiators and amplified the underlying chromogenic substrate signal 10^3-10^6-fold, the resulting 0.14-140 mM pigment concentration would be easily detected by the unaided eye. Earlier studies determined that horseradish peroxidase (HRP) amplification coupled with 3,3′-diaminobenzidine (DAB) deposition [145] and photopolymerization-based signal amplification (PBA) [146] can yield amplification degrees of equivalent order of magnitudes, strengthening the feasibility of our approach.

Based on this principle, we developed pan-cellular perception (panception), a method where biological samples are expanded, pan-stained, and their pan-stain amplified to yield a chromogenic product visible by the un-aided eye.

We further combine panception with transmitted light microscopy modalities and demonstrate that many ultrastructural features, detected previously with fluorescence approaches, can now be revealed with transmitted light alone. This finding suggests that in the context of an expanded sample, single-molecule sensitivity, a property of fluorescence molecules, is not a necessary requirement for nanoscale structural imaging. If two proteins are separated by a sufficient expansion factor, and their pan-stain signal is amplified, nanoscopic features can be revealed with simple magnification optics given that the amplification products do not blur.

5.3. Results

5.3.1. Panception with HRP amplification

Figure 15A outlines the basic workflow of our panception workflow. Cells are first expanded 20-fold with the pan-ExM protocol (see **Methods**), pan-stained with amine reactive NHS ester ligands conjugated to biotin (NHS-PEG4-Biotin) and incubated with streptavidin conjugated to horse radish peroxidase (ST-HRP). The pan-stained hydrogel sample is then sectioned to ~1 mm thickness and stained with chromogenic substrates 3,3′-diaminobenzidine (DAB), aminoethyl carbazole (AEC), or EnzMet metallic silver. The sample is then washed with water and visualized directly.

Figure 15B-E confirms the validity of our concept. Taken with an iPhone 11 camera, panception gels reveal individual cells and their microstructures. We found that DAB, AEC, and EnzMet substrates yielded exceptionally visible brown, red, and black chromogenic contrast respectively, with EnzMet metallography showing cell-stained hydrogels with almost no background signal at all. We can easily discern cellular boundaries, the cell cytosol, the nucleus, and occasionally the nucleolus by eye (**Fig. 15F, Supplementary Fig. 1**).

Furthermore, we found that imaging these samples with transmitted light can reveals sub-cellular features at higher magnifications and with exceptional contrast. **Fig. 15G** and **Fig. 15H** show dark nucleoli stained with DAB and EnzMet respectively. Mitochondria cristae, the nuclear envelope, and nuclear pore complexes (NPCs) can also be discerned (**Fig. 15I-K**). These images resemble those acquired with fluorescently pan-stained cells in pan-ExM but have the benefits of (1) no susceptibility to photobleaching and (2) no degradation of staining over time. The ability to resolve

mitochondria cristae which are ~70 nm apart [25], also suggests that blurring of features from signal amplification is of minimal occurrence on that scale.

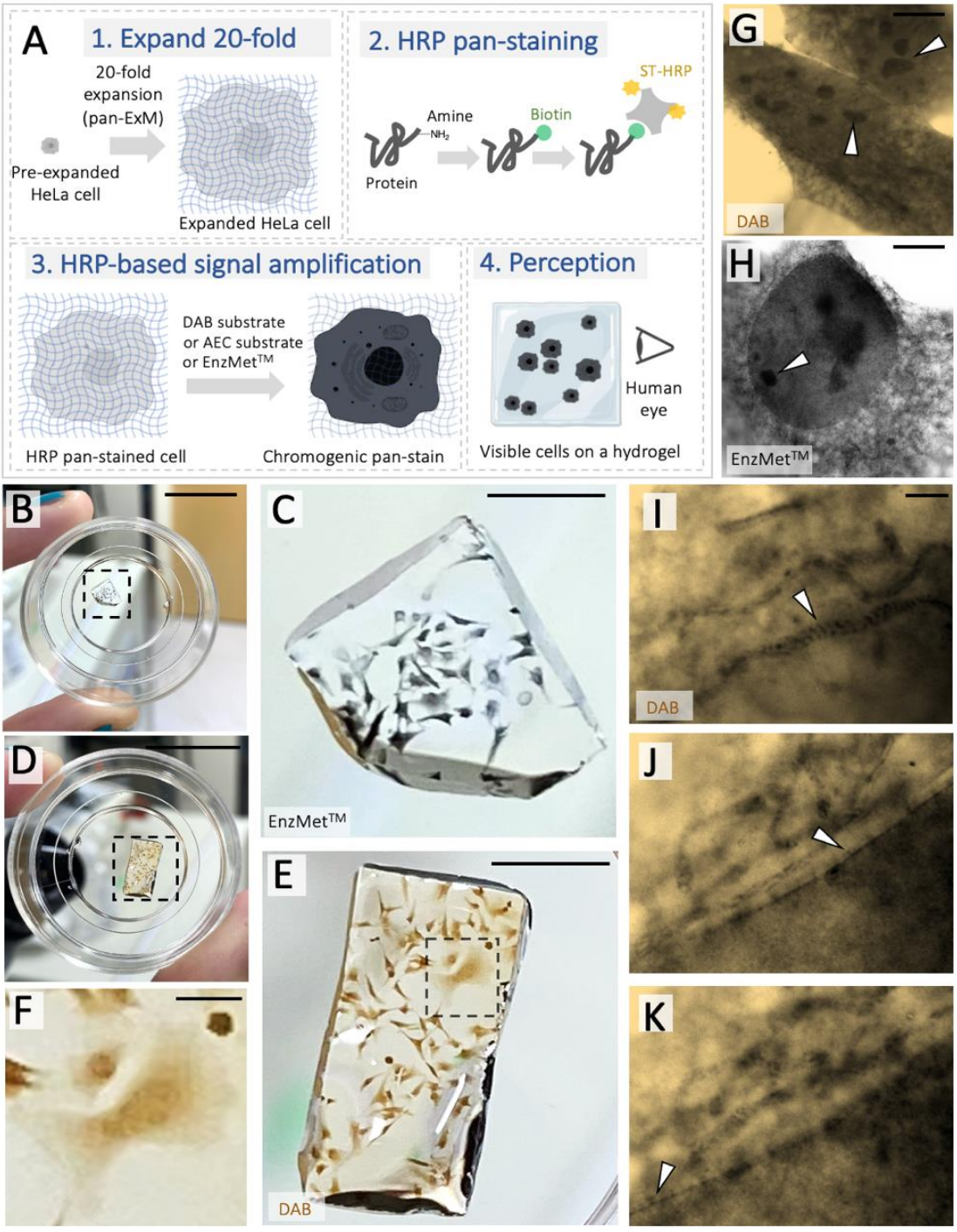

Figure 15: panception with HRP-amplification reveals HeLa cells with the unaided eye. A, Experimental workflow. **B**, Top view of an EnzMet-stained panception sample on a MatTek dish held by hand. **C**, Magnified view of the area

outlined by the black box in **B**. **D**, DAB-stained panception sample. **E**, Magnified view of the area outlined by the black box in **D. F,** Magnified view of the area outlined by the black box in **E**. **G**, Transmitted light microscopy image of an EnzMet-stained panception sample. **H,** Transmitted light microscopy image of a DAB-stained panception sample. White arrows in **G** and **H** point to nucleoli. **I-J**, Transmitted light microscopy images of the edge of a DAB-stained HeLa cell in the same field of view but with different z-positions. White arrow in **I** points to mitochondria cristae. White arrows in **J** and **K** point to nuclear pore complexes (NPCs). Panels **G** and **I-K** are displayed with a yellow background to distinguish from EnzMet™ images. Scale bars are not corrected for the expansion factor. Scale bars, (**B**, **D**) 1 cm, (**C**, **E**), 400 μm, (**F**) 800 μm, (**G**, **H**) 100 μm, (**I-J**) 1 μm.

5.3.2. Panception with Eosin-Y photopolymerization

Next, we questioned whether amplifying the pan-stain using *in situ* polymerization could also render HeLa cells visible by eye and perhaps confer a certain structural sturdiness to the enlarged cells in question. Such development would allow for an orthogonal method of panception, widening its applicability in biological studies.

To amplify pan-stained proteins using *in situ* polymerization, we used a strategy called photopolymerization-based signal amplification (PBA). PBA is commonly used to amplify signals from antibody-antigen binding in immunoassays [147]. Usually, antigens bind to immobilized antibodies and so-called capture antibodies that are conjugated to photo-initiators are introduced. These also bind the antigens and when irradiated with light, in the presence of hydrogel monomers and catalysts, initiate free radical polymerization. PBA is spatially confined to the photo-initiator and yields a polymer film of ~10-250 nm-thickness, depending on the hydrogel monomer composition and photo-initiator density [146].

Most PBA methods use eosin (**Fig. 16A**) as a photo-initiator because it is a high triplet yield fluorophore, and it can partially regenerate in oxygen [148]. Coupled with tertiary amine methyl

diethanolamine (MDEA) and under 530 nm green light irradiation, eosin and MDEA undergo energy transfer and initiate free radical polymerization in the presence of commonly used hydrogel monomers and crosslinkers [148][149].

PBA has also been demonstrated to amplify fluorescence signal in several immunofluorescence studies [150][151]. For example, one study used eosin light-initiated polyethylene (glycol) diacrylate (PEGDA) polymer films to entrap fluorescent nanoparticles onto microtubules, resulting in up to ~10^3 amplification of fluorescence signal [151]. Here, we questioned whether expanded cells pan-stained with eosin can be used to synthesize a densely crosslinked polyacrylamide hydrogel *in situ.* The photopolymer would be ideally capable on entrapping small chromogenic dyes, amplifying the pan-stain accordingly.

Since the cell protein content is significantly diluted following sample expansion (~140 nM), we first tested if eosin surface densities of equivalent concentrations can still initiate photopolymerization. In a solution of 38% (w/v) acrylamide (AAm), 35 mM N-vinylpyrrolidone (VP), 2% (w/w) methylene bisacrylamide (BIS), and 210 mM MDEA, we added eosin in concentrations of 0.03 µM to 12 µM (**Supplementary Table 4**). The forementioned eosin concentrations correspond to the molarity of proteins in a 20-fold expanded cell had they been originally separated by 5 nm and 40 nm respectively. Irradiating these solutions with 530 nm collimated light with intensities between 12 and 55 mW/cm^2, we confirmed that even at 0.03 µM eosin concentration, a photopolymer can still form, with increased thickness when the gelation solution is purged with nitrogen (**Supplementary Fig. 2**). This finding is consistent with a previous report which determined that the eosin concentration threshold for PEGDA and acrylamide photopolymers is 0.03 µM for 5% conversion in 20 min [152].

Next, we investigated if this photopolymer can be labeled with chromogenic dyes. It has been previously shown that Evans Blue (EB) can efficiently stain PEGDA gels [153]. We questioned whether EB could also stain polyacrylamide (pAAm, **Fig. 16F**) and whether it does so without also staining the underlying expansion poly(acrylamide/sodium acrylate) hydrogel (pAAm/SA, **Fig. 16G**). We found that indeed EB stains pAAm gels and not pAAm/SA gels (**Fig. 16B-E**), even when the BIS crosslinker concentration is varied from 0.1% to 2% (w/w) to account for crosslinking density. We hypothesize that this is because EB is sulfonated (**Fig. 16H**) and thus repelled by carboxylic groups in pAAm/SA gels. This finding is also true for the sulfonated textile dye Direct Red 81 (**Supplementary Fig. 3**). However, we chose to use EB in our subsequent experimentation because of its superior visible contrast.

Figure 16I describes the workflow of PBA-based panception in HeLa cells. In brief, cells are first expanded according to the pan-ExM protocol, pan-stained with amine-reactive eosin-5-isothiocynate, incubated in an acrylamide monomer solution with 2% (w/w) BIS concentration, photopolymerized with 530 nm collimated light of 55 mW/cm^2 intensity, and optionally stained with EB.

Indeed, we can observe photopolymerized cells with the un-aided eye (**Fig. 16J-M)**. Even without chromogenic EB staining, photopolymers are still visible against a dark background. This is likely because of the significant polymer refractive index variations between the PBA photopolymer (n> 1.33) and the expansion hydrogel (n~1.33). Like HRP-based panception, we can distinguish between the cellular cytosol and cell nucleus (**Fig. 16K**), delineate cell boundaries, and classify cells by their shapes and sizes. Unlike HRP-based panception however, we can physically excise individual cells with tweezers and manipulate them mechanically (**Supplementary Fig. 4**). This

is due to the mechanical sturdiness of the underlying photopolymer compared to the more fragile and delicate expansion hydrogel.

Moreover, these samples are compatible with phase contrast microscopy. We can observe the fine ultrastructures of nucleoli (**Fig. 17A-B**), filopodia (**Fig. 17C** & **17G**) as well as mitochondria cristae (**Fig. 17D**). Co-staining with fluorescent dyes, correlative imaging shows that PBA and fluorescence images of mitochondria (**Fig. 17D-F**) and filopodia (**Fig. 17G-I**) overlap perfectly.

Finally, our HRP- and PBA-based panception protocols are compatible with mouse brain tissue sections as well (**Fig. 17, Supplementary Fig. 5**). Imaging PBA-processed panception tissue with transmitted light, we can clearly resolve the fine structures of cortical neurons (**Fig. 17J**) as well as axons (**Fig. 17K**). We note that panception shows more overlapping features compared to the counterpart confocal fluorescence images, particularly in thick tissue. This is because our PBA data represent transmitted light images that lack optical sectioning. Combining PBA with 3D phase contrast techniques in the future will substantially enhance image quality.

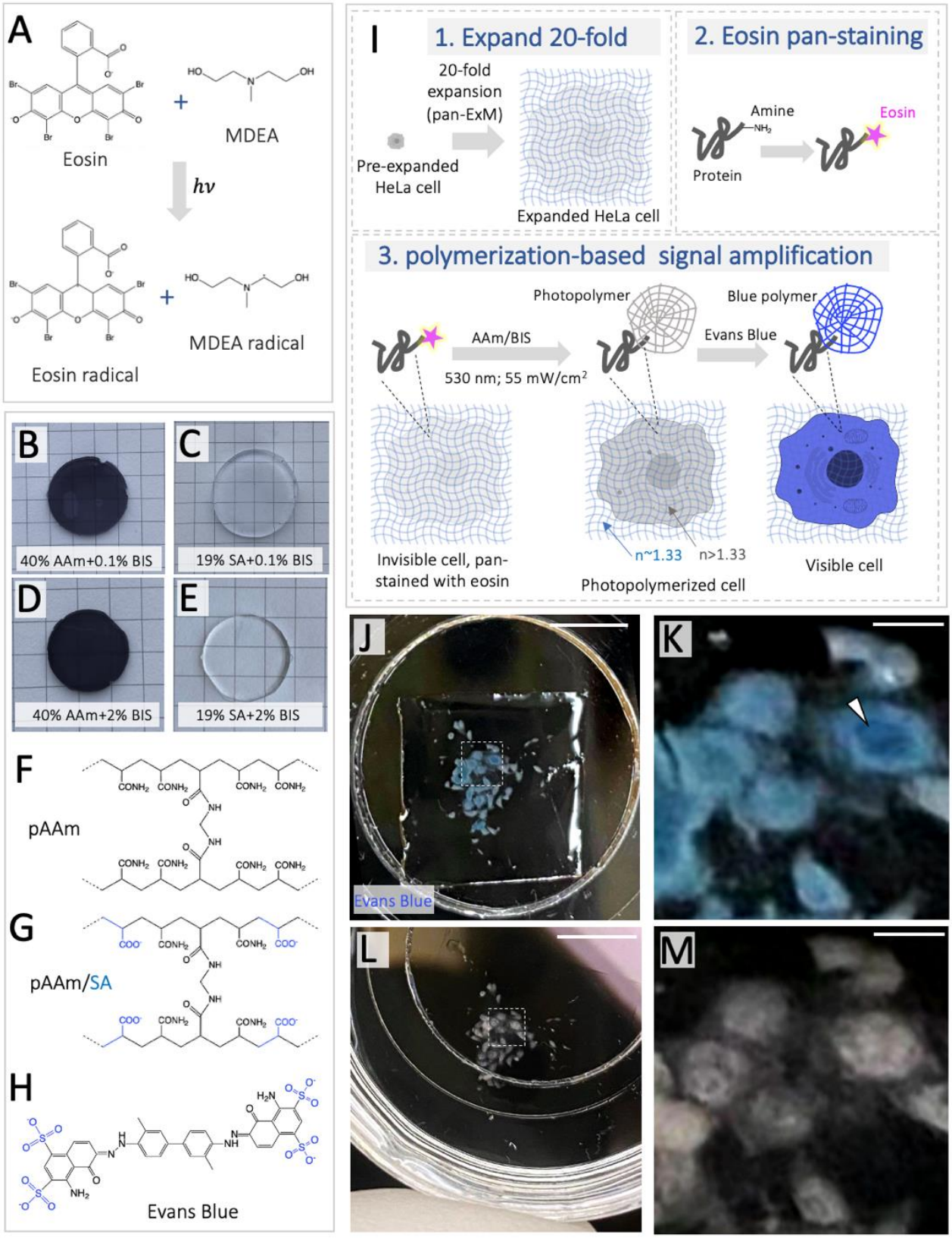
A
Eosin
MDEA
hν
Eosin radical
MDEA radical
I
1. Expand 20-fold
20-fold expansion (pan-ExM)
Pre-expanded HeLa cell
Expanded HeLa cell
2. Eosin pan-staining
Amine
Eosin
Protein
3. polymerization-based signal amplification
Photopolymer
Blue polymer
AAm/BIS
530 nm; 55 mW/cm²
Evans Blue
Invisible cell, pan-stained with eosin
n~1.33
n>1.33
Photopolymerized cell
Visible cell
B
40% AAm+0.1% BIS
C
19% SA+0.1% BIS
D
40% AAm+2% BIS
E
19% SA+2% BIS
F
pAAm
G
pAAm/SA
H
Evans Blue
J
Evans Blue
K
L
M

Figure 16: panception with PBA reveals HeLa cells with the unaided eye. A, The mechanism of light-initiated free-radical generation by eosin and MDEA. **B-E**, Evans Blue, an anionic dye, efficiently stains neutral polyacrylamide hydrogels (**B**, **D**) but not anionic poly(acrylamide/sodium acrylate) co-polymers (**C**, **E**), regardless of hydrogel crosslinker concentration. **F**, Chemical structure of polyacrylamide polymer. **G**, Chemical structure of poly(acrylamide/sodium acrylate) co-polymer (blue: negatively charged carboxylic groups). **H**, Chemical structure of Evans Blue dye (blue: negatively charged sulfate groups that repel carboxylic groups in anionic pAAm/SA hydrogels and prevent their staining. **I**, Experimental workflow. **J,** PBA-stained panception sample stained with Evans Blue visible dye. **K**, Magnified view of the area outlined by the white box in **J**. The white arrow in **K** points to a dark blue cell nucleus. **L**, PBA-stained panception sample that is not stained with Evans Blue. **M**, Magnified view of the area outlined by the white box in **L**. Scale bars are not corrected for the expansion factor. Scale bars, (**J**, **L**) 0.5 cm, (**K**, **M**), 0.5 mm.

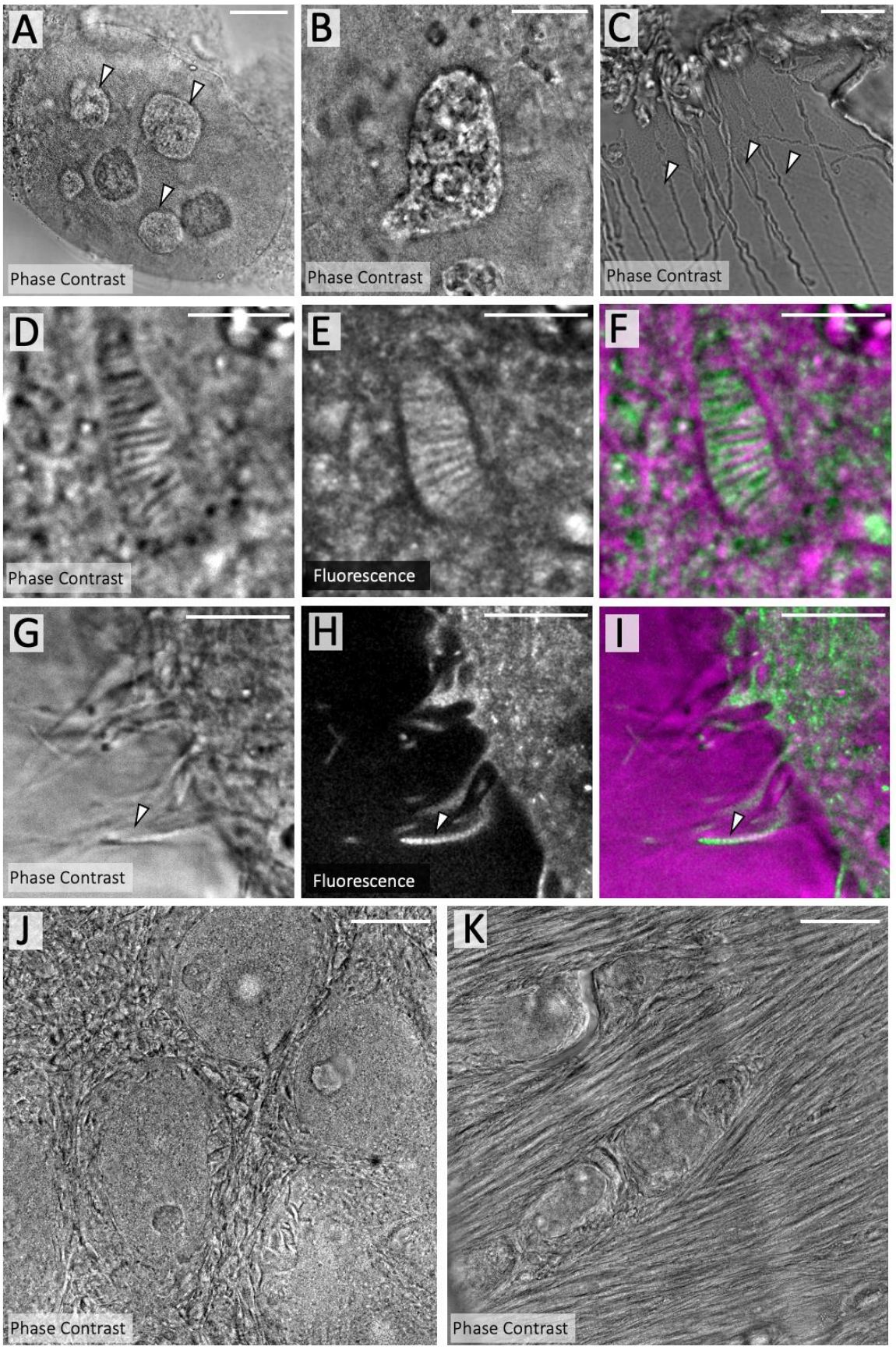
A
Phase Contrast
B
Phase Contrast
C
Phase Contrast
D
Phase Contrast
E
Fluorescence
F
G
Phase Contrast
H
Fluorescence
I
J
Phase Contrast
K
Phase Contrast

Figure 17: panception with PBA reveals sub-cellular features in HeLa cells and mouse brain tissue sections with phase-contrast microscopy. A, PBA-stained cell nucleus showing nucleoli (white arrows). **B**, Magnified view of a PBSA-stained nucleolus showing ultrastructural features. **C**, PBSA-stained HeLa cell filopodia. **D**, PBA-stained mitochondrion showing mitochondria cristae. **E**, Same area as in **D**, showing NHS ester pan-staining. **F**, Overlay of **E** and **D**. **G**, PBSA-stained filopodia. **H**, Same area as in **G**, showing NHS ester pan-staining. **I**, Overlay of **G** and **H**. **J**, PBSA-stained cortical neurons in mouse brain tissue sections. **K**, PBA-stained axons in mouse brain tissue sections**.** Scale bars are not corrected for the expansion factor. Scale bars, (**A**) 40 µm, (**B**, **C**) 20 µm, (**D-F**), 5 µm, (**J,K**), 50 µm.

5.4. Discussion

The data presented demonstrates that by sufficient sample magnification and sufficient signal amplification, cellular microstructures can be revealed without the need for optical instrumentation. While the obtained resolution is too small to reveal ultrastructural details with the unaided eye, larger expansion factors of 100-fold to 1000-fold will render cellular organelles like mitochondria (~500 nm) large enough to see without supplementary optical magnification (~ 100 µm after 200-fold linear expansion).

However, it is important to be cognizant of reaction kinetics when experimenting with larger expansion factors. For example, in the case of the S_N2 nucleophilic substitution reaction of NHS ester with primary amines, the recommended minimum concentration of primary amines before NHS ester hydrolysis becomes dominant is 10 µM [154]. Intermediate amplification steps with streptavidin and biotin [156] at expansion levels of 20-fold will help mediate this problem. In fact, the high affinity ($K_D \sim 10^{-15}$ M) of biotin for streptavidin indicates that this latter can be detected in femto- and pico-molar concentrations [155].

Moreover, our data also demonstrates that fluorescence is not the only contrast mechanism capable of showing ultrastructural details. Simpler and laser-free optical systems such as brightfield and

phase contrast microscopy are well suited to image panception samples. We have shown transmitted light images of nucleoli, mitochondria, filopodia and NPCs at sub-70 nm resolution (**Fig. 15I-K** and **Fig. 17**). However, for panception to reach its full 3D imaging potential and resolve more pan-stained organelles of interest, transmitted light imaging modalities must be implemented with optical sectioning capabilities [157]. Perhaps reflected light confocal microscopy will become popular again [181]. On a positive note, however, these samples cannot be bleached, representing an opportunity to image at essentially infinite signal-to-noise ratio.

Spatial resolution must be evaluated by the structures that can be resolved and not simply the diffraction limit divided by the linear expansion factor. While high amplification magnitudes are desirable for un-aided eye visualization, blurring of features from excessive amplification must be accounted for. To resolve sub-cellular structures at ~20 nm lateral resolution following 20-fold expansion, the layer of amplified polymer or chromogen must not surpass ~75 nm to not blur features of interest.

We have demonstrated here enzyme- (HRP) and photopolymerization- (PBA) based signal amplification in the context of panception imaging. However, other amplification strategies such as nucleic acid-based ones [36] can also be implemented. We have shown contextual imaging by amplifying the pan-stain, but our approach can also be adapted to specific molecule imaging using antibody labels conjugated to HRP or Eosin. Multiplexing is also possible and, in many cases, desirable. One can envision using different color chromogens (e.g., red and blue), different catalytic agents (e.g., alkaline phosphatase (AP) [158]), and different water-soluble photoinitiators (e.g., phenyl-2,4,6-trimethylbenzoylphosphinate (LAP) which is activated with UV light [159]).

While it is unclear what specific biological questions panception can answer that conventional microscopy cannot, we see applications in resource-limited environments (e.g., the space station

and military bases) where high resolution microscopes (e.g., confocal, super-resolution microscopes etc.) are unavailable. For example, identifying contaminating bacterial strains on the space station is notoriously difficult, and current practices are strictly qPCR-based [160]. Combining panception of 100-fold expanded samples with portable magnifying scopes can potentially enable the identification of low-abundance microbes by their shapes. In all cases, we leave it up to the adventurous biologist to explore the proper applications for panception.

Finally, our work here represents the first recorded instance of seeing cellular microstructures by the naked eye and dispels the centuries old conviction that magnifying lenses need to stand in between the human and the specimen. Panception is an opportunity to see and touch a phantom of the building blocks that make us. Previously far beyond what we can see or feel unaided, now they are almost alive, staring back at us, reminding us that we are mere carbon matter.

5.5. Methods

General comments

Please see **Supplementary Tables 1–3** for an overview of the reagents and materials used in this work.

Coverslip preparation

Before plating HeLa, 12-mm round glass coverslips (Electron Microscopy Sciences, catalog no. 72230-01) were cleaned in a sonic bath (Bronson) submerged in 1 M KOH (Macron Fine Chemicals; catalog no. 6984-04) for 15 min and then rinsed with MilliQ water three times. Glass was then sterilized with 100% ethanol and rinsed with sterile phosphate-buffered saline (PBS; Gibco, catalog no. 10010023) before adding media and cells.

Cell culture

HeLa cells were grown in Dulbecco's modified Eagle medium (DMEM; Gibco, catalog no. 21063029), supplemented with 10% fetal bovine serum (FBS; Gibco, catalog no. 10438026), and 1% mL/L penicillin-streptomycin (Gibco, catalog no. 15140122) at 37 °C with 5% CO2. Cells were passaged twice to three times a week and used between passage number 2 and 20. Passaging was performed using 1× PBS and 0.05% Trypsin-EDTA (Gibco, catalog no. 25300054). Approximately 24 h before fixation, cells were seeded on glass coverslips at ~65,000 cells per well.

Cell fixation

Cells were fixed with 3% formaldehyde (FA) and 0.1% glutaraldehyde (GA) (Electron Microscopy Sciences, catalog nos. 15710 and 16019, respectively) in 1× PBS for 15 min at RT. Samples were rinsed three times with 1× PBS and processed according to the pan-ExM protocol immediately after.

Brain perfusion

Thy1-EGFP M (4-8 weeks) mouse was obtained from the Jackson Laboratory. Animal was anesthetized with ketamine (100 mg/kg, Butler Schein: 9952949) and xylazine (10 mg/kg, Akorn: NDC 59399-110-20) in saline (Hudson RCI: 200-59). The mouse was transcardially perfused first with ice cold PBS (Fisher: BP2944-100) and then with 4% PFA (J.T. Baker: S898-07) + 20% acrylamide (Sigma Aldrich: A9099) in PBS, pH 7.4. Brain was isolated and postfixed overnight in 4% PFA + 20% acrylamide in PBS at 4°C. Brain was then washed in PBS and sectioned at 70 μm using vibrating microtome (Leica VT1000, Leica Biosystems, Nussloch, Germany or

Vibratome 1500, Harvard Apparatus, Holliston, MA). Sections were stored in PBS with 0.01% sodium azide (Sigma-Aldrich, St. Louis, MO) at 4°C. All procedures were approved by the Institutional Animal Care and Use Committee and in compliance with National Institutes of Health guidelines.

Polymerization reagents

Acrylamide (AAm; catalog no. A9099), N,N′-(1,2-dihydroxyethylene)bisacrylamide (DHEBA; catalog no. 294381), N,N′-Cystaminebisacrylamide (BAC; catalog no. 9809), N-methyldiethanolamine (MDEA; catalog no. 471828), and N-vinyl-2-pyrrolidone (VP; catalog no. V3409) were purchased from Sigma-Aldrich. Sodium acrylate (SA) was purchased from Santa Cruz Biotechnology (catalog no. sc-236893C). We noticed significant batch-to-batch variability in SA purity. To verify that SA was of acceptable purity, 38% (w/v) solutions were made in water and checked for quality **[37]**. Only solutions that were light yellow were used. Solutions that were yellow and/or had a precipitate were discarded. N,N′-methylenebis(acrylamide) (BIS; catalog no. J66710) was purchased from Alfa Aesar. Solutions with a minimum precipitate were centrifuged at 4000 rpm for 5 min and the supernatant was transferred to a new bottle and stored at 4 °C until use. Ammonium persulfate (APS) was purchased from both American Bio (catalog no. AB00112) and Sigma-Aldrich (catalog no. A3678). N,N,N′,N′-tetramethylethylenediamine (TEMED; catalog no. AB02020) was purchased from American Bio. 10X phosphate buffered saline (10X PBS; catalog no. 70011044) was purchased from Thermofisher.

pan-ExM gelation chamber

The gelation chamber was constructed using a glass microscope slide (Sigma-Aldrich, catalog no. S8400) and two spacers, each consisting of a stack of two no. 1.5 22 × 22 mm coverslips (Fisher

Scientific, catalog no. 12-541B), were glued with superglue to the microscope slide on both sides of the cell-adhered coverslip, with the cell-adhered coverslip glued in between. A no. 1.5 22 × 22 mm coverslip was used as a lid after adding the gel solution. This geometry yielded an initial gel thickness size of ~170 µm.

First round of expansion for HeLa cells

Cells, previously fixed as described in the **Cell fixation** section, were incubated in post-fix solution (0.7% FA + 1% AAm (w/v) in 1× PBS) for 6–7 h at 37 °C. Next, the cells were washed twice with 1× PBS for 10 min each on a rocking platform and embedded in the first expansion gel solution (19% (w/v) SA + 10% AAm (w/v) + 0.1% (w/v) DHEBA + 0.25% (v/v) TEMED + 0.25% (w/v) APS in 1× PBS). Gelation proceeded first for 10-15 min at room temperature (RT) and then for 1.5 h at 37 °C in a humidified chamber. Coverslips with hydrogels were then incubated in ~4 mL denaturation buffer (200 mM SDS + 200 mM NaCl + 50 mM Tris in MilliQ water, pH 6.8) in 6-well plates for 30-45 min at 37 °C. Gels were then transferred to denaturation buffer-filled 1.5 mL Eppendorf tubes and incubated at 74 °C for 1 h. Next, the gels were washed twice with PBS for 20 min each and optionally stored in PBS overnight at 4 °C. Gels were then cut and placed in 6-well plates filled with MilliQ water for the first expansion. Water was exchanged twice every 30 min and once for 1 h. Gels expanded between 4.0× and 4.5× according to SA purity.

First round of expansion for brain tissue sections

Brain tissue, previously fixed and sectioned to 70 µm as described in the **Brain perfusion** section, were first incubated in inactivated first expansion gel solution (18.5% (w/v) SA + 10% AAm (w/v) + 0.1% (w/v) DHEBA in 1× PBS) for 30-45 min on ice and then in activated first expansion gel solution (18.5% (w/v) SA + 10% AAm (w/v) + 0.1% (w/v) DHEBA + 0.075% (v/v)

TEMED + 0.075% (w/v) APS in 1× PBS) for 15-20 min on ice before placing in gelation chamber. The tissue sections were then gelled for 15 min at RT and then for 2 h at 37 °C in a humidified chamber. Next, the brain tissue section-gel hybrids were removed from gelation chamber and incubated in ~4 mL denaturation buffer (200 mM SDS + 200 mM NaCl + 50 mM Tris in MilliQ water, pH 6.8) in 6-well plates for 15 min at 37 °C. Gels were then transferred to denaturation buffer-filled 1.5 mL Eppendorf tubes and incubated at 74 °C for 4 h. The gels were washed twice with PBS for 20 min each and once overnight at RT. Gels were optionally stored in 1× PBS at 4 °C. Gels were then cut and placed in 6-well plates filled with MilliQ water for the first expansion. Water was exchanged three times every 1 h. Gels expanded between 4.0× and 4.5× according to SA purity.

Re-embedding in neutral hydrogel

Expanded hydrogels were incubated in a fresh re-embedding neutral gel solution (10% (w/v) AAm + 0.05% (w/v) DHEBA + 0.05% (v/v) TEMED + 0.05% (w/v) APS) two times for 20 min each on a rocking platform at RT. Immediately after, residual gel solution was removed by extensive but gentle pressing with Kimwipes. The gels were then sandwiched between two pieces of no. 1.5 coverslips and incubated at 37 °C for 1.5 h in a nitrogen-filled humidified chamber. Next, the gels were detached from the coverslip and washed three times with 1× PBS for 200 min each on a rocking platform at RT and optionally stored in 1× PBS at 4 °C. Unlike our previous protocol, no secondary post-fixation was used.

Second round of expansion

For samples that were pan-stained with DAB, AEC, and EnzMet substrates, re-embedded hydrogels were incubated in a fresh second hydrogel gel solution (19% (w/v) SA + 10% AAm

(w/v) + 0.1% (w/v) BIS + 0.05% (v/v) TEMED + 0.05% (w/v) APS in 1× PBS) two times for 15 min each on a rocking platform on ice. For samples that were pan-stained with eosin-5-isothiocyanate, re-embedded hydrogels were incubated in a fresh second hydrogel gel solution (19% (w/v) SA + 10% AAm (w/v) + 0.15% (w/v) BAC + 0.05% (v/v) TEMED + 0.05% (w/v) APS in 1× PBS) two times for 15 min each on a rocking platform on ice. Immediately after, residual gel solution was removed by extensive but gentle pressing with Kimwipes. The gels were then sandwiched between two pieces of no. 1.5 coverslips and incubated at 37 °C for 1.5 h in a humidified nitrogen-filled chamber. To dissolve DHEBA, gels were incubated in 0.2 M NaOH for 1 h on a rocking platform at RT. Gels were next washed three times with 1× PBS for 30 min each on a rocking platform at RT or until the solution pH reached 7.4. The gels were optionally stored in 1× PBS at 4 °C. Subsequently, the gels pan-stained with eosin-5-isothiocyanate, NHS ester-biotin followed by HRP-conjugated streptavidin, or NHS ester-ATTO532 dye and extensively washed with PBS-T. Finally, the gels were cut and placed in 6-well plates filled with MilliQ water for the second expansion. Water was exchanged at least three times every 1 h at RT. Gels expanded ~ 4.0× according to SA purity for a final expansion factor of 16× to 20× and sectioned to a thickness of 1 mm on a Leica VT1000 S vibrating blade microtome.

NHS ester PEG4-biotin pan-staining

Gels were incubated for overnight with 50 µM NHS-PEG4-Biotin (Thermofisher, catalog no. 21330) dissolved in 1× PBS on a rocking platform at 4 °C. The gels were subsequently washed five times in PBS-T for 20 min each on a rocking platform at RT.

Eosin-5-isothiocynate pan-staining

After polymerization-based signal amplification, gels were incubated overnight with 200 µM eosin-5-isothiocyanate (Sigma-Aldrich, catalog no. 45245) dissolved in 100 mM sodium bicarbonate solution (Sigma-Aldrich, catalog no. SLBX3650) on a rocking platform at 4 °C. The gels were subsequently washed three to five times in PBS-T for 20 min each on a rocking platform at RT and washed once overnight at 4 °C.

NHS ester ATTO532 pan-staining

After polymerization-based signal amplification, gels were incubated for 1.5 h with 20 µg/mL NHS ester-ATTO532 (Sigma-Aldrich, catalog no. 88793) dissolved in 100 mM sodium bicarbonate solution on a rocking platform at RT. The gels were subsequently washed three to five times in PBS-T for 20 min each on a rocking platform at RT.

HRP-based signal amplification

After NHS-PEG4-biotin pan-staining, gels were incubated with 1 µg/mL HRP-conjugated streptavidin (Thermofisher, catalog no. N100) in 1× PBS overnight on a rocking platform at RT, washed five times in PBS-T for 20 min each, expanded to its maximum size in MilliQ water, and sectioned with a vibratome as detailed in **Second round of expansion**. Gels were next stained with either DAB (abcam, catalog no. ab64238), AEC (abcam, catalog no. ab64252), or EnzMet™ (Nanoprobes, #6001-30ML) for 3 min, 5 min, and 3 min respectively and according to kit instructions. Staining was stopped by two 5 min MilliQ water exchanges.

Photopolymerization-based signal amplification

After eosin-5-isothiocyanate pan-staining, the gels were incubated in fresh monomer solution (38% AAm (w/v) + 2% BIS (w/w) + 210 mM MDEA + 35 mM VP) two times for 10 min each on

a rocking platform at RT. The samples were then irradiated with 530 nm collimated LED light at 55 mW/cm^2 for 10-20 min or until a photopolymer was visible. The samples were optionally incubated in 1 mg/mL Evans Blue (Sigma, catalog no. E2129) or 2 mg/mL Direct Red 81 (Sigma, catalog no. 195251) for 20 min on a rocking platform at RT and subsequently rinsed with MilliQ water.

Evans Blue hydrogel staining assay

Fig. 2B photopolymer is composed of 210 mM MDEA + 35 mM VP + 40% (w/v) AAm + 0.1% (w/v) BIS + 12.5 µM eosin-5-isothiocyanate. **Fig. 2C** photopolymer is composed of 210 mM MDEA + 35 mM VP + 10% (w/v) AAm + 19% SA (w/v) + 0.1% (w/v) BIS + 12.5 µM eosin-5-isothiocyanate. **Fig. 2D** photopolymer is composed of 210 mM MDEA + 35 mM VP + 40% (w/v) AAm + 2% (w/w) BIS + 12.5 µM eosin-5-isothiocyanate. **Fig. 2E** photopolymer is composed of 210 mM MDEA + 35 mM VP + 10% (w/v) AAm + 19% (w/v) SA + 2% (w/w) BIS + 12.5 µM eosin-5-isothiocyanate. All photopolymers were photopolymerized with 530 nm collimated LED light at 12 mW/cm^2 for 10 min on 30-mm glass MatTek dishes (MatTek life science, catalog no. P50G-1.5-30-F) and stained with 1 mg/mL Evans Blue for 20 min on a rocking platform at RT. Photopolymers were then extensively rinsed with deionized water and photographed with an iPhone 11 camera.

Eosin concentration threshold assay

All photopolymers in **Supplementary Fig. 2** are composed of 210 mM MDEA + 35 mM VP + 40% (w/v) AAm + 2% (w/w) BIS + eosin-5-isothicynate at the indicated concentrations. All photopolymers were polymerized with 530 nm collimated LED light on 30-mm glass MatTek dishes at irradiation intensities and durations described in the figure legend.

Image acquisition

Images shown in **Fig. 1B-E** and **Fig. 2J-M** were acquired using an Apple iPhone 11 camera.

DIC and confocal images were acquired using a Leica SP8 STED 3X equipped with a SuperK Extreme EXW-12 (NKT Photonics) pulsed white light laser as an excitation source. All images were acquired either using a HC FLUOTAR L 25×/0.95 NA water objective or a HC PL APO 63×/1.2 water objective. ATTO532 was imaged with 532-nm excitation. Application Suite X software (LAS X; Leica Microsystems) was used to control imaging parameters.

Image processing

Images were visualized, smoothed, and contrast-adjusted using FIJI/ImageJ software. Confocal images were smoothed for display with a 0.5 to 1-pixel sigma Gaussian blur. Minimum and maximum brightness were adjusted linearly for optimal contrast.

Statistics and reproducibility

For all quantitative experiments, the number of samples and independent reproductions are listed in the figure legends.

Data availability

The datasets generated and/or analyzed during the current study are available from the corresponding author on reasonable request.

Acknowledgements

We would like to thank Phylicia Kidd for assistance with cell culture, Dr. Ilona Kondratiuk for providing mouse brain sample sections, and Hannahmariem Mekbib for LED light collimation. We would also like to thank Dr. Kenny Chung, Dr. James Rothman, and Zach Marin for interesting discussions. This work was supported by grants from the Wellcome Trust (203285/B/16/Z) and NIH (P30 DK045735, S10 OD020142). Both authors filed a patent application with the U.S. patent office covering the presented method (62989158).

6. Conclusions and Outlook

This thesis details my contributions to light microscopy of fixed biological specimen. Previously thought to be strictly within the realm of EM, ultrastructural context imaging is now within the reach of standard light microscopy modalities. My thesis made the conceptual realization that with sufficient sample enlargement and preservation, sample components can be efficiency stained in bulk (pan-stained) with fluorescent dyes (**pan-ExM** and **pan-ExM-t**) or light-scattering chromogens (**panception**), revealing the totality of the fine structures that thoroughly represent a cell. We demonstrated this concept on cultured cells, dissociated neurons, and thick mouse brain tissue sections. We showed that structures like the nuclear envelope, nucleoli, mitochondria cristae, Golgi cisternae, ER tubules, filopodia, NPCs, kinetochores, microtubules, centrioles, chromatin, synapses, pre and postsynaptic densities, blood capillaries, spine apparatuses, axons, dendrites, and cilia can all be revealed with contextual pan-staining alone.

Since the publication of pan-ExM, two reports demonstrated the use of NHS ester pan-stainings in cleared and ~4-fold expanded tissue (FLARE) [39], as well as ~4-fold expanded C. elegans (ExCel) [38]. Virtually every new ExM technique developed after 2020 now incorporates pan-stainings regardless of expansion factor (e.g., TREx [78], Whole-ExM [106], and MAGNIFY [197]). Moreover, in independent labs across the world, pan-ExM was used to resolve individual microtubules in *P. berghei* axoneme [198] and NHS ester pan-staining was used to reveal the disorganization of the rhoptries and the dilated plasma membrane at the apical pole of *Toxoplasma gondii* in the absence of ERK7 protein [199] as well as characterize the ultrastructural phenotype of mini-chromosome maintenance complex binding-protein (MCMBP)-deficient *Plasmodium falciparum* [200]. The adoption of pan-ExM and the widespread use of pan-stainings is a fortunate

outcome of this thesis and we see many more biological insights enabled with these methods in the immediate future.

Certain innovations can help improve pan-ExM, pan-ExM-t, and panception or complement their development. These include:

(1) Development of advanced light sheet microscopes: pan-ExM sample preparation takes approximately three to four days (depending on immunostaining requirements), but multiple samples can be processed in parallel. The rate limiting step is therefore the time it takes to acquire 3D data sets of large tissue volumes (currently limited by the speed of confocal microscopes). pan-ExM would benefit from the development of a new light-sheet microscope which is optimized for extremely large fields of view and has the resolution of a confocal microscope (compatible with high-NA objectives). An ideal light-sheet microscope will speed up imaging by a factor of ~100, shortening data acquisition from hours to minutes.

(2) Automated image segmentation and quantification: pan-ExM data sets are extremely rich in information, but they are impossible to fully analyze manually. Deep-learning algorithms and image analysis pipelines will need to be developed that automatically identify and segment organelles and cellular landmarks from characteristic differential pan-stainings in the pan-ExM datasets.

(3) Novel disulfide-reversible tissue fixatives to enable true molecular decrowding and epitope accessibility. Glutaraldehyde (GA) fixation provides excellent ultrastructural preservation in cells and brain tissue sections but is irreversible and notorious for masking protein antigens. This makes GA incompatible with reliable molecular decrowding and efficient antibody labeling. In pan-ExM, we use the partially reversible fixative formaldehyde (FA)

and only small concentrations of GA (mainly in cell or neuron cultures). This relatively 'weak' fixation should ideally be replaced with stronger fixatives that are also reversible (to ensure subsequent sample expansion). Inspired by EM literature from the 1970s which showed that amine-reactive diimidoesters can preserve fine details as well as antigenicity [204], one could think of testing commercially available disulfide reversible analogs of diimidoesters, such as 3,3'-dithiobispropionimidate (DTBP), whose irreversible analog dimethyl suberimidate (DMS) was shown to preserve the fine structure of liver and other organs similar to GA [204][205][206][207] as well as enable superior immunocytochemical and immunohistochemical reactions relative to GA [206][208][209]. This fixative could potentially transform pan-ExM and enable true molecular decrowding. One could even envision cryogenically fixing cells first (for best preservation) and then using DTBP in the freeze-substitution solution (for subsequent reversible fixation in aqueous solution). Sample preservation is fundamental to ultrastructural visualization and must be optimized carefully. Sample preservation is often overlooked in the world of microscopy, especially today, where we seem to use values inherited by our forefathers in histology. But it must be noted that EM was only brought to the realm of cell biology when sample fixation was perfected.

Finally, in the age of high dimensional imaging, omics driven science, and Artificial Intelligence (AI), this thesis represents a return to first principles. Before attempting to decode every gene and sequence every transcript and protein *in situ*, we need to ask ourselves: *do we even understand the basics?* Do we know how cells in tissue are arranged in 3D? Can we look down at a cell and infer every organelle's place in the synchrony of life? Are we aware of the prerequisites to drawing

complex models of pathology? The pattern seeking mammals we inadvertently are, this thesis presents a fresh opportunity for an unbiased learning of biological matter fundamentals.

Bibliography

[1] Y. Zhang *et al.*
Nanoscale subcellular architecture revealed by multicolor three-dimensional salvaged fluorescence imaging
Nature Methods, **17**, 225–231 (2020)

[2] R. Milo & R. Phillips
Cell Biology by the Numbers
Taylor & Francis, Abingdon (2015)

[3] E.M. Conroy *et al.*
Self-quenching, dimerization, and homo-FRET in hetero-FRET assemblies with quantum dot donors and multiple dye acceptors
The Journal of Physical Chemistry, **120**, 17817–17828 (2016)

[4] D. Baddeley & J. Bewersdorf
Biological insight from super-resolution microscopy: what we can learn from localization-based images
Annual Review of Biochemistry, **87**, 965–989 (2018)

[5] D.P. Hoffman *et al.*
Correlative three-dimensional super-resolution and block-face electron microscopy of whole vitreously frozen cells
Science **367**, eaaz5357 (2020)

[6] F. Chen, P.W. Tillberg & E.S. Boyden
Expansion Microscopy
Science **347**, 543–548 (2015).

[7] T.J. Chozinksi *et al.*
Expansion microscopy with conventional antibodies and fluorescent proteins
Nature Methods, **13**, 485–488 (2016)

[8] P.W. Tillberg *et al.*
Protein-retention expansion microscopy of cells and tissues labeled using standard fluorescent proteins and antibodies
Nature Biotechnology, **34**, 987–992 (2016)

[9] T. Ku *et al.*
Multiplexed and scalable super-resolution imaging of three-dimensional protein localization in size-adjustable tissues
Nature Biotechnology, **34**, 973–981 (2016)

[10] J.B. Chang *et al.*
Iterative expansion microscopy
Nature Methods,**14**, 593–599 (2017)

[11] S. Truckenbrodt *et al.*
X10 expansion microscopy enables 25-nm resolution on conventional microscopes
EMBO Reports, **19**, e45836 (2018)

[12] D. Gambarotto *et al.*
Imaging cellular ultrastructures using expansion microscopy (U-ExM)
Nature Methods, **16**, 71–74 (2019)

[13] S.F. Edwards
Statistical mechanics with topological constraints: I
Proceedings of the Physical Society, **91**, 513–519 (1967)

[14] L.H. Sperling
Interpenetrating Polymer Networks and Related Materials
Springer, New York City, 2012

[15] P. Matricardi *et al.*
Interpenetrating polymer networks polysaccharide hydrogels for drug delivery and tissue engineering
Advanced Drug Delivery Reviews, **65**, 1172–1187 (2013)

[16] A.K. Bajpai *et al.*
Responsive polymers in controlled drug delivery
Progress in Polymer Science, **33**, 1088–1118 (2008)

[17] N. Zoratto *et al.*
Osteochondral Tissue Engineering Advances in Experimental Medicine and Biology
Springer, New York City, 155–188 (2018)

[18] T.A. Brown *et al.*
Superresolution fluorescence imaging of mitochondrial nucleoids reveals their spatial range, limits, and membrane interaction
Molecular and Cellular Biology, **31**, 4994–5010 (2011)

[19] H.D. Ou *et al.*
C*hromEMT: Visualizing 3D chromatin structure and compaction in interphase and mitotic cells*
Science, **357**, eaag0025 (2017)

[20] L. Schermelleh *et al.*
Subdiffraction multicolor imaging of the nuclear periphery with 3D structured illumination microscopy
Science, **320**, 1332–1336 (2008)

[21] J. Laurincik *et al.*
Nucleolar ultrastructure and protein allocation in in vitro produced porcine embryos
Molecular Reproduction and Development, **68**, 327–334 (2004)

[22] S. Brahmachari & J.F. Marko
Chromosome disentanglement driven via optimal compaction of loop-extruded brush structures
PNAS, **116**, 24956–24965 (2019)

[23] I.A. Vorobjev & V.S. Chentsov
The ultrastructure of centriole in mammalian tissue culture cells
Cell Biology International Reports, **4**, 1037–1044 (1980)

[24] K.F. Sonnen *et al.*
3D-structured illumination microscopy provides novel insight into architecture of human centrosomes
Biology Open, **1**, 965–976 (2012)

[25] T. Stephan *et al.*
Live-cell STED nanoscopy of mitochondrial cristae
Scientific Reports, **9**, 12419 (2019)

[26] L.K. Schroeder *et al.*
Dynamic nanoscale morphology of the ER surveyed by STED microscopy
Journal of Cell Biology, **218**, 83–96 (2018)

[27] M. Terasaki *et al.*
Stacked endoplasmic reticulum sheets are connected by helicoidal membrane motifs
Cell, **154**, 285–296 (2013)

[28] M.S. Ladinsky *et al.*
Mastronarde, D. N., McIntosh, J. R., Howell, K. E. & Staehelin, L. A. Golgi structure in three dimensions: functional insights from the normal rat kidney cell
Journal of Cell Biology, **144**, 1135–1149 (1999)

[29] J.H. Billman & A.C. Diesing
Reduction of Schiff bases with sodium borohydride
The Journal of Organic Chemistry, **22**, 1068–1070 (1957)

[30] E.A. Hoffman *et al.*
Formaldehyde crosslinking: a tool for the study of chromatin complexes
Journal of Biological Chemistry, **290**, 26404–26411 (2015)

[31] H.M. Lai *et al.*
Rationalisation and validation of an acrylamide-free procedure in three-dimensional

histological imaging
PLoS ONE, **11**, e0158628 (2016)

[32] A.M. Ernst *et al.*
S-palmitoylation sorts membrane cargo for anterograde transport in the Golgi
Developmental Cell, **47**, 479–493 (2018)

[33] R. Gao *et al.*
Cortical column and whole-brain imaging with molecular contrast and nanoscale resolution
Science, **363**, eaau8302 (2019)

[34] G. Wen *et al.*
E*valuation of direct grafting strategies via trivalent anchoring for enabling lipid membrane and cytoskeleton staining in expansion microscopy*
ACS Nano, https://doi.org/10.1021/acsnano.9b09259 (2020)

[35] E.D. Karagiannis *et al.*
Expansion microscopy of lipid membranes
Preprint at https://doi.org/10.1101/829903 (2019)

[36] S.K. Sarkar *et al.*
Immuno-SABER enables highly multiplexed and amplified protein imaging in tissues
Nature Biotechnology, **37**, 1080–1090 (2019)

[37] S.M. Asano *et al.*
Expansion microscopy: protocols for imaging proteins and RNA in cells and tissues
Current Protocols Cell Biology, **80**, e56 (2018)

[38] C.C. Yu *et al.*
Expansion microscopy of C. elegans
eLife, **9**, e46249 (2020)

[39] C. Mao *et al.*
Feature-rich covalent stains for super-resolution and cleared tissue fluorescence microscopy
Science Adanvces, **6**, eaba4542 (2020)

[40] E.G. Kavalali & E.M. Jorgensen
Visualizing presynaptic function
Nature Neuroscience, **17**, 1: 10-6 (2014)

[41] Gonda M.A.
Electron Microscopy, Immunological Applications
Encyclopedia of Immunology (Second Edition), 790-795 (1998)

[42] M'Saad O. & Bewersdorf J.
Light Microscopy of Proteins in their Ultrastructural Context
Nature Communication, **11**, 1-15 (2020)

[43] Ellinger P.
Fluorescence Microscopy in Biology
Biological Reviews, **15**, 323-347 (1940)

[44] Leake M.C.
Analytical tools for single-molecule fluorescence imaging in cellulo
Physical Chemistry Chemical Physics, **16**, 25:12635-47 (2014)

[45] Shashkova S. & Leake M.C.
Single-molecule fluorescence microscopy review: shedding new light on old problems
Bioscience Reports, **37**, 4: BSR20170031 (2017)

[46] Abbe E.
Beitrage zur Theorie des Mikroskops und der mikroskopischen Wahrnehmung
Arkiv. Mikroskop, **9**, 1:413-418 (1873)

[47] Klar T.A. *et al.*
Fluorescence microscopy with diffraction resolution barrier broken by stimulated emission
PNAS, **97**, 15:8206-10 (2000)

[48] Betzig E. *et al.*
Imaging intracellular fluorescent proteins at nanometer resolution
Science, **313**, 5793:1642-5 (2006)

[49] Hess S.T., Girirajan T.P.K. & Mason M.D.
Photoactivation Localization Microscopy
Biophysical Journal, **91**, 11:4258-4272 (2006)

[50] Rust M.J., Bates M. & Zhuang X.
S*ub-diffraction-limit imaging by stochastic optical reconstruction microscopy (STORM)*
Nature Methods, **3**, 10:793-5 (2006)

[51] Gustafsson M.G.
Surpassing the lateral resolution limit by a factor of two using structured illumination microscopy
Journal of Microscopy, **198**, 2:82-7 (2000)

[52] Juette M.F. *et al.*
Three-dimensional sub-100 nm resolution fluorescence microscopy of thick samples
Nature Methods, **5**, 527-529 (2008)

[53] Gould T.J. *et al.*
Adaptive optics enables 3D STED microscopy in aberrating specimens
Optics Express, **20**, 19:20998-21009 (2012)

[54] Huang F. *et al.*
Video-rate nanoscopy using sCMOS camera-specific single-molecule localization algorithms
Nature Methods, **10**, 653-658 (2013)

[55] Huang F. *et al.*
Ultra-High Resolution 3D Imaging of Whole Cells
Cell, **166**, 4:1028-1040 (2016)

[56] Bottanelli F. *et al.*
Two-colour live-cell nanoscale imaging of intracellular targets
Nature Communications, **7**, 10778 (2016)

[57] Takakura H. *et al.*
Long time-lapse nanoscopy with sponataneously blinking membrane probes
Nature Biotechnology, **35**, 773-780 (2017)

[58] Kenny K.H. *et al.*
Fluorogenic probe for fast 3D whole-cell DNA-PAINT
Preprint at https://doi.org/10.1101/2020.04.29.066886 (2020)

[59] Velasco M.G.V. *et al.*
3D super-resolution deep-tissue imaging in live mice
Optica, **8**, 4:442-450 (2021)

[60] Hao X. *et al.*
Three-dimensional adaptive optical nanoscopy for thick specimen imaging at sub-50-nm resolution
Nature Methods, **18**, 6:688-693 (2021)

[61] Bloom F.E. & Aghajanian G.K.
Cytochemistry of synapses: selective staining for electron microscopy
Science, **154**, 1575-7 (1966)

[62] Dani A. *et al.*
Super-resolution imaging of chemical synapses in the brain
Neuron, **68**, 5:843-856 (2010)

[63] Yang X. & Annaert W.
The Nanoscopic Organization of Synapse Structures: A Common Basis for Cell

Communication
Membranes, **11**, 4:248 (2021)

[64] Acuna C., Liu X. & Sudhof T.C.
H*ow to Make an Active Zone: Unexpected Universal Functional Redundancy between RIMs and RIM-BPs*
Neuron, **91**, 792-807 (2016)

[65] Valtschanoff J.G. & Weinberg R.J.
Laminar Organization of the NMDA Receptor Complex within the Postsynaptic Density
Journal of Neuroscience, **21**, 4:1211-1217 (2001)

[66] Pfenninger K., Akert K., Moor H. & Sandi C.
The fine structure of freeze-fractured presynaptic membranes
Journal of Neurocytology, **I**, 129-149 (1972)

[67] Harlow M.L. *et al.*
The architecture of the active zone material at the frog's neuromuscular junction
Nature, **409**, 479-484 (2001)

[68] Chung K. et al.
Structural and molecular interrogation of intact biological systems
Nature, **497**, 332-337 (2013)

[69] Huerta-Viga A. & Woutersen S.
Protein Denaturation with Guanidium: a 2D-IR Study
The Journal of Physical Chemistry Letters, **4**, 20:3397-3401 (2013)

[70] Hama H. *et al.*
ScaleS: an optical clearing palette for biological imaging
Nature Neuroscience, **18**, 1518-1529 (2015)

[71] Oz S. *et al.*
Tissue expansion of 'cleared' whole brain reduces contrast in ex vivo MRI
Preprint at https://doi.org/10.21203/rs.3.rs-877945/v1 (2021)

[72] Poulsen J.W. *et al.*
U*sing guanidine-hydrochloride for fast and efficient protein digestion and single-step affinity-purification mass spectrometry*
Journal of Proteome Research, **12**, 2:1020-1030 (2013)

[73] Quinn P., Griffiths G. & Warren G.
Density of newly synthesized plasma membrane proteins in intracellular membranes II. Biochemical Studies
Journal of Cell Biology, **98**, 6:2142-7 (1984)

[74] Palade G.E.
A study of fixation for electron microscopy
Journal of Experimental Medicine, **95**, 3:285-298 (1952)

[75] Litman R.B. & Barrnett R.J.
The mechanism of the fixation of tissue components by osmium tetroxide via hydrogen bonding
Journal of Ultrastructure Research, **38**, 1-2:63-86 (1972)

[76] Gotz R. *et al.*
Nanoscale imaging of bacterial infections by sphingolipid expansion microscopy
Nature Communications, **11**, 6173 (2020)

[77] Sun D. *et al.*
Click-ExM enables expansion microscopy for all biomolecules
Nature Methods, **18**, 107-113 (2020)

[78] Damstra H.G.J. *et al.*
Visualizing cellular and tissue ultrastructure using Ten-fold Robust Expansion Microscopy (TREx)
Preprint at https://doi.org/10.1101/2021.02.03.428837 (2021)

[79] Revelo N.H. *et al.*
A new probe for super-resolution imaging of membranes elucidates trafficking pathways
Journal of Cell Biology, **205**, 4:591-606 (2014)

[80] Contreras F. *et al.*
Sphingosine Increases the Permeability of Model and Cell Membranes
Biophysical Journal, **90**, 11:4085-4092 (2006)

[81] Jimenez-Rojo N. *et al.*
Membrane Permeabilization Induced by Sphingosine: Effect of Negatively Charged Lipids
Biophysical Journal, **106**, 12:2577-2584 (2014)

[82] Gomes A.F. & Gozzo F.C.
Chemical cross-linking with a diazirine photoactivatable cross-linker investigated by MALDI- and ESI-MS/MS
Journal of Mass Spectrometry, **45**, 892-9 (2010)

[83] Krieg U.C., Walter P. & Johnson A.E.
Photocrosslinking of the signal sequence of the nascent preprolactin to the 54-kilodalton polypeptide of the signal recognition particle
PNAS, **83**, 8604-8606 (1986)

[84] Beale L.S.
Disease Germs: Their Supposed Nature, An Original Investigation, with Critical Remarks
London:J. Churchill (1870)

[85] Honigsbaum M.
The Pandemic Century: A History of Global Contagion from the Spanish Flu to Covid-19
WH Allen (2020)

[86] Leng L. *et al.*
Pathological features of COVID-19-associated lung injury: a preliminary proteomics report based on clinical samples
Signal Trasduction and Targeted Therapy, **5**, 240 (2020)

[87] Huang Y. *et al.*
Structural and functional properties of SARS-CoV-2 spike protein: potential antivirus drug development for COVID-19
Acta Pharmacologica Sinica, **41**, 1141-1149 (2020)

[88] Sines G. & Sakellarakis Y.A.
Lenses in Antiquity
American Journal of Archaeology, **91**, 2: 191-196 (1987)

[89] Kriss T.C. & Kriss V.M.
History of the Operating Microscope: From Magnifying Glass to Microneurosurgery
Neurosurgery, **42**, 4: 899-907 (1998)

[90] Leewenoek A.
Observation, communicated to the publisher by Mr. Antony van Leewenhoeck, in a Dutch letter of the 9 Octob. 1676 here English'd: concerning little animals by him observed in rain-well-sea and snow water; as also in water wherein pepper had lain infused
Philosophical Transactions of the Royal Society, **12**, 821-831

[91] E. Abbe
Beiträge zur Theorie des Mikroskops und der mikroskopischen Wahrnehmung
Archiv für mikroskopische Anatomie, **9**, 413-418 (1873)

[92] Albani J.R.
Absorption et Fluorescence: Principes et Applications
Lavoisier (2001)

[93] Coons A., Creech H.J. & Jones R.N.
Immunological Properties of An Antibody Containing a Fluorescent Group
Proceedings of the Society for Experimental Biology and Medicine, **47**, 2: 200-202 (1941)

[94] Shimomura O. & Johnson F.H.
Properties of the Bioluminescent Protein Aequorin
Biochemistry, **8**, 10: 3991-3997

[95] Freundlich M.M.
Origin of the Electron Microscope
Science, **142**, 3589: 185-188

[96] Lee K.J., Kang D., & Park H.
Site-Specific Labeling of Proteins Using Unnatural Amino Acids
Molecules and Cells, **42**, 5: 386-396 (2019)

[97] Lakhin A.V., Tarantul V.Z. & Gening L.V.
Aptamers: Problems, Solutions and Prospects
Acta Naturae, **5**, 4: 34-43

[98] Metz B. *et al.*
Identification of formaldehyde-induced modifications in proteins: reaction with model peptides
Journal of Biological Chemistry, **20**, 6235-6243 (2004)

[99] McDonald C.J. & Beaver R.H.
The Mannich Reaction of Poly(acrylamide)
Macromolecules, **12**, 203-208 (1979)

[100] Toews J. *et al.*
Mass spectrometric identification of formaledhyde induced peptide modifications under in vivo protein cross-linking conditions
Analytica Chimica Acta, **23**, 168-183 (2008)

[101] Lai H.M. *et al.*
Rationalization and Validation of Acrylamide-Free Procedure in Three-Dimensional Histological Imaging
Plos One, **11**, 6 (2016)

[102] Freifield L. *et al.*
E*xpansion microscopy of zebrafish for neuroscience and developmental biology studie*s
PNAS, **114**, 50 E10799-E10808 (2017)

[103] Cori K. *et al.*
Superresolution expansion microscopy reveals the three-dimensional organization of the Drosophila synaptonemal complex
PNAS, **114**, 33 E6857-E6866 (2017)

[104] Wang I.E. *et al.*
Hedgehog signaling regulates gene expression in planarian glia
eLife, **5**, e16996 (2016)

[105] Zhao Y. *et al.*
Nanoscale imaging of clinical specimens using pathology-optimized expansion microscopy
Nature Biotechnology, **35**, 8:757-64 (2017)

[106] Sim J. *et al.*
Whole-ExM: Expansion microsocpy imaging of all anatomical structures of whole larval zebrafish
Preprint at https://doi.org/10.1101/2021.05.18.443629 (2021)

[107] Lim Y. *et al.*
Mechanically resolved imaging of bacteria using expansion microscopy
Plos Biology, **17**, 10:e3000268 (2019)

[108] Chen F. *et al.*
Nanoscale imaging of RNA with expansion microscopy
Nature Methods, **13**, 679-684 (2016)

[109] Shi X. *et al.*
Label-retention expansion microscopy
Journal of Cell Biology, **220**, 9: e202105067 (2021)

[110] Alon S. *et al.*
Expansion sequencing: Spatially precise in situ transcriptomics in intact biological systems
Science, **371**, 6528 (2021)

[111] Wang G., Moffit J.R. & Zhuang X.
Multiplexed imaging of high-density libraries of RNAs with MERFISH and expansion microscopy
Scientific Reports, **8**, 4847 (2018)

[112] Gotz R. *et al.*
Expansion Microscopy for Cell Biology Analysis in Fungi
Frontiers Microbiology, **11**, 574 (2020)

[113] Gao M. *et al.*
Expansion Stimulated Emission Depletion Microscopy (ExSTED)
ACS Nano, **12**, 5:4178-4185 (2018)

[114] Kunz T. *et al.*
Detection of Chlamydia Developmental Forms and Secreted Effectors by Expansion

Microscopy
Frontiers in Cellular and Infection Microbiology, **9**, 276 (2019)

[115] Kao P. & Nodine M.D.
*Transcriptional Activation of Arabidopsis Zygotes is Required for Initial Cell Division*s
Scientific Reports, **9**, 1:17159 (2019)

[116] Zwettler F.U. *et al.*
Molecular resolution imaging by post-labeling expansion single-molecule localization microscopy (Ex-SMLM)
Nature Communications, **11**, 3388 (2020)

[117] Wang *et al.*
Combined expansion microscopy with structured illumination microscopy for analyzing protein complexes
Nature Protocol, **13**, 1869-1895 (2018)

[118] During D.N. *et al.*
Expansion Light Sheet Microscopy Resolves Subcellular Structures in Large Portions of the Songbird Brain
Frontier Neuroanatomy, **13**, 2 (2019)

[119] Gao R. *et al.*
A highly homogenous polymer composed of tetrahedron-like monomers for high-isotropy expansion microscopy
Nature Nanotechnology, **16**, 698-707 (2021)

[120] Lee H. *et al.*
Tetra-gel enables superior accuracy in combined super-resolution imaging and expansion microscopy
Scientific Reports, **11**, 16944 (2021)

[121] Kang S. *et al.*
Expansion Microscopy with a Thermally Adjustable Expansion Factor Using Thermoresponsive Biospecimen-Hydrogel Hybrids
ACS Applied Material Interfaces, **13**, 24: 28962-28974 (2021)

[122] Hayat M.A.
Fixation for electron microscopy
Academic Press (1981)

[123] Migneault I. *et al.*
Glutaraldehyde: behavior of aqueous solution, reaction with proteins, and application to *enzyme crosslinking*
Biotechniques, **37**, 790-796 798-802 (2004)

[124] Sabatini D.D., Bensch K. & Barrett R.J.
The preservation of cellular ultrastructure and enzymatic activity by aldehyde fixation
The Journal of Cell Biology, **17**, 19-58 (1963)

[125] Tonnesen J., Inavalli V.V.G.K & Nagerl V.U.
Super-Resolution Imaging of the Extracellular Space in Living Brain Tissue
Cell, **172**, 5:1108-1121 (2018)

[126] O'Connell P.B.H. & Brady C.J.
Polyacrylamide gels with modified crosslinkaged
Analytical Biochemistry, **76**, 1 (1976)

[127] Sarkar D. *et al.*
Expansion Revealing: Decrowding Proteins to Unmask Invisible Brain Nanostructures
Preprint at https://doi.org/10.1101/2020.08.29.273540 (2020)

[128] Luse S.A.
Electron Microscopic Observations of the Central Nervous System
The Journal of Cell Biology, **2**, 5:531-542 (1956)

[129] Feng G. *et al.*
Imaging neuronal subsets in transgenic mice expressing multiple spectral variants of GFP
Neuron, **28**, 1:41-51 (2000)

[130] Senisterra G., Chau I. & Vedadi M.
Thermal Denaturation Assays in Chemical Biology
ASSAY and Drug Development Technology, **10**, 2 (2012)

[131] Vedadi *et al.*
Chemical screening methods to identify ligands that promote protein stability, protein crystallization, and structrue determination
PNAS, 103, 34: 15835-15840 (2006)

[132] Hofman L. *et al.*
An effective thiol reactive probe for differential scanning fluorimetry with a standard RT-PCR device
Anals of Biolchemistry, **499**, 63-65 (2016)

[133] Kasthrui N. *et al.*
Saturated Reconstruction of a Volume of Neocortex
Cell, **162**, 3, 648-661 (2015)

[134] Eichler K *et al.*
The complete connectome of a learning and memory centre in an insect brain
Nature, **548**, 175-182 (2017)

[135] Cook S.J. *et al.*
Whole animal connectomes of both Caenorhabditis elegans sexes
Nature, **571**, 63-71 (2019)

[136] Gallagher B.R. & Zhao Y.
Expansion microscopy: A powerful nanoscale imaging tool for neuroscientists
Neurobiology of Disease, **154**, 105362 (2021)

[137] Fang T. *et al.*
Nanobody immunostaining for correlated light and electron microscopy with preservation of ultrastructure
Nature Methods, **15**, 12:1029-1032 (2018)

[138] Passagot J. *et al.*
Effect of glutarlaldehyde on the antigencity and infectivity of hepatitis A virus
Journal of Virology Methods, **16**, 21-8 (1987)

[139] West A.V. *et al.*
Labeling Preferences of Diazirines with Protein Biomolecules
Journal of the American Chemical Society, **143**, 17: 6691-6700 (2021)

[140] Nahirney P.C. & Tremblay M.
Brain Ultrastructure: Putting the Pieces Together
Frontiers in Cell and Developmental Biology, **9**, 629503 (2021)

[141] Yoon Y. *et al.*
Feasibility of 3D Reconstruction of Neural Morphology Using Expansion Microscopy and Barcode-Guided Agglomeration
Frontiers in Computational Neuroscience, **11**, 97 (2017)

[142] Askary A. *et al.*
I*n situ readout of DNA barcodes and single base edits facilitated by in vitro transcription*
Nature Biotechnology, **38**, 66-75 (2020)

[143] Wroblewska A. *et al.*
Protein Barcodes Enable High-Dimensional Single-Cell CRISPR Screens
Cell, **175**, 1141-1155 (2018)

[144] Anderson S.J, Mullen K.T. & Hess R.F.
Human peripheral spatial resolution for achromatic and chromatic stimuli: limits imposed by optical and retinal factors
Journal of Physiology, **442**, 47-64 (1991)

[145] Adams J.C.
Biotin Amplification of Biotin and Horseradish Peroxidase Signals in Histochemical Stains
The Journal of Histochemistry and Cytochemistry, **40**, 10 : 1457-1463 (1991)

[146] Hansen R.R., Sikes H.D. & Bowman C.N.
Visual Detection of Labeled Oligonucleotides Using Visible-Light-Polymerization-Based Amplification
Biomacromolecules, **9**, 1:355-362 (2008)

[147] Hoang T.X. *et al.*
Advanced Signal Amplification Strategies for Paper-Based Analytical Devices: A Comprehensive Review
Biomedicines, **9**, 5:540 (2021)

[148] Avens H.J. & Bowman C.N.
Mechanism of cyclic dye regeneration during eosin-sensitized photoinitiation in the presence of polymerization inhibitors
Journal of Polymer Science Part A: Polymer Chemistry, **47**, 22:6083-6094 (2009)

[149] Hansen R.R. *et al.*
Quantitative evaluation of oligonucleotide surface concentrations using polymerization-based amplification
Analytical and Bioanalytical Chemistry, 392, 167 (2008)

[150] Avens H.J. *et al.*
Fluorescent polymeric nanocomposite films generated by surface mediated photoinitiation of polymerization
Journal of Nanoparticle Research, **13**, 331-346 (2011)

[151] Avens H.J. *et al.*
Sensitive Immunofluorescent Staining of Cells via Generation of Fluorescent Nanoscale Polymer Films in Response to Biorecognition
Journal of Histochemistry & Cytochemistry, **59**, 1 (2011)

[152] Avens H.J., Randle T.J. & Bowman C.N.
Poylmerization Behavior and Polymer Properties of Eosin-Mediated Surface Modification Reactions
Polymer, **49**, 22:4762-4768 (2008)

[153] Lilly J.L. *et al.*
Interfacial Polymerization for Colorimetric Labeling of Protein Expression in Cells
PLoS ONE, **9**, 12:e115630 (2014)

[154] Smith G.P.
Kinetics of Amine Modification of Proteins
Bioconjugate Chemistry, **17**, 2 501-506 (2006)

[155] Delgadillo R.F. *et al.*
Detailed charactarization of the solution kinetics and thermodynamics of biotin, biocytin

and HABA binding to avidin and streptavidin
PLoS ONE, **14**, 2:e0204194 (2019)

[156] Chu Y.W. *et al.*
Layer by layer assembly of biotinylated protein networks for signal amplification
Chemical Communications, **49**, 23997-2399 (2013)

[157] Chen M., Tian L. & Waller L.
3D differential phase contrast microscopy
Biomedical Optics Express, **7**, 10 3940-3950 (2016)

[158] Stack E.C. *et al.*
Multiplexed immunohistochemistry, imaging, and quantitation: A review with an assessment of Tyramide signal amplification, multispectral imaging and multiplex analysis
Methods, **70**, 1:46-58 (2014)

[159] Tomal W. & Ortyl J.
Water-Soluable Photoinitiators in Biomedical Applications
Polymers, **12**, 5: 1073 (2020)

[160] Sielaff A.C. *et al.*
Charactarization of the total and viable bacterial and fungal communities associated with the International Space Station surfaces
Microbiome, **7**, 50 (2019)

[161] Master B. R.
History of the Electron Microscope in Cell Biology
Encyclopedia of Life Sciences (ELS) DOI: 10.1002/9780470015902.a0021539 (2009)

[162] Porter K.R., Claude A. & Fullam E.
A Study of Tissue Culture Cells by Electron Microscopy
Journal of Experimental Medicine, **81**, 233-246 (1944)

[163] Palade G.E.
A small particulate component of the cytoplasm
The Journal of Biophysical and Biochemical Cytology, **1**, 59-68 (1955)

[164] de Boer P., Hoogenboom J.P., Giepmans B.N.G.
Correlated light and electron microscopy: ultrastructure lights up!
Nature Methods, **12**, 503-513 (2015)

[165] Howland M.C. *et al.*
Charactarization of Physical Properties of Supported Phospholipid Membranes Using Imaging Ellipsometry at Optical Wavelengths
Biophysical Journal, **92**, 1306-1317

[166] Richardson D.S. & Lichtman J.W.
Clarifying Tissue Clearing
Cell, **162**, 2:246-257 (2016)

[167] Spalteholz W.
Uber das Durchsichtigmachen von menschlichen und tierischen Praparaten und seine theoretischen Bedingungen
S. Hirzel, Jena (1911)

[168] Erturk A., Lafkas D. & Chalouni C.
Imaging cleared intact biological systems at a cellular level by 3DISCO
Journal of Visualized Experiments, **89**, 5128 (2014)

[169] Dodt H.U. *et al.*
Ultramicroscopy: three-dimensional visualization of neuronal networks in the whole mouse brain
Nature Methods, **4**, 331–336 (2007)

[170] Renier N. *et al.*
iDISCO: a simple, rapid method to immunolabel large tissue samples for volume imaging
Cell, **159**, 896–910 (2014)

[171] Tsai P.S. *et al.*
Plasma-mediated ablation: an optical tool for submicrometer surgery on neuronal and vascular systems
Current opinion in biotechnology, **20**, 90–99 (2009)

[172] Ke M.T., Fujimoto S. & Imai T.
SeeDB: a simple and morphology preserving optical clearing agent for neuronal circuit reconstruction
Nature Neuroscience, 16, 1154-1161 (2013)

[173] Kuwajima T. *et al.*
ClearT: a detergent-and solvent-free clearing method for neuronal and non-neuronal tissue
Development, 140, 1364–1368 (2013)

[174] Staudt T. *et al.*
2,2'-thiodiethanol: a new water soluble mounting medium for high resolution optical microscopy
Microscopy Research and Technique, **70**, 1–9 (2007)

[175] Hama H. *et al.*
Scale: a chemical approach for fluorescence imaging and reconstruction of transparent mouse brain
Nature Neuroscience, **14**, 1481–1488 (2011)

[176] Susaki E.A. *et al.*
Whole-brain imaging with single-cell resolution using chemical cocktails and computational analysis
Cell, **157**, 726–739 (2014)

[177] Tainaka K. *et al.*
Whole-body imaging with single-cell resolution by tissue decolorization
Cell, **159**, 911–924 (2014)

[178] Yang B. *et al.*
Single-Cell Phenotyping within Transparent Intact Tissue through Whole-Body Clearing
Cell, **158**, 945–958 (2014)

[179] Hausen P. & Dreyer C.
T*he Use of Polyacrylamide as an Embedding Medium for Immunohistochemical Studies of Embryonic Tissues*
Stain Technology, **56**, 5: 287-293 (1981)

[180] Gemoroth P.G., Gourdie R.G. & Thompson R.P.
Confocal microscopy of thick sections from acrylamide gel embedded embryos
Microscopy Research Technology, **30**, 6 :513-20 (1995)

[181] Boyde A.
Stereoscopic images in confocal (tandem scanning) microscopy
Science, **230**, 1270-1272 (1985)

[182] Hecht A., Duplessix R. & Geissler E.
Structural Inhomogeneities in the Range 2.5-2500 Å in Polyacrylamide Gels
Macromolecules, 18, **11**, 2167-2173 (1985)

[183] Di Lorenzo F. & Seiffert S.
Nanostructural heterogeneity in polymer networks and gels
Polymer Chemistry, **6**, 5515-5528 (2015)

[184] Thevathasan J.V. *et al.*
Nuclear pores as versatile reference standards for quantitative super-resolution microscopy
Nature Methods, **16**, 1045-1053 (2019)

[185] Wassie A.T., Zhao Y. & Boyden E.S.
Expansion microscopy: principles and uses in biological research
Nature Methods, **16**, 33-41 (2019)

[186] Fruh S.M. *et al.*
Site-Specifically-Labeled Antibodies for Super-Resolution Microscopy Reveals In Situ

Linkage Errors
ACS Nano, **15**, 7 12161-12170 (2021)

[187] Gonda M.A.
Electron Microscopy, Immunological Applications
Encyclopedia of Immunology, 790-795 (1998)

[188] Schikorski T.
Pre-embedding Immunogold Localization of Antigens in Mammalian Brain Slices
Immunoelectron Microscopy, **657**, 133-144 (2010)

[189] Morris R.E. & Ciraolo
A universal post-embedding protocol for immunogold labelling of osmium-fixed, epoxy resin-embedded tissue
Journal of Electron Microscopy, **46**, 4: 315-319 (1997)

[190] van Rijnsoever C., Oorschot V. & Klumperman J.
Correlative light-electron microscopy (CLEM) combining live-cell imaging and immunolabeling of ultrathin cryosections
Nature Methods, **5**, 973-980 (2008)

[191] Polishchuk R.S. *et al.*
Correlative light-electron microscopy reveals the tubular-saccular ultrastructure of carriers operating between Golgi apparatus and plasma membrane
Journal of Cell Biology, **148**, 1: 45-58 (2000)

[192] Gaietta G. *et al.*
Multicolor and Electron Microscopic Imaging of Connexin Trafficking
Science, **296**, 5567 503-507 (2002)

[193] Gaietta G. *et al.*
Golgi twins in late mitosis revealed by genetically encoded tags for live cell imaging and correlated electron microscopy
PNAS, **103**, 47 17777-17782 (2006)

[194] Sochaki K.A. *et al.*
Correlative super-resolution fluorescence and metal replica transmission electron microscopy
Nature Methods, **11**, 3: 305-308 (2014)

[195] Knott G. et al.
Serial Section Scanning Electron Microscopy of Adult Brain Tissue Using Focused Ion Beam Milling
The Journal of Neuroscience, 28, 12 2959-2964 (2008)

[196] Hayworth K.J. *et al.*
Automating the Collection of Ultrathin Serial Sections for Large Volume TEM Reconstructions
Microscopy Microanalysis, **12**, 86-87 (2006)

[197] Klimas A. *et al.*
Nanoscale Imaging of Biomolecules using Molecule Anchorable Gel-enabled Nanoscale In-situ Fluorescence Microscopy
Preprint at doi: 10.21203/rs.3.rs-858006/v1 (2021)

[198] Rashpa R. & Brochet M.
Ultrastructure expansion microsocpy of plasmo dium gametocytes reveals the molecular architecture of a microtubule organization centre coordinating mitosis with axoneme assembly
Preprint at doi: https://doi.org/10.1101/2021.07.21.453039 (2021)

[199] Pacheco N.D.S. *et al.*
Revisiting the role of Toxoplasma gondii ERK7 in the maintanance and stability of the apical complex
mBio, doi: https://doi.org/10.1128/mBio.02057-21 (2021)

[200] Liffner B. & Absalon S.
Expansion microscopy reveals Plasmodium falciparum blood-stage parasites undergo anaphase with a chromatin bridge in the absence of mini-chromosome maintenance complex binding protein
Preprint at doi: https://doi.org/10.1101/2021.09.25.461816 (2021)

[201] Tricot M.
Comparison of Experimental and Theoretical Persistence Length of Some Polyelectrolytes at Various Ionic Strengths
Macromolecules, **17**, 9 1698-1704 (1984)

[202] Cipriano B.H.
Superabsorbent Hydrogels That are Robust and Highly Stretchable
Macromolecules, **47**, 13 4445-4452 (2014)

[203] Kienberger F. *et al.*
Static and Dynamical Properties of Single Poly(Ethylene Glycol) Molecules Investigated by Force Spectroscopy
Single Molecule, **1**, 123-128 (2000)

[204] Hassell J. & Hand H.R.
Tissue fixation with diimidoesters as an alternative to aldehydes. I. Comparison of cross-linking and ultrastructure obtained with dimethylsuberimidate and glutaraldehyde
Journal of Histochemistry and Cytochemistry, **22**, 223-239 (1974)

[205] Tzaphidou M.
The effects of fixation by combination of glutaraldehyde/dimethyl suberimidate. Use of collagen as a model system
Journal of Histochemistry and Cytochemistry, **31**, 11 1274-1278 (1983)

[206] Hand H.R. & Hassell J.
Tissue fixation with diimidoesters as an alternative to aldehydes. II. Cytochemical and biochemical studies of rat liver fixed with dimethylsuberimidate
Journal of Histochemistry and Cytochemistry, **24**, 9 1000-1011 (1976)

[207] Ono T., Yamamoto N. & Yasuda K.
The Preservation of Fine Structure by Use of Dimethylsuberimidate as a Fixative
Okajimas Folia Anatomica Japonica, **53**, 199-230 (1976)

[208] Dutton A., Adams M. & Singer S.J.
Bifunctional imidoesters as crosslinking reagents
Biochemical and Biophysical Research Communications, **23**, 730 (1966)

[209] Wofsy L. & Singer S.J.
Effects of the amidation reaction on antibody activity and on the physical properties of some proteins
Biochemsitry, **2**, 104 (1963)

[210] North A.J., Gimona M., Cross R.A. & Small J.V.
Calponin is localised in both the contractile apparatus and the cytoskeleton of smooth muscle cells
Journal of Cell Science, **107**, 437-444 (1994)

[211] North A.J., Gimona M., Lando Z. & Small J.V.
Actin isoform compartments in chicken gizzard smooth muscle cells
Journal of Cell Science, **107**, 445-455 (1994)

[212] Xiao B. *et al.*
Homer regulates the association of group 1 metabotropic glutamate receptors with multivalent complexes of homer-related, synaptic proteins
Neuron, **21**, 4:707-16 (1998)

[213] Harrevald A.V., Crowell J. & Malhotra S.K.
A study of extracellular space in central central nervous tissue by freeze-substitution
Journal of Cell Biology, **25**, 1:117–137 (1965)

[214] Korogod N., Petersen C.C.H. & Knott G.W.
Ultrastructural analysis of adult mouse neocortex comparing aldehyde perfusion with cryo fixation
eLife, **4**, e05793 (2015)

[215] Harris K.M. & Weingberg R.J.
Ultrastructure of synapses in the mammalian brain
Cold Spring Harbor Perspective Biology, **4**, 5:a005587 (2012)

[216] Gray E.G.
Axo-somatic and axo-dendritic synapses of the cerebral cortex
Journal of Anatomy, **93**, 420–433 (1959)

[217] Klemen J.H.M.C. & Roubos E.W.
The gray area between synapse structure and function—Gray's synapse types I and II revisited
Synapse, **65**, 1222-1230 (2011)

[218] Nahirne P.C. & Trembley M.
Brain Ultrastructure: Putting the Pieces Together
Frontiers in Cell and Developmental Biology, **9**, 629503 (2021)

[219] Zhang L. et al.
Altered brain energetics induces mitochondrial fission arrest in Alzheimer's Disease
Scientific Reports, **6**, 18725 (2016)

[220] Cserép C., Pósfai B., Schwarcz A.D. & Dénes A.
Mitochondrial Ultrastructure Is Coupled to Synaptic Performance at Axonal Release Sites
eNeuro, **5**, 10.1523/ENEURO.0390-17.2018. (2018)

[221] Haberkant P. *et al.*
Bifunctional Sphingosine for Cell-Based Analysis of ProteinSphingolipid Interactions
ACS Chemical Biology, **11**, 222−230 (2015)

[222] Murakami T.C. *et al.*
A three-dimensional single-cell-resolution whole-brain atlas using CUBIC-X expansion microscopy and tissue clearing
Nature Neuroscience, **21**, 625–637 (2018)

[223] Park H. *et al.*
Scalable and Isotropic Expansion of Tissues with Simply Tunable Expansion Ratio
Advanced Science, **6**, 1901673 (2019)

[224] Shen F. *et al.*
Light microscopy based approach for mapping connectivity with molecular specificity
Nature Communications, **11**, 4632 (2020)

[225] Park C.E. *et al.*
Super-Resolution Three-Dimensional Imaging of Actin Filaments in Cultured Cells and

the Brain via Expansion Microscopy
ACS Nano, **14**, 11, 14999–15010 (2020)

[226] Campbell L.A. *et al.*
Protein-retention expansion microscopy for visualizing subcellular organelles in fixed brain tissue
Journal of Neuroscience Methods, **361**, 109285

Appendix A

Reproducing pan-ExM using the concise protocols outlined in my manuscripts' Methods sections can prove difficult to the inexperienced scientist. In **A.1** and **A.2**, I describe the pan-ExM protocols developed in **Chapters 3 & 4** in sufficient detail to enable every researcher with basic background in biochemistry to perform pan-ExM sample preparation and imaging.

A.1 pan-ExM protocol (adherent cells)

PART I: Preparation

1. Reagents

Reagent	Acronym	Storage	Vendor	Catalog number
40% acrylamide*	AAm	4°C	Sigma-Aldrich	A9099
N,N'-(1,2-dihydroxyethylene)bisacrylamide	DHEBA	RT		294381
Sodium bicarbonate	$NaHCO_3$	RT		S5761
Sodium hydroxide	NaOH	RT		S8045
ATTO594 NHS ester	-	-20°C		08741
Phosphate buffered saline tablets	-	RT		P4417
Triton X-100	TX-100	RT		X100-100ML
Sodium acrylate**	SA	-20°C in desiccator	Santa Cruz Biotechnology	sc-236893C

N,N′-methylenebis(acrylamide)	BIS	RT	Alfa Aesar	J66710
Ammonium persulfate	APS	RT in desiccator	American Bio	AB00112
N,N,N’,N’-tetramethylethylenediamine	TEMED	RT in desiccator		AB02020
Tris [hyroxymethyl] aminomethane	Tris	RT		AB02000
20% sodium dodecyl sulfate solution	SDS	RT		AB01922
Sodium chloride	NaCl	RT	J.T. Baker	3624-01
1x phosphate buffered saline (Gibco)	1X PBS	RT	Thermofisher	10010023
10x phosphate buffered saline (Gibco)	10X PBS	RT		70011044
16% paraformaldehyde	FA	RT	Electron Microscopy Sciences	15710
8% glutaraldehyde	GA	4°C		16019
Bovine serum albumin	BSA	4°C	Jackson Laboratories	001-000-162
Tween 20	-	RT		P7949
SYTOX Green	-	-20°C	Thermofisher	S7020
DMSO, Anhydrous	DMSO	RT		D12345

* Acrylamide (AAm) monomer in powder form can also be used. However, it is much more toxic and requires extensive precautions when handling.

** We recommend purchasing sodium acrylate (SA) from Sigma or Santa Cruz Biotechnology for the time being. However, we do notice significant batch-to-batch variability. To verify that SA is of acceptable purity, we usually make a 38% (w/v) solution in water and check its color. If the solution color is yellow and/or a large precipitate form, please discard and try a different batch. If

the solution is pale yellow and only a small precipitate forms, centrifuge solution at 4000 rpm for 5 minutes and use the supernatant. You must use a pale-yellow 38% SA stock solution without any precipitate (see **Figure 1**).

2. Materials and instruments

Materials	Vendor	Catalog number
N1.5 12-mm round glass coverslips	Electron Microscopy Sciences	72230-01
Glass microscope slide	Sigma-Aldrich	S8400
N1.5 22 x 22 mm square cover glass coverslips	Fisher Scientific	12-541BP
N1.5 18-mm round coverslip	Marienfeld	0117580
50 mm MatTek dish, N1.5 coverslip 30 mm diameter	MatTek life sciences	P50G-1.5-30-F
Picodent twinsil	picodent	1300 1000

Instruments	pH meter, 37°C incubator, nitrogen (or argon) gas tank, dry block incubator, ice bucket, rocker, vortex
Other materials	Superglue, tweezers, razor blades, container (plastic Tupperware), 12-well plates, 6-well plates, 1.5 mL Eppendorf tubes, 15 mL Eppendorf tubes, 50 mL Eppendorf tubs, Kim wipes, beaker, stir bar, paintbrush (brush size No. 2 (1.6 mm)), laminated tape, pH strips, aluminum foil, surgical scissors

3. Solutions

These solutions are referred to in **Part II: Protocol**. Note that some can be made beforehand and stored, while others must be made fresh.

Fixation solution

FA + GA fix (for cytoskeleton, mitochondria, and ER preservation)

Reagent	Amount	Concentration
16% FA	1.875 mL	3% (w/v)
8% GA	125 uL	0.1% (w/v)
10X PBS	1 mL	1X
Ultrapure water	7 mL	-
Total	10 mL	3% FA + 0.1% GA in 1X PBS

FA fix (for NPC and Golgi preservation)

Reagent	Amount	Concentration
16% FA	2.5 mL	4% (w/v)
10X PBS	1 mL	1X
Ultrapure water	6.5 mL	-
Total	10 mL	4% FA in 1X PBS

- These solutions must be made fresh for appropriate preservation of ultrastructure.
- FA and GA are toxic and must be handled in a fume hood. After opening each vial, we transfer these stock solutions to 15 mL Eppendorf tubes and store them for no longer than 24 h at 4°C. For consistent results, please do not use solutions of FA and GA that exceed that storage duration.

Post-fix solution

Reagent	Amount	Concentration
16% FA	440 uL	0.7% (w/v)
40% AAm	250 uL	1% (w/v)
10X PBS	1 mL	1X
Ultrapure water	8.31 mL	-
Total	10 mL	0.7% FA + 1% AAm in 1X PBS

- This solution must be made fresh

DHEBA + AAm stock solution

Reagent	Amount	Concentration
DHEBA	160 mg	0.4% (w/v)
40% AAm	40 mL	40% (w/v)
Total	40 mL	0.4% DHEBA in 40% AAm

- DHEBA is notoriously difficult to dissolve. There are also impurities in recent batches of DHEBA from Sigma that must be removed prior to using the solution.
    - To dissolve DHEBA in 40% AAm solution, vortex vigorously for 15 min, or put a small magnetic stir bar in a falcon tube with the solution, tape it to a magnetic stirrer and stir for at least half an hour.

- Even after excessive vortexing/stirring, you might still notice some ‘flakiness’. These are likely impurities. If that is the case, filter-sterilize the solution to get rid of the impurities.

- Make aliquots of 2.5 mL and store in -20°C. This solution is stable for at least 1 month.

1st gelling solution

Reagent	Amount	Concentration
DHEBA + AAm stock solution	2.5 mL	10% AAm (w/v) + 0.1% DHEBA (w/v)
SA	1.9 g	19% (w/v)
10X PBS	1 mL	1X
Ultrapure water	Until 10 mL	-
Total	10 mL	10% AAm + 0.1% DHEBA + 19% SA in 1X PBS

- Centrifuge this solution at 4000 rpm for about 5 minutes, discard the precipitate, and only use the supernatant.

- Every sample to expand consumes ~200 uL of this solution.

- Make aliquots of 1 mL and store in -20°C. This solution is stable for at least 1 month.

Denaturation buffer

Reagent	Amount	Concentration
NaCl	2.92 g	200 mM
Tris	1.51 g	50 mM

20% SDS	72.1 mL	200 mM
Ultrapure water	Until 250 mL	-
Total	250 mL	200 mM SDS + 50 mM Tris + 50 mM NaCl

- Add reagents to a beaker with a stir bar and stir heated to 40°C to dissolve. Note that SDS precipitates at temperatures below 20°C.
- Cool to room temperature and adjust pH to 6.8 with hydrochloric acid (HCl).
    - Tris buffer pH is sensitive to temperature. The solution must have its pH adjusted at RT (~19°C).
- This solution is stored at RT and is stable for at least 12 months.

2nd gelling solution

Reagent	Amount	Concentration
40% AAm	12.5 mL	10% (w/v)
DHEBA	25 mg	0.05% (w/v)
Ultrapure water	37.5	-
Total	50 mL	10% AAm + 0.05% DHEBA

- Every sample to expand consumes 6 mL of this solution. Since the number of samples we process at once is generally around 6, we make 50 mL of this solution and discard the remnant.

3rd gelling solution

Reagent	Amount	Concentration
40% AAm	6.25 mL	10% (w/v)
BIS	25 mg	0.1% (w/v)
SA	4.75 g	19% (w/v)
10X PBS	2.5 mL	1x
Ultrapure water	Until 25 mL	-
Total	25 mL	10% AAm + 0.1% BIS + 19% SA in 1X PBS

- Every sample to expand consumes 4 mL of this solution. Since the number of samples we process at once is generally around 6, we make 25 mL of this solution and discard the remnant.

25% APS stock solution

Reagent	Amount	Concentration
APS	500 mg	25% (w/v)
Ultrapure water	Until 1 mL	-
Total	1 mL	25% APS

- This solution must be made fresh and kept on ice. We use it to make ***Activated 1st gelling solution***. We usually discard it if left on ice for more than 6 hours.

25% TEMED stock solution

Reagent	Amount	Concentration
TEMED	250 uL	25% (v/v)
Ultrapure water	750 uL	-
Total	1 mL	25% TEMED

- This solution must be made fresh and kept on ice. We use it to make ***Activated 1st gelling solution***. We usually discard it if left on ice for more than 6 hours.

10% APS stock solution

Reagent	Amount	Concentration
APS	100 mg	10% (w/v)
Ultrapure water	Until 1 mL	-
Total	1 mL	10% APS

- This solution must be made fresh and kept on ice. We use it to make ***Activated 2nd gelling solution*** or ***Activated 3rd gelling solution***. We usually discard it if left on ice for more than 6 hours.

10% TEMED stock solution

Reagent	Amount	Concentration

TEMED	100 uL	10% (v/v)
Ultrapure water	900 uL	-
Total	1 mL	10% TEMED

- This solution is made fresh and kept on ice. We use it to make ***Activated 2nd gelling solution*** or ***Activated 3rd gelling solution***. We usually discard this working solution if left on ice for more than 6 hours.

NaOH solution

Reagent	Amount	Concentration
NaOH	800 mg	200 mM
Ultrapure water	Until 100 mL	-
Total	100 mL	200 mM NaOH

- Please be cautious when handling this solution as it is highly caustic (pH ~13).
- You can store this solution at room temperature.

PBS-T buffer

Reagent	Amount	Concentration
PBS tablets	5 tablets	1X
Tween 20	1 mL	0.1% (v/v)
Ultrapure water	1 L	-

Total	1 L	0.1% Tween 20 in 1X PBS

- This solution can be stored at room temperature.
- Alternatively, you can add 1 mL of Tween 20 to 1 L of pre-made 1X PBS solution.

Block buffer

Reagent	Amount	Concentration
PBS tablets	5 tablets	1X
Triton X-100	1 mL	0.1% (v/v)
Bovine serum albumin (BSA)	10 g	1% (w/v)
Ultrapure water	Until 1 L	-
Total	1 L	0.1% TX-100 + 1% BSA in 1X PBS

- This solution must be stored at 4°C.

NHS ester dye stock

Reagent	Amount	Concentration
NHS ester ATTO594 (Sigma-Aldrich 08741)	1 mg	2 mg/mL
DMSO	500 uL	-
Total	500 uL	2 mg/mL ATTO594 NHS ester

- Make 50 uL aliquots and store desiccated at -20°C.

- NHS ester is very sensitive to moisture and must be stored in a desiccator. In the absence of a desiccator, place the reagent in a container containing desiccant beads.

PART II: Protocol

1. Fixation

This protocol is optimized for monolayer cells plated on 12-mm round coverslips.

1. Aspirate cell media
2. Immediately add ***fixation solution***
    - For ER, mitochondria, and cytoskeleton preservation, we prefer using the fixative 3% FA + 0.1% GA in 1X PBS for 15 min at RT; For Golgi and NPC preservation, we prefer using the fixative 4% FA for 1 h.
    - Fixing longer than 1 h prevents antibody labeling post-expansion because of hydrogel epitope masking and fixing less than 15 min results in poor ultrastructure preservation.
3. Rinse three times with 1X PBS

- This step is critical. Please make sure that the fixation solution is added immediately after media removal (i.e., do not include a PBS rinsing step). The faster the cells are fixed, the better ultrastructure is preserved.

- Note that we prefer supplementing the fixative with GA because it preserves ultrastructure best and it also increases retention of proteins in the hydrogel (we found that FA fixation

alone results in ~30% protein loss relative to GA fixation). However, many antibodies are not validated for GA fixation. If you need to omit GA in the fixative, we recommend fixing cells with 4% FA in 1X PBS for 1 h.

- Do not permeabilize your cells. This will destroy sample ultrastructure.

2. Post-fix

1. Aspirate PBS
2. Incubate fixed cells in ***post-fix solution*** for 6-7 hours at 37°C

- Please add this solution immediately after cell fixation. It is believed that formaldehyde fixation goes into completion after ~48 hours but is partially reversible within that time frame. Adding acrylamide monomers in this step is meant to prevent protein-protein inter-crosslinking since acrylamide covalently reacts with the intermediate Schiff bases formed during formaldehyde crosslinking.

3. Gelation chamber construction

Please refer to **Figure 2** for a visual diagram

1. To make one gelation chamber spacer, glue two N1.5 22x22 mm coverglasses using superglue
    - For every gelation chamber, make two of these spacers.
2. Glue each spacer on the microscope slide spaced about (or slightly more) than 12 mm from each other
    - The space between these spacers will be used to glue the cell-adhered coverslip.

3. As a chamber lid, we use one N1.5 22x22 mm coverslip
    - This lid is used to seal the chamber after pouring 1st gelling solution onto the sample.

4. 1st gelation

1. Remove ***post-fix solution***
2. Wash cells x3 with 1X PBS on rocker for 15 min each
3. Thaw ***1st gelling solution***
4. Make ***25% APS stock solution*** fresh
5. Make ***25% TEMED stock solution*** fresh
6. Place all three solutions above on ice

For this next step, refer to **Figure 3** for a visual representation of steps **1**, **4**, **9** and **10**

Samples are embedded in 1st hydrogel one-by-one. For every single sample:

5. Put a small droplet of superglue at the center of the space between the gelation chamber spacers
6. Take cell-adhered coverslip out of 24-well plate using tweezers
7. Gently place coverslip on a Kim wipe to remove residual PBS from its non-cell adhered side
8. Glue coverslip to the gelation chamber

9. Make sure that cells remain hydrated by adding a droplet of PBS on top of the coverslip

10. Remove PBS from the coverslip with a Kim wipe, such that only some moisture can be seen

    - This step is critical: you must not allow the coverslip to dry out completely and you also must not leave a significant layer of PBS above the cells since it might dilute the gel.

11. Take one 1.5 mL Eppendorf tube and mix:

Activated 1st gelling solution

Solution	Volume	Final concentration
1st gelling solution	196 uL	19% SA + 10% AAm + 0.1% DHEBA (all w/v) in 1X PBS
25% APS stock solution	2 uL	0.25% (w/v)
25% TEMED stock solution	2 uL	0.25% (v/v)
Total	200 uL	19% SA + 10% AAm + 0.1% DHEBA + 0.25% APS + 0.25% TEMED in 1X PBS

Note that this step is very time sensitive as premature gelation of the solution might affect protein retention.

12. Vortex for 2 seconds

13. Pour ***Activated 1st gelling solution*** onto the coverslip to cover it entirely

- Use the same pipette used for handling the 196 uL gel solution to avoid spending time calibrating pipettes, which could cause premature gelation.
- Use roughly two-thirds of the 196 uL volume or slightly more.

14. Seal chamber immediately with the gelation chamber lid
    - Avoid air bubbles in the gel solution.
    - Remove residual gel solution with Kim wipes.
15. Place gelation chambers in a humidified container (Tupperware with wet Kim wipes will suffice)
16. Incubate for 1.5 h at 37°C

5. Denaturation

Refer to **Figure 4** for a visual representation of steps **2-5**

Remember to turn the dry block incubator on and set to 76°C before these following step

1. Remove gelation chambers from container
2. With a razor blade, gently remove the gelation lid from gelation chamber
3. With a razor blade, gently remove the gelation chamber spacers
4. Remove coverslip from microscope slide with a razor blade by gently placing the blade in between the sample coverslip and the microscope slide
    - Do not peel the gel off the coverslip.
5. Place coverslips in a 6-well plate and add 4 mL denaturation buffer in each well

6. Incubate for 15 min at 37°C

    - The gel should peel off the coverslip on its own during this step.

7. With a No. 2 paintbrush, gently pick up the gel and move to a 1.5 mL Eppendorf tube and add 1 mL of denaturation buffer

8. Incubate in heat block at 76°C for 1 h

    - Because heat is transferred to the Eppendorf tube through air, the actual temperature of the solution will be 73°C (the desired temperature) and not 76°C.

    - Water has higher thermal conductivity. So, if you are using a water bath, set it to 73°C.

9. Move gel with a paintbrush to a microscope glass slide and flatten it

10. With a new razor blade, cut a 0.75x0.75 cm square gel from the total gel and transfer to a new 6-well plate using a paintbrush

11. Wash the gel x3 with 1X PBS for 20 min each to remove residual SDS

    - You may wish to save the remaining gel in 4°C after washing residual SDS for future use.

    - You may wish to pause the protocol here for a couple of days by storing the gel in PBS at 4°C.

6. 1st expansion

In this step, the gel will expand a factor of 4× to 4.5×

1. In the same 6-well plate, remove PBS and replace with ultrapure water
2. Incubate in water x2 for 30 min each and x1 for 1 h or until the size of the gel plateaus

7. 2nd gelation

The ideal re-embedded gel size is 1.5x1.5 cm.

1. Thaw ***2nd gelling solution***
2. Make ***10% APS stock solution*** fresh
3. Make ***10% TEMED stock solution*** fresh
4. Place all solutions above on ice
5. For every six samples to be expanded, in a 15 mL Eppendorf tube mix:

Activated 2nd gelling solution

Solution	Volume	Final concentration
2nd gelling solution	12 mL	10% (w/v) AAm + 0.05% (w/v) DHEBA
10% APS stock solution	60 uL	0.05% (w/v)
10% TEMED stock solution	60 uL	0.05% (v/v)
Total	~12 mL	10% AAm + 0.05% DHEBA + 0.05% APS + 0.05% TEMED

- Note that this solution will replace water within the expanded gel prior to its polymerization.

- As described below, we incubate each gel x2 with 2 mL of this solution (made fresh each time) for 20 min each before we immobilize them in gelation chambers and polymerize at 37°C.

6. Vortex ***Activated 2nd gelling solution*** for 5 seconds

7. Remove water from the 6-well plates

8. Add ***Activated 2nd gelling solution***

    - Make sure that the gels are not adhered to the plate and can move freely.

9. Incubate for 20 min at RT on a rocker

    - 5 minutes before the incubation time is over, make the same solution again fresh.

10. Remove ***Activated 2nd gelling solution*** from wells using a p1000 pipette and make sure that there is minimum residual solution

11. Repeat steps **5-10** again for a total of 2 incubations

12. After removing residual solution, move each gel with laminated tape to a glass microscope slide

    - Laminated tape is used to handle gels from this step onwards.

13. Remove residual ***Activated 2nd gelling solution*** on one side of the gel by gently pressing on it using a Kim wipe

14. Flip the gel and repeat step **13**

    - It is important to not have residual gel on the gel because after the final expansion, you risk expanding a layer of gel underneath the cells which would limit how deep

you can image (high NA microscope working objectives usually have limited working distances).

15. Sandwich the gel with a N1.5 22x22 mm glass coverslip (see **Figure 5**)

    - It is important to not have air bubbles between the microscope slide and the coverslip, so position (or re-position) the coverslip properly.
    - Now the gel is sandwiched between a microscope slide and a coverslip.

16. Place in a humidified degassing chamber (see **Figure 6)**

    - Tupperware with two holes as inlet and outlet on its plastic lid is acceptable.
    - You can use a compass to punch holes into the plastic lid.
    - You can use wet Kim wipes to humidify the chamber.
    - Alternatively, you can use a plastic Ziploc as a degassing chamber. In that case, place a container inside a Ziploc and poke two holes to create an inlet and outlet.

17. Perfuse chamber with nitrogen or argon gas for 10 min

    - Use a Pasteur pipette as a nitrogen/argon gas inlet and use leave the outlet open to let the air escape.

18. After perfusion, remove nitrogen/argon gas inlet and seal both inlet holes with tape immediately to prevent re-oxygenation of the chamber

19. Incubate at 37°C for 1.5 hours

20. Remove gel from gelation chamber and place it onto a new glass microscope slide using tweezers

21. With a new razor blade, cut and discard the edges of the gel

    - Cut roughly 2-3 mm off every edge.
    - Press very firmly with the razor blade to remove edges.
    - The gel size should be ~1x1 cm.

22. Transfer gels to a new 12-well plate and hydrate with PBS

    - If you wish to pause the protocol, you can store the gels in PBS at 4°C for a couple of days, else you can proceed to the 3rd gelation step.

8. 3rd gelation

1. Make ***3rd gelling solution***
2. Make ***10% APS stock solution*** fresh
3. Make ***10% TEMED stock solution*** fresh
4. Place the three solutions above on ice
5. For every six samples to be expanded, in a 15 mL Eppendorf tube labelled mix:

Activated 3rd gelling solution

Solution	Volume	Final concentration
3rd gelling solution	12 mL	19% SA + 10% AAm + 0.1% BIS (all w/v) in 1X PBS
10% APS stock solution	60 uL	0.05% (w/v)
10% TEMED stock solution	60 uL	0.05% (v/v)

Total	~12 mL	19% SA + 10% AAm + 0.1% BIS + 0.05% APS + 0.05% TEMED

- Note that this solution will replace water within the expanded gel prior to its polymerization.
- As described below, we incubate each gel x2 with 2 mL of this solution (made fresh each time) for 20 min each before we immobilize them in gelation chambers and polymerize at 37°C.

6. Vortex ***Activated 3rd gelling solution*** for 5 seconds
7. Add this solution to the gels in the 12-well plate they were stored in
    - Make sure the gels are not adhered to the plate and can move freely.
8. Incubate for 15 min <u>on ice</u> on a rocker
    - 5 minutes before the incubation time is over, make the same solution again fresh.
9. Remove ***Activated 3rd gelling solution*** from wells using a p1000 pipette and make sure that there is minimum residual solution
10. Repeat steps **5-9** again for a total of 2 incubations
11. After removing residual solution, move each gel with laminated tape to a glass microscope slide
12. Remove residual ***Activated 3rd gelling solution*** on one side of the gel by gently pressing on it using a Kim wipe

13. Flip the gel and repeat step **12**

    - It is important to not have residual gel on the gel because after the final expansion, you risk expanding a layer of gel underneath the cells which would limit how deep you can image (high NA microscope working objectives usually have limited working distances).

14. Sandwich the gel with a N1.5 22x22 mm glass coverslip (see **Figure 5**)

    - It is important to not have air bubbles between the microscope slide and the coverslip.

    - Now the gel is sandwiched between a microscope slide and coverslip.

15. Place in a humidified degassing chamber (see **Figure 6)**

16. Perfuse chamber with nitrogen or argon gas for 10 min

    - Use a Pasteur pipette as a nitrogen/argon gas inlet and leave the other inlet open to let the air escape.

17. Remove nitrogen/argon gas inlet and seal both inlet holes with tape immediately to prevent re-oxygenation of the chamber

23. Incubate at 37°C for 1.5 hours

9. Dissolution of 1st and 2nd gel crosslinks

1. Remove gels from the humidified container and re-embedding gel chamber using tweezers

- Do not rip the coverslip lid off the gel harshly. Instead, hydrate the interface between the coverslip lid and gel with some PBS prior to removing the lid.

2. Place in a new 6-well plate
3. Add 4 mL of 200 mM ***NaOH solution***
    - Verify that the gel is not stuck to the 6-well plate and can swim freely in the NaOH solution.
4. Incubate on a rocker for 1 h at RT
5. Remove NaOH solution and move gels to a new 6-well plate using laminated tape
6. Wash x3 with 1X PBS for 20 min each or until the pH of the PBS solution is 7.4
    - You can use pH strips to measure pH.
7. Move gel to a new glass microscope slide using laminated tape
8. With a new razor blade, cut a 1x1 cm square gel from the total gel and transfer to a new 12-well plate
    - If you wish to pause the protocol, you can store the gels in PBS at 4°C for a couple of days.

10. Immunofluorescence

Important notes:

- Antibody staining must precede pan-staining of the proteome because we noticed less efficient antibody staining if the order is reversed.

- There is no permeabilization step because the denaturation treatment extracts lipids.
- IF is performed in 12-well plates. We use 2 mL volume per well.

1. Dilute primary antibody in ***block buffer***
    - A dilution of 1:200 to 1:500 of common antibodies is recommended.
2. Incubate in primary antibody on a rocker for 12-24 h at RT or 4°C
3. Wash x3 with ***PBS-T buffer*** for 20 min each on a rocker at RT
4. Dilute secondary antibody in ***block buffer***
    - A dilution of 1:200 to 1:500 of common antibodies is recommended.
5. Incubate in secondary antibody on a rocker for 12 h at RT or 4°C
6. Wash x3 with ***PBS-T buffer*** for 20 min each on a rocker at RT
7. Rinse x1 with 1X PBS

11. Pan-staining of the proteome

1. Thaw ***NHS ester dye stock*** at RT for 30 min
    - Since NHS esters are easily hydrolyzed by water, the stock solution must be allowed to thaw for ~30 min prior to usage to prevent condensation of moisture on the product.

- Our favorite NHS ester dye is ATTO594 since it is hydrophilic and exceptionally photostable. ATTO594 is sulfonated; we noticed efficient proteome staining and less apparent aggregation with sulfonated dyes.
- Other preferred NHS ester dyes are ATTO532 and ATTO643.
- Hydrophobic dyes (e.g., OG488 and ATTO647N) are not recommended since they do not label the proteome efficiently.
- We noticed that cyanine dyes (e.g., Dy634, AF647) are bleached quickly with confocal illumination.

2. To label six gels in a 12-well plate, we make 12 mL ***NHS ester dye working solution*** and we use it immediately:

NHS ester dye working solution

Solution	Volume/Mass	Final concentration
Sodium bicarbonate solution	100 mg	100 mM
NHS ester dye stock	120 uL	20 ug/mL
Ultrapure water	Until 12 mL	-
Total	12 mL	20 ug/mL NHS ester in 100 mM $NaHCO_3$

3. Add 2 mL ***NHS ester dye working solution*** to each of the 6 wells
4. Incubate protected from light on a rocker for 1.5 h at RT
    - You can use aluminum foil to cover your samples.
5. Wash x3 with ***PBS-T buffer*** for 20 min each on a rocker at RT

6. Optional but recommended: Label gels with a chromatin marker
    - We recommend staining with SYTOX green DNA (Thermo; cat no. S7020) used at a dilution of 1:3,000 in phosphate-free buffer for 30 min to 1 h at RT.
    - Co-staining with NHS ester dye in sodium bicarbonate buffer is also possible.

12. 2nd expansion

In this step, the gel will expand a factor of ~16×

1. Place gels in a new 6-well plate
2. Exchange water x2 for 30 min each and x1 for 1 h or until the size of the gel plateaus

13. Gel mounting

First, the orientation of the cells on the gel the be determined. The most reliable way of doing this is by imaging the gel with a table-top fluorescence microscope that is compatible with GFP or RFP imaging.

1. Make sure that the gel is about or less than 2x2 cm
2. Place the gel onto a 30 mm N1.5 glass coverslip MatTek dish
3. Remove residual water
4. Move MatTek dish to microscope and try to find the sample focal plane using a 10x air objective (4x or 20x air objective is also appropriate)
    - It is preferable (and easier) to use the microscope eye pieces and not a camera.
    - Set lamp power (or LED) at maximum excitation.

5. Now flip the gel
6. Try to find the focal plane again. If you need to move the objective upwards (assuming this is an inverted microscope), then the cells are on the top of the gel. If you need to move downwards, then the cells are on the bottom of the gel
7. Place in water again

Refer to **Figure 7** for a schematic describing steps **4** and **6** below

Now that the gel orientation is determined, for every single gel to be mounted:

1. Place a 18 mm round coverglass on top of the gel to sandwich it
2. Mix 3 mL yellow and blue Picodent twinsil in a 1:1 ratio for a final volume of 6 mL
3. Pour Picodent twinsil on top of the 18 mm coverslip such that the coverslip and MatTek dish are entirely submerged
4. Let Picodent twinsil cure for ~15 min

A few notes on sample mounting:

- Note that there are other ways of securing a gel onto a MatTek dish for imaging on an inverted microscope system, but this is our preferred way. Pouring low-melt agarose (instead of a Picodent twinsil) is an option, but it dries out over time.

- The gel is stable and will not shrink for about 3 days. For best results, the gels are imaged within a day or two of mounting them. Organic dyes that are stable in water will remain bright for weeks.

14. Imaging on a conventional confocal microscope

1. Secure MatTek dish on microscope stage
2. Use the microscope eyepieces to localize cells
    - If SYTOX green is used, use the GFP channel to localize cell nuclei.
3. Acquire images

A few notes on imaging:

- To localize cells, we recommend using a bright chromatin marker like SYTOX green. If that is not desirable, we recommend using the pan-stain as a guide.
- Localizing antibody staining through the microscope eyepieces is possible but not recommended because the signal is likely too dim. It is worthwhile to note that a ~16x linear expansion corresponds to a >4,000-fold reduction in local concentration of fluorophores.
- Using 100% of the maximum output laser power during confocal imaging is normal and expected, especially with immuno-stained structures of interest.
- Sometimes even maximum power for IF samples can give you the impression that the staining did not work. Try increasing line averages and scanning slower (e.g., 16 line averaged for scan speed 600 Hz).

- Because the pan-stain (NHS ester) signal is generally much brighter than the IF signal, be aware of potential crosstalk between color channels. Choose your spectral detection bands, photomultiplier voltages and excitation wavelengths and powers carefully and consider line-sequential imaging of different color channels.
- Use a high-NA water-immersion objective since you most likely will image several tens of microns deep in the sample with a refractive index close to water. Be aware of the limited free working distance of high-NA objectives. If the gel is too thick you might not be able to reach the cells with your objective.

PART III: Figures

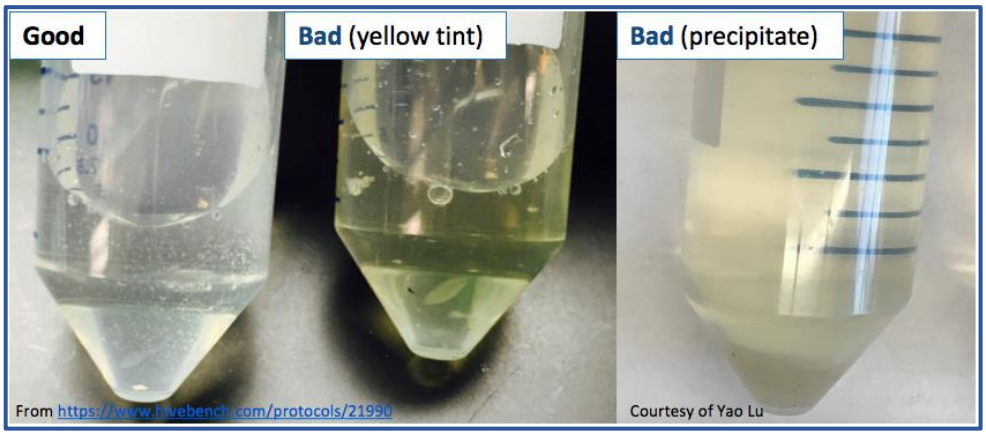

Figure 1: 38% (w/v) sodium acrylate solution

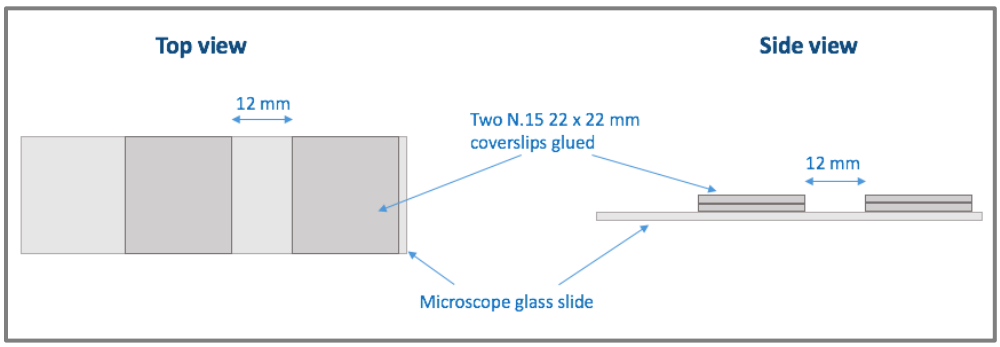

Figure 2: pan-ExM gelation chamber

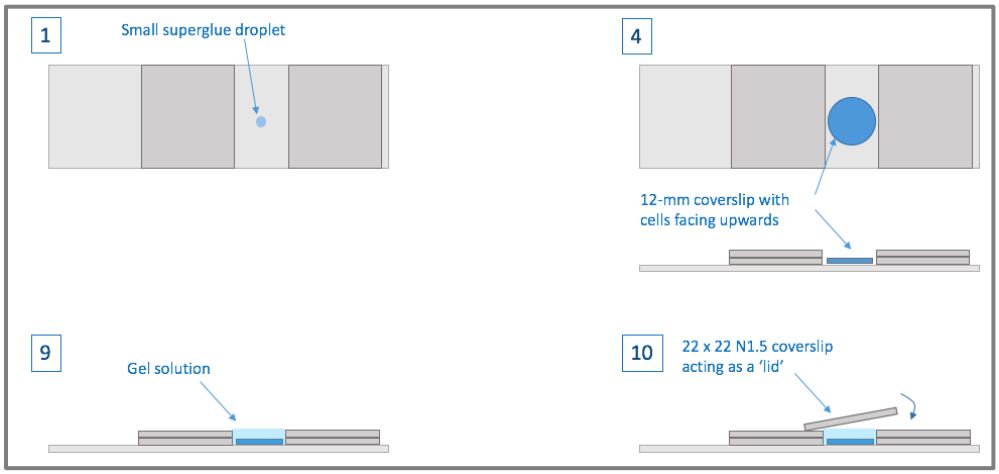

Figure 3: pan-ExM 1st gelation schematic

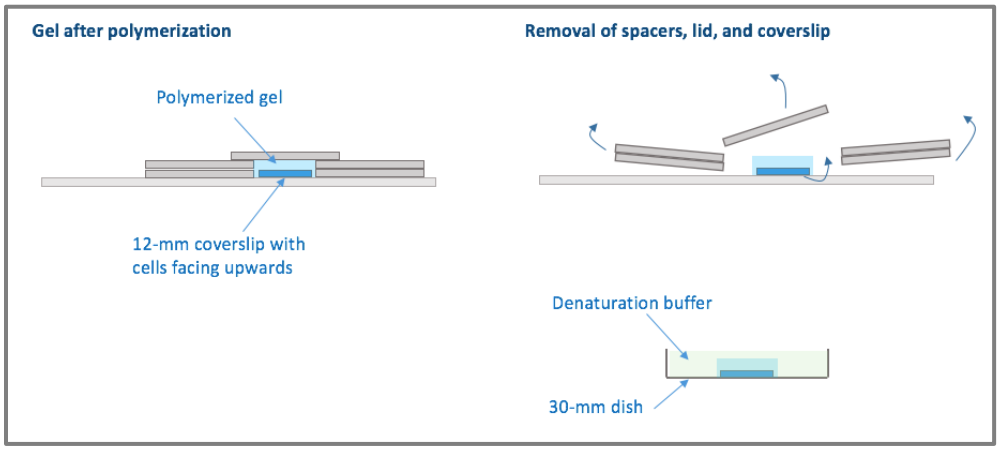

Figure 4: Removal of gel from gelation chamber and denaturation

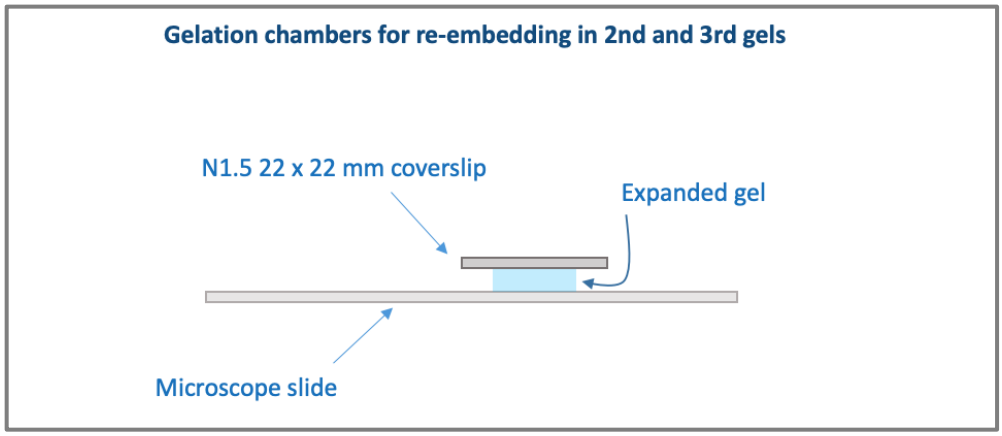

Figure 5: Gelation chamber for re-embedding in 2nd and 3rd gels schematic

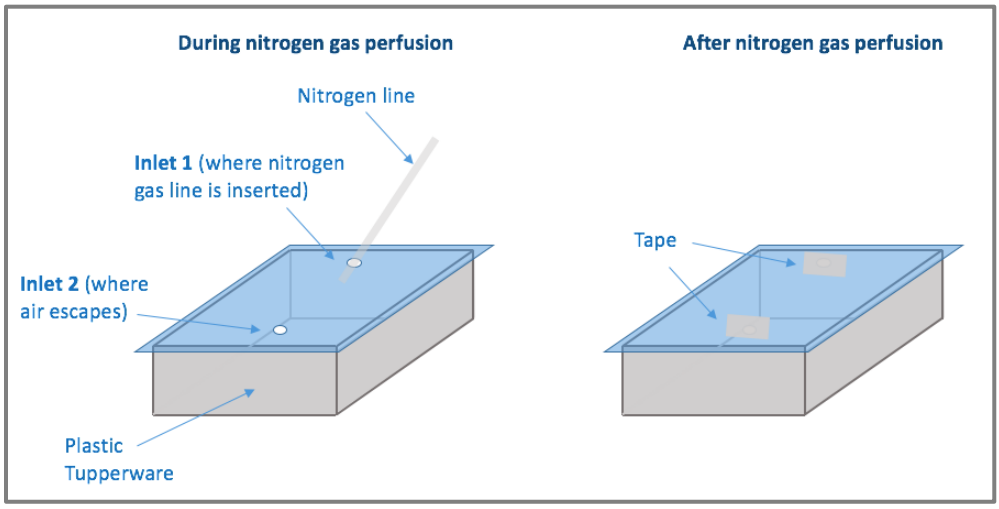

Figure 6: Degassing chamber schematic

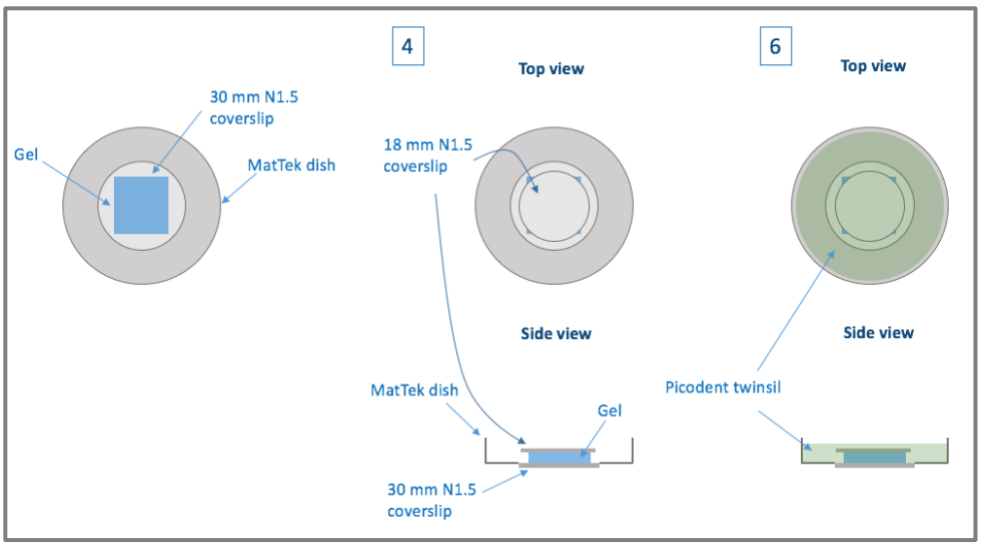

Figure 7: Gel mounting schematic

A.2 pan-ExM-t protocol (brain tissue sections)

This protocol is optimized for pan-ExM-t of **50-100 µm mouse brain tissue** sections.

PART I: Preparation

1. Reagents

Reagent	Acronym	Storage	Vendor	Catalog number
40% acrylamide*	AAm	4°C	Sigma-Aldrich	A9099
N,N'-(1,2-dihydroxyethylene)bisacrylamide	DHEBA	RT		294381
Sodium bicarbonate	$NaHCO_3$	RT		S5761
Sodium hydroxide	NaOH	RT		S8045
ATTO532 NHS ester	-	-20°C		88793
Phosphate buffered saline tablets	-	RT		P4417
Triton X-100	TX-100	RT		X100-100ML
Sodium acrylate**	SA	-20°C in desiccator	Santa Cruz Biotechnology	sc-236893C
N,N′-methylenebis(acrylamide)	BIS	RT	Alfa Aesar	J66710
Ammonium persulfate	APS	RT in desiccator	American Bio	AB00112
N,N,N’,N’-tetramethylethylenediamine	TEMED	RT in desiccator		AB02020

Tris [hyroxymethyl] aminomethane	Tris	RT		AB02000
20% sodium dodecyl sulfate solution	SDS	RT		AB01922
Sodium chloride	NaCl	RT	J.T. Baker	3624-01
1x phosphate buffered saline (Gibco)	1X PBS	RT	Thermofisher	10010023
10x phosphate buffered saline (Gibco)	10X PBS	RT		70011044
16% paraformaldehyde	FA	RT	Electron Microscopy Sciences	15710
8% glutaraldehyde	GA	4°C		16019
Bovine serum albumin	BSA	4°C	Jackson Laboratories	001-000-162
Tween 20	-	RT		P7949
SYTOX Green	-	-20°C	Thermofisher	S7020
DMSO, Anhydrous	DMSO	RT		D12345

* Acrylamide (AAm) monomer in powder form can also be used. However, it is much more toxic and requires extensive precautions when handling.

** We recommend purchasing sodium acrylate (SA) from Sigma or Santa Cruz Biotechnology for the time being. However, we do notice significant batch-to-batch variability. To verify that SA is of acceptable purity, we usually make a 38% (w/v) solution in water and check its color. If the solution color is yellow and/or a large precipitate form, please discard and try a different batch. If the solution is pale yellow and only a small precipitate forms, centrifuge solution at 4000 rpm for 5 minutes and use the supernatant. You must use a pale-yellow 38% SA stock solution without any precipitate (see **Figure 1**).

2. Materials and instruments

Materials	Vendor	Catalog number
N1.5 12-mm round glass coverslips	Electron Microscopy Sciences	72230-01
Glass microscope slide	Sigma-Aldrich	S8400
N1.5 22 x 22 mm square cover glass coverslips	Fisher Scientific	12-541BP
N1.5 18-mm round coverslip	Marienfeld	0117580
50 mm MatTek dish, N1.5 coverslip 30 mm diameter	MatTek life sciences	P50G-1.5-30-F
Picodent twinsil	picodent	1300 1000

Instruments	pH meter, 37°C incubator, nitrogen (or argon) gas tank, dry block incubator, ice bucket, rocker, vortex
Other materials	Superglue, tweezers, razor blades, container (plastic Tupperware), Petri dishes, 12-well plates, 6-well plates, 1.5 mL Eppendorf tubes, 15 mL Eppendorf tubes, 50 mL Eppendorf tubs, Kim wipes, beaker, stir bar, paintbrush (brush size No. 2 (1.6 mm)), laminated tape, pH strips, aluminum foil, surgical scissors

3. Solutions

These solutions are referred to in **Part II: Protocol**. Note that some can be made beforehand and stored, while others must be made fresh.

Fixation solution

Reagent	Amount	Concentration
16% FA	2.5 mL	4% (w/v)

20% AAm	5 mL	
10X PBS	1 mL	1X
Ultrapure water	1.5 mL	-
Total	10 mL	4% FA + 20% AAm in 1X PBS

- This solution must be made fresh for appropriate preservation of ultrastructure.
- FA is toxic and must be handled in a fume hood. After opening each vial, we transfer these stock solutions to 15 mL Eppendorf tubes and store them for no longer than 24 h at 4°C. For consistent results, please do not use solutions of FA that exceed that storage duration.

DHEBA + AAm stock solution

Reagent	Amount	Concentration
DHEBA	160 mg	0.4% (w/v)
40% AAm	40 mL	40% (w/v)
Total	40 mL	0.4% DHEBA in 40% AAm

- DHEBA is notoriously difficult to dissolve. There are also impurities in recent batches of DHEBA from Sigma that must be removed prior to using the solution.
    - To dissolve DHEBA in 40% AAm solution, vortex vigorously for 15 min, or put a small magnetic stir bar in a falcon tube with the solution, tape it to a magnetic stirrer and stir for at least half an hour.

- Even after excessive vortexing/stirring, you might still notice some 'flakiness'. These are likely insoluble impurities. If that is the case, filter-sterilize the solution to get rid of the impurities.

- Make aliquots of 2.5 mL and store in -20°C. This solution is stable for at least 1 month.

1st gelling solution

Reagent	Amount	Concentration
DHEBA + AAm stock solution	2.5 mL	10% AAm (w/v) + 0.1% DHEBA (w/v)
SA	1.9 g	19% (w/v)
10X PBS	1 mL	1X
Ultrapure water	Until 10 mL	-
Total	10 mL	10% AAm + 0.1% DHEBA + 19% SA in 1X PBS

- Centrifuge this solution at 4000 rpm for about 5 minutes, discard the precipitate, and only use the supernatant.

- Every sample to expand consumes ~200 uL of this solution.

- Make aliquots of 1 mL and store in -20°C. This solution is stable for at least 1 month.

Denaturation buffer

Reagent	Amount	Concentration
NaCl	2.92 g	200 mM
Tris	1.51 g	50 mM

20% SDS	72.1 mL	200 mM
Ultrapure water	Until 250 mL	-
Total	250 mL	200 mM SDS + 50 mM Tris + 50 mM NaCl

- Add reagents to a beaker with a stir bar and stir heated to 40°C to dissolve. Note that SDS precipitates at temperatures below 19°C.
- Cool to room temperature and adjust pH to 6.8 with hydrochloric acid (HCl).
    - The pH of Tris buffer is sensitive to temperature. The solution must have its pH adjusted at RT (~19°C).
- This solution is stored at RT and is stable for at least 12 months.

2nd gelling solution

Reagent	Amount	Concentration
40% AAm	12.5 mL	10% (w/v)
DHEBA	25 mg	0.05% (w/v)
Ultrapure water	37.5	-
Total	50 mL	10% AAm + 0.05% DHEBA

- Every sample to expand consumes 6 mL of this solution. Since the number of tissue samples we process at once is generally around 6, we make 50 mL of this solution and discard the remnant.

3rd gelling solution

Reagent	Amount	Concentration
40% AAm	6.25 mL	10% (w/v)
BIS	25 mg	0.1% (w/v)
SA	2.25 g	9% (w/v)
10X PBS	2.5 mL	1x
Ultrapure water	Until 25 mL	-
Total	25 mL	10% AAm + 0.1% BIS + 9% SA in 1X PBS

- Centrifuge this solution at 4000 rpm for about 5 minutes, discard the precipitate, and only use the supernatant.
- Every sample to expand consumes 4 mL of this solution. Since the number of samples we process at once is generally around 6, we make 25 mL of this solution and discard the remnant.

15% APS stock solution

Reagent	Amount	Concentration
APS	150 mg	15% (w/v)
Ultrapure water	Until 1 mL	-
Total	1 mL	15% APS

- This solution must be made fresh and kept on ice. We use it to make ***Activated 1st gelling solution***. We usually discard it if left on ice for more than 6 hours.

15% TEMED stock solution

Reagent	Amount	Concentration
TEMED	150 uL	15% (v/v)
Ultrapure water	750 uL	-
Total	1 mL	15% TEMED

- This solution must be made fresh and kept on ice. We use it to make ***Activated 1st gelling solution***. We usually discard it if left on ice for more than 6 hours

10% APS stock solution

Reagent	Amount	Concentration
APS	100 mg	10% (w/v)
Ultrapure water	Until 1 mL	-
Total	1 mL	10% APS

- This solution must be made fresh and kept on ice. We use it to make ***Activated 2nd gelling solution*** or ***Activated 3rd gelling solution***. We usually it if left on ice for more than 6 hours.

10% TEMED stock solution

Reagent	Amount	Concentration
TEMED	100 uL	10% (v/v)
Ultrapure water	900 uL	-
Total	1 mL	10% TEMED

- This solution is made fresh and kept on ice. We use it to make ***Activated 2nd gelling solution*** or ***Activated 3rd gelling solution***. We usually discard this working solution if left on ice for more than 6 hours.

NaOH solution

Reagent	Amount	Concentration
NaOH	800 mg	200 mM
Ultrapure water	Until 100 mL	-
Total	100 mL	200 mM NaOH

- Please be cautious when handling this solution as it is highly caustic (pH ~13).
- You can store this solution at room temperature.

PBS-T buffer

Reagent	Amount	Concentration
PBS tablets	5 tablets	1X

Tween 20	1 mL	0.1% (v/v)
Ultrapure water	1 L	-
Total	1 L	0.1% Tween 20 in 1X PBS

- This solution can be stored at room temperature.
- Alternatively, you can add 1 mL of Tween 20 to 1 L of pre-made 1X PBS solution.

Block buffer

Reagent	Amount	Concentration
PBS tablets	5 tablets	1X
Triton X-100	1 mL	0.1% (v/v)
Bovine serum albumin (BSA)	10 g	1% (w/v)
Ultrapure water	Until 1 L	-
Total	1 L	0.1% TX-100 + 1% BSA in 1X PBS

- This solution must be stored at 4°C.

NHS ester dye stock

Reagent	Amount	Concentration
NHS ester ATTO532 (Sigma-Aldrich 88793)	1 mg	2 mg/mL
DMSO	500 uL	-
Total	500 uL	2 mg/mL ATTO594 NHS ester

- Make 50 uL aliquots and store desiccated at -20°C.
- NHS ester is very sensitive to moisture and must be stored in a desiccator. In the absence of a desiccator, place the reagent in a container containing desiccant beads.

PART II: Protocol

1. Fixation

1. Perfuse mice with ***fixation solution***
2. Extract brains and incubate in the same fixation solution for 24 h at 4°C
3. Store in PBS at 4°C

2. Vibratome sectioning

1. Make ~70 um-thick sections using a vibratome at RT
2. Store sections in PBS at 4°C

3. Gelation chamber construction

Please refer to **Figure 2** for a visual diagram

1. To make one gelation chamber spacer, glue two single N1.5 22x22 mm coverslips on a microscope slide spaced about 12 mm from each other
    - The space between these spacers will be used to place the tissue sample.
2. As a chamber lid, we use one N1.5 22x22 mm coverslip

- This lid is used to seal the chamber after pouring 1st gelling solution onto the sample.

3. **1st gelation**

1. Thaw ***1st gelling solution***
2. Make ***15% APS stock solution*** fresh
3. Make ***15% TEMED stock solution*** fresh
4. Place all three solutions above on ice

For this next step, refer to **Figure 3** for a visual representation of steps **7**, **8** and **9**

We recommend beginners embed at most 2 samples at once

Samples are embedded in 1st hydrogel two-by-two. For every single tissue section sample:

5. Using a paintbrush, place in a 1.5 mL Eppendorf tube filled with 500 uL ***1st gelling solution***
6. Incubate on ice for 30 min on a rocking platform
7. Immediately before use, take one 1.5 mL Eppendorf tube and mix:

Activated 1st gelling solution

Solution	Volume	Final concentration
1st gelling solution	400 uL	19% SA + 10% AAm + 0.1% DHEBA (all w/v) in 1X PBS

15% APS stock solution	2 uL	0.075% (w/v)
15% TEMED stock solution	2 uL	0.075% (v/v)
Total	~400 uL	19% SA + 10% AAm + 0.1% DHEBA + 0.075% APS + 0.075% TEMED in 1X PBS

Note that this step is very time sensitive as premature gelation of the solution might affect protein retention.

8. Vortex for 2 seconds
9. Using a paintbrush, transfer brain tissue section to the ***Activated 1st gelling solution***
10. Incubate on ice for 15 min
    - Extending this incubation even by 5 min risks premature gelation.
11. Using a paintbrush, transfer brain tissue to the N1.5 22x22 mm glass coverslip lid and gently flatten
    - Quickly remove residual ***Activated 1st gelling solution*** with Kim wipes to ease tissue flattening.
12. Add ~100 uL of iced ***Activated 1st gelling solution*** to the center of the gelation chamber
13. Seal the chamber with the N1.5 22x22 mm glass coverslip lid holding the flattened sample
    - Remove residual gel with a Kim wipe.
14. Place gelation chambers in a humidified container (Tupperware with wet Kim wipes will suffice)

15. Incubate for 1.5 h at 37°C

5. Denaturation

Refer to **Figure 4** for a visual representation of steps **2-5**.

Remember to turn the dry block incubator on and set to 76°C before these following steps.

1. Remove gelation chambers from container
2. With a razor blade, gently remove the gelation lid from gelation chamber
3. With a razor blade, scrape off the gel areas that do not contain any tissue
    - At this stage, you are still able to see the tissue sample. After SDS denaturation, the sample will be transparent. So, it is important to get rid of non-tissue embedded gel at this stage.
4. Peel off the gel-embedded sample from the gelation lid with tweezers
5. Place coverslips in a 6-well plate and add 4 mL denaturation buffer in each well
6. Incubate for 30 min at 37°C
7. With a No. 2 paintbrush, gently pick up the gel and move to a 1.5 mL Eppendorf tube and add 1 mL of denaturation buffer
8. Incubate in heat block at 76°C for **4 h**
    - Because heat is transferred to the Eppendorf tube through air, the actual temperature of the solution will be 73°C (the desired temperature) and not 76°C.

- Water has higher thermal conductivity. So, if you are using a water bath, set it to 73°C.

9. Move gel with a paintbrush to a Petri dish and flatten it
10. With a new razor blade, cut a 0.75x0.75 cm square gel from the total gel and transfer to a new 6-well plate using a paintbrush
    - You can cut multiple 0.75x0.75 cm squares if you wish to make multiple samples.
11. Wash the gel x3 with 1X PBS for 20 min each to remove residual SDS
    - You may wish to save the remaining gel in 4°C after washing residual SDS for future use.
    - You may wish to pause the protocol here for a couple of days by storing the gel in PBS at 4°C.

6. 1st expansion

In this step, the gel will expand a factor of 4× to 4.5×

1. In the same 6-well plate, remove PBS and replace with ultrapure water
2. Incubate in water x2 for 30 min each and x1 for 1 h or until the size of the gel plateaus

7. 2nd gelation

The ideal re-embedded gel size is 1.5x1.5 cm.

1. Thaw ***2nd gelling solution***
2. Make ***10% APS stock solution*** fresh

3. Make ***10% TEMED stock solution*** fresh

4. Place all solutions above on ice

5. For every six samples to be expanded, in a 15 mL Eppendorf tube mix:

Activated 2nd gelling solution

Solution	Volume	Final concentration
2nd gelling solution	12 mL	10% (w/v) AAm + 0.05% (w/v) DHEBA
10% APS stock solution	60 uL	0.05% (w/v)
10% TEMED stock solution	60 uL	0.05% (v/v)
Total	~12 mL	10% AAm + 0.05% DHEBA + 0.05% APS + 0.05% TEMED

- Note that this solution will replace water within the expanded gel prior to its polymerization.
- As described below, we incubate each gel x2 with 2 mL of this solution (made fresh each time) for 20 min each before we immobilize them in gelation chambers and polymerize at 37°C.

1. Vortex ***Activated 2nd gelling solution*** for 5 seconds

2. Remove water from the 6-well plates

3. Add ***Activated 2nd gelling solution***

- Make sure that the gels are not adhered to the plate and can move freely.

4. Incubate for 20 min at RT on a rocker

    - 5 minutes before the incubation time is over, make the same solution again fresh.

5. Remove ***Activated 2nd gelling solution*** from wells using a p1000 pipette and make sure that there is minimum residual solution

6. Repeat steps **5-10** again for a total of 2 incubations

7. After removing residual solution, move each gel with laminated tape to a glass microscope slide

    - Laminated tape is used to handle gels from this step onwards.

8. Remove residual ***Activated 2nd gelling solution*** on one side of the gel by gently pressing on it using a Kim wipe

9. Flip the gel and repeat step **13**

    - It is important to not have residual gel on the gel because after the final expansion, you risk expanding a layer of gel underneath the cells which would limit how deep you can image (high NA microscope working objectives usually have limited working distances).

10. Sandwich the gel with a N1.5 22x22 mm glass coverslip (see **Figure 5**)

    - It is important to not have air bubbles between the microscope slide and the coverslip, so position (or re-position) the coverslip properly.

    - Now the gel is sandwiched between a microscope slide and a coverslip.

11. Place in a humidified degassing chamber (see **Figure 6)**

- Tupperware with two holes as inlet and outlet on its plastic lid is acceptable.
- You can use a compass to punch holes into the plastic lid.
- You can use wet Kim wipes to humidify the chamber.
- Alternatively, you can use a plastic Ziploc as a degassing chamber. In that case, place a container inside a Ziploc and poke two holes to create an inlet and outlet.

12. Perfuse chamber with nitrogen or argon gas for 10 min

- Use a Pasteur pipette as a nitrogen/argon gas inlet and use leave the outlet open to let the air escape.

13. After perfusion, remove nitrogen/argon gas inlet and seal both inlet holes with tape immediately to prevent re-oxygenation of the chamber

14. Incubate at 37°C for 1.5 hours

15. Remove gel from gelation chamber and place it onto a new glass microscope slide using tweezers

16. With a **new** razor blade, cut and discard the edges of the gel

- Cut roughly 2-3 mm off every edge.
- Press very firmly with the razor blade to remove edges.
- The gel size should be ~1x1 cm.
- This step is to ensure that the gel is flat for the 3rd gelation step.

17. Transfer gels to a new 12-well plate and hydrate with PBS

- If you wish to pause the protocol, you can store the gels in PBS at 4°C for a couple of days, else you can proceed to the 3rd gelation step.

8. 3rd gelation

1. Make ***3rd gelling solution***
2. Make ***10% APS stock solution*** fresh
3. Make ***10% TEMED stock solution*** fresh
4. Place the three solutions above on ice
5. For every six samples to be expanded, in a 15 mL Eppendorf tube labelled mix:

Activated 3rd gelling solution

Solution	Volume	Final concentration
3rd gelling solution	12 mL	9% SA + 10% AAm + 0.1% BIS (all w/v) in 1X PBS
10% APS stock solution	60 uL	0.05% (w/v)
10% TEMED stock solution	60 uL	0.05% (v/v)
Total	~12 mL	9% SA + 10% AAm + 0.1% BIS + 0.05% APS + 0.05% TEMED

- Note that this solution will replace water within the expanded gel prior to its polymerization.

- As described below, we incubate each gel x2 with 2 mL of this solution (made fresh each time) for 20 min each before we immobilize them in gelation chambers and polymerize at 37°C.

6. Vortex ***Activated 3rd gelling solution*** for 5 seconds
7. Add this solution to the gels in the 12-well plate they were stored in
    - Make sure the gels are not adhered to the plate and can move freely.
8. Incubate for 15 min <u>on ice</u> on a rocker
    - 5 minutes before the incubation time is over, make the same solution again fresh.
9. Remove ***Activated 3rd gelling solution*** from wells using a p1000 pipette and make sure that there is minimum residual solution
10. Repeat steps **5-9** again for a total of 2 incubations
11. After removing residual solution, move each gel with laminated tape to a glass microscope slide
12. Remove residual ***Activated 3rd gelling solution*** on one side of the gel by gently pressing on it using a Kim wipe
13. Flip the gel and repeat step **12**
    - It is important to not have residual gel on the gel because after the final expansion, you risk expanding a layer of gel underneath the tissue which would limit how deep you can image (high NA microscope working objectives usually have limited working distances),

14. Sandwich the gel with a N1.5 22x22 mm glass coverslip (see **Figure 5**)
    - It is important to not have air bubbles between the microscope slide and the coverslip.
    - Now the gel is sandwiched between a microscope slide and coverslip.
15. Place in a humidified degassing chamber (see **Figure 6)**
16. Perfuse chamber with nitrogen or argon gas for 10 min
    - Use a Pasteur pipette as a nitrogen/argon gas inlet and leave the other inlet open to let the air escape.
17. Remove nitrogen/argon gas inlet and seal both inlet holes with tape immediately to prevent re-oxygenation of the chamber
18. Incubate at 37°C for 1.5 hours

9. Dissolution of 1st and 2nd gel crosslinks

1. Remove gels from the humidified container and re-embedding gel chamber using tweezers
    - Do not rip the coverslip lid off the gel harshly. Instead, hydrate the interface between the coverslip lid and gel with some PBS prior to removing the lid.
2. Place in a new 6-well plate
3. Add 4 mL of 200 mM ***NaOH solution***
    - Verify that the gel is not stuck to the 6-well plate and can swim freely in the NaOH solution.

4. Incubate on a rocker for 1 h at RT
5. Remove NaOH solution and move gels to a new 6-well plate using laminated tape
6. Wash x3 with 1X PBS for 20 min each or until the pH of the PBS solution is 7.4
    - You can use pH strips to measure pH.
7. Move gel to a new Petri dish using laminated tape
8. With a new razor blade, cut a 1x1 cm square gel from the total gel and transfer to a new 12-well plate
    - If you wish to pause the protocol, you can store the gels in PBS at 4°C for a couple of days.

10. Immunofluorescence

Important notes:

- Antibody staining must precede pan-staining of the proteome because we noticed less efficient antibody staining if the order is reversed.
- There is no permeabilization step because the denaturation treatment extracts lipids.
- IF is performed in 12-well plates. We use 2 mL volume per well.
- We recommend using ATTO594 and ATTO647N secondary antibodies (with preference for ATTO594).

1. Dilute primary antibody in ***block buffer***

- A dilution of 1:250-1:500 of common antibodies is recommended (~5 ug/mL).
- For structural tissue markers (e.g., GFAP antibody), we recommend 1:500 dilution (~5 ug/mL) and for synaptic proteins, we recommend 1:250 dilution (~10 ug/mL).

2. Incubate in primary antibody on a rocker for ~30 h at 4°C
3. Wash x5 with ***PBS-T buffer*** over the course of 1 day
    - Wash x3 for 20 min each on a rocker at RT.
    - Wash x1 overnight at 4°C.
    - Wash x1 for 20 min.
4. Dilute secondary antibody in ***block buffer***
    - A dilution of 1:250-1:500 of common antibodies is recommended.
5. Incubate in secondary antibody on a rocker for ~30 h at 4°C
6. Wash x5 with ***PBS-T buffer*** over the course of 1 day
    - Wash x3 for 20 min each on a rocker at RT.
    - Wash x1 overnight at 4°C.
    - Wash x1 for 20 min.

11. Pan-staining of the proteome

1. Thaw ***NHS ester dye stock*** at RT for 30 min

- Since NHS esters are easily hydrolyzed by water, the stock solution must be allowed to thaw for ~30 min prior to usage to prevent condensation of moisture on the product.
- Our favorite NHS ester dye is ATTO532 and ATTO594 since they are hydrophilic and exceptionally photostable. These dyes are sulfonated; we noticed efficient proteome staining and less apparent aggregation with sulfonated dyes.
- We prefer using ATTO532 NHS ester if antibody labeling with ATTO594 or ATTO647N was performed.
- We recommend that the pan-stain dye is green-shifted relative to the dyes used for antibody labeling to avoid quenching effects.
- Hydrophobic dyes (e.g., OG488 and ATTO647N) are not recommended since they do not label the proteome efficiently.
- We noticed that cyanine dyes (e.g., Dy634, AF647) are bleached quickly with confocal illumination.

2. To label six gels in a 12-well plate, we make 12 mL ***NHS ester dye working solution*** and we use it immediately:

NHS ester dye working solution

Solution	Volume/Mass	Final concentration
Sodium bicarbonate solution	100 mg	100 mM
NHS ester dye stock	180 uL	30 ug/mL

Ultrapure water	Until 12 mL	-
Total	12 mL	30 ug/mL NHS ester in 100 mM $NaHCO_3$

3. Add 2 mL ***NHS ester dye working solution*** to each of the 6 wells
4. Incubate protected from light on a rocker for 2.5 h at RT
    - You can use aluminum foil to cover your samples.
5. Wash x3 with ***PBS-T buffer*** for 20 min each on a rocker at RT
6. Wash x1 in ***PBS-T buffer*** overnight
7. Optional but recommended: Label gels with a chromatin marker
    - We recommend staining with SYTOX green DNA (Thermo; cat no. S7020) used at a dilution of 1:3,000 in phosphate-free buffer for 30 min to 1 h at RT.
    - Co-staining with NHS ester dye in sodium bicarbonate buffer is also possible.

12. 2nd expansion

In this step, the gel will expand a factor of ~16×

1. Place gels in a new 6-well plate
2. Exchange water x2 for 30 min each and x1 for 1 h or until the size of the gel plateaus

13. Gel mounting

First, the orientation of the cells on the gel the be determined. The most reliable way of doing this is by imaging the gel with a table-top fluorescence microscope that is compatible with GFP or RFP imaging.

1. Make sure that the gel is about or less than 2x2 cm^2
2. Place the gel onto a 30 mm N1.5 glass coverslip MatTek dish
3. Remove residual water
4. Move MatTek dish to microscope and try to find the sample focal plane using a 10x air objective (4x or 20x air objective is also appropriate)
    - It is preferable (and easier) to use the microscope eye pieces and not a camera.
    - Set lamp power (or LED) at maximum excitation.
5. Now flip the gel
6. Try to find the focal plane again. If you need to move the objective upwards (assuming this is an inverted microscope), then the cells are on the top of the gel. If you need to move downwards, then the cells are on the bottom of the gel
7. Place in water again

Refer to **Figure 7** for a schematic describing steps **4** and **6** below.

Now that the gel orientation is determined, for every <u>single</u> gel to be mounted:

5. Place a 18 mm round coverglass on top of the gel to sandwich it
6. Mix 3 mL yellow and blue Picodent twinsil in a 1:1 ratio for a final volume of 6 mL

7. Pour Picodent twinsil on top of the 18 mm coverslip such that the coverslip and MatTek dish are entirely submerged

8. Let Picodent twinsil cure for ~15 min

A few notes on sample mounting:

- Note that there are other ways of securing a gel onto a MatTek dish for imaging on an inverted microscope system, but this is our preferred way. Pouring low-melt agarose (instead of a Picodent twinsil) is an option, but it dries out over time.

- The gel is stable and will not shrink for about 3 days. For best results, the gels are imaged within a day or two of mounting them. Organic dyes that are stable in water will remain bright for weeks.

14. Imaging on a conventional confocal microscope

4. Secure MatTek dish on microscope stage

5. Use the microscope eyepieces to localize tissue

    - If SYTOX green is used, use the GFP channel to localize cell nuclei.

6. Acquire images

A few notes on imaging:

- To localize tissue, we recommend using a bright chromatin marker like SYTOX green. If that is not desirable, we recommend using the pan-stain as a guide.

- Localizing antibody staining through the microscope eyepieces is possible but not recommended because the signal is likely too dim. It is worthwhile to note that a ~16x linear expansion corresponds to a >4,000-fold reduction in local concentration of fluorophores.
- Using 100% of the maximum output laser power during confocal imaging is normal and expected, especially with immuno-stained structures of interest.
- Sometimes even maximum power for IF samples can give you the impression that the staining did not work. Try increasing line averages and scanning slower (e.g., 8-16 line averaged for scan speed 600 Hz).
- Because the pan-stain (NHS ester) signal is generally much brighter than the IF signal, be aware of potential crosstalk between color channels. Choose your spectral detection bands, photomultiplier voltages and excitation wavelengths and powers carefully and consider line-sequential imaging of different color channels.
- To image tissue processed with pan-ExM, you need to use a high WD (~2 mm) and high-NA (>0.9) water-immersion objective since you most likely will image several tens of microns deep in the sample with a refractive index close to water. Be aware of the limited free working distance of high-NA objectives. If the gel is too thick you might not be able to reach the cells with your objective.
    i. One great water objective is Leica's 25X 0.95 NA water immersion objective (WD = 2 mm)
    ii. If you can only use objectives with lower WD, you might need to section the expanded gel with a vibratome (after labeling)

PART III: Figures

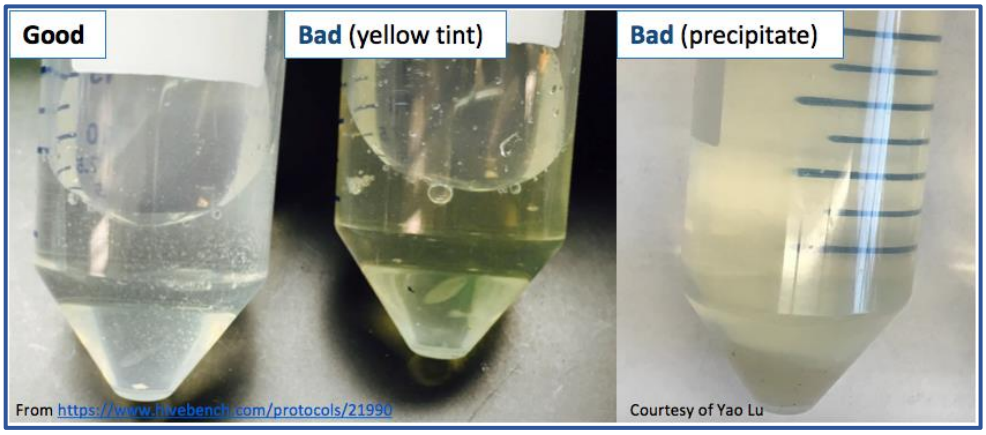

Figure 1: 38% (w/v) sodium acrylate solution

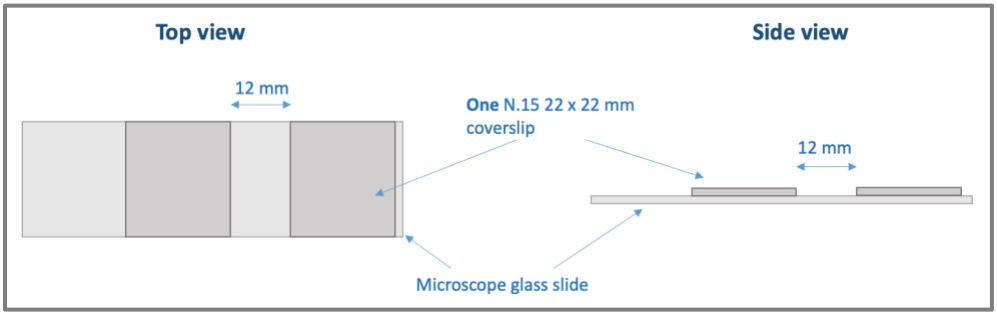

Figure 2: pan-ExM-t gelation chamber

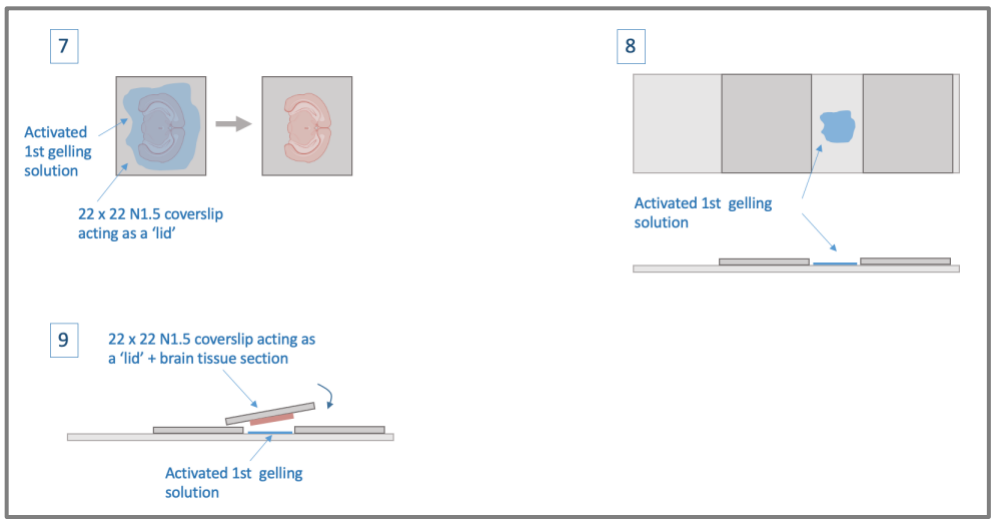

Figure 3: pan-ExM-t 1st gelation schematic

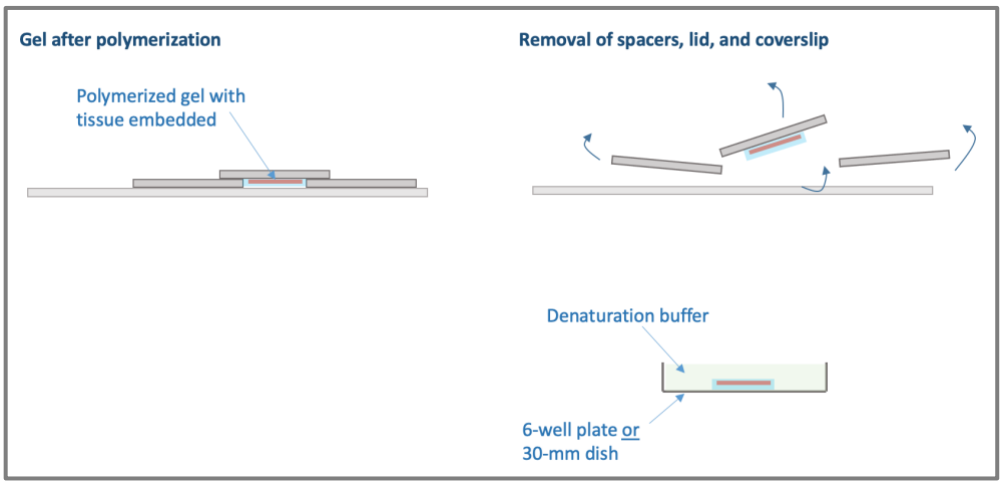

Figure 4: Removal of gel from gelation chamber and denaturation

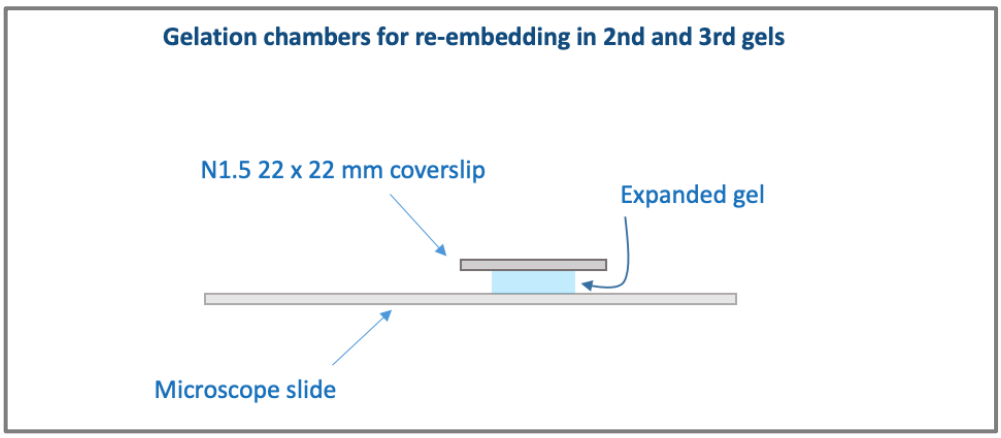

Figure 5: Gelation chamber for re-embedding in 2nd and 3rd gels schematic

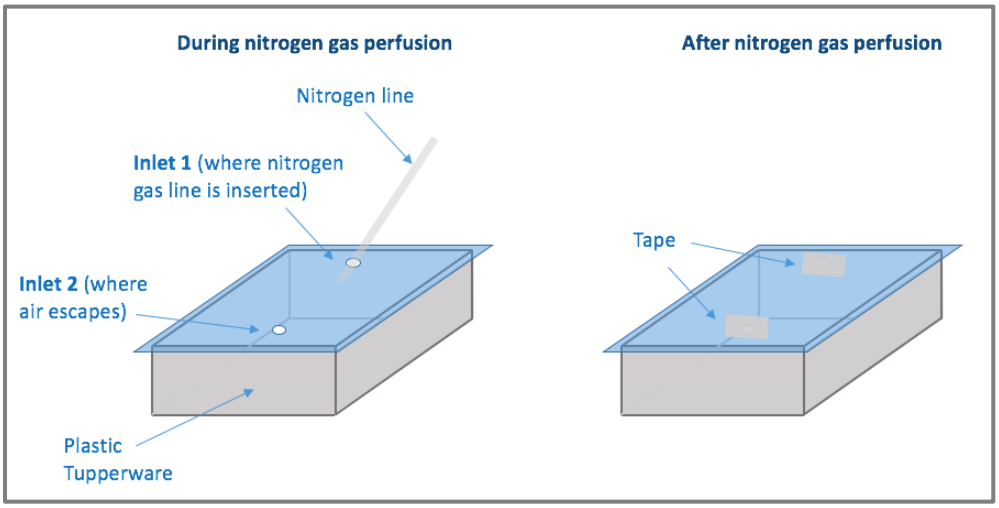

Figure 6: Degassing chamber schematic

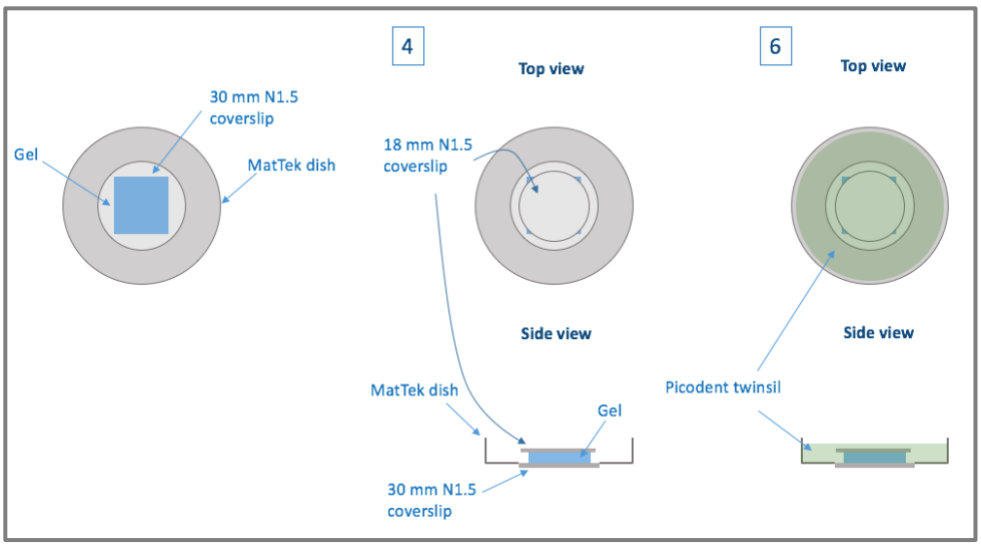

Figure 7: Gel mounting schematic